NOVEL ROLES OF EXTRACELLULAR MATRIX AND NON-MUSCLE MYOSIN II IN REGULATING EPITHELIAL MIGRATION AND PROLIFERATION

by

Kim-Vy Nguyen-Ngoc

A dissertation submitted to Johns Hopkins University in conformity with the requirements for the degree of Doctor of Philosophy

Baltimore, Maryland

February 2015

Abstract

The extracellular matrix (ECM) provides physical support for tissue development and is co-opted in cancer. The mammary gland includes two distinct types of ECMs: a collagen I-rich stroma, and basement membrane (BM) that separates epithelial tissue from the stroma. The ECM is continuously remodeled to control tissue integrity while its abnormal remodeling correlates with breast cancer metastasis. However, how ECM microenvironments differentially regulate epithelial cell behavior of normal and tumor tissues remains elusive. We explanted ductal groups, called organoids, from normal and tumor mammary epithelium into 3D gels of BM (Matrigel) and collagen I. We found that the local ECM primarily determined cell migratory behavior. While collagen I induced protrusive invasion in normal and tumor organoids while they grew indolently in Matrigel. However, different from tumor cells that persistently invaded, normal cells ceased to protrude, and restored epithelial structure. Inhibition of actomyosin contractility abolished the epithelial reorganization. Moreover, the addition of Matrigel suppressed collagen I-triggered invasion. Interestingly, we identified a mix of Matrigel and collagen I as a better ECM microenvironment to recapitulate branching morphogenesis.

We next aimed to uncover how myosin II-mediated contractility regulates epithelial reorganization. We used Cre-lox-based gene deletion to induce the deletion of non-muscle myosin II (NMII) isoforms. Surprisingly, concurrent deletion of NMIIA and NMIIB (NMIIA,B) stimulated excessive proliferation in

quiescent and actively growing epithelial tissues. The genetic mosaic analysis revealed that the hyper-proliferation was a non-cell autonomous effect. Our data unravel a novel cooperative role of NMIIA,B as negative regulators for cell proliferation and tissue growth.

Advisor: Dr. Andrew Ewald

Reader: Dr. Douglas Robinson

Acknowledgements

First and foremost I would like to thank my advisor Andrew Ewald. It has been a great honor to be his first graduate student. He has taught me how to approach, ask and investigate important scientific questions, how to interpret difficult experimental results, and how to write and present my work. I appreciate his dedication of time, ideas, and efforts for my scientific skills, career development, and his enormous support for whatever I want to do. His encouragement and motivation help me get through tough time during the Ph.D pursuit.

The members of the Ewald group have contributed immensely to my professional and personal life at Hopkins. The group has always been the source of friendship as well as scientific discussion and collaboration. I have been extremely fortunate to spend my PhD time with Kevin Cheung, Eliah Shamir, and Robert Huebner. I am especially grateful for Eliah, who is always willing to help me with editing and writing. I have learned a lot from her diligence, discipline, and self-motivation. I want to thank Kevin for many inspiring discussions and good advice. I really enjoy talking with Robert about scientific ideas and family issues, of which we have had many similarities. In the last year of my PhD, I am lucky to work with a new group of members: Neil Neumann, Amanda Fairchild, Dan Georgess, Vanesa Silvestri, Katarina Sirka, and Veena Padmanaba, who are very talented, enthusiastic, passionate, and caring. They have brought a new,

lively dynamic to the lab. I owe a special thank to Vanesa for her help and collaboration to complete our last two papers.

I gratefully acknowledge various members of Hopkins community for their support during my training: the BCMB program, particularly Carolyn Machamer, Lesley Brown, and Arhonda Gogos; the department of Cell Biology, the Hay Fellowship program, the Lewis travel award program; Dr. Sarah Poynton for enormous help in manuscript and thesis editing. I want to especially acknowledge my thesis committee: Doug Robinson, Pierre Coulombe, and Debbie Andrew, for their time dedication and helpful suggestions.

My time at Hopkins was made enjoyable in large part due to my friends that have become a part of my life. I want to thank my wonderful classmate friends: Cassandra Patenaude, Robert Huebner and his wife, Ouma Onguka and his wife, Hoku West-Foyle and his wife, Elizabeth Hwang-Wong, Nina Rajpurohit, Danfeng Cai, Yawen Lu, and Jose Wong. I also want to thank my Vietnamese friends at Hopkins: Khanh-An Huynh, Hoai-Nghia Nguyen, Sang Tang, Nam Chu, Nhat Le, and many others.

I cannot complete my PhD and be a mother at the same time without enormous help and encouragement from my big family. My words cannot express enough my truly gratitude to the love of my parents and brother, who have been always by my side through many ups and downs, twists and turns. Their firm belief in my ability has always motivated me to strive for new goals and achievements. I am very thankful for my in-law family, particularly my mother in-

law for her caring and love for us. And most of all for the loves of my life: my husband and son. We have been married and had a child while living apart, which is not always easy. I am deeply grateful for his endless love, faithful support, and even criticism. All in all, whatever he does is to help me improve myself and be more successful. I am very lucky to have my son, who always shows his support by being healthy, happy, and caring. His smile simply shines my day.

Kim-Vy Nguyen-Ngoc
Johns Hopkins School of Medicine
March 2015

Table of Contents

List of Figures

CHAPTER 1

Remodeling the extracellular matrix in mammary epithelial development and breast cancer

Remodeling the extracellular matrix in mammary epithelial development

The extracellular matrix (ECM) is a three-dimensional (3D), non-cellular structure that contributes to the development and organization of all mammalian organs. Our understanding of the functional roles of the ECM has expanded beyond that of structural support, to recognizing that the ECM also provides biological signals and mechanical inputs through cell-matrix adhesion complexes. The ECM proteins and supramolecular structures play a crucial role in cell fate determination, proliferation, survival, polarity, migration, and tissue homeostasis. The dynamic ECM structure is continuously remodeled to provide proper physical support for organ integrity. However, when there is abnormal remodeling of ECMs in mature organs, this is associated with a number of diseases including cancer (Bonnans et al., 2014). Therefore, understanding how ECM remodeling regulates cellular phenotypes will help us gain better insights into both development and disease.

The mammary gland is mainly composed of two types of tissues: epithelium and connective. Mammary epithelium is structured from apical luminal epithelial cells and basal myoepithelial cells. Luminal epithelial cells shape the collecting ducts, and differentiate into milk-producing alveoli during pregnancy and lactation. Myoepithelial cells form a contractile layer for milk secretion. The interstitial connective tissue, or stroma, contains single, loosely-adherent cells, and a large variety of ECM proteins such as collagens, proteoglycans, and

glycoproteins (Hynes and Naba, 2012).

In respect to location and shape, ECMs are divided into two types: (i) stromal matrix, which surrounds cells and provides physical support for tissues; and (ii) basement membrane, which is a specialized sheet of ECMs that entirely ensheathes and separates the epithelium from the stroma. Stromal ECMs form a complex microenvironment, which serves as supply sources and regulators of nutrients, immune defenses, and molecular signals, as well as the scaffolding structure for epithelial tissue.

Cellular basis of mammary branching morphogenesis

The mammary gland is a unique branched organ, in which full development requires a long period of time, initiating around embryonic mid-gestation, and completely elaborating a ductal network with alveoli in adulthood (Deugnier et al., 1995). The mammary epithelium is derived from epidermal placodes that migrate into the mesenchyme (Balinsky, 1950). The placodes develop into bud-like structures with a stratified organization (Hogg et al., 1983), which quickly resolves into a small network of polarized simple epithelium, or epithelial rudiment, and grows very slowly until puberty (Hogg et al., 1983).

At the onset of puberty, an increasing wave of pituitary growth hormone, ovarian hormone, estrogen, and various growth factors, such as IGF1, FGFs, stimulates epithelial rudiments to enter a phase of rapid proliferation and migration throughout the fat pad (Macias and Hinck, 2012). A tremendous surge

in cell growth leads to an important structural switch of epithelial duct: the transition from a simple bilayered structure to a stratified structure, which is called a terminal end bud (TEB) (Williams and Daniel, 1983; Hinck and Silberstein, 2005; Huebner et al., 2014). The TEB is the major engine for ductal elongation and bifurcation.

The TEB contains multiple layers of luminal epithelial cells that stained positively for keratin 8 (K8) and E-Cadherin; and myoepithelial cells that stained positively with the basal markers K14 and P-Cadherin (Daniel et al., 1995), and by the contractile marker smooth muscle actin (SMA) (Deugnier et al., 1995). Epithelial cells in the TEBs are constantly proliferative, have few intercellular junctions, and incomplete apico-basal polarity (Ewald et al., 2008; Ewald et al., 2012). Derived from apically-located luminal epithelial cells and through asymmetric cell division, the newly divided cells collectively form *de novo* internal layers of cells (Huebner et al., 2014). If the TEB is considered as an engine for branching morphogenesis, these internal cells are the cellular fuel that allows the engine to function.

Concurrent with proliferation, epithelial cells in the TEB collectively migrate across the mammary fat pad. The mammary epithelial cells do not extend subcellular protrusions directed to surrounding ECMs, which differs from the models of ductal elongation in other types of epithelium such as *Drosophila* border cells (Montell et al., 2012), *Drosophila* salivary gland elongation (Andrew and Ewald, 2010), and cancer invasion (Friedl and Gilmour, 2009). Extensive

analyses with a combination of several imaging techniques including time-lapse, confocal, and transmission electron microscopy, in both *in vivo* and *ex vivo* elongating ducts, have revealed that the epithelial cells that are in direct contact with ECMs always maintain a non-protrusive morphology, and the basal interface between epithelium and ECMs is strikingly smooth (Ewald et al., 2008; Ewald et al., 2012). In contrast, there are cells with actin-based protrusion inside the TEBs, yet they do not interact with the ECM. These observations suggest a role for the ECM in regulating cell morphology and migration during normal development, and imply a role in cancer invasion.

Basement membrane structure and remodeling

Localized outside myoepithelial cells, the basement membrane creates a specific ECM microenvironment and an interface between the mammary epithelium and stroma (William and Daniel, 1983). The basement membrane is present in all mammary epithelial developmental stages: from epithelial rudiments to pubertal ductal networks and lactating alveoli.

The basement membrane is organized as a sheet, 50 – 100 nm thick, which is constructed on assembled networks of laminin and collagen IV proteins, and decorated with abundant glycoproteins and proteoglycans. Four types of laminin proteins are expressed in the mammary gland: laminin 111, 322, 511, and 521 (known as laminin 1, 5, 10, and 11, respectivey), which form $\alpha\beta\gamma$ trimers, and serve as core proteins for basement membrane assembly (Muschler

and Streuli, 2010). In particular, laminin 111 is produced by myoepithelial cells and stabilizes epithelial cell polarity (Gudjonsson et al., 2002).

Basement membrane is not merely a physical barrier, it is also required for mammary branching morphogenesis by modulating multiple cellular processes. Since basement membrane contains many protein constituents with different types of ligands, the epithelial cells use a variety of integrin $\alpha\beta$ dimers, which link basement membrane ECMs to both actin and intermediate filament cytoskeletons, and integrate with signaling pathways involved in cell migration, proliferation, polarity, and functions (Muschler and Streuli, 2010). A 3D culture model using basement membrane ECM (Matrigel) as a substrate, with the addition of nanomolar growth factor, recapitulates important features of epithelial branching morphogenesis (Ewald et al., 2008). In this *ex vivo* model of branching morphogenesis, mammary epithelial cells do not exhibit subcellular protrusions, rather they maintain a smooth basal surface and stimulate TEB-like structure formation via cell proliferation and rearrangement (Ewald et al., 2008). To accommodate epithelial growth *in vivo*, the thin sheet of basement membrane must constantly undergo remodeling, involving cleavage, disassembly, and reassembly (William and Daniel, 1983; Page-McCaw et al., 2007).

Stromal ECMs and fibrillar collagen remodeling

The structure of stromal ECMs is heterogeneous, tissue specific, and dependent on developmental stage (Schedin and Keely, 2010, Lu et al., 2012).

Mammary stroma contains a diversity of ECM proteins, with 90% of the content being fibrillar collagen type I. Produced and secreted to the extracellular space as protocollagen, collagen fibers are then assembled via a highly hierarchical process with multiple chemical modifications. Mature collagen fibers can be crosslinked by extracellular enzymes to form a supramolecular structure with high stability and enhanced mechanical properties (Mouw et al., 2014). In addition, other ECM components such as elastic fibers and fibronectin further crosslink collagen fibers, and significantly change key physical properties of the collagen meshwork, such as fiber thickness, orientation, density, stiffness and pore size. These collagen structures influence cell function by mechanosensation/transduction with downstream signaling pathways (Butcher et al., 2009).

The mammary gland is a collagen-rich organ. Collagen I exists only in the stromal space, and is separated from the epithelial tissue via a basement membrane. Normal mammary epithelial cells require endogenous or exogenous addition of laminin proteins to achieve a bilayered structure in a 3D collagen matrix (Gudjonsson et al., 2002).

It is increasingly evident that collagen I plays an important role in epithelial organization and development. The presence of collagen I around mammary ducts may have different effects. First, most stromal collagen I is accumulated around epithelial ducts. In particular, the accumulation occurs along nascent ducts that are repolarized from TEBs (Silberstein and Daniel, 1982; Provenzano

et al., 2006). The bundles of collagen fibers wrapping around epithelial ducts provide physical support, and molecular signals to re-establish bilayered structure from the stratified TEBs. Second, orientation of collagen fibers in front of TEBs act as guidance cues for ductal elongation. Before puberty, collagen fiber networks are pre-disposed in the fat pad, and could provide a pre-determined route for ductal elongation (Brownfield et al., 2014). During branching morphogenesis, TEBs are surrounded with a array of collagen fibers, which directly guide epithelial cell migration to the end of the fat pad (Ingman et al, 2006, Brownfield et al., 2014). These lines of evidence not only demonstrate the contribution of collagen I to epithelial architecture and migration, but also raise questions about the molecular basis of the interaction between epithelial cells and collagen fibers.

Abnormal ECM remodeling in breast tumors

Given the great importance of the ECM during epithelial development and for tissue integrity maintenance, when ECM remodeling is abnormal, epithelial function is affected and cancer can develop. Tumor progression and metastasis can be promoted by the global accumulation of stromal ECMs, including fibrillar collagen I, which increases matrix stiffness thereby activating mechano-sensing and transducing pathways (Egeblad et al., 2010). Basement membrane provides essential signals for cell polarity and suppresses tumor invasion; thus the existence of basement membrane is often used as a histological signature,

distinguishing ductal carcinoma *in situ* (DCIS) (in which basement membrane is present) from invasive cancers (in which basement membrane is absent) (Polyak, 2010).

Local breach in basement membrane

Invasion of tumor through the basement membrane, is an important step in the transition from benign to invasive breast cancer. The breach in the basement membrane, that allows the invasion, could result from defects in matrix synthesis and degradation, and alterations in cell-matrix adhesion (Hood and Cheresh, 2002; Mercurio et al., 2001). Breaching of the basement membrane is well-known, and has been extensively studied in worm, mouse, fly, and chick embryonic development (Kelley et al., 2014).

The mechanisms of basement membrane breaching in breast cancer, however, remain unclear. Increased proteolysis due to MMP induction has been a widely accepted model (Rowe and Weiss, 2008). In mammary epithelial tissue, proteolysis alone might not be sufficient for breaking basement membrane. Focal breach of the basement membrane is often associated with dysfunction of myoepithelial cells, which are the key producer of basement membrane components. In mammary tumors, myoepithelial cells, or acquired basal cells, fail to synthesize and secrete laminin 111, the critical protein for basement membrane assembly (Gudjonsson et al., 2002). In addition to the basement membrane, the myoepithelial cells themselves are considered as a suppressor,

acting to prevent tumor invasion (Clarke et al., 2005).

Even though crossing of tumor cells through the basement membrane is one of the hallmarks of invasive cancer, it remains unclear how the ECM microenvironments in the basement membrane and stroma directly dictate tumor cell behavior, and how normal epithelial cells respond to acute breaks due to benign lesions.

Collagen-rich ECM remodeling in cancer progression and metastasis

For decades, mammography has been used for early screening for breast cancer. Increasing mammographic density is associated with a 4-6 fold higher risk of developing breast cancer, and is correlated with a higher fraction of stroma including collagen fibers (Boyd et al., 2001; Guo et al., 2001). In addition, breast tumor tissue is palpably hard, which is partially due to massive accumulation of stromal collagen (Butcher et al., 2011).

Indeed, both the local and global architectures of the collagen matrix in breast tumors are adversely changed. In normal breast tissue, collagen I fibers are typically curly and anisotropic (Provenzano et al., 2006). However, during tumorigenesis, the fibers become linearized and progressively thicken (Provenzano et al., 2006; Levental et al., 2009; Condeelis and Segall, 2003). These abnormal structures of collagen fibers are prominent at the invasive sites (Provenzano et al., 2006), thereby are predicted to promote tumor invasion by providing a “fiber track” for cell migration.

At the larger scale, the stroma which is highly enriched with collagen fibers is mechanically stiffer than normal stroma, and this stiffness deregulates epithelial structure, activates proliferative and oncogenic programs (Paszek et al. 2005; Provenzano et al. 2009), and consequently accelerates tumor progression (Provenzano et al. 2009; Levental et al., 2009).

Collectively, these lines of evidence: (i) support the proposal that abnormal mechanical changes in surrounding collagen ECMs, directly, and indirectly, promote tumor formation, and (ii) indicate that breaching of the basement membrane allows tumor invasion into a collagen-rich stroma, thus facilitating metastasis. However, direct evidence of changing cell behaviors due to ECM alteration is lacking, and the underlying mechanisms by which tumor cells organize and migrate along linearized collagen fibers, are incompletely understood.

My graduate work has focused on understanding how ECM micro-environmental composition and structures influence mammary epithelial cells. We adapted the *ex vivo* 3D culture model, which allows us to separately test the effect of different types of ECMs on normal and tumor cells during branching morphogenesis and cancer invasion, respectively. Using powerful imaging technique, I can visualize, track, and compare behavioral changes in reponse to acute or permanent ECM alteration. I can also study the dynamic interaction between epithelial cells and surrounding ECMs. Furthermore, to gain the molecular understanding of cell-matrix interaction, I used Cre-lox based gene

deletion method to genetically perturb non-muscle myosin II isoforms and study the effects on epithelial organization.

References

1. Andrew DJ, Ewald AJ. (2010) Morphogenesis of epithelial tubes: Insights into tube formation, elongation, and elaboration. Dev Biol. 341(1):34-55.
2. Balinsky BI. (1950) On the prenatal growth of the mammary gland rudiment in the mouse. J Anat. 84(3):227-35.
3. Bonnans C, Chou J, Werb Z. (2014) Remodelling the extracellular matrix in development and disease. Nat Rev Mol Cell Biol. 15(12):786-801.
4. Boyd NF, Martin LJ, Rommens JM, Paterson AD, Minkin S, Yaffe MJ, Stone J, Hopper JL. (2009) Mammographic density: A heritable risk factor for breast cancer. Methods Mol Biol 472: 343–360.
5. Brownfield DG, Venugopalan G, Lo A, Mori H, Tanner K, Fletcher DA, Bissell MJ. (2014) Patterned collagen fibers orient branching mammary epithelium through distinct signaling modules. Curr Biol. 23(8):703-9.
6. Butcher DT, Alliston T, Weaver VM. (2009) A tense situation: forcing tumour progression. Nat Rev Cancer. 9(2):108-22.
7. Clarke C, Sandle J, Lakhani SR. (2005) Myoepithelial cells: pathology, cell separation and markers of myoepithelial differentiation. J Mammary Gland Biol Neoplasia. 10(3):273-80.
8. Condeelis J, Segall JE. (2003) Intravital imaging of cell movement in tumours. Nat Rev Cancer. 3(12):921-30.
9. Daniel CW, Strickland P, Friedmann Y. (1995) Expression and functional role of E- and P-cadherins in mouse mammary ductal morphogenesis and growth. Dev Biol. 169(2):511-9.
10. Deugnier MA, Moiseyeva EP, Thiery JP, Glukhova M. (1995) Myoepithelial cell differentiation in the developing mammary gland: progressive acquisition of smooth muscle phenotype. Dev Dyn. 204(2):107-17.
11. Egeblad M, Rasch MG, Weaver VM. (2010) Dynamic interplay between the collagen scaffold and tumor evolution. Curr Opin Cell Biol. 22(5):697-706.
12. Ewald AJ, Brenot A, Duong M, Chan BS, Werb Z (2008) Collective epithelial migration and cell rearrangements drive mammary branching morphogenesis. Dev Cell. 14(4):570-81.
13. Ewald AJ, Huebner RJ, Palsdottir H, Lee JK, Perez MJ, Jorgens DM, Tauscher AN, Cheung KJ, Werb Z, Auer M (2012) Mammary collective cell migration involves transient loss of epithelial features and individual cell migration within the epithelium. J Cell Sci. 125(Pt 11):2638-54.
14. Friedl P, Gilmour D. (2009) Collective cell migration in morphogenesis, regeneration and cancer. Nat Rev Mol Cell Biol. 10(7):445-57.
15. Gudjonsson T1, Rønnov-Jessen L, Villadsen R, Rank F, Bissell MJ, Petersen OW. (2002) Normal and tumor-derived myoepithelial cells differ in their ability to interact with luminal breast epithelial cells for polarity and basement membrane deposition. J Cell Sci. 115(Pt 1):39-50.
16. Guo YP,Martin LJ, HannaW, BanerjeeD, Miller N, Fishell E, Khokha R,

Boyd NF. (2001) Growth factors and stromal matrix proteins associated with mammographic densities. Cancer Epidemiol Biomarkers Prev 10: 243–248.
17. Hinck L, Silberstein GB. (2005) Key stages in mammary gland development: the mammary end bud as a motile organ. Breast Cancer Res. 7(6):245-51.
18. Hogg NA, Harrison CJ, Tickle C. (1983) Lumen formation in the developing mouse mammary gland. J Embryol Exp Morphol. 73:39-57.
19. Hood JD, Cheresh DA. (2002) Role of integrins in cell invasion and migration. Nat Rev Cancer. 2(2):91-100.
20. Huebner RJ, Lechler T, Ewald AJ. (2014) Developmental stratification of the mammary epithelium occurs through symmetry-breaking vertical divisions of apically positioned luminal cells. Development. 141(5):1085-94.
21. Hynes RO, Naba A. (2012) Overview of the matrisome--an inventory of extracellular matrix constituents and functions. Cold Spring Harb Perspect Biol. 1;4(1).
22. Ingman WV, Wyckoff J, Gouon-Evans V, Condeelis J, Pollard JW. (2006) Macrophages promote collagen fibrillogenesis around terminal end buds of the developing mammary gland. Dev Dyn. 235(12):3222-9.
23. Kelley LC, Lohmer LL, Hagedorn EJ, Sherwood DR. (2014) Traversing the basement membrane in vivo: a diversity of strategies. J Cell Biol. 204(3):291-302.
24. Levental KR, Yu H, Kass L, Lakins JN, Egeblad M, Erler JT, Fong SF, Csiszar K, Giaccia A, Weninger W, Yamauchi M, Gasser DL, Weaver VM. (2009) Matrix crosslinking forces tumor progression by enhancing integrin signaling. Cell. 139(5):891-906.
25. Lu P, Weaver VM, Werb Z. (2012) The extracellular matrix: a dynamic niche in cancer progression. J Cell Biol. 196(4):395-406.
26. Macias H, Hinck L. (2012) Mammary gland development. Wiley Interdiscip Rev Dev Biol. 1(4):533-57.
27. Mercurio AM, Bachelder RE, Chung J, O'Connor KL, Rabinovitz I, Shaw LM, Tani T. (2001) Integrin laminin receptors and breast carcinoma progression. J Mammary Gland Biol Neoplasia. 6(3):299-309.
28. Montell DJ, Yoon WH, Starz-Gaiano M. (2012) Group choreography: mechanisms orchestrating the collective movement of border cells. Nat Rev Mol Cell Biol. 13(10):631-45.
29. Mouw JK, Ou G, Weaver VM. (2014) Extracellular matrix assembly: a multiscale deconstruction. Nat Rev Mol Cell Biol. 15(12):771-85.
30. Muschler J, Streuli CH. (2010) Cell-matrix interactions in mammary gland development and breast cancer. Cold Spring Harb Perspect Biol. 2(10).
31. Page-McCaw A, Ewald AJ, Werb Z. (2007) Matrix metalloproteinases and the regulation of tissue remodelling. Nat Rev Mol Cell Biol. 8(3):221-33.
32. Paszek MJ, Zahir N, Johnson KR, Lakins JN, Rozenberg GI, Gefen A, Reinhart-King CA, Margulies SS, Dembo M, Boettiger D, Hammer DA,

Weaver VM (2005) Tensional homeostasis and the malignant phenotype. Cancer Cell. 8(3):241-54.
33. Polyak K. (2010) Molecular markers for the diagnosis and management of ductal carcinoma in situ. J Natl Cancer Inst Monogr. 2010;2010(41):210-3.
34. Provenzano PP, Eliceiri KW, Campbell JM, Inman DR, White JG, Keely PJ. (2006) Collagen reorganization at the tumor-stromal interface facilitates local invasion. BMC Med.4(1):38.
35. Provenzano PP, Inman DR, Eliceiri KW, Keely PJ. (2009) Matrix density-induced mechanoregulation of breast cell phenotype, signaling and gene expression through a FAK-ERK linkage. Oncogene. 28(49):4326-43.
36. Rowe RG, Weiss SJ. (2008) Breaching the basement membrane: who, when and how? Trends Cell Biol. 18(11):560-74.
37. Schedin P, Keely PJ. (2010) Mammary gland ECM remodeling, stiffness, and mechanosignaling in normal development and tumor progression. Cold Spring Harb Perspect Biol. 3(1).
38. Silberstein GB, Daniel CW. (1982) Glycosaminoglycans in the basal lamina and extracellular matrix of the developing mouse mammary duct. Dev Biol. 90(1):215-22.
39. Williams JM, Daniel CW. (1983) Mammary ductal elongation: differentiation of myoepithelium and basal lamina during branching morphogenesis. Dev Biol. 97(2):274-90.`

CHAPTER 2

Mammary ductal elongation and myoepithelial migration are regulated by the composition of the extracellular matrix

(Modified from Nguyen-Ngoc and Ewald, J Microsc. 2013)

Abstract

Mammary branching morphogenesis occurs over a period of weeks deep inside an adipocyte-rich stroma. The adipocytes contain light-scattering lipid droplets that limit the depth of penetration of visible light. Organotypic culture methods were developed to enable high-resolution optical monitoring of branching morphogenesis ex vivo. A challenge has been to identify the best culture conditions to model specific developmental events. We recently demonstrated that collagen I induces protrusive invasion in both normal and neoplastic mammary epithelium. In this study, we observed that the abundance of collagen I fibrils correlated strongly with invasive behaviour, even when the collagen I concentration was identical. We found that the extent of fibril assembly was experimentally manipulable by varying the incubation time at 4°C following pH neutralization. We next tested the capacity of collagen I fibrils to induce invasive behaviour when presented in combination with basement membrane proteins (Matrigel). We found that epithelial organoids in mixed gels of collagen I and basement membrane proteins exhibited more extensive branching morphogenesis but did not initiate protrusions into the matrix. Organoids in pure Matrigel produced many small epithelial buds that were bare of myoepithelial cells. Surprisingly, organoids in mixed gels of collagen I and Matrigel produced fewer epithelial buds, the buds elongated further, and the elongating buds remained covered by myoepithelial cells. Our mixed gels therefore provide a more physiologically accurate model of mammary branching morphogenesis. Our

results also suggest that changes in the composition of the extracellular matrix could induce migration of epithelial cells past myoepithelial coverage.

Introduction

The mammary epithelium forms as a placode in the embryo and elaborates into a small branched network of ducts during fetal development (Hogg et al., 1983). This ductal rudiment persists until the beginning of puberty, when increasing levels of steroid hormones induce a rapid phase of branching morphogenesis (Sternlicht et al., 2006). Mammary ducts are organized before and after puberty as a bilayered tube (Hogg et al., 1983), with an apically located luminal epithelial cell layer and a basally located myoepithelial cell layer (Deugnier et al., 2002). However, ductal elongation and bifurcation are accomplished by a specialized structure at the end of the duct known as the terminal end bud (TEB) (Williams & Daniel, 1983; Hinck & Silberstein, 2005). Epithelial organization within the TEB is distinct from that of a bilayered duct, with multiple luminal cell layers and a single, basally positioned myoepithelial cell layer. Normal mammary morphogenesis therefore involves large changes in proliferation, apico-basal polarity and tissue architecture (Mailleux et al., 2007; Ewald et al., 2008; Ewald et al., 2012).

The critical events of mouse mammary branching morphogenesis occur over a period of weeks during postnatal development, with the ducts embedded deep inside an adipocyte-rich stroma. These adipocytes, or fat cells, contain abundant lipid droplets that scatter, and therefore limit the depth of penetration of, visible wavelengths of light. It is possible to observe stromal cell dynamics around the TEB using advanced two-photon microscopy (Ingman et al., 2006),

but there are no published studies reporting how epithelial cell dynamics within the TEB in vivo accomplish ductal elongation.

The experimental and optical inaccessibility of mammary branching morphogenesis in vivo has led our group and others to develop a diverse array of three dimensional (3D) culture systems to model mammary epithelial morphogenesis (Simian et al., 2001; Debnath et al., 2003; Nelson et al., 2006; Fata et al., 2007; Ewald et al., 2008; Nelson et al., 2008; Provenzano et al., 2009; Ewald, 2010). These assays have distinct cellular inputs and technical foundations but share the goal of developing more accurate models of epithelial morphogenesis than are possible in conventional 2D cell culture. We specifically optimised our culture methods to enable continuous optical monitoring of branching morphogenesis (Fata et al., 2007; Ewald et al., 2008; Ewald, 2010; Ewald et al., 2012).

These diverse organotypic culture assays have in common the combination of epithelial cells and 3D gels of extracellular matrix (ECM) proteins. A major challenge is to identify the appropriate culture conditions to model specific developmental events, as the composition and organization of the ECM can induce profound changes in epithelial cell behaviour (Weaver & Roskelley, 1997; Hagios et al., 1998; Nelson & Bissell, 2005; Provenzano et al., 2008). We recently demonstrated that collagen I induces protrusive and disseminative behaviours in both normal and neoplastic mammary epithelium (Nguyen-Ngoc et al., 2012). In vivo analysis of the TEB at different stages of branching

morphogenesis revealed no epithelial protrusions or dissemination into the surrounding stromal ECM (Williams & Daniel, 1983; Mailleux et al., 2007; Ewald et al., 2008; Ewald et al., 2012). Therefore, 3D culture in pure collagen I gels can transiently induce epithelial cell behaviours that are not observed during normal development in vivo. Our published imaging analyses of the cell dynamics underlying mammary branching morphogenesis instead relied on culture of mammary epithelium in Matrigel, a commercial matrix composed chiefly of laminin I, collagen IV, and entactin (Kleinman & Martin, 2005). Careful comparison of the epithelium in 3D culture and in vivo revealed a close correspondence in epithelial organization, especially in the proliferation, polarity, and cell–cell interactions within the multilayered luminal compartment (Ewald et al., 2008; Ewald et al., 2012). However, elongating epithelial buds in Matrigel frequently migrated free of myoepithelial coverage, a rare event in vivo (Ewald et al., 2008).

In this study, we varied the composition of the ECM in organotypic cultures to answer two questions. First, we sought to identify features of collagen I gels that correlated with invasive behaviour. Second, we sought to test the capacity of collagen I to induce protrusions and dissemination in the presence of competing signals from basement membrane proteins.

Results

The supramolecular organization of collagen I correlated with the extent of epithelial invasion

Collagen I is a fibrillar collagen and has multiple hierarchical states of organization (Prockop & Kivirikko, 1995). Collagen I polymers can assemble into fibrils, and these fibrils can assemble into larger fibers. The organization and orientation of collagen I fibers correlate with the extent of breast cancer invasion and patient prognosis (Provenzano et al., 2006; Wolf et al., 2009; Conklin et al., 2011). Native type I collagen is commercially available as an acid-solubilised solution purified from rat tails. The solution needs to be adjusted to a neutral pH for gellation to occur. We previously reported that direct contact between mammary epithelial cells and pure collagen I gels induced protrusive and disseminative behaviours (Nguyen-Ngoc et al., 2012). However, we observed variation in the extent of invasion of epithelial cells into collagen I gels prepared according to different protocols. We hypothesized that the time interval between neutralization at 4°C and gellation at 37°C could influence fibril assembly and epithelial cell behaviour.

To test this hypothesis, we varied the time at 4°C between neutralization and gellation, which we termed as ‘preincubation’, in samples from the same batch of 3 mg mL−1 collagen I (Fig. 2-1A). We then used second-harmonic generation (SHG) microscopy to visualize the supramolecular organization of collagen I in the resulting gels. With a brief preincubation period of 5 min at 4°C,

we observed no detectable collagen fibrils by SHG (Fig. 2-1B). Small, sparse collagen fibrils became evident with a 30 min preincubation period (Fig. 2-1C), and the density of fibrils rapidly increased with a preincubation time of 1–2 h (Fig. 2-1D,E). The timing of fibril assembly in our study is similar to that observed in previous work analysing glioma invasion (Yang et al., 2010).

We next tested whether these large differences in the size and abundance of collagen I fibrils affected epithelial cell behaviours. We compared the response of epithelial organoids derived from the same mouse to gels prepared from the same batch of neutralized 3 mg mL−1 collagen I (Fig. 2-1A). We only varied the preincubation time of the collagen I at 4°C following pH neutralization. At the end of the preincubation interval, epithelial organoids were added to the collagen I solution and the mixture was allowed to gel at 37°C. We observed protrusive organoids in gels corresponding to all preincubation intervals tested. However, the frequency of subcellular protrusions into the ECM and the extent of epithelial growth correlated strongly with the preincubation time and the density of collagen fibrils (Fig. 2-1B'–E'). With a brief preincubation at 4°C, epithelial cells initiated fewer ECM-directed protrusions, and the extent of epithelial growth was reduced (Fig. 2-1B'). With longer preincubation times at 4°C (1–2 h), the number of ECM-directed protrusions (red arrows, Fig. 2-1) and the extent of epithelial growth increased (Figs. 1C'–E' and 2I).

Our data indicate that the supramolecular organization of collagen I regulates the protrusive and migratory response of epithelial cells, even at equal

protein concentrations. Our data are consistent with past experiments comparing collagen I fibril organization following gellation at different temperatures (Raub et al., 2007).

The extent of ECM-directed protrusions and epithelial migration were both independent of collagen I concentration

The protein concentration of collagen I can affect its supramolecular organization and the mechanical properties of the resulting gel (Provenzano et al., 2009). Changes in collagen I concentration can influence mammary epithelial cell behaviour considerably in some assays (Provenzano et al., 2008; Provenzano et al., 2009). As such, we used SHG to compare collagen I gels with the same preincubation time but gelled at different protein concentrations. We tested the effect of collagen I concentration via two strategies. First, we preincubated 3 mg mL−1 collagen I for 1 h, then diluted aliquots to 2 and 1 mg mL−1 and gelled each at 37°C (Fig. 2-2A). We observed a broadly similar organization of collagen I fibrils by SHG in each concentration (Fig. 2-2B–D), suggesting that much of the fibril assembly occurred during preincubation at 4°C. We next asked whether the protein concentration of collagen I during gellation influenced epithelial invasion. We cultured mammary organoids from the same mouse in collagen I gels preincubated at 3 mg mL−1 for 1 h and adjusted to 2 mg mL−1 or 1 mg mL−1 before combining with organoids. The morphology (Fig. 2-2B'–D') and frequency (Fig. 2-2J) of protrusive invasion were similar at all tested

concentrations.

We next tested whether the concentration of collagen I during preincubation had a significant impact on either the organization of collagen I as measured by SHG or on the epithelial response to the resulting gel. We neutralized the collagen I and adjusted the concentration to 1, 2, or 3 mg mL−1, preincubated all samples for 1 h, and then created both empty gels for SHG and organoid-containing gels. We observed a broadly similar supramolecular organization of collagen I by SHG at each concentration when preincubated for 1 h at 4°C (Fig. 2-2F–H), though there appeared to be an increased density of fibrils at 3 mg mL−1. However, the epithelial response to the collagen I was indistinguishable across the different concentrations tested (Fig. 2-2F'–H',K). We cannot exclude the possibility that the different concentrations would generate very different supramolecular organizations of collagen I with a different preincubation interval.

In summary, the duration of preincubation at 4°C had a stronger effect on epithelial behaviour than the protein concentration of the collagen I (Fig. 2-2I vs. Fig. 2-2J,K). With preincubation times longer than 1 h, the resulting gels were more opaque, limiting their usefulness for live imaging. We therefore chose a 1 h preincubation and a 3 mg mL−1 concentration for the remaining experiments and termed this preparation 'preassembled collagen I'.

Mixed gels of collagen I and Matrigel did not induce protrusive invasion

We next sought to determine whether collagen I would still induce protrusive invasion when presented in the context of basement membrane proteins, such as laminin I and collagen IV. These proteins are in high concentration in the commercial ECM Matrigel. We first tested whether the organization of the collagen I fibrils would be maintained after we mixed the preassembled collagen I solution with Matrigel (Fig. 2-3A). SHG imaging revealed that collagen I fibrils were maintained in the mixed gels and that we could vary their abundance by varying the fractions of Matrigel and preassembled collagen I (Fig. 2-3B–F). The fact that collagen I fibrils were still detectable even when gelled in the presence of Matrigel was consistent with their preassembly in the preincubation interval. In the remaining experiments, we describe mixed gels based on the ratio of Matrigel and preassembled collagen I, for example, 3 parts Matrigel to 7 parts collagen I is referred to as 3M7C.

We next used these mixed gels to compare the behaviour of mammary organoids isolated from the same mouse and embedded in gels in which the only difference was the relative proportion of Matrigel and preassembled collagen I (Fig. 2-3G). Organoids in pure gels of collagen I (3 mg mL−1) were highly protrusive (246/246 buds; Fig. 2-3L,L’,M). In contrast, we observed essentially no protrusions into the matrix during epithelial bud elongation in mixed gels containing Matrigel (Fig. 2-3H–K and M). Epithelial buds in Matrigel and in mixed gels typically exhibited a smooth, nonprotrusive surface during collective migration (Fig. 2-3H’–’), while epithelial buds in pure collagen I formed

protrusions into the matrix (red arrows, Fig. 2-3L').

The extent of epithelial elongation correlated with collagen I density in mixed gels

Surprisingly, we observed that the pattern of branching morphogenesis and the extent of epithelial elongation depended strongly on the fraction of collagen I in the gel (Fig. 2-3H–L). The average length of epithelial buds increased from 58 μm in Matrigel to 104 μm and 95 μm in 5M5C and 3M7C (Fig. 2-3O). Similarly, only 8% of organoids in Matrigel had at least one bud longer than 100 μm (Fig. 2-3 H',N), while we observed elongated buds in 63% of 7M3C organoids and 83% of 5M5C and 3M7C organoids (Fig. 2-3 I'-K',N). These data suggested that the percentage of preassembled collagen I in the mixed ECMs required to induce extensive epithelial elongation was between 50% and 70%.

Mammary organoids undergo branching morphogenesis in Matrigel through the initiation and elongation of new epithelial buds (Ewald et al., 2008). We next used time-lapse differential interference contrast (DIC) microscopy to compare branching morphogenesis in the mixed ECM gels (Fig. 2-4). We did not observe epithelial protrusions into the ECM during initiation or elongation in any of the mixed gels (three independent experiments, minimum of 30 movies per condition, Figs. 3 M, 4A–C'). We observed a strong correlation between the persistence of elongation and the fraction of collagen I in the gel. In particular, organoids embedded within 3M7C gels typically displayed very extensive

epithelial elongation (Fig. 2-4C,C').

The extent of myoepithelial coverage during epithelial elongation correlated with collagen I density

Mammary ducts in vivo are elongated by the TEB, a specialized region of mammary epithelium with multiple luminal cell layers enclosed by an essentially complete single layer of cells expressing myoepithelial markers (Williams & Daniel, 1983; Hinck & Silberstein, 2005). Organoids in Matrigel initiate many small epithelial buds, and these buds often elongate free of myoepithelial coverage (Fig. 2-5A and Ewald et al., 2008). Since the extent of epithelial elongation varied in the mixed gels, we next asked whether the extent of myoepithelial coverage varied as well. We monitored the relative position of cell types in elongated buds using antibodies raised against the luminal epithelial cell marker keratin-8 and the myoepithelial cell markers keratin-14 and smooth muscle actin (SMA). We found that elongated buds in Matrigel, 7M3C and 5M5C gels were typically free of myoepithelial cells (Fig. 2-5A–C), while elongating buds in 3M7C and pure collagen I remained covered by a complete layer of myoepithelial cells (Fig. 2-5D–E). The fraction of myoepithelium-covered epithelial buds consistently correlated with the fraction of collagen I using three tested myoepithelial cell markers (Fig. 2-5F–H).

We next used time-lapse confocal microscopy to distinguish whether myoepithelial coverage was maintained during epithelial elongation or restored

afterward. We utilized dual fluorescent transgenic reporter mice in which all cell membranes were labelled with a red fluorescent protein (mT/mG, Muzumdar et al., 2007) and myoepithelial cells were labelled with a green fluorescent protein under the control of the myoepithelial-specific keratin-14 promoter (Vaezi et al., 2002). We found that, similar to Matrigel, new epithelial buds in 7M3C and 5M5C gels initiated and elongated free of myoepithelial cells. However, myoepithelial cells occasionally caught up and restored full coverage by the end of imaging (Fig. 2-6A–C). Importantly, complete myoepithelial coverage was typically maintained during initiation and elongation in the majority of organoids in 3M7C gels (Fig. 2-6D). These data suggest that either the composition or supramolecular organization of the ECM regulates myoepithelial coverage of luminal epithelial cells.

Discussion

In this study, we used 3D organotypic culture to test the influence of collagen I on mammary epithelial cells in two contexts. We first explanted organoids from the same mouse into gels with equal concentrations of collagen I but varied polymerisation conditions. We found that the capacity of collagen I to induce protrusive invasion and dissemination (Nguyen-Ngoc et al., 2012) depended strongly on the preincubation interval prior to gellation, with longer intervals correlating with more extensive fibril assembly. We next demonstrated that the preassembled collagen I fibrils were maintained in mixtures with Matrigel. We then used these mixed gels to test whether collagen I could still induce protrusive invasion in the context of basement membrane proteins. Epithelial organoids in mixed collagen I/Matrigel gels did not initiate protrusions or disseminate cells into the matrix. The extent of epithelial elongation correlated positively with the concentration of collagen I fibrils in the mixed gel. Surprisingly, the extent of myoepithelial coverage also correlated positively with the concentration of collagen I fibrils in mixed gels. To our knowledge this is the first report that ECM composition can regulate myoepithelial coverage. The observation of cancer cells beyond myoepithelial coverage defines invasive breast cancer in clinical samples (Sternlicht & Barsky, 1997; Leonard & Swain, 2004; Hu et al., 2008; Polyak, 2010). Our data suggest that the composition of the ECM could directly regulate myoepithelial coverage of breast tumours and thereby impact the in situ to invasive transition.

Technical implications for organotypic models of epithelial morphogenesis

Many 3D culture models rely on collagen I to support cell survival and migration, and previous studies have identified differences in collagen I organization between pepsinized and acid-solubilised collagen I (Wolf et al., 2009). We identified the time interval between neutralization of acid-solubilised collagen I and gelling as a critical parameter that determines the abundance of fibrils in the final gel. Unintended variation in this time interval could result in highly varying ECM microenvironments, even when the same source and final concentration of collagen I are used. In the specific context of mammary branching morphogenesis, our mixed 3M7C gels supported a more organotypic form of branching, with more extensive epithelial elongation and more complete myoepithelial coverage, similar to that of TEBs in vivo (Williams & Daniel, 1983; Hinck & Silberstein, 2005). The organisation and dynamics of the luminal cells were broadly similar in mixed gels and pure Matrigel. Matrigel cultures are technically easier to prepare and will suffice for many analyses. However, in future studies focused either on the pattern of branching morphogenesis or on the interactions between luminal and myoepithelial cells, our mixed 3M7C gels provide a more organotypic model than Matrigel alone. Future studies will be required to determine the relative contributions of matrix rigidity, ECM protein composition, and Matrigel-associated growth factors to epithelial phenotypes in the mixed gels.

Implications for understanding mammary branching morphogenesis

The stroma surrounding mammary ducts in vivo contains abundant collagen I fibers located just outside the basement membrane (William & Daniel, 1983). In our previous study, we demonstrated that direct contact with pure collagen I gels induced protrusive invasion in normal mammary epithelial cells (Nguyen-Ngoc et al., 2012). However, mammary epithelial cells would not normally have direct access to the collagen I fibers as a complete basement membrane is maintained during TEB elongation in vivo (Williams & Daniel, 1983). Our data suggest that collagen I in the stroma could nonetheless influence the extent and pattern of branching morphogenesis.

Translational implications for breast cancer

Ductal carcinoma in situ (DCIS) describes neoplastic epithelial growths in the breast that remain confined within the basement membrane (Leonard & Swain, 2004). Clinically, invasive breast cancer is distinguished from DCIS by observation of cancer cells invading past myoepithelial coverage (Polyak & Hu, 2005; Polyak, 2010). In our previous study, we demonstrated that direct contact with pure collagen I was sufficient to induce protrusive invasion of both normal and neoplastic mammary epithelial cells (Nguyen-Ngoc et al., 2012). In this study, we reveal that changes in the relative abundance of collagen I, collagen IV, and laminin I are sufficient to induce migration of epithelial cells past

myoepithelial coverage. Taken together, our data suggest that both the protein composition and the supramolecular organization of the ECM can rapidly induce changes in epithelial behaviour similar to those observed during malignant progression. Importantly, these responses were observed in normal epithelial cells, suggesting that breast cancers may achieve important steps in malignant progression, such as invasion past myoepithelial coverage, through changes in cell–matrix interactions and/or changes in ECM composition.

Materials and methods

Mouse lines and breeding. All experiments were done in accordance with an approved protocol from the Johns Hopkins University Animal Care and Use Committee. Most experiments were done with Charles River FVB/N mice. For confocal time-lapse imaging, myoepithelial cells were visualized using keratin-14::actin-GFP transgenic mice (Vaezi et al., 2002), in which the keratin-14 promoter drives cell-type specific expression of an actin-GFP fusion protein. Cell membranes were visualized using the membrane TdTomato signal in the mT/mG transgenic line (Muzumdar et al., 2007). Keratin-14::actin-GFP were generously provided by Elaine Fuchs (Rockefeller University, NY, NY, USA), and mT/mG mice were obtained from Jackson Laboratory and back-crossed to FVB/N.

Isolation of primary mouse mammary organoids. We isolated organoids following previously described protocols (Ewald et al., 2008; Nguyen-Ngoc et al., 2012). In short, we collected mammary glands, minced the tissue with a sterile scalpel, and isolated the epithelial fraction following collagenase and trypsin treatment. Epithelial organoids were separated from single cells by differential centrifugation.

Collagen gel preparation. We used acid-solubilised rat tail collagen I (BD Bioscience #354326) as starting material. We combined 8 µL NaOH 1N, 25 µL 10X DMEM and 217 µL collagen I into 250 µL of solution. The volume was scaled up as necessary. Collagen solution was mixed until it had a stable, uniform colour. The pH was adjusted to 7.0–7.5. The concentration of collagen I

varies between commercial lots and was always adjusted to 3 mg mL−1 by 1x DMEM. 10–20 µL of the collagen I solution was used to make a thin underlay for each well. The rest of the collagen I solution was preincubated at 4°C, on wet ice, from 5 min to 2 h (Fig. 2-1A). At the end of the specified preincubation interval, the collagen I solution was mixed with epithelial organoids, and the mixture was plated on top of the underlay and incubated at 37°C for 1 h to allow gellation before addition of culture medium. To generate the mixed gels, preassembled collagen I solutions (3 mg mL−1, preincubated for 1 h at 4°C) were mixed with Matrigel (BD Biosciences #354230, Growth Factor Reduced) in 3:7, 5:5, and 7:3 (v/v) ratios. The mixtures were then combined with epithelial organoids plated, and incubated at 37°C for 1 h for gellation. Organoids were combined at an approximate ratio of two organoids per microliter of ECM solution.

Antibody staining. Organoids cultured in all matrix conditions were fixed with 4% (v/v) paraformaldehyde in PBS for 20 min, washed twice with PBS for 10 min, permeabilised with 0.5% (v/v) Triton X-100 in PBS for 20 min, and washed twice for 10 min. Samples were then blocked with 10% FBS (v/v) in PBS for 2 h, incubated with primary antibody in 10% FBS for 2 h at RT, washed twice, and blocked another 1 h in 10% FBS in PBS. They were next stained with secondary antibody for 1h and washed twice with 10% FBS in PBS before imaging. Primary antibodies were anti-keratin 8 (1:100) (TROMA-1, Developmental Studies Hybridoma Bank), anti-keratin 14 (1:500) (PRB-155P Covance) and anti smooth muscle actin-FITC conjugate (1:250) (F3777, Sigma).

Time-lapse imaging. Live DIC imaging was conducted using a Zeiss Cell Observer system with a Zeiss AxioObserver Z1 and an AxioCam MRM camera. Images were collected at 20 min intervals with exposure time of approximately 250 ms and analysed by Axiovision software. Live confocal imaging was performed using a custom spinning disc microscope (Ewald et al., 2008; Ewald, 2010). Temperature was maintained at 37°C and CO2 at 5%.

Image acquisition. Confocal images were acquired using a custom spinning disc microscope with 40× c-APO oil and 20× air objectives. Second harmonic generation (SHG) was conducted using a Zeiss LSM 710 laser-scanning microscope with a 25× water objective. SHG excitation was via a Coherent Inc. Chameleon laser tuned to 880 nm. For SHG imaging, laser power was set to 35, gain was in the range of 800–1000 depending on sample intensity, the digital offset was 1200, and the digital gain was 1.0. SHG images in the figures were collected with equivalent gain settings and are presented with equivalent digital contrast, brightness, and levels. Images were assembled using Imaris software.

Author contribution

K-V. N-N principally designed, performed and analyzed the experiments.

K-V. N-N also contributed to writing the manuscript.

References

1. Conklin MW, Eickhoff JC, Riching KM, Pehlke CA, Eliceiri KW, Provenzano PP, Friedl A, Keely PJ. (2011) Aligned collagen is a prognostic signature for survival in human breast carcinoma. Am J Pathol. 178(3):1221-32.
2. Debnath J, Muthuswamy SK, Brugge JS. (2003). Morphogenesis and oncogenesis of MCF-10A mammary epithelial acini grown in three-dimensional basement membrane cultures. Methods 30:256-268.
3. Deugnier MA, Moiseyeva EP, Thiery JP, Glukhova M. (1995) Myoepithelial cell differentiation in the developing mammary gland: progressive acquisition of smooth muscle phenotype. Dev Dyn. 204(2):107-17.
4. Ewald AJ (2013) Practical Considerations for Long-Term Time-Lapse Imaging of Epithelial Morphogenesis in Three-Dimensional Organotypic Cultures. Cold Spring Harb Protoc. 2013 Feb 1;2013(2):100-17. Ewald, A.J., Brenot, A., Duong, M., Chan, B.S., and Werb, Z. (2008). Collective epithelial migration and cell rearrangements drive mammary branching morphogenesis. Dev Cell 14, 570-581.
5. Ewald AJ, Huebner RJ, Palsdottir H, Lee JK, Perez MJ, Jorgens DM, Tauscher AN, Cheung KJ, Werb Z, Auer M (2012) Mammary collective cell migration involves transient loss of epithelial features and individual cell migration within the epithelium. J Cell Sci. 125(Pt 11):2638-54.
6. Fata JE, H Mori, AJ Ewald, H Zhang, E Yao, Z Werb and MJ Bissell. (2007). The MAPK(ERK-1,2) pathway integrates distinct and antagonistic signals from TGFalpha and FGF7 in morphogenesis of mouse mammary epithelium. Dev Biol 306:193-207.
7. Hagios C, Lochter A, & Bissell MJ (1998) Tissue architecture: the ultimate regulator of epithelial function? Philos Trans R Soc Lond B Biol Sci 353(1370):857-870.
8. Hinck L, GB Silberstein. (2005). Key stages in mammary gland development: the mammary end bud as a motile organ. Breast Cancer Res 7:245-51.
9. Hogg NA, Harrison CJ, Tickle C. (1983) Lumen formation in the developing mouse mammary gland. J Embryol Exp Morphol. 73:39-57.
10. Ingman WV, Wyckoff J, Gouon-Evans V, Condeelis J, Pollard JW. (2006) Macrophages promote collagen fibrillogenesis around terminal end buds of the developing mammary gland. Dev Dyn. 235(12):3222-9.
11. Leonard, GD, Swain SM. (2004). Ductal carcinoma in situ, complexities and challenges. J Natl Cancer Inst 96, 906-920.
12. Mailleux AA, Overholtzer M, Schmelzle T, Bouillet P, Strasser A, Brugge JS. (2007). BIM regulates apoptosis during mammary ductal morphogenesis, and its absence reveals alternative cell death mechanisms. Dev Cell. 12, 221-234.
13. Muzumdar MD, Tasic B, Miyamichi K, Li L, Luo L. (2007). A global double-

fluorescent Cre reporter mouse. Genesis 45, 593-605.
14. Nelson CM and MJ Bissell. (2005). Modeling dynamic reciprocity: engineering three-dimensional culture models of breast architecture, function, and neoplastic transformation. Semin Cancer Biol 15:342-52.
15. Nelson, C.M., Vanduijn, M.M., Inman, J.L., Fletcher, D.A., and Bissell, M.J. (2006). Tissue geometry determines sites of mammary branching morphogenesis in organotypic cultures. Science 314, 298-300.
16. Nelson CM, JL Inman, MJ Bissell. (2008) Three-dimensional lithographically defined organotypic tissue arrays for quantitative analysis of morphogenesis and neoplastic progression. Nat Protoc 3:674-8.
17. Nguyen-Ngoc KV, KJ Cheung, A Brenot, ER Shamir, RS Gray, WC Hines, P Yaswen, Z Werb, AJ Ewald. (2012). The ECM microenvironment regulates collective migration and local dissemination in normal and malignant mammary epithelium. Proc Natl Acad Sci U S A. 109(39):E2595-604.
18. Polyak K (2010) Molecular markers for the diagnosis and management of ductal carcinoma in situ. J Natl Cancer Inst Monogr 2010(41):210-213.
19. Polyak K, Hu M. (2005). Do myoepithelial cells hold the key for breast tumor progression? J Mammary Gland Biol Neoplasia 10, 231-247.
20. Prockop DJ, Kivirikko KI. (1995). Collagens: molecular biology, diseases, and potentials for therapy. Annu Rev Biochem 64, 403-434.
21. Provenzano PP, Eliceiri KW, Campbell JM, Inman DR, White JG, Keely PJ. (2006) Collagen reorganization at the tumor-stromal interface facilitates local invasion. BMC Med.4(1):38.
22. Provenzano PP, DR Inman, KW Eliceiri, JG Knittel, L Yan, CT Rueden, JG White and PJ Keely. (2008). Collagen density promotes mammary tumor initiation and progression. BMC Med 6:11.
23. Provenzano PP, Inman DR, Eliceiri KW, Keely PJ. (2009) Matrix density-induced mechanoregulation of breast cell phenotype, signaling and gene expression through a FAK-ERK linkage. Oncogene. 28(49):4326-43.
24. Raub CB, Suresh V, Krasieva T, Lyubovitsky J, Mih JD, Putnam AJ, Tromberg BJ, George SC. (2007) Noninvasive assessment of collagen gel microstructure and mechanics using multiphoton microscopy. Biophys J 92, 2212-2222.
25. Simian M, Y Hirai, M Navre, Z Werb, A Lochter and MJ Bissell. (2001). The interplay of matrix metalloproteinases, morphogens and growth factors is necessary for branching of mammary epithelial cells. Development 128:3117-31.
26. Sternlicht MD, SW Sunnarborg, H Kouros-Mehr, Y Yu, DC Lee and Z Werb. (2005). Mammary ductal morphogenesis requires paracrine activation of stromal EGFR via ADAM17-dependent shedding of epithelial amphiregulin. Development 132:3923-33.
27. Vaezi A, Bauer C, Vasioukhin V, Fuchs E (2002) Actin cable dynamics and Rho/Rock orchestrate a polarized cytoskeletal architecture in the early steps of assembling a stratified epithelium. Dev Cell 3(3):367-381.

28. Weaver, VM, Roskelley CD (1997). Extracellular matrix: the central regulator of cell and tissue homeostasis. Trends Cell Biol 7, 40-42.
29. Williams JM, Daniel CW. (1983) Mammary ductal elongation: differentiation of myoepithelium and basal lamina during branching morphogenesis. Dev Biol. 97(2):274-90.`
30. Wolf K, Alexander S, Schacht V, Coussens LM, von Andrian UH, van Rheenen J, Deryugina E, Friedl P. (2009) Collagen-based cell migration models in vitro and in vivo. Semin Cell Dev Biol. 20(8):931-41.

Figure 2-1

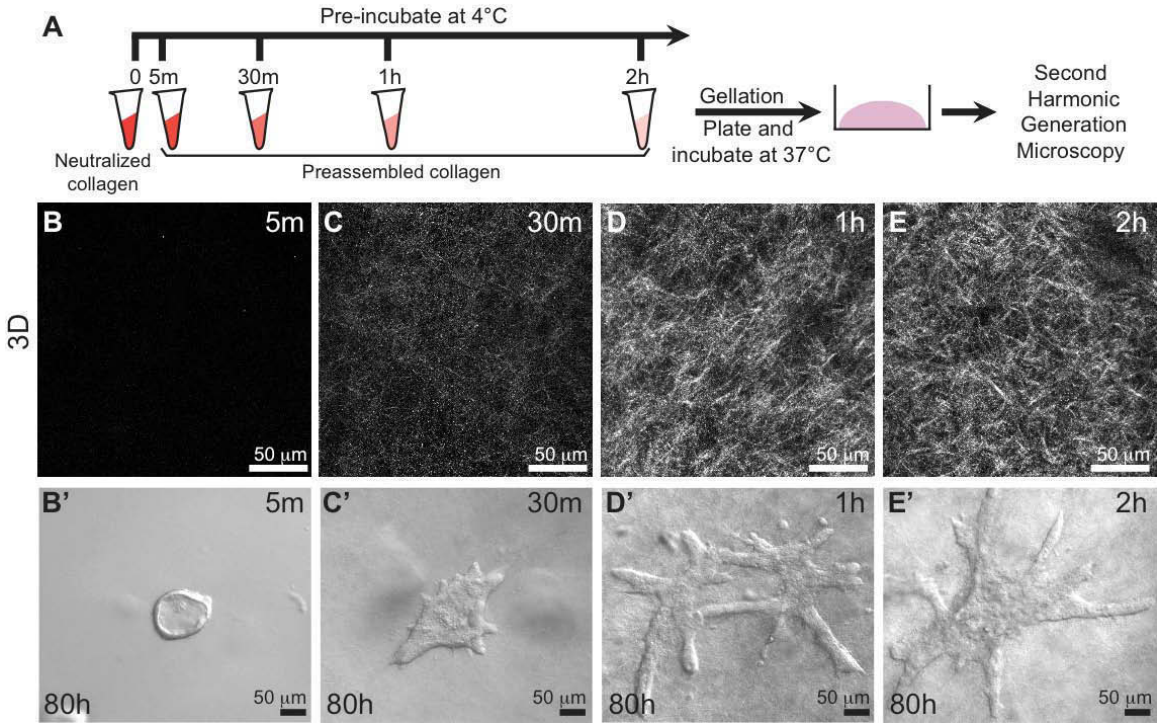

Organization of collagen I correlates with the extent of epithelial invasion. (A) Schematic description of preparation of collagen gels in vitro. (B-E) SGH images of collagen I organization following pre-incubation for (B) 5 min, (C) 30 min, (D) 1h, and (E) 2h. (B'-E') DIC images of representative epithelial organoids cultured in collagen I gels with varying pre-incubation times (B-E, respectively).

Figure 2-2

Fibril formation and invasive response are independent of collagen concentration. (A) Schematic description of preparation of collagen gels in which the concentration is adjusted after pre-incubation. (B-D) SGH images showing collagen I organization at (B) 1 mg/mL, (C) 2 mg/mL, and (D) 3 mg/mL. (B'-D') Representative DIC images of organoids cultured in gels of different collagen I concentration (B-D, respectively). (E) Schematic description of preparation of collagen gels in which the concentration is adjusted before pre-incubation. (F-H) SGH images showing collagen I organization at (F) 1 mg/mL, (G) 2 mg/mL, and (H) 3 mg/mL. (F'-H') Representative DIC images of organoids cultured in gels of different collagen I concentration (F-H, respectively). (I-K) Percent of organoids showing epithelial invasion into collagen gels with (I) different pre-incubation times (3 biological replicates), (J) collagen concentration adjusted after preassembly (3 biological replicates), and (K) collagen concentration adjusted before preassembly ((3 biological replicates).

Figure 2-2

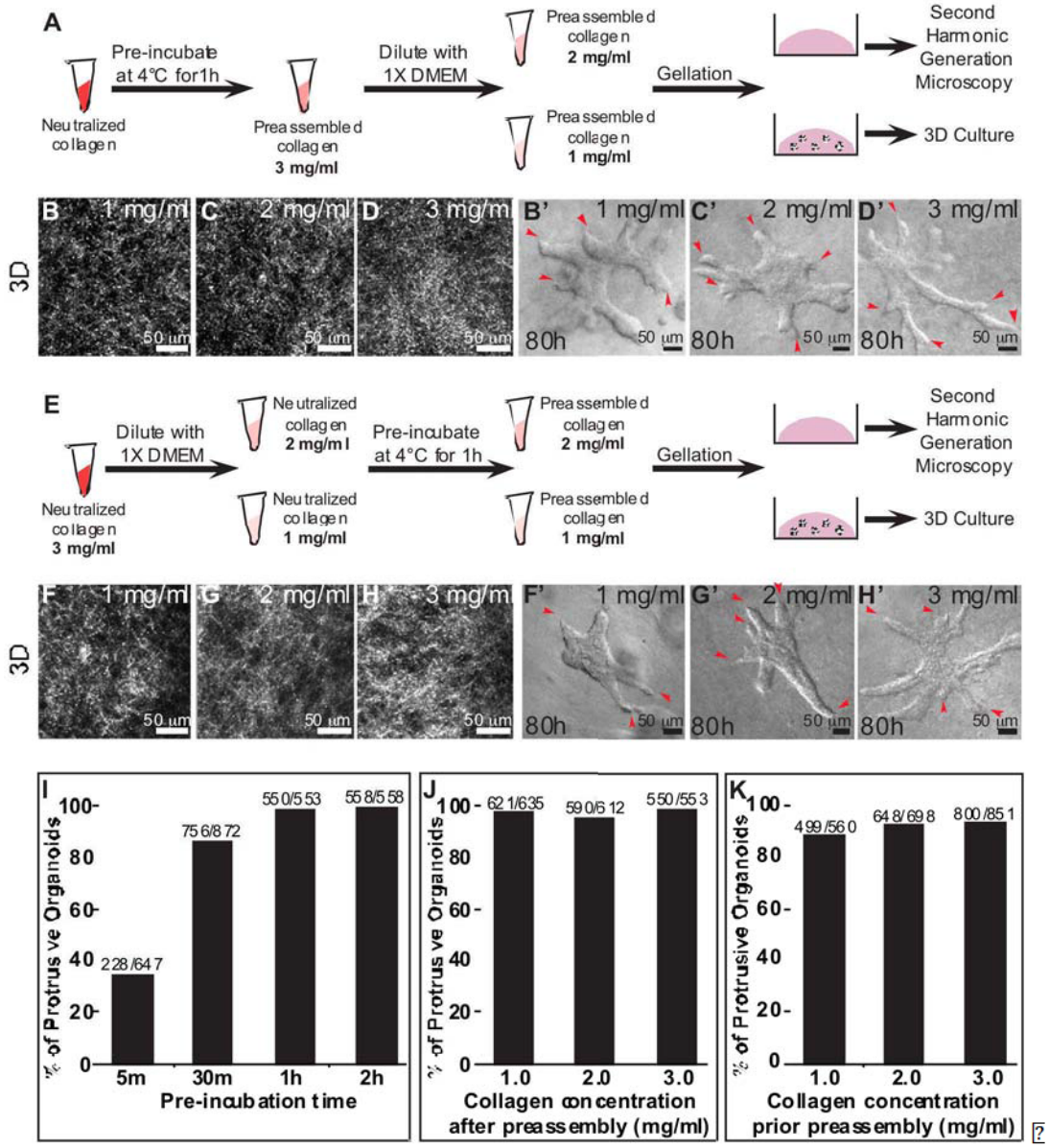
A
Pre-incubate at 4°C for1h
Neutralized collagen
Preassembled collagen 3 mg/ml
Dilute with 1X DMEM
Preassembled collagen 2 mg/ml
Preassembled collagen 1 mg/ml
Gellation
Second Harmonic Generation Microscopy
3D Culture
3D
B 1 mg/ml
C 2 mg/ml
D 3 mg/ml
B' 1 mg/ml
C' 2 mg/ml
D' 3 mg/ml
80h
50 µm
E
Dilute with 1X DMEM
Neutralized collagen 3 mg/ml
Neutralized collagen 2 mg/ml
Neutralized collagen 1 mg/ml
Pre-incubate at 4°C for 1h
Preassembled collagen 2 mg/ml
Preassembled collagen 1 mg/ml
Gellation
Second Harmonic Generation Microscopy
3D Culture
F 1 mg/ml
G 2 mg/ml
H 3 mg/ml
F' 1 mg/ml
G' 2 mg/ml
H' 3 mg/ml
I
% of Protrusive Organoids
228/647
756/872
550/553
558/558
5m
30m
1h
2h
Pre-incubation time
J
621/635
590/612
550/553
1.0
2.0
3.0
Collagen concentration after preassembly (mg/ml)
K
499/560
648/698
800/851
Collagen concentration prior preassembly (mg/ml)

Figure 2-3

The extent of mammary branching morphogenesis varies with ECM composition. (A) Schematic description of preparation of mixed ECM gels. (B-F) SGH images showing collagen fibrils in mixed ECM gels of different ratios of Matrigel (M) and collagen I (C): (B) Matrigel only, (C) 7M3C, (D) 5M5C, (E) 3M7C, and (F) collagen I only. (G) Schematic description of 3D organotypic culture in different mixed ECMs. (H- L) Representative DIC images of epithelial organoids after 100h of culture in mixed gels with different ratios of Matrigel and collagen I (B-F, respectively). Arrows indicate the buds that will be shown at higher magnification. (H'-L') Selected buds showing the non- protrusive leading front in (H') Matrigel only, (I') 7M3C, (J') 5M5C, and (K') 3M7C, and the protrusive leading front in (L') collagen I only. Red arrows indicate protrusive leading fronts. Dash-lines indicate how bud length is measured. (M) Percent of epithelial buds with at least one protrusion into the ECM observed during time-lapse imaging of elongation. (N) Percent of organoids with at least one epithelial bud greater than 100 μm cultured in different mixed ECMs (3 biological replicates). (O) Distribution of epithelial elongation of organoids cultured in different mixed ECMs (3 biological replicates, P-value determined by Student's t-test, two tailed, unequal variance).

Figure 2-3

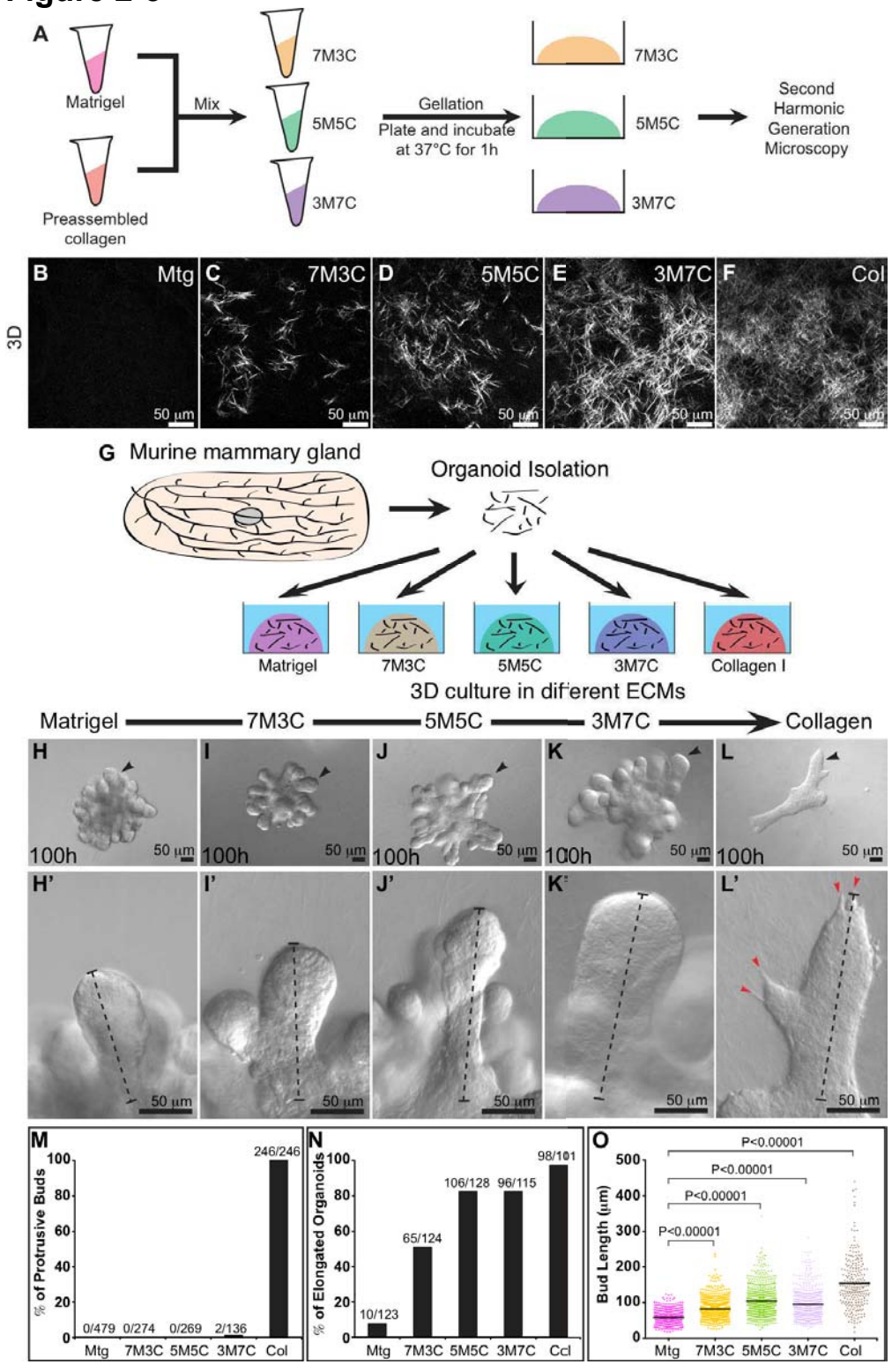
A
Matrigel
Preassembled collagen
Mix
7M3C
5M5C
3M7C
Gellation
Plate and incubate at 37°C for 1h
Second Harmonic Generation Microscopy
3D
B Mtg
C 7M3C
D 5M5C
E 3M7C
F Col
50 μm
G Murine mammary gland
Organoid Isolation
Matrigel
7M3C
5M5C
3M7C
Collagen I
3D culture in different ECMs
Matrigel 7M3C 5M5C 3M7C Collagen
H
I
J
K
L
100h
H'
I'
J'
K'
L'
M
% of Protrusive Buds
0/479 0/274 0/269 2/136 246/246
Mtg 7M3C 5M5C 3M7C Col
N
% of Elongated Organoids
10/123 65/124 106/128 96/115 98/101
Mtg 7M3C 5M5C 3M7C Ccl
O
Bud Length (μm)
P<0.00001
Mtg 7M3C 5M5C 3M7C Col

Figure 2-4

Epithelial elongation is greater in mixed ECMs. (A-C) Representative frames from DIC time-lapse movies of organoids cultured in (A) 7M3C, (B) 5M5C, and (C) 3M7C mixed ECM gels. (A'-C') Insets show bud elongation at higher magnification from organoids in (A-C), respectively.

Figure 2-4

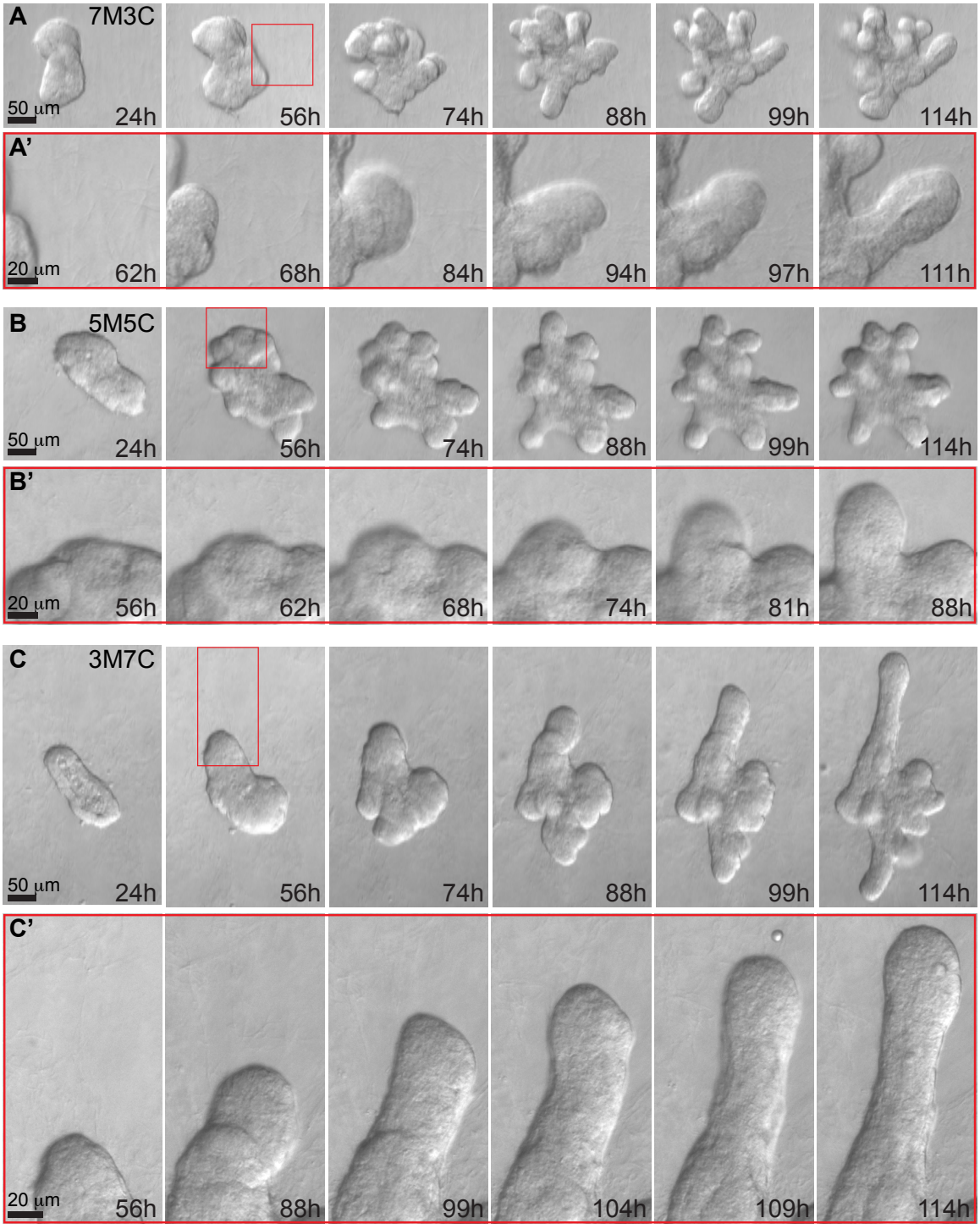
A
7M3C
50 μm
24h
56h
74h
88h
99h
114h
A'
20 μm
62h
68h
84h
94h
97h
111h
B
5M5C
50 μm
24h
56h
74h
88h
99h
114h
B'
20 μm
56h
62h
68h
74h
81h
88h
C
3M7C
50 μm
24h
56h
74h
88h
99h
114h
C'
20 μm
56h
88h
99h
104h
109h
114h

Figure 2-5

Myoepithelial coverage correlates with the fraction of collagen I in mixed ECMs. (A-E) Immuno-fluorescence staining of keratin 14 and keratin 8 in epithelial buds of organoids cultured in (A) Matrigel, (B) 7M3C, (C) 5M5C, (D) 3M7C, and (E) collagen I gels. (F-H) Percent of epithelial buds covered by (F) SMA+ cells, (G) K14+ cells, and (H) keratin-14::actin-GFP+ cells.

Figure 2-5

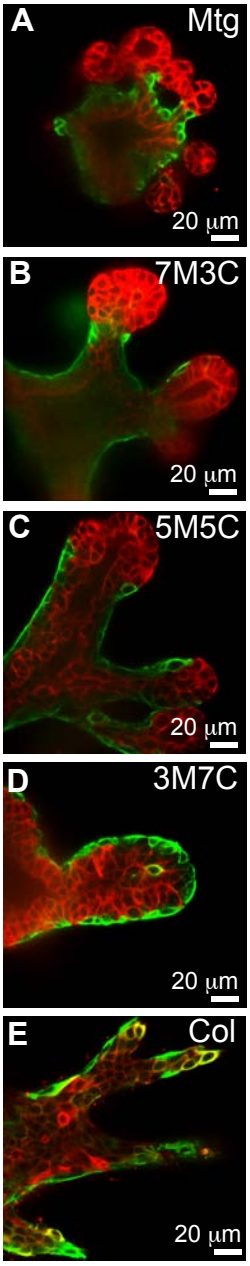
A
Mtg
20 μm
B
7M3C
20 μm
C
5M5C
20 μm
D
3M7C
20 μm
E
Col
20 μm
Keratin 8
Keratin 14

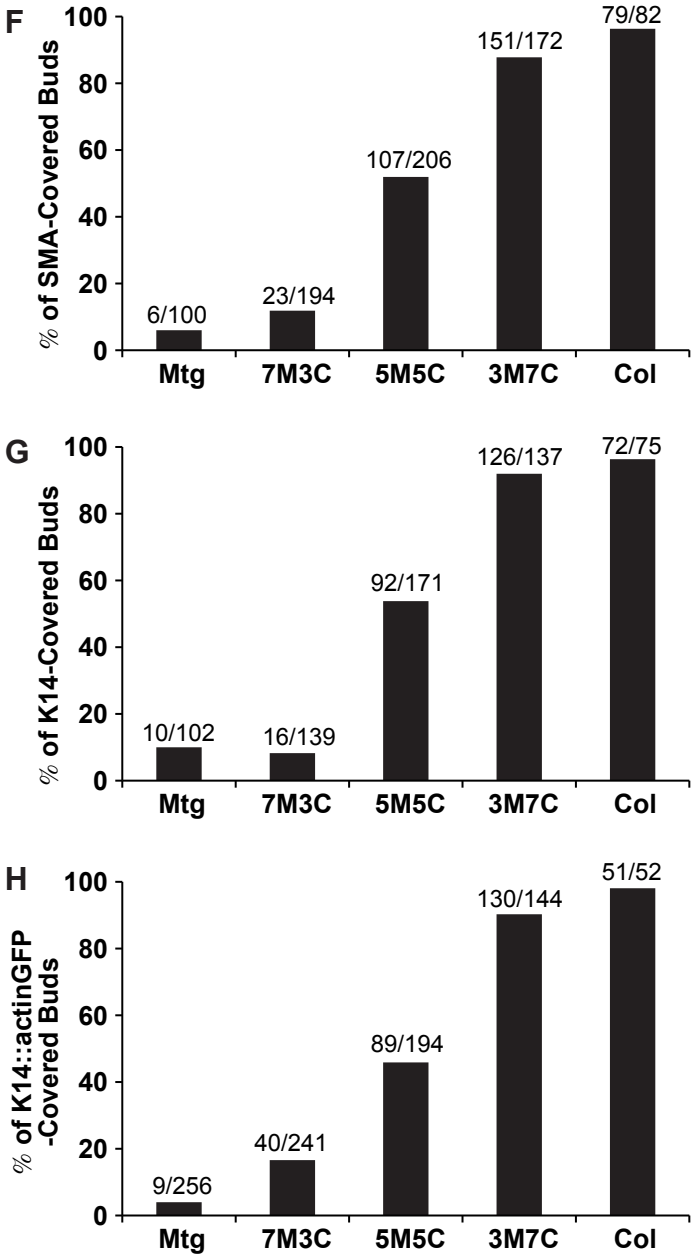
F
% of SMA-Covered Buds
100
80
60
40
20
0
6/100
23/194
107/206
151/172
79/82
Mtg
7M3C
5M5C
3M7C
Col
G
% of K14-Covered Buds
10/102
16/139
92/171
126/137
72/75
H
% of K14::actinGFP -Covered Buds
9/256
40/241
89/194
130/144
51/52

Figure 2-6

Myoepithelial coverage is maintained during elongation in mixed ECM gels with a high fraction of collagen I. (A-D) Frames of confocal time-lapse movies showing myoepithelial cells (green, keratin- 14::actin-GFP) and cell membranes (membrane tomato) elongating buds in (A) Matrigel, (B) 7M3C, (C) 5M5C and (D) 3M7C.

Figure 2-6

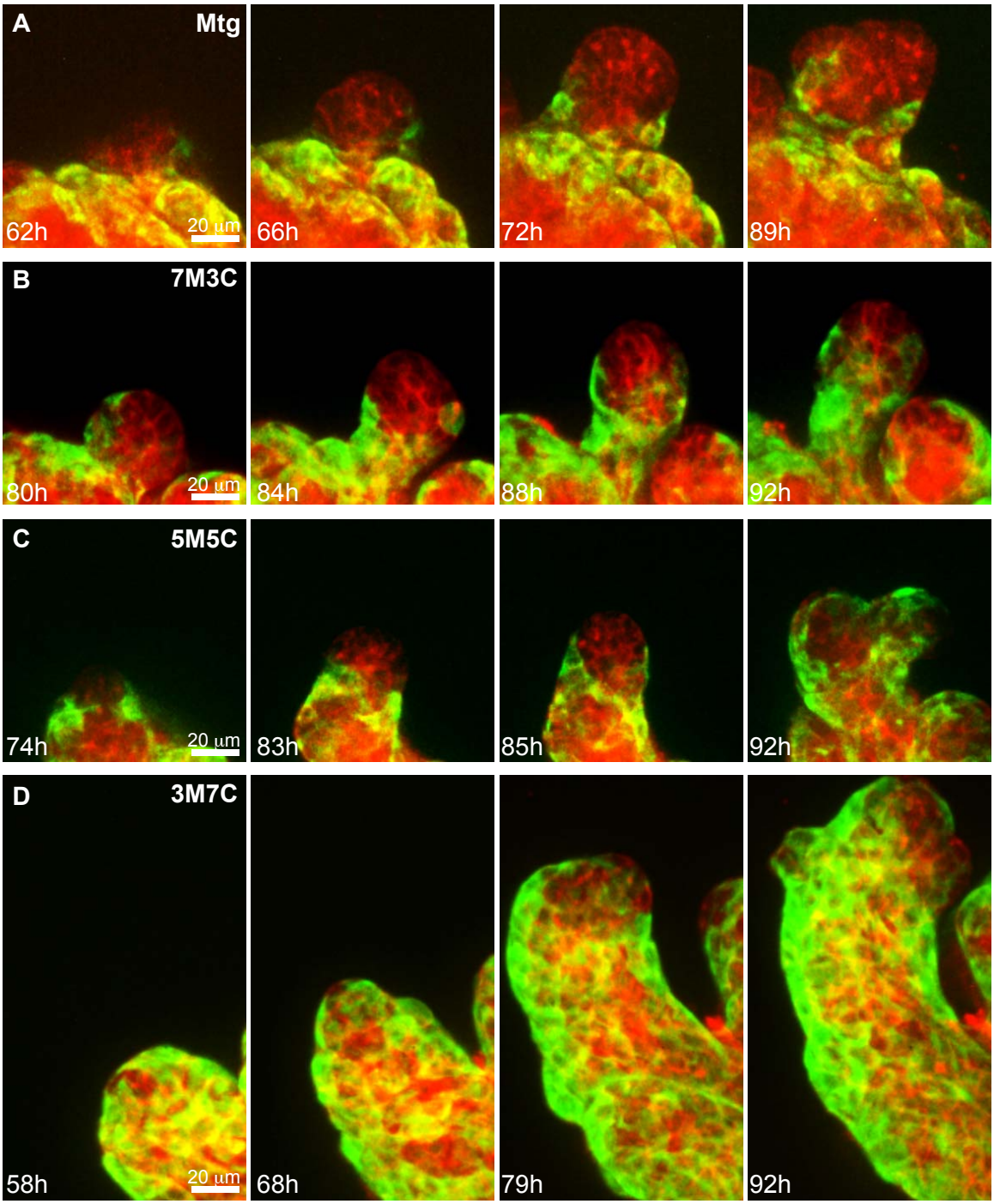

All cell membrane (mTmG) Myoepithelial cells (Keratin 14::actin-GFP)

CHAPTER 3

3D Culture Assays of Murine Mammary Branching Morphogenesis and Epithelial Invasion

(Modified from Nguyen-Ngoc et al., Methods Mol Biol. 2015)

Abstract

Epithelia are fundamental tissues that line cavities, glands, and outer body surfaces. We use three-dimensional (3D) embedded culture of primary murine mammary epithelial fragments, called “organoids”, to recapitulate in days in culture epithelial programs that occur over weeks deep within the body. Modulating the composition of the extracellular matrix (ECM) allows us to model cell- and tissue-level behaviors observed in normal development, such as branching morphogenesis, and in cancer, such as invasion and dissemination. Here, we describe a collection of protocols for 3D culture of mammary organoids in different ECMs and for immunofluorescence staining of 3D culture samples and mammary gland tissue sections. We illustrate expected phenotypic outcomes of each assay and provide troubleshooting tips for commonly encountered technical problems.

1. Introduction

Mammary gland development occurs postnatally from a simple epithelial rudiment (Sternlicht, 2006). During puberty, this rudiment undergoes stratification and initiates branching morphogenesis to form a network of epithelial tubes. The functional unit of elongation is a proliferative, multilayered front called the terminal end bud (TEB) (Williams and Daniel, 1983; Hinck and Silberstein, 2005). Behind the TEB, repolarization to a mature duct reestablishes a simple, bi-layered architecture, characterized by an inner layer of luminal epithelial cells and an outer layer of myoepithelial cells. These fundamental programs involve concurrent changes in cell proliferation, migration, polarity, and tissue architecture and are modulated by signaling cues from stromal cells and the extracellular matrix (ECM) (Sternlicht et al., 2006).

Because mammary epithelium develops within a fat pad with limited optical accessibility, various groups have used 3D culture to facilitate direct observation and manipulation of epithelial cell behaviors (Mroue and Bissell, 2012; Vidi et al., 2012; Griffith and Swartz, 2006; Gudjonsson et al., 2003; Nelson and Bissell, 2005; Nelson et al., 2008; Wozniak and Keely, 2005; Provenzano et al., 2010; Debnath et al., 2003). Cultures of primary mammary tissues were first developed half a century ago (Ichinose and Nandi, 1964; Ichinose and Nandi, 1966), but the past decade has seen significant improvements in and increasing utilization of 3D culture models (Ewald et al., 2008; Simian et al., 2001; Fata et al., 2007; Nelson et al., 2006). While many

conventional methods rely on immortalized cell lines or primary single cells, we use freshly isolated, murine mammary epithelial fragments, which we term “organoids”. The organoid assay arose from a series of papers published in the Bissell and Werb Labs (Ewald et al., 2008; Simian et al., 2001; Fata et al., 2007; Sternlicht et al., 2005). There are technical differences among the papers, but all involve mechanical disruption, enzymatic digestion, and differential centrifugation to separate mammary epithelial organoids from surrounding adipocytes and stromal cells. Purified organoids can be embedded in various ECMs to model distinct epithelial programs.

Our recent studies have revealed many of the cellular mechanisms driving epithelial morphogenesis and demonstrated that the ECM microenvironment regulates the migration and dissemination of mammary epithelial cells (Ewald et al., 2008; Ewald et al., 2012; Nguyen-Ngoc et al., 2012; Nguyen-Ngoc and Ewald, 2013). Normal development in vivo occurs within a basement membrane, and we use Matrigel, a basement membrane-rich ECM, as an experimentally convenient model for the normal ductal microenvironment. Culture of organoids in basal medium, without supplemental growth factors, induces formation of simple, bi-layered cysts, while culture with growth factor induces a stereotyped program of branching morphogenesis. In contrast, cancer progression involves breaks in the basement membrane, and the microenvironment around a tumor is enriched in collagen I (Provenzano et al., 2006; Provenzano et al., 2008; Conklin et al., 2011; Egeblad et al., 2010; Paszek et al., 2005; Levental et al., 2009). We

demonstrated that collagen I-rich microenvironments induce a conserved program of invasion and dissemination in normal and malignant mammary epithelium (Nguyen-Ngoc et al., 2012). Conversely, defined mixtures of Matrigel and collagen I can reproduce a more physiological organization of the elongating TEB (Nguyen-Ngoc and Ewald, 2013).

Building on our previously published methods (Ewald et al., 2008; Ewald et al., 2012; Nguyen-Ngoc et al., 2012; Ewald, 2013), this protocol seeks to provide a comprehensive guide to utilizing the mammary organoid assay (Fig. 3-1A). We introduce several variations on the assay in different ECMs and growth conditions that model different aspects of epithelial development and disease. We also provide optimized protocols for immunofluorescence staining of organoids in 3D embedded culture and of tissue sections of whole mammary glands.

2. Materials

2.1 Mice

We have successfully isolated and cultured organoids from mice ranging in age from E18.5 through 1.5 years of age. There are variations in response to growth factors with age and strain. All protocols below are optimized for FVB mice between 8-12 weeks of age. Once euthanized, mammary tissue is optimally isolated and cultured immediately, but successful organoid cultures have been established from mice sacrificed and then kept at 4°C overnight.

2.2 Reagents

1. Collagenase solution in DMEM/F12: 2 mg/mL collagenase, 2 mg/mL trypsin, 5% v/v fetal bovine serum (FBS), 5 µg/mL insulin, and 50 µg/mL gentamicin.

a. Collagenase from Clostridium histolyticum (Sigma C2139): Dissolve 1 g in 10 mL DMEM/F12, and make 200 µL aliquots. Store at -20°C.

b. Trypsin: Dissolve 1 g in 10 mL DMEM/F12, and make 200 µL aliquots. Store at -20°C.

2. Dulbecco's phosphate buffered saline (DPBS, with Ca2+, Mg2+).

3. Phosphate buffered saline (PBS, without Ca2+, Mg2+).

4. BSA solution: 2.5% bovine serum albumin (BSA) in DPBS.

5. 2000 U DNase (Sigma D4263): Dissolve in 1 mL of PBS, and make 40 µL aliquots. Store at -20°C.

6. Organoid medium in DMEM/F12: 1% penicillin/streptomycin and 1% insulin-transferrin-selenium-X (ITS) (GIBCO 51500).
7. FGF2, 25 µg (Sigma F0291): Dissolve in 250 µL of PBS, and make 20 µL aliquots. Store at -20°C.
8. Growth Factor Reduced Matrigel (BD Biosciences 354230).
9. Rat tail collagen I (BD Biosciences 354236).
10. DMEM 10X, low glucose.
11. 1.0 N NaOH.
12. 4% paraformaldehyde (PFA) in DPBS.
13. OCT compound.
14. 0.5% Triton X-100 in DPBS.
15. 10% FBS in DPBS.
16. Mounting Medium (Sigma F4680-25ML).
17. Primary antibodies.
18. Secondary antibodies conjugated to fluorescent probes

2.3 Instructions for Preparing Solutions

Prepare solutions as follows:

1. Collagenase solution (10 mL per mouse): Combine 9 mL DMEM/F12, 500 µL FBS, 5 µL insulin (10 mg/mL stock), 10 µL gentamicin (50 mg/mL stock), 200 µL collagenase (100 mg/mL stock), and 200 µL trypsin (100 mg/mL stock) in a 15 mL tube. Filter sterilize through a 0.2 µm filter into a

new tube. This solution should be made fresh for each experiment.

2. BSA solution: Combine 46 mL DPBS and 4.1 mL BSA (30% stock solution). Filter sterilize, and store at 4°C. This solution can be reused for several experiments if kept sterile but should be monitored for contamination.

3. Organoid medium: Remove 10 mL of DMEM/F12 from a 500 mL bottle of medium. Add 5 mL penicillin/streptomycin (10,000 units penicillin and 10 mg streptomycin/mL stock) and 5 mL ITS. For the branching morphogenesis assays (Sections 3.10.2 and 3.10.3) and the invasion assay (Section 3.10.4), supplement organoid medium with growth factor at the desired concentration. Diverse growth factors induce branching in the 1-10 nM range, including EGF ligands (EGF, TGF-α, amphiregulin, heregulin, neuregulin), FGF ligands (FGF2, FGF7), and HGF. We typically use 2.5 nM FGF2 for 8-12 week old FVB mice. It is necessary to optimize the growth factor concentration for the specific age and strain of mouse.

2.4 Tools and instruments

1. One Spencer Ligature scissors, delicate pattern (FTS 14028-10): For mouse exterior.

2. One standard forceps, narrow pattern (FTS 11003-12): For mouse exterior.

3. One Iris scissors, straight pattern (FTS 14060-09): For mouse interior

(sterile).

4. One Graefe forceps (FTS 11051-10): For mouse interior (sterile).
5. Sterile scalpel, #10 blade.
6. Polystyrene Petri dish.
7. Benchtop incubator orbital shaker (Thermo Scientific MaxQ 4450).
8. IncublockTM microtube incubator with two blocks set to 37°C (Denville Scientific Inc I0540).
9. Ice bucket.
10. Centrifuge tubes, 15 mL and 50 mL.
11. SensoPlate, black, 24W multiwell plate, glass bottom, sterile, w/lid (Greiner Bio-One 662892).
12. Chambered coverglass, 2-well and 4-well (Thermo Scientific).
13. 24-well glass plate cover (MatTek Corp P24GTOP-1.5-F).
14. Disposable base molds: 15x15x5 mm, 24x24x5 mm, and 30x24x5 mm (Fisher Scientific).
15. Superfrost® Plus Gold precleaned microscope slides (Fisher Scientific 15-188-48).
16. Cover glass, 50 x 22 mm.
17. Orbital Shaker (Reliable Scientific, Inc.).
18. StainTray with black lid (Simport M920-2).
19. Cryostat

3. Methods

3.1 Collecting mouse mammary glands

Mice have five pairs of mammary glands located beneath the skin and outside the peritoneum. This section describes how to collect glands #3, #4, and #5 for organoid isolation and how to limit contamination by other tissues.

1. Generally, use female mice between 8 to 12 weeks old.
2. Sterilize the dissecting area with 70% Ethanol.
3. Sterilize the dissecting tools by heat in a glass bead sterilizer.
4. Euthanize the mouse in a CO2-saturated chamber for 3-5 minutes followed by cervical dislocation.
5. Pin the mouse face-up to a protected Styrofoam board.
6. Wet the mouse thoroughly with 70% EtOH. Use the back of the standard forceps to smooth down the fur. Wipe away any feces with a 70% EtOH damp Kimwipe.
7. Use the standard forceps to grasp the skin above the groin.
8. Use the Spencer Ligature scissors to cut along the ventral midline from the groin to the chin (Fig. 3-1B). Be careful to cut only the skin and not the peritoneum underneath.
9. Make four incisions from the midline cut towards the four legs (Fig. 3-1B).
10. Use the standard forceps to pull back the skin one side at a time to expose the mammary glands (Fig. 3-1C). Use the back of the Graefe forceps to help separate the skin from the peritoneum (Fig. 3-1D).

11. Push back a thin yellow layer of muscle located on top of gland #3 to expose only the mammary gland (Fig. 3-1E-E').
12. Use the Graefe forceps to remove the inguinal lymph node located at the intersection of three blood vessels in gland #4 (Fig. 3-1F-F').
13. Use the Graefe forceps and Iris scissors to grasp and pull out mammary glands #3, #4, and #5 from both right and left sides. Pool glands in a sterile Petri dish (Fig. 3-2A) (see Note 1).

3.2 Isolating mammary epithelial organoids

Mammary epithelium is embedded inside a fat pad containing adipose tissue and collagen-rich stroma. This section describes how to purify fragments of mammary epithelium ("organoids") using enzymatic and mechanical digestion. All centrifugation speeds refer to a Sorvall Legend X1R benchtop swinging bucket centrifuge (1500 rpm, 1250 rcf). We have achieved similar results with 1500 rpm spins in similar benchtop centrifuges from other manufacturers.

1. In a sterile hood, mince mammary glands with a scalpel, ~25-50 times per mouse, until the tissue relaxes (Fig. 3-2A'). Use a separate scalpel for each mouse type.
2. Use the scalpel to transfer the minced glands to collagenase solution in a 15 mL or 50 mL tube (Fig. 3-2B). We use 10 mL of collagenase solution per mouse.
3. Shake the suspension at 110 rpm for 30-40 min (see Note 2) at 37°C until

the tissue breaks up into smaller pieces and is relatively dispersed (Fig. 3-2B'). We typically use a Thermo Scientific MaxQ 4450 for this purpose.

4. Spin the tube in a centrifuge at 1500 rpm for 10 min at room temperature. The tube will have 3 layers: a fatty layer on top, an aqueous layer in the middle, and a red pellet of epithelium on the bottom (Fig. 3-2C).
5. Precoat (Fig. 3-3A) (see Note 3) a 15 mL tube with BSA solution. Use one tube per mouse type. For all subsequent steps, precoat all pipette tips and tubes with BSA solution prior to contact with mammary tissue (Fig. 3-3).
6. To recover additional epithelial tissue, use a pipette to transfer the opaque fatty layer into the BSA-coated 15 mL tube. Add DMEM/F12 up to 10 mL. Pipette up and down vigorously to disperse the fatty layer (Fig. 3-2D). Spin the tube at 1500 rpm for 10 min at room temperature. Aspirate the supernatant, and save the pellet (Fig. 3-2E).
7. Aspirate (see Note 4) the aqueous layer in the tube with the original pellet.
8. Add 10 mL DMEM/F12 to the tube with the original pellet, and transfer to the 15 mL "fatty layer" tube (step 7). Pipette up and down vigorously to resuspend both pellets.
9. Spin the tube at 1500 rpm for 10 min at room temperature.
10. Aspirate the supernatant, and add up to 4 mL DMEM/F12 to the combined pellet (Fig. 3-2F). At this stage during isolation, the suspension contains small clusters of organoids and stromal cells attached to one another (Fig. 3-2F-F").

11. Add 40 µL DNase (2 U/µL) into the 4 mL organoid suspension, and gently invert by hand for 2-5 min at room temperature to break up the clusters and detach organoids from single cells (Fig. 3-2G'-G'').
12. Add 6 mL of DMEM/F12, and pipette up and down thoroughly.
13. Spin the tube at 1500 rpm for 10 min at room temperature. The pellet should now appear red and more compact (Fig. 3-2H-H').

Next perform differential centrifugation to wash out enzymes and separate single stromal cells from the epithelial organoids. The protocol suggests aspiration of the supernatant assuming that the stromal cells will be discarded. If recovery of mammary stromal populations is desired, then transfer the supernatant after each spin to a 50 mL tube.

14. Aspirate the supernatant to the 0.5 mL mark.
15. Resuspend the pellet in 10 mL DMEM/F12, and mix thoroughly.
16. Pulse to 1500 rpm, and stop the centrifuge 3-4 sec after it reaches speed.
17. Repeat step 15-17 three more times (see Note 5).
18. The final pellet should be off-white and consist mostly of organoids, without single cells (Fig. 3-2I-I",J). However, the organoid suspension may be contaminated with other tissue types, most commonly nerve bundles (Fig. 3-2K) and muscle (Fig. 3-2L).

3.3 Organoid density determination

This section describes how to determine the density of the organoid suspension and the overall yield.

1. Resuspend the pellet in 10 mL DMEM/F12 to form a homogeneous mixture (see Note 6).
2. Mix thoroughly (e.g. by rocking the tube by hand), and transfer 50 µL of the suspension to a 30 mm Petri dish. Count the number of organoids in this sample volume under a microscope (Fig. 3-2I',J).

$$\text{Total number of organoids} = \frac{\text{Number of organoids}}{\text{Sample Volume (e.g. 50 µL)}} \times \text{Remaining volume (e.g. 9950 µL)}$$

3. Calculate the total number of organoids collected according to the following formula. For example, if 20 organoids were counted in a 50 µL sample removed from a 10 mL total volume (9950 µL remaining), then the total number of organoids would be (20/50) x 9950 = 3980 organoids.
4. Calculate the organoid density (see Note 7), and re-adjust to 1000 organoids/mL to simplify allocation to ECM gels.
5. Calculate the number of organoids and the respective volume of suspension required for each experiment.
6. Aliquot the required volumes of organoid suspension into BSA-coated 1.5 mL microcentrifuge tubes (Fig. 3-3C), and spin the tubes at 1500 rpm for 5 min at room temperature.
7. Carefully remove the supernatant so as not to disturb the pellet (see Note 8).

8. Calculate the volume of ECM solution required to reach a final density of 2 organoids/μL (see Note 9).

3.4 Plating mammary organoids in Matrigel

Mammary epithelium develops in vivo within a basement membrane. 3D culture in Matrigel, a basement membrane-rich gel, recapitulates important features of epithelial development (Ewald et al., 2008; Fata et al., 2007; Ewald et al., 2012; Nguyen-Ngoc et al., 2012). This section describes how to embed organoids in 3D Matrigel.

1. Thaw Matrigel at 4°C for 3-4 h prior to plating. If the Matrigel is put at 4°C to thaw at the start of the prep, it will be ready to use by the end of the prep. During plating, always keep Matrigel on ice.
2. Use a plate with a glass bottom for time-lapse imaging.
3. Pre-incubate the plate at 37°C for 5 min.
4. Set up the tissue culture hood in preparation for plating (Fig. 3-4A).
5. Set the heating block to 37°C, and place the plate in direct contact with the block (Fig. 3-4B-C') (see Note 10).
6. Add the required volume of liquid Matrigel to a microcentrifuge tube with organoids. Since Matrigel is quite viscous, first pipette up and down slowly a few times to coat the tip and ensure an accurate volume.
7. Keep the Matrigel-containing tube on ice or in a cold block. Resuspend the organoid pellet gently to avoid introducing air bubbles. Do not try to take

up the entire volume into the pipette tip while mixing.

8. Plate the appropriate volume of Matrigel/organoid suspension into the wells according to the following table (Fig. 3-5A). Pipette up and down to resuspend the organoids before plating each sample, and pipette out only until the first stop.

Type of plate	Volume of gel / well (µL)	Volume of medium / well (µL)
24-well plate	50 – 150	750 – 1000
4-well chamber	50 – 75	750 – 1000
2-well chamber	150 – 300	1500 – 2000

9. Keep the plate on the heating block for several minutes to allow further gelation before returning it to the incubator.
10. Incubate the plate at 37°C, 5% CO_2 for 30-60 min.
11. Gently add pre-warmed organoid medium to the wells. For the cyst formation assay (Section 3.10.1), use basal medium without supplemental growth factors. For the branching morphogenesis assay (Section 3.10.2), supplement the medium with nanomolar concentrations of growth factor. A variety of growth factors may be used, including EGF ligands (EGF, TGF-α, amphiregulin, heregulin, neuregulin), FGF ligands (FGF2, FGF7), and HGF. We most commonly use 2.5 nM FGF2.
12. Add sterile water or PBS to the empty wells to prevent desiccation.
13. Label the wells. Return the plate to the incubator.
14. If the plate will be used for DIC imaging, use a glass plate cover for better image quality.

3.5 Preparing collagen I solution

Collagen I solubilized from rat tail is commonly used to study 3D migration of many cell types. However, the properties of collagen I gels vary depending on multiple factors during preparation, such as temperature, pH, and collagen concentration. We demonstrated that the extent of collagen fiber assembly correlated strongly with invasive behavior (Nguyen-Ngoc and Ewald, 2013). This section describes how to properly prepare a collagen I solution (Fig. 3-5B).

1. Rat tail collagen I is used to prepare a collagen solution according to the following formula. The steps below describe how to make a 250 µL solution. Scale up the volume as needed.

Total volume (µL)	250	500	1000	2000	5000
1.0 N NaOH (µL)	8	16	32	64	160
DMEM 10X (µL)	25	50	100	200	500
collagen I stock (µL)	217	434	868	1763	4340

2. Perform all steps on ice. To work with a large volume of collagen solution, use a 1000 µL extra long pipette tip to avoid the collagen solution getting stuck to the filter barrier during pipetting.
3. First, combine 25 µL DMEM 10X and 8 µL NaOH, and mix well. The solution will turn a dark pink color (Fig. 3-5C_1).
4. Add 217 µL collagen I (Fig. 3-5C_2) (see Note 11). Since collagen I is quite viscous, pipette up and down slowly a few times to coat the pipette tip.
5. Mix the solution well until the color remains stable. When the pH changes

from acidic → neutral → basic, the color changes from light green/yellow → light pink/orange → dark pink, respectively (Fig. 3-5C_{3-7}). The desired color is light pink or salmon, which corresponds to a pH of 7.0-7.5 (see Note 12). The pH can be tested using pH strips.

6. Use DMEM 1X to adjust the neutralized collagen I solution to the desired collagen concentration (see Note 13). For the invasion assay (Section 3.10.4), we use a collagen concentration of 3 mg/mL.

3.6 Plating mammary organoids in collagen I

Fibrillar collagen I, the most abundant structural protein in mammary glands, plays an important role in normal development as well as in breast cancer. Our previous studies have demonstrated that collagen I induces a conserved response of protrusive invasion in both normal and tumor organoids (Nguyen-Ngoc et al., 2012). This section describes how to properly prepare pre-assembled collagen I and embed mammary organoids in a 3D gel.

2. Use a plate with a glass bottom for time-lapse imaging.
3. Use 20-30 µL of neutralized collagen to make a thin underlay on the coverglass of the well at room temperature (**Fig. 3-5E**). The underlay helps the top collagen/organoid suspension attach better to the coverglass.
4. Incubate the plate with the underlays at 37°C until ready for plating.
5. Pre-incubate the neutralized collagen I solution (used for the top gel) on

ice for 60-120 min for pre-assembly (Nguyen-Ngoc and Ewald, 2012) (see Note 14). The collagen I solution will turn cloudy and fibrous (Fig. 3-5D$_{1-6}$) (see Note 15), a state we term pre-assembled collagen I.

6. Set up the tissue culture hood in preparation for plating (Fig. 3-4A).
7. Set the heating block to 37°C, and place the plate on top, in direct contact with the block (Fig. 3-4B-C') (see Note 10).
8. Always keep the collagen I solution (or a Matrigel/collagen I mix) on ice. Add the desired amount of pre-assembled collagen I to the organoid pellet in a microcentrifuge tube. Since collagen I is quite viscous, first pipette up and down slowly a few times to coat the tip and ensure an accurate volume.
9. Keep the tube on ice or in a cold block. Resuspend the organoid pellet gently to avoid introducing air bubbles. Do not try to take up the entire volume into the pipette tip while mixing.
10. Plate the appropriate volume of collagen/organoid suspension (see table in Section 3.4) on top of the underlay (Fig. 3-5E'). Pipette up and down to resuspend the organoids before plating each sample, and pipette out only until the first stop.
11. Keep the plate on the heating block for several minutes to allow further gelation before returning it to the incubator (see Note 16).
12. Incubate the plate at 37°C, 5% CO_2 for 45-60 min. After gelation, collagen I fibrils are visible under the microscope at 10X and 40X (Fig. 3-5F-F').

13. Gently add pre-warmed organoid medium supplemented with growth factor to the wells. A variety of growth factors may be used, including EGF ligands (EGF, TGF-α, amphiregulin, heregulin, neuregulin), FGF ligands (FGF2, FGF7), and HGF. We most commonly use 2.5 nM FGF2.
14. Add sterile water or PBS to the empty wells to prevent desiccation.
15. Label the wells. Return the plate to the incubator.
16. If the plate will be used for DIC imaging, use a glass plate cover for better image quality.

3.7 Plating mammary organoids in a mixture of Matrigel and collagen I

A mixture of Matrigel and collagen I represents a more physiological ECM microenvironment for mammary branching morphogenesis. The presence of collagen I significantly improves epithelial ductal elongation and myoepithelial coverage (Nguyen-Ngoc and Ewald, 2013). We do not observe epithelial protrusions into mixed Matrigel/collagen I gels (Nguyen-Ngoc and Ewald, 2013). This section describes how to properly prepare a mixture of Matrigel and pre-assembled collagen I and how to embed mammary organoids in this mixed matrix.

1. Prepare collagen I solution as described in Section 3.5.
2. Repeat steps 1-4 in Section 3.6 to make underlays and prepare pre-assembled collagen I.
3. Combine Matrigel and pre-assembled collagen I at the desired ratio.

Gently pipette up and down a few times to form a homogeneous solution (Fig. 3-5B').

4. Always keep the mixed matrix solution on ice. Add the desired amount to the organoid pellet in a microcentrifuge tube.
5. Plate the mixed matrix/organoid suspension as described in steps 5 – 15 in Section 3.6 (Fig. 3-5E').

3.8 Immunofluorescence staining of 3D culture samples

The thickness of 3D gels and the multicellular structure of mammary organoids often results in reduced antibody accessibility for immunofluorescence (IF) staining and poor visualization during imaging. This section describes two methods for performing IF staining in 3D culture samples. First, fix gels as follows:

1. Remove organoid medium from the wells.
2. Fix samples with 4% PFA for 10-15 min at room temperature (see Note 17) on an orbital shaker at 20 rpm.
3. Remove PFA, and wash samples 2-3X 10 min with DPBS.

From here, you can perform antibody staining directly in intact 3D gels or on cut sections on slides. The whole gel staining works well with high-quality antibodies and probes such as Phalloidin (stains for F-actin), smooth muscle actin (SMA), and keratin 14. For many other antibodies, staining sections on slides is preferable.

3.8.1 Staining whole gels

1. Permeabilize the gel with 0.5% Triton X-100 for 30-60 min.
2. After permeabilization, immediately block samples with 10% FBS (*see* Note 18) for 1-3 h at room temperature or overnight at 4°C.
3. Remove the blocking solution, add primary antibody in 10% FBS (*see* Note 18) at the desired ratio, and incubate for 2-3 h at room temperature or overnight at 4°C.
4. Remove the primary antibody solution, and wash samples 3X 10 min with 10% FBS or DPBS at room temperature.
5. Optional: Block the samples again with 10% FBS for 30-60 min at room temperature.
6. Add secondary antibody in 10% FBS (*see* Note 18) at the desired ratio, and incubate for 1-2 h at room temperature.
7. Wash 3X 10 min with DPBS at room temperature.
8. Store samples in DPBS at 4°C, but remove DPBS before imaging. If the gel has detached from the coverslip, leaving the DPBS in the well causes the gel to wiggle or float and go out of focus.

3.8.2 Staining sections on slides

1. Gently detach the gel from the culture plate and transfer to a small disposable base mold (15x15x5 mm) filled with a thin layer of OCT.

2. Freeze the mold at -80°C for 5-10 min.
3. Fill up the mold with OCT to cover the sample, and return to -80°C for long-term storage.
4. During sectioning, store molds on dry ice. Set up the cryostat with OT at -20°C and CT at -20°C.
5. Remove an OCT block from its mold, and cut sections at 20-100 μm thickness.
6. Transfer sections to slides using a fine camel hair brush or a pair of forceps.
7. Keep slides at -80°C for long-term storage.
8. For antibody staining, thaw slides at room temperature (*see* Note 19).
9. Wash slides 2-3X 10 min with DPBS to remove OCT.
10. Permeabilize with 0.5% Triton X-100 for 30-60 min (*see* Note 20).
11. Wash 2X 10 min with DPBS to remove Triton.
12. Block slides with 10% FBS for 2 h at room temperature or overnight at 4°C.
13. Remove the blocking solution, add primary antibody in 10% FBS, and incubate for 2-3 h at room temperature or overnight at 4°C (*see* Note 21).
14. Wash 3X 10 min with 10% FBS or DPBS.
15. Add secondary antibody in 10% FBS, and incubate for 2 h at room temperature or overnight at 4°C.
16. Wash 3X 10 min with DPBS.

17. Mount slides with mounting medium and 50 x 22 mm coverslips.
18. Let the slides dry at room temperature in a dry StainTray or in a dark drawer before imaging.

3.9 Immunofluorescence staining of mammary gland tissue sections

The opacity and thickness of the mammary fat pad limits the accessibility of mammary epithelium to whole gland staining and imaging. This section describes how to perform IF staining in mammary gland tissue sections.

1. Collect mouse mammary glands #3 and/or #4, as described in **Section 3.1**, taking care to keep the entire gland intact (*see* **Note 22**). Spread out the gland on the bottom of a 1- or 2-well chambered coverglass.
2. Fix the tissue with 4% PFA for 4 h at room temperature or overnight at 4°C.
3. Wash 3X 15 min with DPBS to remove PFA.
4. Transfer the gland to a medium (24x24x5 mm) or large (30x24x5 mm) disposable base mold filled with a thin layer of OCT.
5. Freeze the mold at -80°C for 5-10 min.
6. Fill up the mold with OCT to cover the gland, and return to -80°C for long-term storage.
7. During sectioning, store molds on dry ice. Set up the cryostat with OT at -40°C and CT at -30°C.
8. Remove an OCT block from its mold, and cut sections at 50-200 μm

thickness.

9. Transfer sections to slides using a fine camel hair brush or a pair of forceps.
10. Keep slides at -80°C for long-term storage.
11. Repeat steps 8-17 in **Section 3.8.2** for IF staining (*see* **Note 23**).

3.10 Assays

In vivo, mammary epithelium develops within a basement membrane surrounded by collagen-rich stromal tissue. The ability to manipulate the ECM microenvironment in 3D organotypic culture allows us to isolate the effects of individual matrix components on mammary epithelial cell behaviors. This section describes four assays that use different ECM compositions or growth conditions to model distinct epithelial programs (Fig. 3-6A).

3.10.1 Cyst formation assay

In 3D Matrigel in basal medium, mammary organoids reorganize from a multilayered fragment to establish a simple bi-layered epithelium with an internal lumen, termed a cyst (Fig. 3-6B, Fig. 3-7A). The extent of lumen formation varies with the initial size of the organoid and with the mouse strain (Fig. 3-7A_1-A_4). The resulting morphologies include a minimal or barely detectable lumen (Fig. 3-7A_1), a partial lumen (Fig. 3-7A_2), a complete lumen in a small cyst (Fig. 3-7A_3), and a complete lumen in a large cyst (Fig. 3-7A_4). Epithelial cells in the cyst always

maintain a smooth basal surface with the ECM (Fig. 3-7$A_{4'}$). We have observed that C57BL6 organoids form cysts with complete lumens (Fig. 3-6B) more efficiently than FVB organoids. Although the appearance of the lumen varies by light microscopy, immunofluorescence staining for SMA and F-actin can confirm establishment of a simple bi-layered structure of internal luminal epithelial cells and basal myoepithelial cells (Fig. 3-8A). We use this assay to model the formation of mammary epithelial ducts in vivo (Fig. 3-8D).

3.10.2 Branching morphogenesis assay in Matrigel

In 3D Matrigel, nanomolar concentrations of growth factor induce mammary organoids to undergo branching morphogenesis (Fig. 3-6C). The branching program includes sequential steps of lumen clearing, stratification, bud initiation, and bud elongation (Fig. 3-6C) (Ewald et al., 2008). We observe variation in morphology depending on the extent of progression through this program. Organoids that only complete stratification or bud initiation (Fig. 3-7B_1), or that form fewer than three buds (Fig. 3-7B_2-B_4), are not scored as “branched” (Fig. 3-7B). Only organoids with three or more elongated buds are scored as “branched” (Fig. 3-7C). However, the morphology of branched organoids varies based on the initial size of the organoid, the mouse strain, and the types of growth factors added. Here, we present four examples of branching in Matrigel (Fig. 3-7C_1-C_4). The first two show organoids with multiple multilayered, elongating buds without any regions of repolarization (Fig. 3-7C_1-C_2). In contrast,

the second two show organoids that have re-established simple epithelial architecture in the central lumen (Fig. 3-7C_3) or within buds (Fig. 3-7C_4). During bud elongation in Matrigel, the leading front of the bud is always non-protrusive (Fig. 3-7$B_{4'}$, 7$C_{4'}$). Notably, these buds lack or are incompletely covered by myoepithelial cells (SMA^+, Fig. 3-8B). These gaps in myoepithelial coverage can be observed in vivo, particularly in side branches of the mammary ductal tree (Fig. 3-8E).

3.10.3 Branching morphogenesis assay in a mix of Matrigel and collagen I

In a mixture of Matrigel and collagen I, mammary organoids undergo a similar program of branching morphogenesis to that in Matrigel alone, with several notable differences (Nguyen-Ngoc and Ewald, 2013) (Fig. 3-6D). Branched organoids in the mixed matrix generally have fewer buds, but the buds elongate much further into the ECM. We have demonstrated that ratios of 5:5 and 3:7 Matrigel to collagen I induce the highest average bud lengths (Nguyen-Ngoc and Ewald, 2013). Here, we present four examples of branching in the mixed matrices. Organoids may contain both short and long buds, without repolarization (Fig. 3-7D_1) or with partial repolarization (Fig. 3-7D_2,D_4). We also observe bifurcation at the ends of elongated buds (Fig. 3-7D_3). As in Matrigel alone, the leading front of the bud is always non-protrusive (Fig. 3-7$D_{4'}$). Importantly, a mix of 3:7 Matrigel to collagen I yields a high percentage of epithelial buds that maintain complete myoepithelial coverage throughout bud

initiation and elongation (Fig. 3-8C). This phenomenon more closely models elongation of the terminal end bud in vivo (Fig. 3-8F).

3.10.4 Invasion assay

Collagen I induces a conserved protrusive response in mammary epithelium (48 h, Fig. 3-6E). Organoids invade collectively into collagen I, with branches varying in shape and length, from short and thin (Fig. 3-7E_1-E_2) to elongated and wide (Fig. 3-7E_3-E_4). Initially, we observe extensive subcellular protrusions. However, these protrusions cease, and the epithelium reestablishes a smooth basal surface upon formation of a basement membrane between the epithelium and ECM (Fig. 3-6E) (Nguyen-Ngoc et al., 2012). The extent of invasion and epithelial reorganization varies, even within the same organoid. At day 5 in culture, we observe both protrusive (violet unfilled arrowheads, Fig. 3-7$E_{4'}$) and non-protrusive, round tips (violet filled arrowheads, Fig. 3-7E_1-E_4) at the ends of multicellular invasive structures. We also observe single cell dissemination into collagen I (blue arrowheads, Fig. 3-7E_1,E_4).

4. Technical Issues

Here we present several technical problems that we commonly encounter during 3D culture. First, epithelial organoids located very close to the cover glass tend to lose their 3D structure and spread out in 2D as sheets of cells (Fig. 3-7F_1-F_2). Second, organoids may be surrounded by spiky or stringy cells, which likely

results from stromal or other non-epithelial cells attaching to organoids during their isolation (Fig. 3-7F_3). Non-epithelial contaminating species appear distinct and behave differently from organoids. We have observed groups of dead cells (Fig. 3-7F_4), clusters of spiky stromal cells (Fig. 3-7F_5), and nerve bundles (Fig. 3-7F_6), which tend to locally disseminate cells into the matrix.

5. Notes

1. Mammary gland #1 is very small. Mammary gland #2 is located in the neck and is hard to distinguish from other tissues. Generally, do not collect these glands so as to avoid contamination by other tissues (e.g. muscle or epithelial glands) (Fig. 3-2L).
2. Incubation in collagenase solution can require up to 60 min to adequately break up the fat pad. Check the status of the suspension after 30 min of shaking. We have observed incorrect incubation times increase the amount of contaminating tissues in the final organoid suspension (Fig. 3-2K). If shaking is done in an incubator that is also used for bacterial cultures, wipe the outside of the tube with 70% ethanol before bringing it into the biosafety cabinet.
3. Always precoat new pipette tips and tubes with BSA solution to prevent organoids from sticking to the plastic. This precoating (Fig. 3-3) is critical to achieving a high final yield of organoids, especially at younger ages or with C57BL6 mice.

4. Never aspirate the supernatant completely to avoid sucking up the pellet.
5. Carefully examine the pellet after each quick spin before aspirating the supernatant. If the organoids are not well pelleted, mix the suspension thoroughly again, and increase the centrifugation time.
6. The appropriate volume of DMEM/F12 to use for counting varies depending on the estimated yield. If the yield is low, add less medium. If the yield is high, dilute the suspension further 2-10X.
7. The yield varies significantly with mouse strain and age. We generally obtain 2000-4000 organoids per FVB mouse and 500-2000 organoids per C57BL6 mouse.
8. Always check the pellet after every centrifugation. Be careful not to disturb the pellet when removing the supernatant. Use small pipette tips if necessary.
9. The optimal density of organoids in the gel differs for different ECMs and mouse strains. For example, C57BL6 organoids tend to be more contractile than FVB organoids when embedded in collagen I, resulting in contraction of the gel and detachment from the glass bottom if plated too densely.
10. In a 24-well plate, the glass bottom is slightly recessed from the edge of the plastic wall. When both blocks are present in the heating block (Fig. 3-4B), there is a small gap between the plate and the heating block surface, resulting in a temperature at the glass bottom less than 37°C. To establish

direct contact between the glass bottom and the heating block, remove one of the blocks and set up the plate as in Fig. 3-4C-C'.

11. When preparing the collagen I solution, always wait for the solution to come down to the tip, and pipette it out completely. This is particularly important during collagen I neutralization to ensure an accurate volume and concentration of collagen.

12. Since the concentration and pH of rat tail collagen I vary among batches, adjust the pH using small volumes of collagen stock (up to 30 µL) or small amounts of 1.0 N NaOH (<0.5 µL).

a. If the adjustment requires addition of a large amount of collagen I stock, you will need to add more DMEM 10X to maintain ionic balance. However, this complicates calculation of the final concentration of neutralized collagen solution.

b. If you find that your collagen I stock is more basic, prepare the collagen solution with 7.0-7.5 µL of 1.0 N NaOH per 250 µL, and then adjust the final pH with small volumes of 1.0 N NaOH. This will avoid the need to add large volumes of collagen I stock to achieve the appropriate pH.

13. If you are concerned about the accuracy of the final collagen concentration, try to use the same pipette tip for mixing throughout neutralization and pH adjustment to limit loss of collagen solution inside the pipette tip.

14. The pre-incubation time will determine the density of pre-assembled

collagen fibrils. Due to batch variability in collagen stocks, the time required to obtain a gel with visible collagen fibrils varies considerably from 45-120 min. To examine the extent of fibril formation during pre-incubation, plate 30 µL of collagen solution onto a small Petri dish, let it gel for several minutes, and examine under the microscope.

15. If the neutralized collagen I solution is pre-incubated for more than 3-4 h on ice, it will become very cloudy and fibrous (Fig. 3-5D$_6$), and the resulting gel will be less transparent, impairing visibility during imaging.

16. Collagen I gels tend to detach from the coverglass when kept too long on the heating block. Therefore, if you have Matrigel and collagen I gels on the same plate, plate the Matrigel samples first and the collagen I samples last.

17. In PFA, Matrigel becomes very fragile, especially after more than 4 days in culture. To avoid disintegration of the gel, reduce the PFA concentration to 2% with lighter shaking or incubate the gel with 4% PFA for 8-10 min.

18. In our lab, we have identified two successful approaches for performing antibody staining that use slightly different solutions and incubation times. The first one, described in Sections 3.8 and 3.9, uses 10% FBS in DPBS as both the blocking buffer and the dilution buffer for antibodies. The other method uses 10% FBS, 1% BSA in DPBS as a blocking buffer and 1% FBS, 1% BSA in DPBS as the dilution buffer for antibodies.

19. From this step on, slides are kept in a StainTray with a black lid filled with

a shallow layer of water to prevent desiccation and photo-bleaching of fluorescent probes.

20. If you plan to stain for extracellular proteins, such as basement membrane components, permeabilize the samples before embedding into OCT and sectioning. Direct permeabilization on slides can extract too many of these proteins.

21. To conserve primary antibodies, especially ones that require a high concentration, use a PAP pen to draw a hydrophobic border around the section, and add primary antibody solution within this area.

22. For mice less than 4 weeks of age, we typically use only gland #4 and remove the fat pad distal to the lymph nodes. Since the glands at this age are very small, pool several glands into one OCT block for sectioning.

23. To improve antibody staining in mammary gland tissue sections, it is sometimes useful to significantly increase the incubation times. For example, we sometimes permeabilize with Triton X-100 for 1 h at room temperature; incubate with primary antibody for 48 h at 4°C; and incubate with secondary antibody for 6 h at room temperature or overnight at 4°C. In addition, for incubation with antibodies, it is preferable to draw a hydrophobic border around the tissue with a PAP pen to reduce the volume of solution required and to ensure that the tissue is always immersed in solution. Do not let samples air-dry.

Author contribution

K-V. N-N prepared and organized all the figures

K-V. N-N also contributed to writing the manuscript.

References

1. Conklin MW, Eickhoff JC, Riching KM, Pehlke CA, Eliceiri KW, Provenzano PP, Friedl A, Keely PJ. (2011) Aligned collagen is a prognostic signature for survival in human breast carcinoma. Am J Pathol. 178(3):1221-32.
2. Debnath J, Muthuswamy SK, Brugge JS. (2003). Morphogenesis and oncogenesis of MCF-10A mammary epithelial acini grown in three-dimensional basement membrane cultures. Methods 30:256-268.
3. Egeblad M, MG Rasch and VM Weaver. (2010). Dynamic interplay between the collagen scaffold and tumor evolution. Curr Opin Cell Biol 22:697-706.
4. Ewald AJ, Brenot A, Duong M, Chan BS, & Werb Z (2008) Collective epithelial migration and cell rearrangements drive mammary branching morphogenesis. Dev Cell 14(4):570-581.
5. Ewald AJ, Huebner RJ, Palsdottir H, Lee JK, Perez MJ, Jorgens DM, Tauscher AN, Cheung KJ, Werb Z, Auer M. (2012). Mammary collective cell migration involves transient loss of epithelial features and individual cell migration within the epithelium. J Cell Sci 125:2638-54.
6. Ewald AJ. (2013). Isolation of mouse mammary organoids for long-term time-lapse imaging. Cold Spring Harb Protoc 2013
7. Fata JE1, Mori H, Ewald AJ, Zhang H, Yao E, Werb Z, Bissell MJ. (2007). The MAPK(ERK-1,2) pathway integrates distinct and antagonistic signals from TGFalpha and FGF7 in morphogenesis of mouse mammary epithelium. Dev Biol 306:193-207.
8. Griffith LG & Swartz MA (2006) Capturing complex 3D tissue physiology in vitro. Nat Rev Mol Cell Biol 7(3):211-224.
9. Gudjonsson T, L Ronnov-Jessen, R Villadsen, MJ Bissell, OW Petersen. (2003). To create the correct microenvironment: three-dimensional heterotypic collagen assays for human breast epithelial morphogenesis and neoplasia. Methods 30:247-55.
10. Hinck L, GB Silberstein. (2005). Key stages in mammary gland development: the mammary end bud as a motile organ. Breast Cancer Res 7:245-51.
11. Ichinose RR, S Nandi. (1966). Influence of hormones on lobulo-alveolar differentiation of mouse mammary glands in vitro. J Endocrinol 35:331-40.
12. Levental KR, H Yu, L Kass, JN Lakins, M Egeblad, JT Erler, SF Fong, K Csiszar, A Giaccia, W Weninger, M Yamauchi, DL Gasser, VM Weaver. (2009). Matrix crosslinking forces tumor progression by enhancing integrin signaling. Cell 139:891-906.
13. Mroue R and MJ Bissell. (2012). Three-dimensional cultures of mouse mammary epithelial cells. Methods Mol Biol 945:221-50.
14. Nelson CM, MJ Bissell. (2005). Modeling dynamic reciprocity: engineering three-dimensional culture models of breast architecture, function, and neoplastic transformation. Semin Cancer Biol 15:342-52.

15. Nelson CM, MM Vanduijn, JL Inman, DA Fletcher and MJ Bissell. (2006). Tissue geometry determines sites of mammary branching morphogenesis in organotypic cultures. Science 314:298-300.
16. Nelson CM, JL Inman, MJ Bissell. (2008) Three-dimensional lithographically defined organotypic tissue arrays for quantitative analysis of morphogenesis and neoplastic progression. Nat Protoc 3:674-8.
17. Nguyen-Ngoc KV, KJ Cheung, A Brenot, ER Shamir, RS Gray, WC Hines, P Yaswen, Z Werb, AJ Ewald. (2012). The ECM microenvironment regulates collective migration and local dissemination in normal and malignant mammary epithelium. Proc Natl Acad Sci U S A. 109(39):E2595-604.
18. Nguyen-Ngoc KV, AJ Ewald. (2013). Mammary ductal elongation and myoepithelial migration are regulated by the composition of the extracellular matrix. J Microsc. 251(3):212-23.
19. Paszek MJ, N Zahir, KR Johnson, JN Lakins, GI Rozenberg, A Gefen, CA Reinhart-King, SS Margulies, M Dembo, D Boettiger, DA Hammer and VM Weaver. (2005). Tensional homeostasis and the malignant phenotype. Cancer Cell 8:241-54.
20. Provenzano PP, Eliceiri KW, Campbell JM, Inman DR, White JG, Keely PJ. (2006) Collagen reorganization at the tumor-stromal interface facilitates local invasion. BMC Med.4(1):38.
21. Provenzano PP, DR Inman, KW Eliceiri, JG Knittel, L Yan, CT Rueden, JG White, PJ Keely. (2008). Collagen density promotes mammary tumor initiation and progression. BMC Med 6:11.
22. Provenzano PP, KW Eliceiri, DR Inman, PJ Keely. (2010). Engineering three-dimensional collagen matrices to provide contact guidance during 3D cell migration. Curr Protoc Cell Biol Chapter 10:Unit 10 17.
23. Simian M, Y Hirai, M Navre, Z Werb, A Lochter, MJ Bissell. (2001). The interplay of matrix metalloproteinases, morphogens and growth factors is necessary for branching of mammary epithelial cells. Development 128:3117-31.
24. Sternlicht MD, SW Sunnarborg, H Kouros-Mehr, Y Yu, DC Lee, Z Werb. (2005). Mammary ductal morphogenesis requires paracrine activation of stromal EGFR via ADAM17-dependent shedding of epithelial amphiregulin. Development 132:3923-33.
25. Sternlicht MD, H Kouros-Mehr, P Lu, Z Werb. (2006). Hormonal and local control of mammary branching morphogenesis. Differentiation 74:365-81.
26. Sternlicht MD. (2006). Key stages in mammary gland development: the cues that regulate ductal branching morphogenesis. Breast Cancer Res 8:201.
27. Vidi PA, MJ Bissell, SA Lelievre. (2012). Three-dimensional culture of human breast epithelial cells: the how and the why. Methods Mol Biol 945:193-219.
28. Williams JM, Daniel CW. (1983) Mammary ductal elongation: differentiation of myoepithelium and basal lamina during branching

morphogenesis. Dev Biol. 97(2):274-90.`
29. Wozniak MA, PJ Keely. (2005) Use of three-dimensional collagen gels to study mechanotransduction in T47D breast epithelial cells. Biol Proced Online 7:144-61.

Figure 3-1.

Collection of mouse mammary glands for organoid isolation and 3D culture. (A) Schematic description of isolation and 3D culture of mouse mammary organoids. (B) Scheme for surgically accessing the mammary glands. Numbers indicate the order of cuts. (C) Locations of the ten mammary glands. (D) Expose glands #3, #4, and #5 by pushing back the abdomen (blue dotted line) with the back of the Graefe forceps. (E-E') A thin layer of muscle partially covers gland #3 (E) and should be pushed back before dissection (E'). Dotted line in (E') indicates the region of gland #3 to be collected. (F) Use the Graefe forceps to pluck out the lymph node in gland #4. Dotted line in (F') indicates the approximate region of glands #4 and #5 to be collected.

Figure 3-1

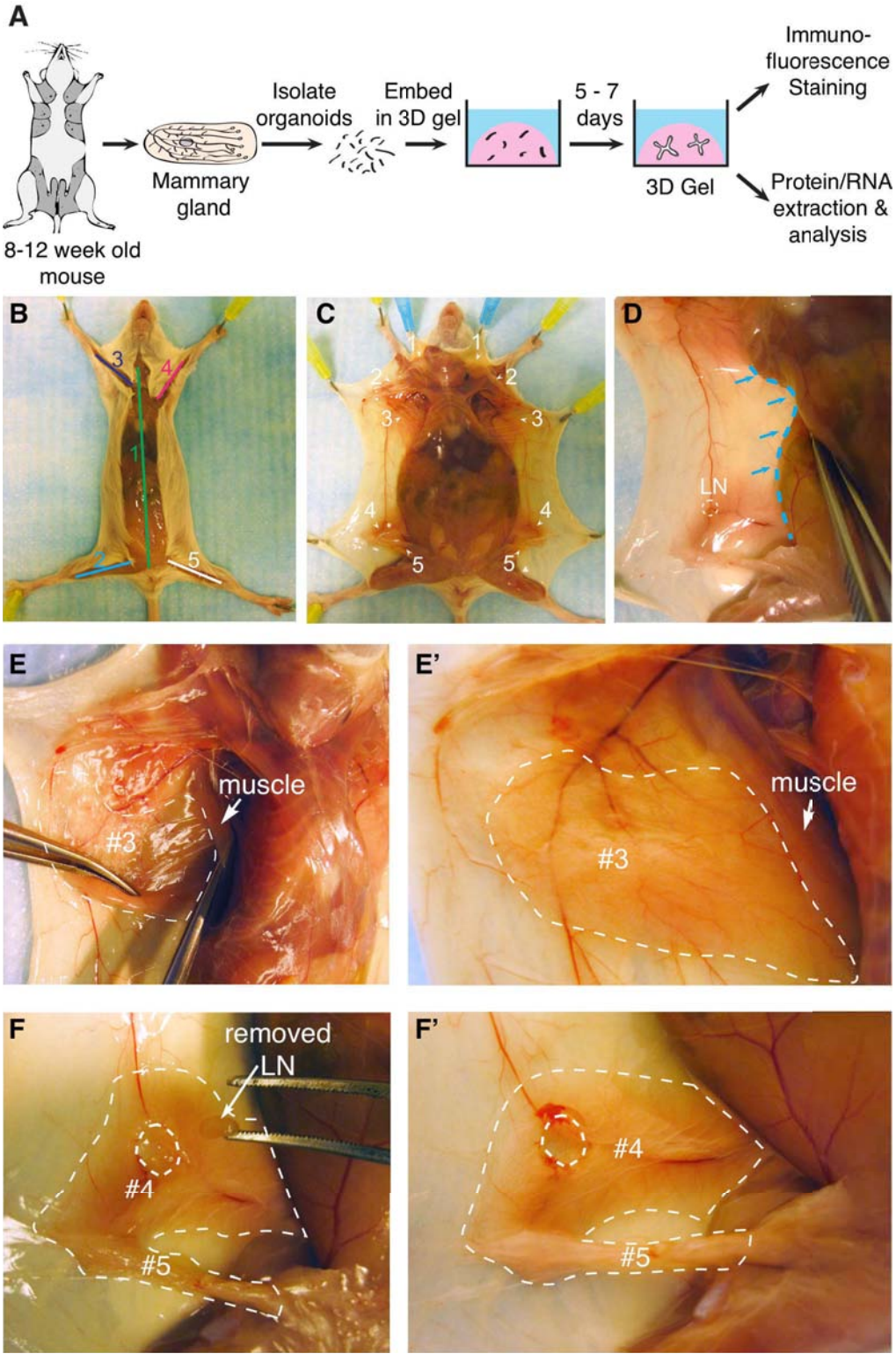
A
8-12 week old mouse
Mammary gland
Isolate organoids
Embed in 3D gel
5 - 7 days
3D Gel
Immuno-fluorescence Staining
Protein/RNA extraction & analysis
B
C
D
LN
E
muscle
#3
E'
muscle
#3
F
removed LN
#4
#5
F'
#4
#5

Figure 3-2.

Mammary organoid isolation. (A-A') Collected mammary glands are pooled in a Petri dish (A) and minced until the tissue relaxes, typically 25-50 cuts (A'). (B-B") Incubation in collagenase solution breaks up the fat pad (B) into smaller pieces that are relatively dispersed (B'). Too long of a digestion (B'') will cause organoids to be too small and not grow well. (C) Following incubation in collagenase solution, centrifugation separates the suspension into three layers, with a top opaque layer of fat and a pellet (#1) of epithelium and stroma. (D) The fatty layer is transferred to a new tube and resuspended in 10 mL DMEM/F12. (E) Centrifugation of the dispersed fatty layer recovers additional epithelium in the pellet (#2). (F-F") The combined pellets from (C) and (E) are resuspended in 4 mL DMEM/F12 with DNase (F). Before DNase treatment, organoids (pink arrowheads) are loosely attached to each other and to stromal cells (F'), forming visible clusters in the tube (F"). (G-G") DNase treatment causes organoids (pink arrowheads) to detach from one another (G') and the clusters to disappear (G"). (H-H') Centrifugation of the suspension in (G) results in a compact red pellet (H'). (I-I") Differential centrifugation removes single cells from the suspension (I') and results in an off-white pellet of purified epithelial organoids (I''). Organoids (pink arrowheads) may appear rounded and small or more elongated and even branched (I'). Larger organoids typically survive and branch more efficiently in our assays. (J) Close-up view of an organoid. (K-L) Non-epithelial tissues can be observed in the final suspension, including nerve bundles (K) and muscle (L).

Figure 3-2

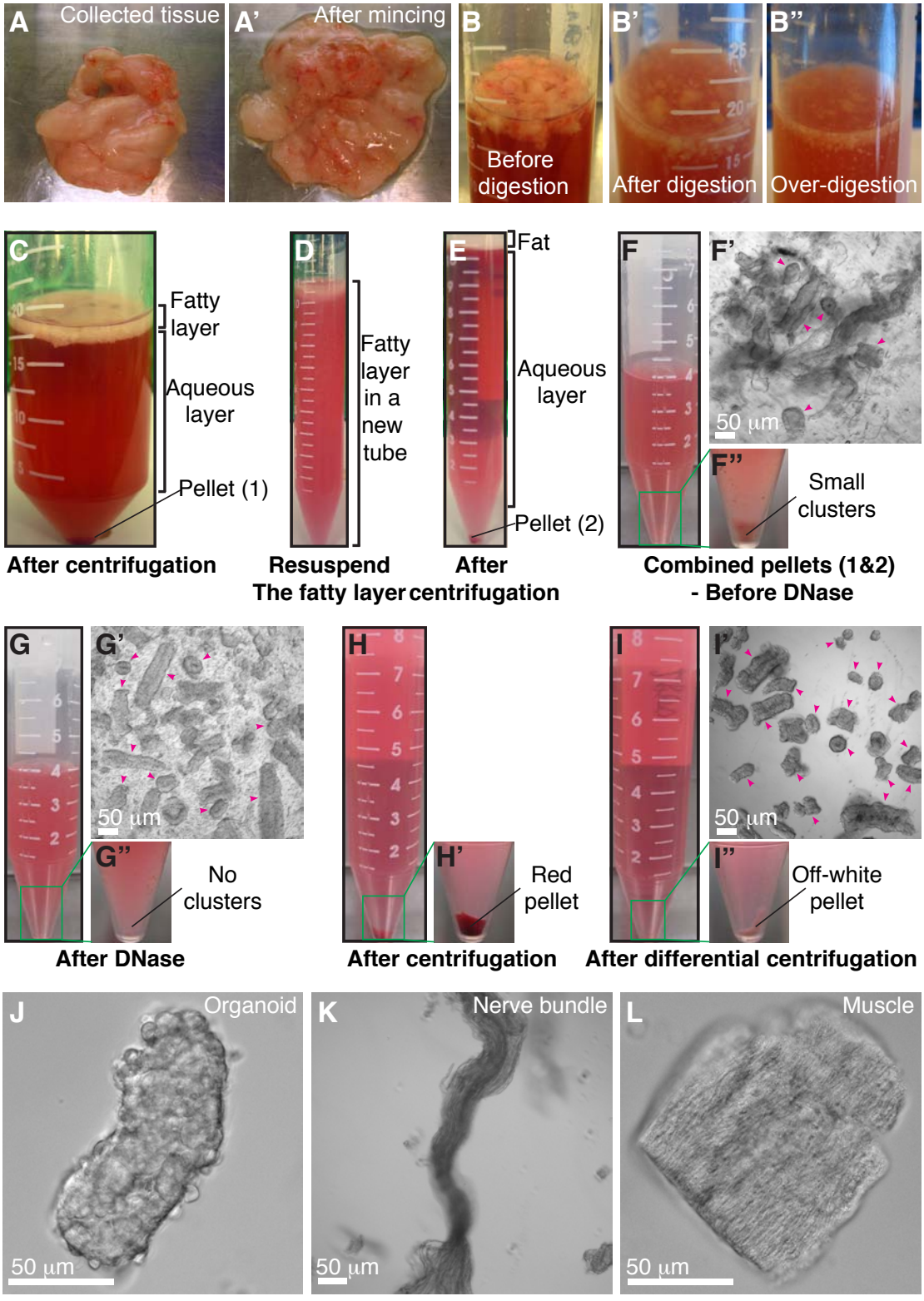
A
Collected tissue
A'
After mincing
B
Before digestion
B'
After digestion
B"
Over-digestion
C
Fatty layer
Aqueous layer
Pellet (1)
After centrifugation
D
Fatty layer in a new tube
Resuspend The fatty layer
E
Fat
Aqueous layer
Pellet (2)
After centrifugation
F
F'
50 µm
F"
Small clusters
Combined pellets (1&2) - Before DNase
G
G'
50 µm
G"
No clusters
After DNase
H
H'
Red pellet
After centrifugation
I
I'
50 µm
I"
Off-white pellet
After differential centrifugation
J
Organoid
50 µm
K
Nerve bundle
50 µm
L
Muscle
50 µm

Figure. 3-3

Precoating tubes and pipette tips with BSA. Fresh tissue can adhere to uncoated plastic surfaces, and this protocol involves many pipetting steps. Accordingly, it is essential to precoat the plastic surfaces with BSA solution to maximize final organoid yield. (A) Precoat a 15 mL tube by filling the tube with BSA solution, inverting the tube to precoat the cap, and removing the BSA solution. (B) Precoat a 10 mL pipette tip by taking up BSA solution to fill the entire pipette and ejecting back out. (C-D) Use the same approach to precoat a microcentrifuge tube (C) and a small pipette tip (D) with BSA solution.

Figure 3-3

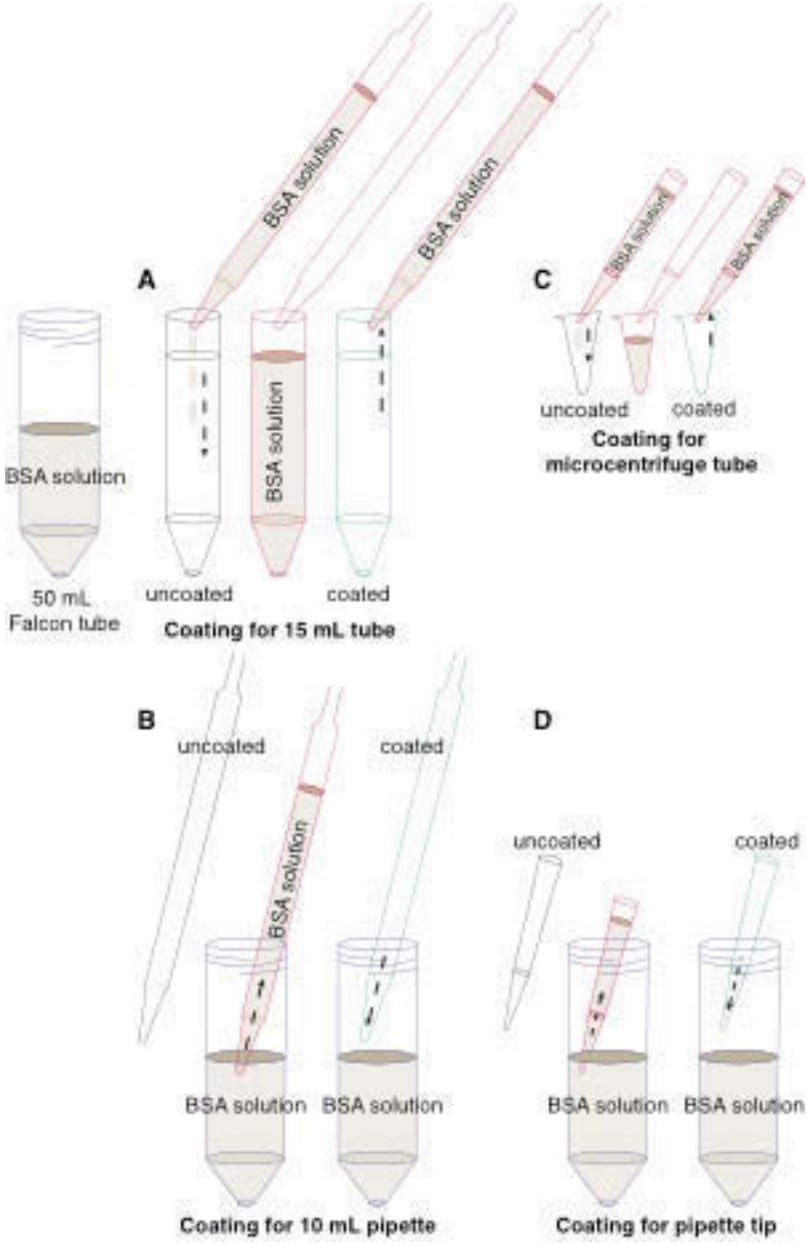
A
BSA solution
BSA solution
BSA solution
BSA solution
50 mL
Falcon tube
uncoated
coated
Coating for 15 mL tube
C
uncoated
coated
Coating for
microcentrifuge tube
B
uncoated
coated
BSA solution
BSA solution
BSA solution
Coating for 10 mL pipette
D
uncoated
coated
BSA solution
BSA solution
Coating for pipette tip

Figure. 3-4

Setting up the tissue culture hood for plating. (A) Sample layout of reagents, tools, and equipment used for plating 3D culture samples. (B) Heating block set-up for plating in 2-well or 4-well chambers. (C-C') To plate in a 24-well dish, remove one of the blocks from the heating block (C) to establish direct contact between the remaining block and the plate bottom (C').

Figure 3-4

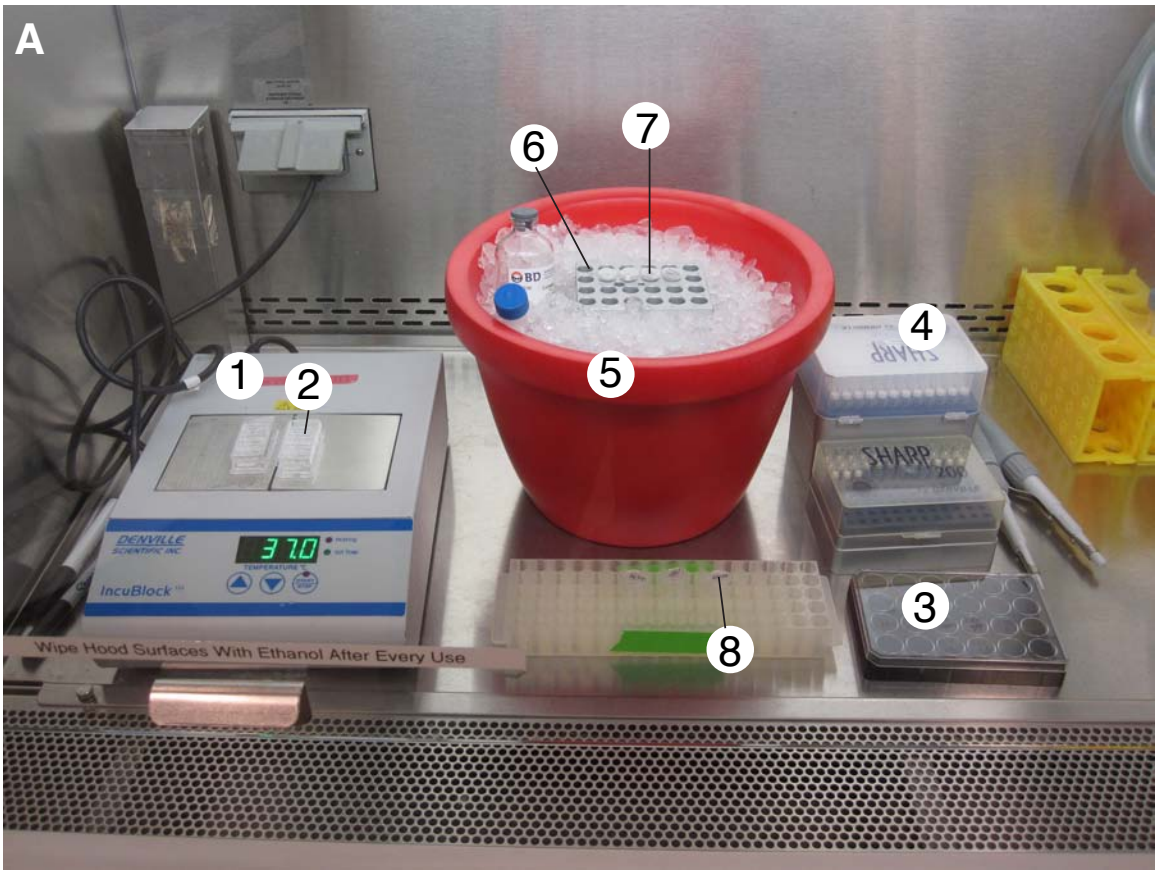

1. Heating block	4. 1 mL extra long tips	7. Collagen I solution being pre-incubated
2. 4-well chamber	5. Ice bucket	
3. 24-well plate	6. Cold block	8. Organoid samples

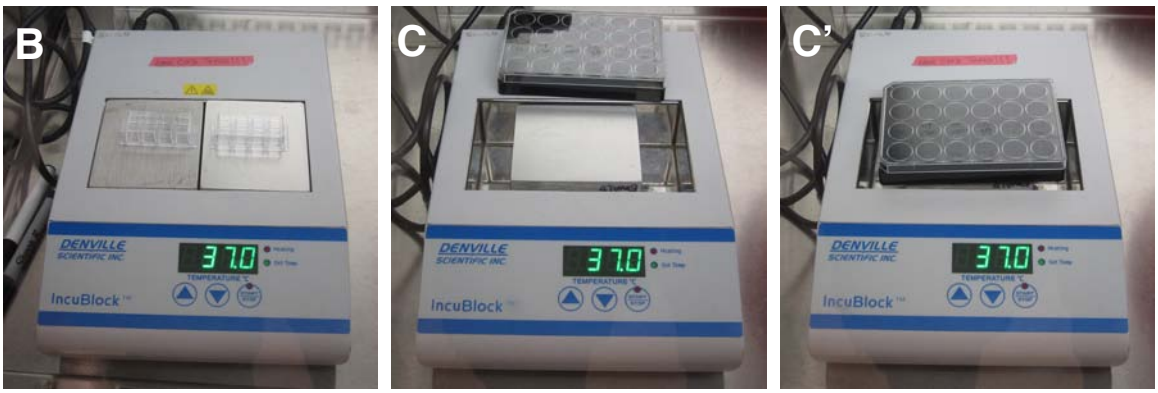

Figure 3-5

Plating organoids in 3D Matrigel and collagen I. (A) Schematic description of plating organoids in Matrigel. (B-B') Schematic description of preparing pre-assembled collagen I (B), which can be used alone or mixed with Matrigel (B'). (C_1-C_7) Color indicators for the pH of the collagen I solution during neutralization. (D_1-D_6) Decreasing transparency of the collagen I solution during pre-incubation on ice. (E-E') Schematic description of plating organoids in 3D collagen I or in a mixture of Matrigel and collagen I. (E) shows a top view for making an underlay on the coverglass. (E') shows a side view of how to plate the organoid/collagen I suspension on top of the gelled underlay. (F-F') Representative DIC images of collagen I fibers at low (F) and high (F') magnification.

Figure 3-5

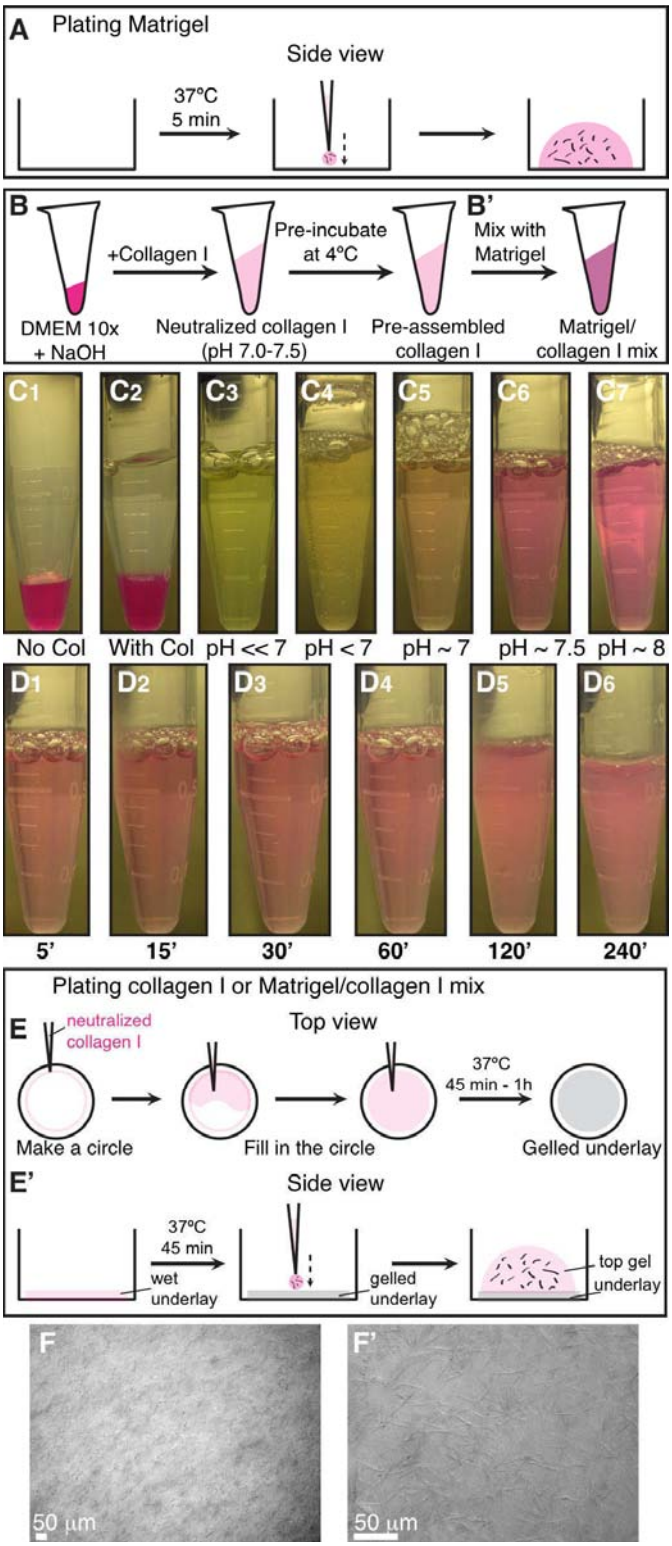
A
Plating Matrigel
Side view
37°C
5 min
B
+Collagen I
Pre-incubate
at 4°C
B'
Mix with
Matrigel
DMEM 10x
+ NaOH
Neutralized collagen I
(pH 7.0-7.5)
Pre-assembled
collagen I
Matrigel/
collagen I mix
C1
C2
C3
C4
C5
C6
C7
No Col
With Col
pH << 7
pH < 7
pH ~ 7
pH ~ 7.5
pH ~ 8
D1
D2
D3
D4
D5
D6
5'
15'
30'
60'
120'
240'
Plating collagen I or Matrigel/collagen I mix
E
neutralized
collagen I
Top view
37°C
45 min - 1h
Make a circle
Fill in the circle
Gelled underlay
E'
Side view
37°C
45 min
wet
underlay
gelled
underlay
top gel
underlay
F
50 µm
F'
50 µm

Figure 3-6

3D organotypic culture assays. (A) Schematic description of four assays that use different extracellular matrix compositions to model specific epithelial behaviors. (B-E) Representative frames of DIC time-lapse movies showing cyst formation in Matrigel in basal medium (B), branching morphogenesis in Matrigel induced by FGF2 (C), branching morphogenesis in a mixture of Matrigel and collagen I induced by FGF2 (D), and epithelial cell invasion into pure collagen I induced by FGF2 (E).

Figure 3-6

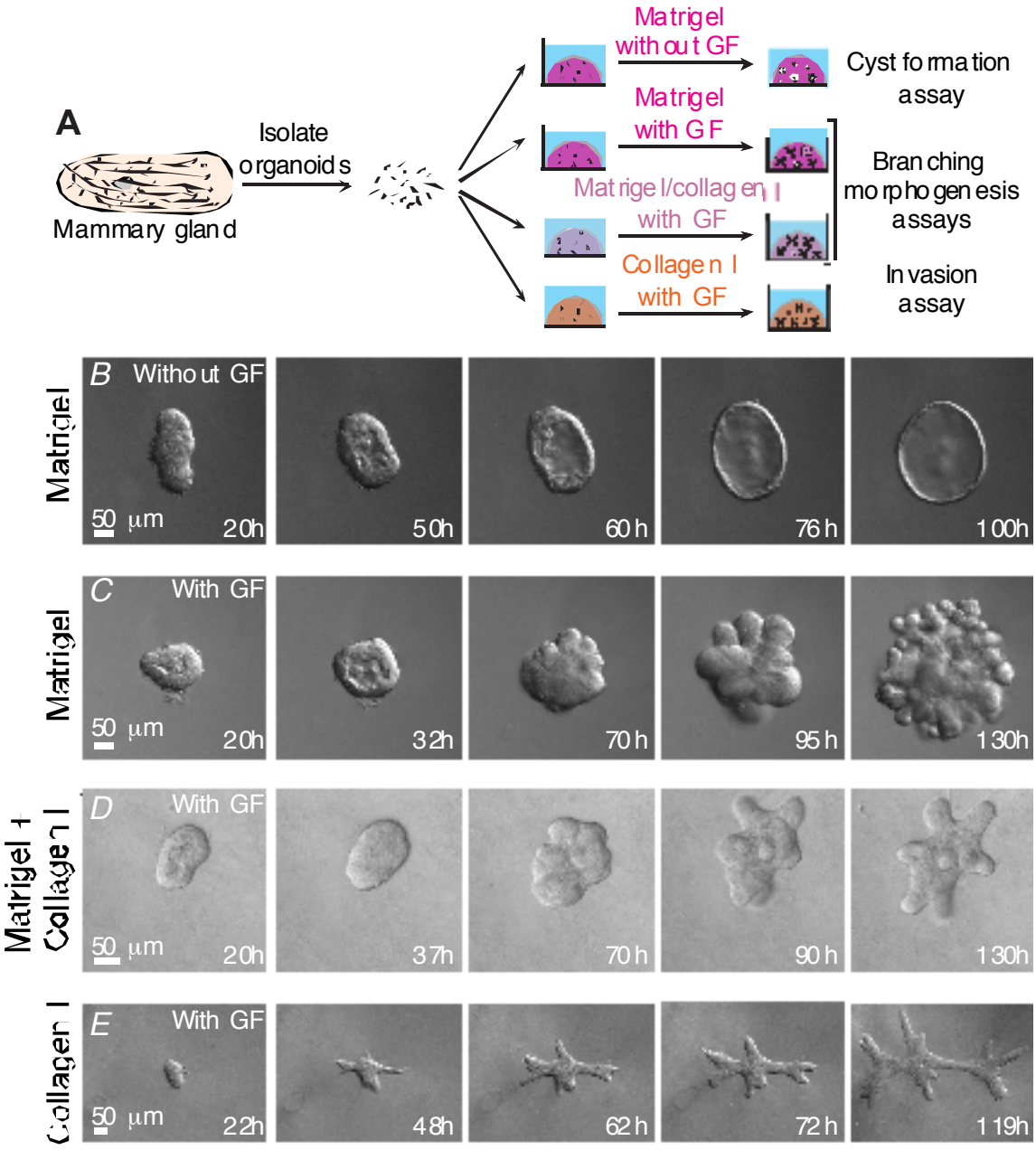
A
Isolate organoids
Mammary gland
Matrigel without GF
Matrigel with GF
Matrigel/collagen I with GF
Collagen I with GF
Cyst formation assay
Branching morphogenesis assays
Invasion assay
Matrigel
Matrigel + Collagen I
Collagen I
B Without GF
C With GF
D With GF
E With GF
50 µm
20h
50h
60 h
76 h
100h
32h
70 h
95 h
130h
37h
90 h
22h
48h
62 h
72 h
119h

Figure 3-7

Phenotypic variability in assay outcomes. (A) Schematic description of a cyst. (A_1-A_4) DIC images showing variation in cyst morphology. ($A_{4'}$) An inset of (A_4) showing a smooth basal surface with Matrigel. (B) Schematic description of a stratified, unbranched organoid. (B_1-B_4) DIC images showing examples of stratified, unbranched organoids in Matrigel. ($B_{4'}$) An inset of (B_4) showing a smooth basal surface with Matrigel. (C) Schematic description of a branched organoid in Matrigel. (C_1-C_4) DIC images showing variation in branching morphology. ($C_{4'}$) An inset of (C_4) showing a smooth basal surface with Matrigel. (D) Schematic description of a branched organoid in a mixture of Matrigel and collagen I. (D_1-D_4) DIC images showing variation in branching morphology. ($D_{4'}$) An inset of (D_4) showing a smooth basal surface with the mixed matrix. (E) Schematic description of an organoid with protrusive tips in collagen I. (E_1-E_4) DIC images showing variation in protrusive invasion. ($E_{4'}$) An inset of (E_4) showing protrusive tips into collagen I. (F) DIC images showing commonly observed technical issues. (F_1-F_2) Organoids lose their 3D organization in Matrigel (F_1) and collagen I gels (F_2) when they make contact with the cover glass. (F_3) Non-epithelial species (red arrowheads) attached to organoids may appear elongated and mesenchymal (ECM: Matrigel). (F_4) A group of dead cells beside a branching organoid (ECM: collagen I). (F_5) A cluster of elongated, non-epithelial cells (ECM: Matrigel). (F_6) A nerve bundle disseminating single cells into the surrounding matrix (ECM: Matrigel).

Figure 3-7

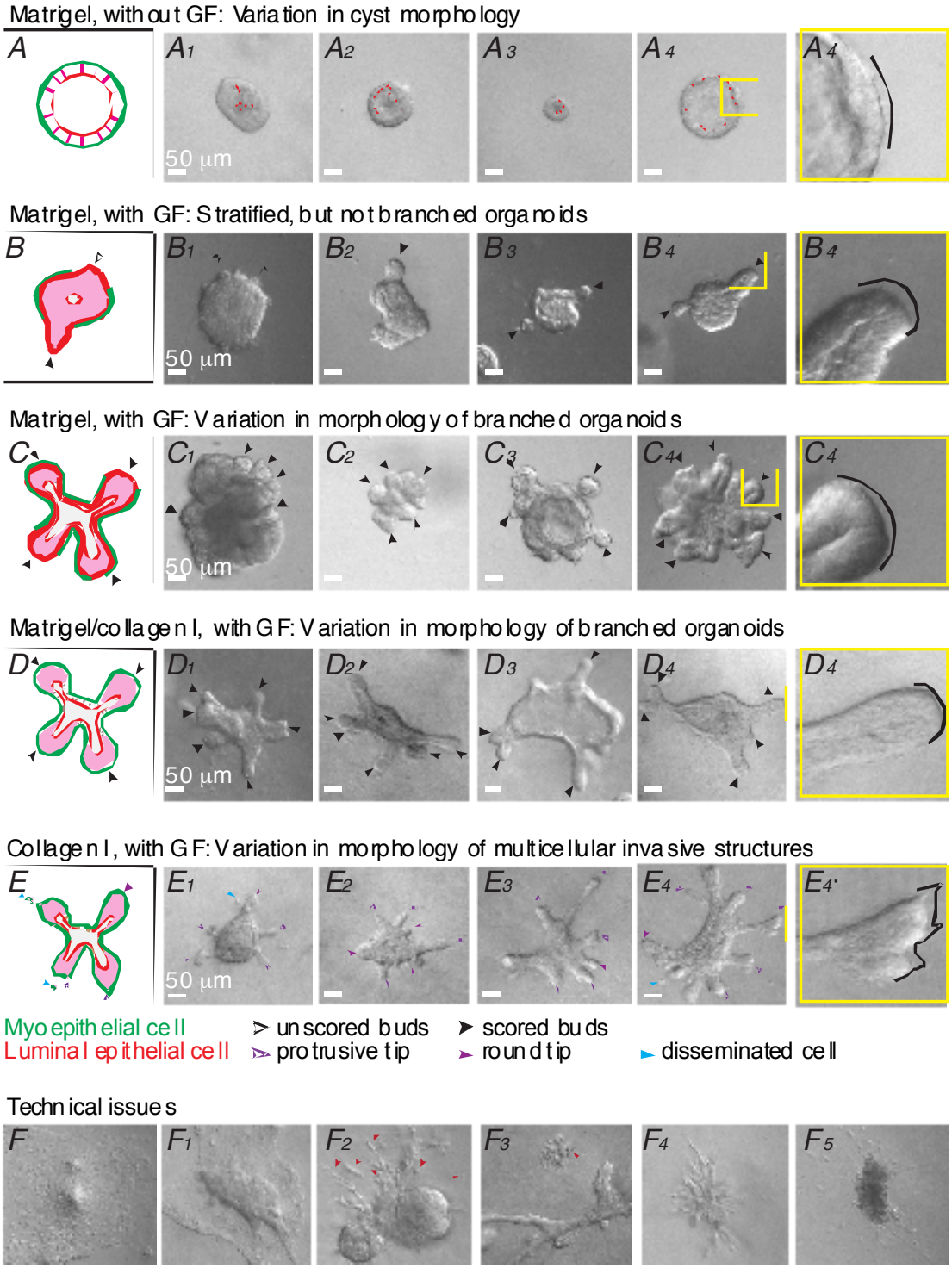
Matrigel, without GF: Variation in cyst morphology
A
A1
A2
A3
A4
A4'
50 μm
Matrigel, with GF: Stratified, but not branched organoids
B
B1
B2
B3
B4
B4'
50 μm
Matrigel, with GF: Variation in morphology of branched organoids
C
C1
C2
C3
C4
C4'
50 μm
Matrigel/collagen I, with GF: Variation in morphology of branched organoids
D
D1
D2
D3
D4
D4'
50 μm
Collagen I, with GF: Variation in morphology of multicellular invasive structures
E
E1
E2
E3
E4
E4'
50 μm
Myoepithelial cell
Luminal epithelial cell
unscored buds
protrusive tip
scored buds
round tip
disseminated cell
Technical issues
F
F1
F2
F3
F4
F5

Figure 3-8

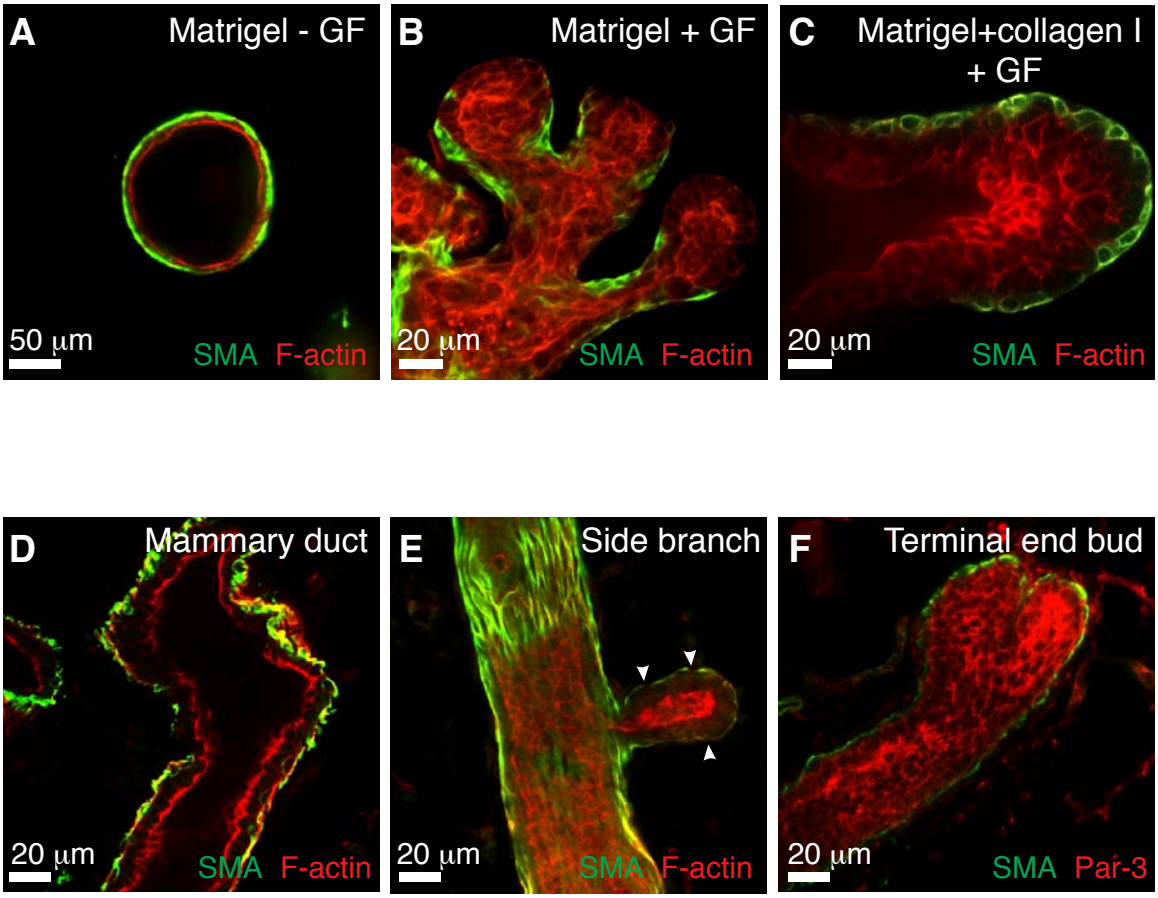

Correlation between epithelial morphologies in 3D organotypic assays and *in vivo*. (A-C) Representative confocal images of a cyst in Matrigel (A), branched buds in Matrigel (B), and a stratified, elongating bud in a mixture of Matrigel and collagen I (C). (D-F) Representative confocal images from mammary gland tissue sections of a bilayered duct (D), a side branch (E), and a terminal end bud (F).

CHAPTER 4

ECM microenvironment regulates collective migration and local dissemination in normal and malignant mammary epithelium

(Modified from Nguyen-Ngoc et al., PNAS. 2012)

Abstract

Breast cancer progression involves genetic changes and changes in the extracellular matrix (ECM). To test the importance of the ECM in tumor cell dissemination, we cultured epithelium from primary human breast carcinomas in different ECM gels. We used basement membrane gels to model the normal microenvironment and collagen I to model the stromal ECM. In basement membrane gels, malignant epithelium either was indolent or grew collectively, without protrusions. In collagen I, epithelium from the same tumor invaded with protrusions and disseminated cells. Importantly, collagen I induced a similar initial response of protrusions and dissemination in both normal and malignant mammary epithelium. However, dissemination of normal cells into collagen I was transient and ceased as laminin 111 localized to the basal surface, whereas dissemination of carcinoma cells was sustained throughout culture, and laminin 111 was not detected. Despite the large impact of ECM on migration strategy, transcriptome analysis of our 3D cultures revealed few ECM-dependent changes in RNA expression. However, we observed many differences between normal and malignant epithelium, including reduced expression of cell-adhesion genes in tumors. Therefore, we tested whether deletion of an adhesion gene could induce sustained dissemination of non-transformed cells into collagen I. We found that deletion of P-cadherin was sufficient for sustained dissemination, but exclusively into collagen I. Our data reveal that metastatic tumors preferentially disseminate in specific ECM microenvironments. Furthermore, these data suggest that breaks

in the basement membrane could induce invasion and dissemination via the resulting direct contact between cancer cells and collagen I.

Introduction

Collective cell migration is an important mechanism for both normal epithelial development and cancer invasion (Friedl and Gilmour, 2009). During collective cell migration, cells move in coordinated groups and maintain cell–cell adhesion. In the normal mammary gland, ducts transition from a polarized bilayer into a proliferative, motile, multilayered epithelium and then migrate collectively through the stromal tissue (Ewald et al., 2008, Ewald et al., 2012). Mammary carcinomas also originate from a polarized adult epithelium, transition from a simple to multilayered organization, and migrate collectively (Hanahan and Weinberg, 2000; Friedl et al., 1995). Despite these similarities, normal ductal morphogenesis in vivo does not involve local dissemination of cells and eventually results in restoration of polarized simple epithelial architecture. In contrast, breast carcinomas continue to grow, disseminate cells locally, and frequently metastasize to distant sites (Nguyen et al., 2009). These observations raise the fundamental question: What features of tumor progression can regulate the transition from a collective to a disseminative phenotype?

Cancer is a genetic disease, and sequencing has revealed that genes encoding cell–cell and cell–matrix adhesion proteins frequently are mutated (Vogelstein and Kinzler, 1993; Wood et al., 2007). However, breast cancer also involves characteristic changes in the ECM and the tumor microenvironment (Egeblad et al., 2010a; Egeblad et al., 2010b; Polyak et al., 2009; Egeblad et al., 2008). For example, collagen I is enriched and aligned at the stromal border in

breast tumors (Egeblad et al., 2010b; Provenzano et al., 2006), changes in collagen I organization are independent negative prognostic indicators (Conklin et al., 2011), and increased collagen I crosslinking accelerates progression in experimental cancer models (Levental et al., 2009). Additionally, basement membrane proteins and their integrin receptors have been shown to regulate carcinoma cell behavior (Petersen et al., 1992; Weaver et al., 1997; Hagio et al., 1998). A major challenge today is to distinguish the relative contributions of specific genetic and microenvironmental changes to the migration and local dissemination of carcinoma cells.

In vivo, there are vast differences in the soluble signals, the stromal cells, and the ECM microenvironments surrounding carcinomas and normal ducts (Egeblad et al., 2010a). It is difficult to manipulate these signals independently in an intact tumor and even more challenging to assess the acute cell behavioral consequences of experimental manipulations. The relative optical inaccessibility of mammalian tissues led our laboratory and others to establish 3D ex vivo models of both normal and malignant mammary epithelial growth (Friedl et al., 1995, Debnath and Brugge, 2005; Griffith and Swartz, 2006; Ewald, 2010; Simian et al., 2001; Gudjonsson et al., 2003; Nelson and Bissell, 2005). We have applied these techniques to test the relative importance of genetic and microenvironmental changes in regulating the pattern of collective cell migration and the likelihood of local dissemination.

Results

An epithelial cell in a mammary duct exists in a highly structured 3D environment and receives extensive inputs from cell–cell, cell–matrix, and soluble signals. We previously identified the critical conditions that enable primary mammary epithelium to undergo an organotypic program of branching morphogenesis (Ewald et al., 2008). We found that, despite extensive cell migration, normal mammary morphogenesis in 3D Matrigel cultures and in vivo occurs without ECM-directed protrusions (Ewald et al., 2008, Ewald et al., 2012). In contrast, carcinomas in vivo can migrate with protrusions and can disseminate cells locally and to distant sites (Nguyen et al., 2009, Friedl et al., 2004). Because the tumor microenvironment changes in parallel with genetic changes in the cancer cells (Egeblad et al., 2010b), it is unclear whether the protrusive migration and dissemination of carcinoma cells are the result of cell-intrinsic motility differences or of interactions of the cancer cells with their microenvironment. Therefore, we exploited organotypic culture techniques to isolate and culture fragments from individual primary human mammary carcinomas in different ECM microenvironments (Fig. 4-1A). We first optimized the medium conditions to yield consistent branching morphogenesis in samples of normal human breast epithelium (Fig. 4-2 A–D). We then focused on two ECM environments: a gel composed of basement membrane proteins (Matrigel) to model the normal breast epithelial microenvironment and 3 mg/mL collagen I to model the stromal matrix encountered by invading mammary carcinomas

(Egeblad et al., 2010b). Although fibrillar collagen I is present near normal mammary ducts, it remains outside an intact basement membrane even during branching morphogenesis, limiting contact with normal epithelial cells (Williams and Daniel, 1983).

Human Mammary Carcinomas Invade and Disseminate Preferentially into Collagen I.

We explanted fragments from primary human mammary carcinomas (n = 7 tumors) (Fig. 4-2E) into 3D ECM cultures (Fig. 4-1A). The starting point for culture was epithelial fragments of a few hundred to a few thousand cells. We allocated fragments of the same tumor to different 3D ECM microenvironments and observed ECM-dependent carcinoma migration strategies (Fig. 4-1 B–C"). In 3D Matrigel, we observed both indolent behavior and collective epithelial migration (Fig. 4-1 B – B"). We observed single-cell protrusions from the epithelium in Matrigel only rarely and did not observe robust collective protrusive migration. In contrast, fragments from the same primary human mammary carcinoma exhibited protrusive migration and disseminated cells extensively into 3D gels of 3 mg/mL collagen I (Fig. 4-1 C–C", H, and I). Although the extent of invasion and dissemination varied among tumor fragments (Fig. 4-3 A–C), the borders of carcinoma fragments cultured in Matrigel maintained an epithelial appearance without protrusions (150/155 fragments from five human tumors) (Fig. 4-1H), whereas the borders of carcinoma fragments in collagen I were

protrusive (90/109 fragments from five human tumors) and exhibited extensive local dissemination (89/109 fragments) (Fig. 4-1 H and I).

Current, Local ECM Microenvironment Determines the Cellular Strategy of Invasion for Primary Human Mammary Carcinomas.

We next sought to determine whether protrusive migration and dissemination could be reversed if the ECM composition returned to basement membrane-like composition. To test this concept, we first cultured primary human tumor fragments in either Matrigel or collagen I until the pattern of migration was clear and then digested the ECM and transferred the tumor fragments to another ECM environment (Fig. 4-1 D–G). We tested all reciprocal combinations, including transfer from Matrigel to Matrigel, from Matrigel to collagen I, from collagen I to Matrigel, and from collagen I to collagen I. Transfer between Matrigel and Matrigel resulted in a restarting of collective migration (Fig. 4-1D). Transfer from Matrigel to collagen I resulted in protrusive migration in the new environment (Fig. 4-1E), whereas transfer from collagen I to Matrigel resulted in a retraction of protrusions and confined, collective growth (Fig. 4-1F). Carcinoma fragments transferred from collagen I to collagen I were protrusive but on average were less disseminative (Fig. 4-1 G–I), suggesting there may be a limited subpopulation of highly invasive cells in a tumor. However, we cannot exclude the possibility that the more extensive enzymatic digestion required to free epithelial fragments from a collagen I gel might have reduced their invasive

behavior. We therefore conclude that the current, local ECM environment determines the migration strategy and likelihood of dissemination.

Collagen I Induces Protrusive Migration and Local Dissemination of Murine Carcinoma Cells.

Our investigations with human breast carcinomas suggested that the local ECM microenvironment is sufficient to induce or repress protrusive and disseminative behavior. However, live primary human carcinoma tissue is scarce, and the details of tumor pathology vary widely from one available sample to the next (Fig. 4-2E). Therefore we modeled this regulatory interaction using mouse mammary carcinomas. We selected a mammary carcinoma model in which the mouse mammary tumor virus long terminal repeat drives the expression of the polyomavirus middle T oncogene (MMTV-PyMT), because it exhibits progressive cellular and molecular changes that parallel those observed in human breast cancer (Guy et al., 1992; Lin et al., 2003). Gene expression in this model clusters with the highly aggressive luminal B subtype of human breast cancer (Herschkowitz et al., 2007).

We isolated epithelial fragments of 200–1,000 cells from advanced murine mammary carcinomas (12–15 wk, 1.5- to 2-cm tumors) and embedded them into Matrigel or collagen I (Fig. 4-4A). Carcinoma fragments in Matrigel culture developed into budded structures with high efficiency (Fig. 4-4B). Cells within these fragments remained in a stratified organization, without lumens, throughout

their time in Matrigel culture, and cells at the ECM border maintained an epithelial appearance, without protrusions (Fig. 4-4 B and B'). Although the MMTV-PyMT model metastasizes to the lungs with high efficiency in vivo, 90% of the carcinoma fragments did not disseminate cells into Matrigel (Fig. 4-4D and 45/50 movies). In contrast, carcinoma fragments embedded in 3 mg/mL collagen I developed extensive protrusions and frequently (98%) disseminated cells into collagen I (Fig. 4-4 C–D and 47/48 movies). Both the protrusions and dissemination were detectable by transmitted light microscopy (Fig. 4-4 C and C'). We conclude that the ECM microenvironment determines the collective cell migratory strategy and the likelihood of local dissemination in both human breast cancer cells and murine mammary carcinoma models.

Normal Mammary Epithelial Cells Exhibit Protrusive Migration and Local Dissemination in a Collagen I Microenvironment.

We next asked whether a protrusive, disseminative response to collagen I was tumor specific. We isolated epithelial fragments (organoids) from the mammary glands of FVB mice and cultured them in Matrigel or 3 mg/mL collagen I (Fig. 4-4E). Again, the cell-migratory strategy and likelihood of local dissemination depended on the ECM microenvironment. In Matrigel, normal organoids migrated collectively to accomplish branching morphogenesis without protrusions into the ECM (Fig. 4-4 F and F'), as we previously reported (Ewald et al., 2008). In collagen I, organoids isolated from the same mouse migrated with

extensive protrusions, and cells disseminated locally into the ECM (Fig. 4-4 G and G'). To test the reversibility of the ECM-induced changes in migratory program, we next cultured normal epithelial fragments for 90 h in Matrigel or collagen I (Fig. 4-5 A–C) and then recovered and re-embedded the epithelium in either the same or the opposite matrix (Fig. 4-5D). Similar to the results observed in human carcinoma fragments (Fig. 4-1 G–H), the current, local ECM microenvironment dictated the migratory pattern, with collective epithelial migration in Matrigel (Fig. 4-5 E and G) and collective protrusive migration in collagen I (Fig. 4-5 F and H).

Mammary Carcinomas Exhibit Sustained Local Dissemination in Collagen I.

To understand better how epithelia transition from collective migration to individual cell dissemination, we quantified specific dissemination behaviors. Carcinoma fragments disseminated cells into collagen I throughout culture, with an average of 13 cells observed to leave each tumor mass (612 disseminating cells observed in 48 movies). We classified the disseminating tumor cells, based on previous morphological definitions (Friedl and Gilmour, 2009; Calvo et al., 2011), as mesenchymal, amoeboid, or collective (Fig. 4-6 A–D). Most carcinoma cells disseminated with a mesenchymal morphology (60%) as they protruded into the ECM and maintained an elongated morphology while migrating through the collagen I matrix (Fig. 4-6A). Other carcinoma cells (34%) disseminated in an amoeboid fashion as rounded cells that rolled or squeezed through the collagen I

matrix (Fig. 4-6B). In a minority of cases (6%), we also observed collective dissemination of groups of cells (Fig. 4-6C). Individual carcinoma fragments typically exhibited both mesenchymal and amoeboid dissemination (Fig. 4-6F). Most disseminated carcinoma cells remained motile in the ECM during the entire period of observation (69%), but 17% of the disseminated cells died, and 14% rejoined the tumor fragment (Fig. 4-6E). Once in the matrix, individual cancer cells were observed to convert between elongated and rounded morphologies, consistent with a previous report on melanoma cells (Sanz-Moreno et al., 2008). Despite local dissemination, carcinoma cells localized E-cadherin to intercellular borders in both Matrigel and collagen I (Fig. 4-6 H and J).

Protrusive Migration and Local Dissemination Are Transient Responses of Normal Myoepithelial Cells to Collagen I.

We previously observed no ECM-directed protrusions at the front of elongating mammary ducts in Matrigel or in vivo (Ewald et al., 2008). In contrast, collagen I induced acute protrusive and disseminative behaviors in both normal and malignant mammary epithelium (Fig. 4-6 F and G, 1–50 h). We observed dissemination from 79% (34/43 movies) of normal epithelial organoids (Fig. 4-4H), with an average of five cells leaving each epithelial group (210 disseminating cells observed in 43 movies), typically at the protrusive borders (Fig. 4-7 A and A”). Despite local dissemination, cells in the main epithelial group remained E-cadherin+ in both Matrigel and collagen I (Fig. 4-6 I and K). The main

difference in cell behavior between normal and carcinoma cells was that both protrusions and dissemination were transient in normal epithelial cells (Fig. 4-6G), because normal epithelial organoids ceased protrusive activity and reverted to a program of branching morphogenesis. The protrusive normal cells stained positive for the myoepithelial marker smooth muscle α-actin (SMA) (Fig. 4-4G') in 67/69 samples. Using a transgenic myoepithelial cell reporter to visualize the protrusive behavior in real time (Fig. 4-7B, keratin-14::actin-GFP, and Vaezi et al., 2002), we observed subcellular protrusions extending and retracting from single myoepithelial cells (Fig. 4-7B') as well as multicellular extensions of myoepithelial cells (Fig. 4-7B"). Live imaging revealed that the transition from protrusive to epithelial organization at the ECM interface (Fig. 4-7A') represented a change in cell behavior in individual myoepithelial cells (Fig. 4-7B'). In contrast, in Matrigel, myoepithelial cells remained closely adherent to the luminal epithelial cells and did not extend protrusions into the ECM (Ewald et al., 2008).

Normal Mammary Organoids Progressively Organize a Basement Membrane in Collagen I.

We observed a shift from protrusive to smooth, organized basal surfaces in normal mammary organoids cultured in collagen I (Fig. 4-7 A and B). To test whether this shift might relate to reestablishment of a basement membrane, we used antibodies to stain for laminin 111, laminin 332, and collagen IV. We observed a negative correlation between protrusions and basement membrane

organization. We observed single-cell protrusions (Fig. 4-7 C and C') and multicellular protrusive groups (Fig. 4-7 D and D') that extended through gaps in the laminin 111. Collagen IV staining was diffuse and incomplete in protrusive areas of normal epithelium (Fig. 4-7 E and E'). Late in culture in collagen I, normal epithelium typically became covered by a complete basement membrane that stained positive for all three markers (Fig. 4-7 F–H'). In contrast, at the ECM border of carcinoma fragments, we observed no laminin 111 and only scattered laminin 332 and incomplete collagen IV coverage (Fig. 4-7 I–K'). The most striking difference between tumor and normal epithelium in collagen I was the lack of laminin 111 along tumor borders, even late in culture (Fig. 4-7 I and I' vs. F and F').

ECM Microenvironment Has Minor Effects on Average Gene Expression.

Taken together, our results suggest that the pattern of epithelial migration and local dissemination are constrained by the local ECM microenvironment. We next sought to identify changes in RNA expression that could regulate these changes in cell behavior. Accordingly, we collected RNA from normal and malignant epithelium during active growth at day 4 of culture in either Matrigel or collagen I. Our goal was to compare average gene expression, so we isolated RNA from whole cultures. We hybridized the resulting RNA to Agilent single-color microarrays (Fig. 4-8A), with a minimum of three biologically independent microarray replicates per condition. To test the relative importance of the ECM to

gene expression, we performed complete-linkage hierarchical clustering. Normal samples clustered together regardless of their ECM microenvironment, distinct from all tumor samples (Fig. 4-8B). A principal component analysis confirmed that the first principal component was whether the epithelium was normal or tumor, and the second principal component was the ECM condition (Fig. 4-8C). Using a fold change ≥2 and a false discovery rate (FDR) ≤0.05 as criteria for significance we found only 15 or 16 genes were differentially expressed based on ECM condition in normal or tumor epithelium, respectively (Fig. 4-8 E–G). However, these genes did not have obvious mechanistic connections to dissemination (Fig. 4-8 F and G). Thus, the ECM microenvironment had a relatively small impact on average RNA expression, despite its large effects on migratory strategy and local dissemination. Our experimental design cannot exclude the possibility of changing gene expression within subpopulations of the epithelium.

Normal and Malignant Epithelia Differ in Their Expression of Cell-Adhesion Genes and Modifiers of the Extracellular Microenvironment.

In contrast to the modest differences observed between ECM environments, we found significant differences in gene expression between normal and malignant epithelia, even when cultured in the same ECM: 1,455 genes were differentially expressed between normal and tumor samples in Matrigel, and 599 genes were differentially expressed between normal and tumor

samples in collagen I (Fig. 4-8 D and E). These data suggest that normal epithelium and tumors accomplish morphologically similar migration processes despite widely different gene expression.

We next sought gene-expression signatures that might explain the sustained dissemination of carcinoma cells in collagen I (Fig. 5A). The epithelial-to-mesenchymal transition (EMT) has been proposed as a mechanism for cancer metastasis (Yang and Weinberg, 2008). Conceptual models of EMT center on decreased expression of E-cadherin and increased expression of genes such as N-cadherin and vimentin (Yang and Weinberg, 2008). However, the local dissemination we observed in collagen I was achieved with membrane-localized E-cadherin (Fig. 4-6 J and K). Surprisingly, E-cadherin RNA expression was not statistically significantly different between any two conditions (Fig. 4-9C). Furthermore, carcinoma cells displayed reduced levels of both N-cadherin and vimentin RNA, and the EMT regulators Snail-1, Snail-2, and Twist-1 also were not differentially expressed (defined as a greater-than-twofold change, FDR <0.05) in any condition (Fig. 4-9C). Our results suggest that a classic molecular EMT program is not activated in the tumor or in response to a collagen microenvironment, despite vigorous dissemination of cells into the ECM.

Importantly, our enrichment analysis using the Database for Annotation, Visualization and Integrated Discovery (DAVID) functional annotation revealed large and statistically significant differences between normal tissue and tumors in gene sets for cell adhesion and for proteins that function in the extracellular

space (Fig. 4-9 A and B). Analysis of mRNA expression of genes defined by structural motifs related to adhesion (e.g., cadherins and integrins) and of ECM and ECM-remodeling genes [e.g., collagens and matrix metalloproteinases (MMPs)] (Figs. 4-9B and 4-10) revealed widespread changes across gene families. Moreover, adhesion gene sets (cadherins, immunoglobulin cell-adhesion molecules, integrins, lectins, and other cell-adhesion molecules) were down-regulated in tumor relative to normal epithelium (~60% of differentially expressed genes higher in normal epithelium; $P \leq 0.0003$, Wilcoxon rank sum test). We specifically observed strong down-regulation in the cadherin gene family, with 75% of differentially expressed genes down-regulated in tumor relative to normal tissue ($P \leq 0.0001$, Wilcoxon rank sum test) (Fig. 4-9B). These data suggest that down-regulation of cell-adhesion genes may contribute to the sustained dissemination of carcinoma cells in collagen I.

Reduced Intercellular Adhesion Cooperates with a Collagen I Microenvironment to Permit Sustained Dissemination of Nontransformed Cells.

Recent breast cancer genome-sequencing efforts have revealed mutations in multiple families of cell-adhesion genes, including both classical cadherins and protocadherins (Leary et al., 2008). More than 70% of breast tumors in a recent study had mutations in a cell-adhesion gene, but few of these mutations occurred in more than one tumor (Velculescu et al., 2008). We chose

to test genetically whether altering cell adhesion is sufficient to enable sustained dissemination of nontransformed cells into collagen I. Because myoepithelial cells were the only protrusive or disseminative cells in our normal epithelial cultures, we focused on P-cadherin (Cdh3), a classical cadherin specifically expressed in myoepithelial but not luminal epithelial cells (Daniel et al., 1995). Deletion of P-cadherin in vivo results in precocious alveolar differentiation and luminal epithelial hyperplasia (Radice et al., 1997). We hypothesized that loss of P-cadherin might synergize with a collagen I-rich microenvironment to induce sustained myoepithelial dissemination. In Matrigel, we observed precocious branching (Fig. 4-11 A and B) and increased branching efficiency (Fig. 4-11C) in P-cadherin–null epithelial fragments but no protrusions or dissemination. In contrast, P-cadherin–null epithelial fragments explanted into collagen I disseminated more cells relative to controls, and dissemination was sustained throughout culture (Fig. 4-11 D–F). Disseminating cells were myoepithelial in nature (K14+) (Fig. 6H), and they survived and proliferated in collagen I (Fig. 4-11I). Indeed, we frequently observed nearly complete depletion of myoepithelial cells from the surface of P-cadherin–null organoids (Fig. 4-11H). We conclude that deletion of a cell-adhesion gene is sufficient to induce sustained myoepithelial dissemination in specific ECM microenvironments.

Discussion

In the present study we sought to isolate the specific role of the ECM in regulating collective epithelial migration and local dissemination by explanting fragments from the same epithelium into different ECM microenvironments. We found that murine and human mammary carcinomas cultured in 3D Matrigel were indolent or migrated collectively as a multilayered epithelium. Surprisingly, we observed local dissemination only rarely in Matrigel, even from metastatic human and murine mammary carcinomas. This result demonstrates that a metastatic genotype is not sufficient for local dissemination in all ECM microenvironments. In contrast, both normal and malignant mammary epithelium disseminated vigorously into collagen I.

Epithelial Cells Have ECM-Specific Migration Programs.

We observed large, ECM-specific differences in the pattern of collective migration and frequency of local dissemination with fragments from the same epithelium and identical culture medium. Moreover, these large differences in migratory pattern had few corresponding ECM-specific differences in gene expression. Despite the local dissemination of epithelial cells into collagen I, we did not detect a classic molecular EMT response in either normal or tumor tissue. However, all our transcriptome experiments compared RNA extracted from whole cultures, so our experimental design cannot exclude gene-expression or signaling changes in the cells directly in contact with the ECM. Comparable

molecular profiling studies comparing in situ and invasive breast cancer at the tissue level also have failed to define a gene signature predictive of invasion (Polyak, 2010).

Taken together, our data suggest that cancer cells could possess all the gene expression required for sustained local dissemination but remain indolent while the basement membrane remains intact. However, if the basement membrane were disrupted, the resulting direct contact between cancer cells and the stromal collagen I matrix could induce protrusive and disseminative cell behaviors rapidly. Breach of the basement membrane can be accomplished by MMP-based proteolysis by the cancer cells (Egeblad et al., 2010b, Wolf et al., 2007), by immune cells recruited during inflammatory processes, or by the actions of carcinoma-associated macrophages (DeNardo et al., 20009) or fibroblasts (Gaggioli et al., 2007). Consistent with this model, correlative studies in human breast tumors show that even microscopic breaks in the myoepithelium correlate with poor patient prognosis (Man and Sang, 2004).

Stromal ECM Is Not Sufficient for Sustained Dissemination.

The acute reaction of normal and carcinoma-derived epithelium to collagen I was very similar, because both exhibited protrusive migration and a mixture of amoeboid and mesenchymal dissemination. All the individual cell behaviors observed in the tumor fragments were observed in the normal fragments also. However, this similarity was transient: Normal epithelium

reestablished basement membrane coverage and underwent branching morphogenesis. In contrast, dissemination from carcinoma fragments was sustained throughout culture, and polarized epithelial architecture was not restored. Taken together, our data support a requirement for coordinate changes in both the cancer cell and the microenvironment to enable sustained dissemination. Our data also suggest that the final signal triggering invasion and local dissemination can be provided by changes in the ECM microenvironment rather than by genetic changes in the cancer cell. This suggestion is consistent with recent sequencing efforts that identified similar gene expression and mutations within in situ and invasive breast tumors (Polyak, 2010; Miron et al., 2010). Additionally, central fibrosis, which is characterized by high levels of collagen I, independently correlates negatively with patient outcome even among the most aggressive types of breast cancers (Kreike et al., 2007).

Cell–Cell Adhesion and the ECM Microenvironment Coordinately Regulate Dissemination.

Cell-adhesion genes frequently are down-regulated or mutated in metastatic human tumors (Vogelstein and Kinzler, 1993; Wood et al., 2007) and in our mouse carcinoma model. Our data support the hypothesis that deletion of a cell-adhesion gene can enable sustained dissemination of otherwise normal cells. Because the transiently disseminating normal cells were myoepithelial, we focused on P-cadherin (Radice et al., 1997), the major classical cadherin in

myoepithelial cells (Daniel et al., 1995). The phenotype of P-cadherin deletion in Matrigel and in vivo was luminal epithelial hyperplasia. However, the phenotype of P-cadherin deletion in collagen I was excess, sustained myoepithelial dissemination. The consequences of molecular perturbations therefore can be qualitatively different in different ECM microenvironments with respect to clinically important variables such as local dissemination. Our data are consistent with recent reports that myoepithelial cells are structurally and molecularly abnormal in nonmalignant regions adjacent to primary human breast tumors (Trujillo et al., 2011). Our data suggest that observed changes in the ECM composition of the tumor microenvironment in these regions may help explain these abnormalities (Trujillo et al., 2011).

Translational Implications for Breast Cancer.

Our data indicate that the cellular migratory strategy and the likelihood of local dissemination depend not only on the genetic state of the cancer cells but also on the ECM in the tumor microenvironment. Importantly, we demonstrated through matrix-switching experiments that, even after an ECM-induced transition to protrusive migration and local dissemination, human malignant carcinomas can revert to confined, nonprotrusive growth in response to basement membrane signals. Our data are consistent with past work on the normalization of tumor architecture by basement membrane signals such as laminin 111 (Weaver et al., 1997; Nelson and Bissell, 2006; Gudjonsson et al., 2002) and on the invasion-

associated behavior of cells in collagen I (Egeblad et al., 2010b; Provenzano et al., 2006; Greenburg and Hay, 1982).

Future Directions.

It is now necessary to isolate the molecular basis for the differential effects of different ECM microenvironments on collective cell migration and dissemination. Collagen I and Matrigel have distinct rigidity, protein composition, and supramolecular organization. It remains unclear which of these variables is most important to dissemination, although past studies suggest a role for increased matrix rigidity in cancer progression (Egeblad et al., 2010b). Our data also suggest that deletion of a single adhesion gene is sufficient to induce sustained dissemination of nontransformed cells into a stromal matrix such as collagen I. It will be important to determine whether deletion of other adhesion genes will promote local dissemination similarly. Because the collective migration strategy of epithelial cells differs in different ECMs, it also is possible that specific genetic perturbations contribute to invasion and dissemination only in specific microenvironmental contexts.

Materials and Methods

Isolation of Primary Murine Mammary Organoids. We isolated mouse mammary organoids from normal mice using previously described techniques (Ewald et al., 2008; Fata et al., 2007). Briefly, we dissected the no. 3 and no. 4 mammary glands and digested this tissue into epithelial fragments by a combination of mechanical disruption and collagenase/trypsin digestion. We then separated these fragments from single cells by differential centrifugation. The final pellet was composed of epithelial fragments, each containing several hundred cells; we term these fragments “organoids.” Tumors were harvested from mice at 12–16 wk of age, when carcinomas were poorly differentiated. We surgically isolated the largest tumor in each mouse and processed it as above. Any incompletely digested large tumor fragments were removed before differential centrifugation. We also added additional rounds of differential centrifugation as needed to remove single cells. This protocol was adapted further for isolation of organoids from primary human mammary tumor.

Isolation of Primary Human Mammary Tumor Organoids. Primary human breast tumor specimens were acquired from the Cooperative Human Tissue Network (CHTN), a program funded by the National Cancer Institute. Use of these anonymous samples was granted exemption status by the local Institutional Review Board according to the Code of Federal Regulations (45 CFR 46.101[b]). Tissue samples were shipped overnight on wet ice and upon receipt were washed 3-5 times with PBSA to reduce traces of blood. Tissues

were then cut into small fragments using a sterile razor blade and then incubated in collagenase overnight, rocking at 37°C (typically 10 ml of solution in a 15 ml Falcon tube). Digested tumor fragments were then pelleted in a centrifuge at 100x g for 3 minutes, and the supernatant was discarded. The PBSA wash solution consisted of 1X Dulbecco's PBS supplemented with Penn/Strep (penicillin at 200 U/ml and streptomycin at 200 µg/ml; Invitrogen 15140-155) and fungizone (~5 µg/ml; Invitrogen 15290-018). Collagenase solution consisted of DMEM (high glucose, Sigma D6546), 2 mM glutamine (5.1 ml), Penn/Strep (as above), and 1 mg/ml collagenase I (Invitrogen 17100-017). Human mammary epithelial tissue was cultured in mammary epithelial medium, which consisted of DMEM (Sigma D6546), 2 mM glutamine (ATCC or Invitrogen), Penn/Strep (100 U/ml penicillin / 100 µg/ml streptomycin), 10 mM Hepes (Sigma H3375-250g), 0.075% BSA (Sigma A8412), 10 ng/ml cholera toxin (Sigma C8052), 0.47 µg/ml hydrocortisone (Sigma H6909), 5 µg/ml Insulin (Sigma I0516), and 5 ng/ml EGF (Invitrogen 13247-051)).

Primary Murine Mammary Organoid Culture. We embedded organoids derived from normal and tumor epithelium in 3D Matrigel (354230; BD Biosciences) or rat-tail collagen I (354236; BD Biosciences). Cultures were set up in 24-well coverslip-bottomed plates (EK-42892; E&K Scientific) or in two-well or four-well coverslip-bottomed chambers (155383; Nunc). Acid-solubilized rat-tail collagen I gels (3 mg/mL collagen I, pH 7–7.5) were prepared as described below. For each matrix, organoids were mixed to yield a suspension of two or

three organoids/μL. A 100-μL suspension of organoids was plated in each well on a 37-°C heating block, followed by incubation at 37 °C for 45 min to allow polymerization. Epithelial fragments in collagen I were plated on top of an underlay of cell-free collagen I of the same concentration. Murine samples were cultured in 1 mL of 2.5-nM FGF2 in murine organoid medium (Ewald et al., 2008).

Time-Lapse Differential Interference Contrast Microscopy. Live imaging of normal and tumor murine organoids was conducted using a Zeiss Cell Observer system with a Zeiss AxioObserver Z1 and an AxioCam MRM camera. In general, images were collected at 20-min intervals with exposure times of ∼250 ms. Some of the movies of human tumor were collected on a Zeiss Axiovert S-100 microscope and a Cohu CCD camera, as previously reported (2). Temperature was held at 37 °C and CO2 at 5%.

Gene-Expression Analysis of Normal and Tumor Fragments in Parallel ECM Conditions. In total, four different conditions were profiled (tumor vs. normal; collagen I vs. Matrigel); each was replicated at least three times in biologically independent experiments. Sample preparation, labeling, and array hybridizations were performed according to standard protocols from the University of California, San Francisco Shared Microarray Core Facilities and Agilent Technologies (http://www.arrays.ucsf.edu and http://www.agilent.com). Equal amounts of Cy3-labeled target were hybridized to Agilent whole mouse genome 4 × 44K Ink-jet arrays. Arrays were scanned using the Agilent microarray scanner, and raw

signal intensities were extracted with Feature Extraction v. 9.1 software (Agilent). Samples were confirmed to be of good quality and were quantile normalized using R/Bioconductor packages. Pairwise differentially expressed genes were detected using the limma package in R. q-Values ≤0.05 were deemed statistically significant. A stand-alone program written in Java was developed to interface with the R program via the command-line to generate heatmaps for publication (available upon request). Genes changed by twofold or more and with q-values ≤0.05 were used as input for DAVID Gene Set Analysis (Huang et al., 2009). Gene sets associated with structurally similar gene families (including cell–cell adhesion, cytoskeletal networks, and actin–myosin contractility) were curated manually from Mouse Genome Informatics and Interpro (available upon request). Lists of cell-adhesion genes were cross-referenced further with OKCAM, an online database of cell-adhesion molecules (Li et al., 2009). Microarray data have been made available on the National Center for Biotechnology Information's GEO database (accession no. GSE39173).

P-Cadherin–Deletion Experiments. The P-cadherin and mT/mG mouse lines were acquired from the Jackson Laboratory. The keratin-14::actin-GFP transgenic line (Vaezi et al., 2002; Radice et al., 1997; Muzumdar et al., 2007) was a kind gift of Elaine Fuchs (The Rockefeller University, New York). P-cadherin−/− and P-cadherin+/−, mT/mG, K14-Actin-GFP mammary organoids were isolated as described above. Organoids were grown in Matrigel or collagen I with 2.5 nM FGF2. Branching in Matrigel was quantified on day 7 in three

independent biological replicates and scored as three or more buds per organoid. Organoids were grown in 3 mg/mL collagen I for 4–5 d, and cell dissemination was quantified from differential interference contrast (DIC) and confocal time-lapse movies in three independent biological replicates.

Matrix Switching Experiments. In some experiments, epithelial organoids were cultured in one matrix environment (e.g. Matrigel) and then switched to another after several days of culture. To remove epithelial organoids from Matrigel, the gel was transferred manually to a 1.7 ml Eppendorf tube and dispersed into culture medium by repeated pipetting. To remove organoids from collagen I, the gel was transferred manually to a 1.7 ml Eppendorf tube, briefly treated with collagenase solution (prepared as in (1, 2)), and then dispersed into culture medium by repeated pipetting. Recovered organoids were centrifuged at 500x g for 1-2 minutes, the supernatant was discarded, and the organoids were embedded in either Matrigel or collagen I.

Antibody Staining. Organoids cultured in both Matrigel and collagen I were fixed with 4% PFA for 20 min, rinsed two times in PBS for 10 min, permeabilized with 0.5% Triton X-100 in PBS for 20 min, and rinsed two times in PBS for 10 min. Samples were then embedded in OCT and frozen at -80°C. OCT blocks were sectioned by cryostat at -20°C at 100 µm thickness. Samples on slides were rinsed two times in PBS for 10 min, blocked in 10% fetal bovine serum in PBS for 1 hour, incubated with primary antibodies overnight at 4°C, and rinsed two times in PBS. Slides were incubated with secondary antibodies for 2-3h and

rinsed two times in PBS for 10 min. Slides were finally mounted with Fluoromount (Sigma F4680) and sealed with coverslips. F-actin was stained with Alexa 647 Phallodin (1:100) (Invitrogen A22287), and nuclei were stained with DAPI (1:1000) (Invitrogen D3571). Immunofluorescent stainings for each antibody were done three independent times and imaged for at least 15 organoids per condition each time. Primary antibodies were mouse anti-laminin 1α (1:100) (R&D System MAB2549), rabbit anti-laminin 5 (1:1000) (gift of Peter Marinkovich, Stanford University and Monique Aumailley, University of Cologne, Germany), goat anti-collagen IV (1:80) (Millipore AB769), rat anti-E-cadherin (1:250) (Invitrogen 13-1900), and FITC-conjugated mouse anti-SMA (1:250) (Sigma F3777).

Confocal Imaging. Confocal imaging was done on a Solamere Technology Group spinning disk confocal microscope (Ewald et al., 2008) with a 40x C-Apochromat objective lens (Zeiss Microimaging). Acquisition of both fixed and time-lapse images was done using a combination of μManager (Edelstein et al, 2010) and Piper (Stanford Photonics). Levels were adjusted across entire images in Adobe Photoshop to maximize clarity in the figures.

Gene Expression Analysis of Normal and Tumor Fragments in Parallel ECM Conditions. Normal fragments were obtained from normal FVB mammary gland. Tumor fragments were isolated from advanced carcinomas from the MMTV-PyMT mouse model. Fragments were embedded in 3D Matrigel or collagen I and cultured in serum-free organoid media supplemented with 2.5 nM FGF2 (Ewald et al., 2008; Ewald, 2010). In total, 4 unique conditions were profiled (tumor vs.

normal; collagen I vs. Matrigel), each replicated at least 3 times with biologically independent replicates (Table S4-1). Each array replicate corresponds to independent mice unless otherwise noted. These experiments were performed in two batches. In batch #1, tissue was taken from four mice, labeled A-D, with each group having one sample from each mouse except for D. In batch #2, each tumor fragment was derived from a PyMT mouse that was split into parts for culture in different microenvironments and time-points. BWM4F RNA was hybridized twice: once in batch #1 and again in batch #2. After averaging BWM4F, there were a total of 13 unique arrays.

Microarray Sample Preparation. Sample preparation, labeling, and array hybridizations were performed according to standard protocols from the UCSF Shared Microarray Core Facilities and Agilent Technologies (http://www.arrays.ucsf.edu and http://www.agilent.com). Total RNA quality was assessed using a Pico Chip on an Agilent 2100 Bioanalyzer (Agilent Technologies, Palo Alto, CA). RNA was amplified and labeled with Cy3-CTP using the Agilent low RNA input fluorescent linear amplification kits following the manufacturers protocol (Agilent). Labeled cRNA was assessed using the Nanodrop ND-100 (Nanodrop Technologies, Inc., Wilmington DE), and equal amounts of Cy3-labeled target were hybridized to Agilent whole mouse genome 4x44K Ink-jet arrays (Agilent). Hybridizations were performed for 14 hrs, according to the manufacturers protocol (Agilent). Arrays were scanned using the Agilent microarray scanner (Agilent), and raw signal intensities were extracted

with Feature Extraction v9.1 software (Agilent).

Quality Control and Normalization Analyses of Microarray Data. Analyses were conducted using R and the Bioconductor packages Agi4x44PreProcess, ArrayQualityMetrics, and ggplot2. Plain text files generated from Agilent Feature Extraction were parsed into ExpressionSet objects. The ProcessedSignal intensities, generated by Agilent Feature Extraction, were used in this analysis. Array quality was assessed using box plots, hierarchical clustering, and MA plots generated by the ArrayQualityMetrics package (Reimers, 2010). The array dataset was then normalized using quantile normalization without background subtraction. Following this normalization, as anticipated, boxplots of gMedian Intensity were then all on the same scale. Batch effects were evaluated using hierarchical clustering and principle component analysis (Leek et al., 2010) arrays clearly segregate according to tumor and time, rather than by batch. Since RNA from sample BWMF4 was applied to two chips from two batches (BWMF4 and BWMF4.1), post-normalized intensities for these two samples were averaged. Otherwise, all other samples were biologic rather than technical replicates.

Probe to Gene Mapping. Probes were mapped to their corresponding genes based on identifiers supplied by the Agilent file GEO GPL4134-5647. RefSeq IDs, Refseq Predicted, GenBank Accession No., EmblID, Entrez Gene ID, UNIGENE_ID, Wiki_Genename, and Ensembl_transcript_ID were used to map to ENSEMBL gene IDs using Biomart, with the mouse genome sequence

"ENSEMBL Genes 58, NCBIM37 Mus Musculus". Altogether, probes were mapped to 19693 genes, selecting the probe with the maximal intensity across conditions.

Clustering and Differential Gene Expression Analyses. Hierarchical clustering and principle component analysis was done using the limma and affycoretools packages (Smyth, 2004). Pairwise differentially expressed genes were detected using the limma package in R. Q-values less than 0.05 were deemed statistically significant. A program was written in Java to generate heatmaps for publication. Positive enrichment scores such as log fold changes or modified t statistics correspond to enrichment in tumor or collagen I matrix conditions. Negative enrichment scores correspond to enrichment in normal or Matrigel conditions. Genes 2-fold changed or greater and with FDR less than or equal to 0.05 were used as input for DAVID Gene Set Analysis (Huang da et al., 2009).

Gene Family Analysis. Gene sets associated with structurally similar gene families were manually curated from Mouse Genome Informatics and Interpro. These gene sets include genes involved in cell-cell adhesion, cytoskeletal networks, and actin-myosin contractility. Cell adhesion gene lists were further cross-referenced with OKCAM, an online cell adhesion database (Li et al., 2009). For gene family heatmaps, we constructed a linear model incorporating tissue source (normal or tumor) and microenvironment (Matrigel or collagen I) for each gene using the lmFit function in the limma package. Genes were sorted

according to their enrichment with respect to normal versus tumor conditions.

Author contribution

K-V. N-N principally designed, performed and analyzed the ECM experiments.

K-V. N-N also contributed to writing the manuscript.

Supplemental data

Movies will be available on the ASCB Cell: An Image Library website

References

1. Calvo F, Sanz-Moreno V, Agudo-Ibáñez L, Wallberg F, Sahai E, Marshall CJ, Crespo P. (2011) RasGRF suppresses Cdc42-mediated tumour cell movement, cytoskeletal dynamics and transformation. Nat Cell Biol 13(7):819-826.
2. Conklin MW, Eickhoff JC, Riching KM, Pehlke CA, Eliceiri KW, Provenzano PP, Friedl A, Keely PJ. (2011) Aligned collagen is a prognostic signature for survival in human breast carcinoma. Am J Pathol. 178(3):1221-32.
3. Daniel CW, Strickland P, Friedmann Y. (1995) Expression and functional role of E- and P-cadherins in mouse mammary ductal morphogenesis and growth. Dev Biol. 169(2):511-9.
4. Debnath J, Brugge JS (2005) Modelling glandular epithelial cancers in three-dimensional cultures. Nat Rev Cancer 5(9):675-688.
5. DeNardo DG, Barreto JB, Andreu P, Vasquez L, Tawfik D, Kolhatkar N, Coussens LM. (2009) CD4(+) T cells regulate pulmonary metastasis of mammary carcinomas by enhancing protumor properties of macrophages. Cancer Cell 16(2):91-102.
6. Edelstein A, Amodaj N, Hoover K, Vale R, Stuurman N (2010) Computer control of microscopes using μManager. Curr Protoc Mol Biol. Chapter 14:Unit14.20.
7. Egeblad M, Ewald AJ, Askautrud HA, Truitt ML, Welm BE, Bainbridge E, Peeters G, Krummel MF, Werb Z. (2008) Visualizing stromal cell dynamics in different tumor microenvironments by spinning disk confocal microscopy. Dis Model Mech 1(2-3):155-167; discussion 165.
8. Egeblad M, Nakasone ES, Werb Z (2010) Tumors as organs: complex tissues that interface with the entire organism. Dev Cell 18(6):884-901.
9. Egeblad M, Rasch MG, & Weaver VM (2010) Dynamic interplay between the collagen scaffold and tumor evolution. Curr Opin Cell Biol 22(5):697-706.
10. Ewald AJ, Brenot A, Duong M, Chan BS, & Werb Z (2008) Collective epithelial migration and cell rearrangements drive mammary branching morphogenesis. Dev Cell 14(4):570-581.
11. Ewald AJ, Huebner RJ, Palsdottir H, Lee JK, Perez MJ, Jorgens DM, Tauscher AN, Cheung KJ, Werb Z, Auer M (2012) Mammary collective cell migration involves transient loss of epithelial features and individual cell migration within the epithelium. J Cell Sci. 125(Pt 11):2638-54.
12. Ewald AJ (2013) Practical Considerations for Long-Term Time-Lapse Imaging of Epithelial Morphogenesis in Three-Dimensional Organotypic Cultures. Cold Spring Harb Protoc. 2013 Feb 1;2013(2):100-17.
13. Fata JE1, Mori H, Ewald AJ, Zhang H, Yao E, Werb Z, Bissell MJ. (2007) The MAPK(ERK-1,2) pathway integrates distinct and antagonistic signals from TGFalpha and FGF7 in morphogenesis of mouse mammary epithelium. Dev Biol 306:193-207.

14. Friedl P, Hegerfeldt Y, & Tusch M (2004) Collective cell migration in morphogenesis and cancer. Int J Dev Biol 48(5-6):441-449.
15. Friedl P, Gilmour D. (2009) Collective cell migration in morphogenesis, regeneration and cancer. Nat Rev Mol Cell Biol. 10(7):445-57.
16. Gaggioli C, Hooper S, Hidalgo-Carcedo C, Grosse R, Marshall JF, Harrington K, Sahai E.. (2007) Fibroblast-led collective invasion of carcinoma cells with differing roles for RhoGTPases in leading and following cells. Nat Cell Biol 9(12):1392-1400.
17. Greenburg G & Hay ED (1982) Epithelia suspended in collagen gels can lose polarity and express characteristics of migrating mesenchymal cells. J Cell Biol 95(1):333-339.
18. Griffith LG, Swartz MA (2006) Capturing complex 3D tissue physiology in vitro. Nat Rev Mol Cell Biol 7(3):211-224.
19. Gudjonsson T, L Ronnov-Jessen, R Villadsen, MJ Bissell, OW Petersen. (2003). To create the correct microenvironment: three-dimensional heterotypic collagen assays for human breast epithelial morphogenesis and neoplasia. Methods 30:247-55.
20. Guy CT, Cardiff RD, & Muller WJ (1992) Induction of mammary tumors by expression of polyomavirus middle T oncogene: a transgenic mouse model for metastatic disease. Mol Cell Biol. 12(3):954-961.
21. Hagios C, Lochter A, Bissell MJ (1998) Tissue architecture: the ultimate regulator of epithelial function? Philos Trans R Soc Lond B Biol Sci 353(1370):857-870.
22. Hanahan D, Weinberg RA (2011) Hallmarks of cancer: the next generation. Cell. 144: 646–674.
23. Herschkowitz JI, Simin K, Weigman VJ, Mikaelian I, Usary J, Hu Z, Rasmussen KE, Jones LP, Assefnia S, Chandrasekharan S, Backlund MG, Yin Y, Khramtsov AI, Bastein R, Quackenbush J, Glazer RI, Brown PH, Green JE, Kopelovich L, Furth PA, Palazzo JP, Olopade OI, Bernard PS, Churchill GA, Van Dyke T, Perou CM. (2007) Identification of conserved gene expression features between murine mammary carcinoma models and human breast tumors. Genome Biol 8(5):R76.
24. Huang da W, Sherman BT, Lempicki RA (2009) Systematic and integrative analysis of large gene lists using DAVID bioinformatics resources. Nat Protoc 4(1):44-57.
25. Kreike B, van Kouwenhove M, Horlings H, Weigelt B, Peterse H, Bartelink H, van de Vijver MJ. (2007) Gene expression profiling and histopathological characterization of triple-negative/basal-like breast carcinomas. Breast Cancer Res. 9(5):R65.
26. Leary RJ, Lin JC, Cummins J, Boca S, Wood LD, Parsons DW, Jones S, Sjöblom T, Park BH, Parsons R, Willis J, Dawson D, Willson JK, Nikolskaya T, Nikolsky Y, Kopelovich L, Papadopoulos N, Pennacchio LA, Wang TL, Markowitz SD, Parmigiani G, Kinzler KW, Vogelstein B, Velculescu VE. (2008) Integrated analysis of homozygous deletions, focal amplifications, and sequence alterations in breast and colorectal cancers.

Proc Natl Acad Sci U S A 105(42):16224-16229.
27. Leek JT, Scharpf RB, Bravo HC, Simcha D, Langmead B, Johnson WE, Geman D, Baggerly K, Irizarry RA. (2010) Tackling the widespread and critical impact of batch effects in high-throughput data. Nat Rev Genet 11(10):733-739.
28. Levental KR, H Yu, L Kass, JN Lakins, M Egeblad, JT Erler, SF Fong, K Csiszar, A Giaccia, W Weninger, M Yamauchi, DL Gasser, VM Weaver. (2009). Matrix crosslinking forces tumor progression by enhancing integrin signaling. Cell 139:891-906.
29. Li CY, Liu QR, Zhang PW, Li XM, Wei L, Uhl GR. (2009) OKCAM: an ontology-based, human-centered knowledgebase for cell adhesion molecules. Nucleic Acids Res 37(Database issue):D251-260.
30. Lin EY, Jones JG, Li P, Zhu L, Whitney KD, Muller WJ, Pollard JW. (2003) Progression to malignancy in the polyoma middle T oncoprotein mouse breast cancer model provides a reliable model for human diseases. Am J Pathol. 163(5):2113-2126.
31. Man YG, Sang QX (2004) The significance of focal myoepithelial cell layer disruptions in human breast tumor invasion: a paradigm shift from the "protease-centered" hypothesis. Exp Cell Res. 301(2):103-118.
32. Miron A, Varadi M, Carrasco D, Li H, Luongo L, Kim HJ, Park SY, Cho EY, Lewis G, Kehoe S, Iglehart JD, Dillon D, Allred DC, Macconaill L, Gelman R, Polyak K. (2010) PIK3CA mutations in in situ and invasive breast carcinomas. Cancer Res 70(14):5674-5678.
33. Muzumdar MD, Tasic B, Miyamichi K, Li L, Luo L. (2007). A global double-fluorescent Cre reporter mouse. Genesis. 45:593-605.
34. Nelson CM, MJ Bissell. (2005). Modeling dynamic reciprocity: engineering three-dimensional culture models of breast architecture, function, and neoplastic transformation. Semin Cancer Biol 15:342-52.
35. Nelson CM, Bissell MJ. (2006) Of extracellular matrix, scaffolds, and signaling: tissue architecture regulates development, homeostasis, and cancer. Annu Rev Cell Dev Biol. 22:287-309.
36. Nguyen DX, Bos PD, & Massague J (2009) Metastasis: from dissemination to organ-specific colonization. Nat Rev Cancer 9(4):274-284.
37. Petersen OW, Ronnov-Jessen L, Howlett AR, Bissell MJ (1992) Interaction with basement membrane serves to rapidly distinguish growth and differentiation pattern of normal and malignant human breast epithelial cells. Proc Natl Acad Sci U S A 89(19):9064-9068.
38. Polyak K (2010) Molecular markers for the diagnosis and management of ductal carcinoma in situ. J Natl Cancer Inst Monogr 2010(41):210-213.
39. Polyak K, Haviv I, & Campbell IG (2009) Co-evolution of tumor cells and their microenvironment. Trends in Genetics 25(1):30-38.
40. Provenzano PP, Eliceiri KW, Campbell JM, Inman DR, White JG, Keely PJ. (2006) Collagen reorganization at the tumor-stromal interface facilitates local invasion. BMC Med.4(1):38.

41. Radice GL, Ferreira-Cornwell MC, Robinson SD, Rayburn H, Chodosh LA, Takeichi M, Hynes RO. (1997) Precocious mammary gland development in P-cadherin-deficient mice. J Cell Biol. 139(4):1025-32.
42. Reimers M (2010) Making informed choices about microarray data analysis. PLoS Comput Biol 6(5):e1000786.
43. Simian M, Y Hirai, M Navre, Z Werb, A Lochter, MJ Bissell. (2001). The interplay of matrix metalloproteinases, morphogens and growth factors is necessary for branching of mammary epithelial cells. Development 128:3117-31.
44. Smyth GK (2004) Linear models and empirical bayes methods for assessing differential expression in microarray experiments. Stat Appl Genet Mol Biol 3:Article3.
45. Vaezi A, Bauer C, Vasioukhin V, Fuchs E (2002) Actin cable dynamics and Rho/Rock orchestrate a polarized cytoskeletal architecture in the early steps of assembling a stratified epithelium. Dev Cell. 3(3):367-381.
46. Velculescu VE (2008) Defining the blueprint of the cancer genome. Carcinogenesis 29(6):1087-1091.
47. Vogelstein B, Kinzler KW (1993) The multistep nature of cancer. Trends Genet 9(4):138-141.
48. Weaver VM, Petersen OW, Wang F, Larabell CA, Briand P, Damsky C, Bissell MJ. (1997) Reversion of the malignant phenotype of human breast cells in three-dimensional culture and in vivo by integrin blocking antibodies. J Cell Biol 137(1):231-245.
49. Williams JM, Daniel CW. (1983) Mammary ductal elongation: differentiation of myoepithelium and basal lamina during branching morphogenesis. Dev Biol. 97(2):274-90.`
50. Wolf K, Wu YI, Liu Y, Geiger J, Tam E, Overall C, Stack MS, Friedl P. (2007) Multi-step pericellular proteolysis controls the transition from individual to collective cancer cell invasion. Nat Cell Biol 9(8):893-904.
51. Wood LD, Parsons DW, Jones S, Lin J, Sjöblom T, Leary RJ, Shen D, Boca SM, Barber T, Ptak J, Silliman N, Szabo S, Dezso Z, Ustyanksky V, Nikolskaya T, Nikolsky Y, Karchin R, Wilson PA, Kaminker JS, Zhang Z, Croshaw R, Willis J, Dawson D, Shipitsin M, Willson JK, Sukumar S, Polyak K, Park BH, Pethiyagoda CL, Pant PV, Ballinger DG, Sparks AB, Hartigan J, Smith DR, Suh E, Papadopoulos N, Buckhaults P, Markowitz SD, Parmigiani G, Kinzler KW, Velculescu VE, Vogelstein B. (2007) The genomic landscapes of human breast and colorectal cancers. Science 318(5853):1108-1113.
52. Yang J, Weinberg RA (2008) Epithelial-mesenchymal transition: at the crossroads of development and tumor metastasis. Dev Cell. 14(6):818-829.

Figure 4-1

ECM microenvironments modulate the pattern of collective migration and local dissemination in human mammary carcinomas. (A) Schematic description of isolation and 3D culture of human mammary carcinoma fragments. In the first round of culture, tumor fragments were embedded in either 3D Matrigel or collagen I. In the second round of culture, the same tumor fragments were freed from the 3D gels and were re-embedded in the same or were swapped to the other microenvironment. (B–C") Representative DIC time-lapse sequences of human mammary carcinomas in Matrigel (B) or collagen I (C). (B' and C') Enlarged views of B and C at 30 h showing the smooth and protrusive leading fronts, respectively. (B" and C") Micrographs of the border of the same mammary carcinoma embedded in Matrigel or collagen and stained with phalloidin–F-actin and DAPI. (D–G) Representative frames of DIC time-lapse movies of human mammary carcinomas switched from Matrigel to Matrigel (M–M) (D), Matrigel to collagen I (M–C) (E), collagen I to Matrigel (C–M) (F), or collagen I to collagen I (C–C) (G) at 0 or 1 h in culture (Left) or 45 h in culture (Right). (H and I) Bar graphs showing the number of tumor fragments in each ECM condition with protrusive migration (H) or local dissemination (E) relative to the number of primary human tumor fragments analyzed in each condition.

Figure 4-1

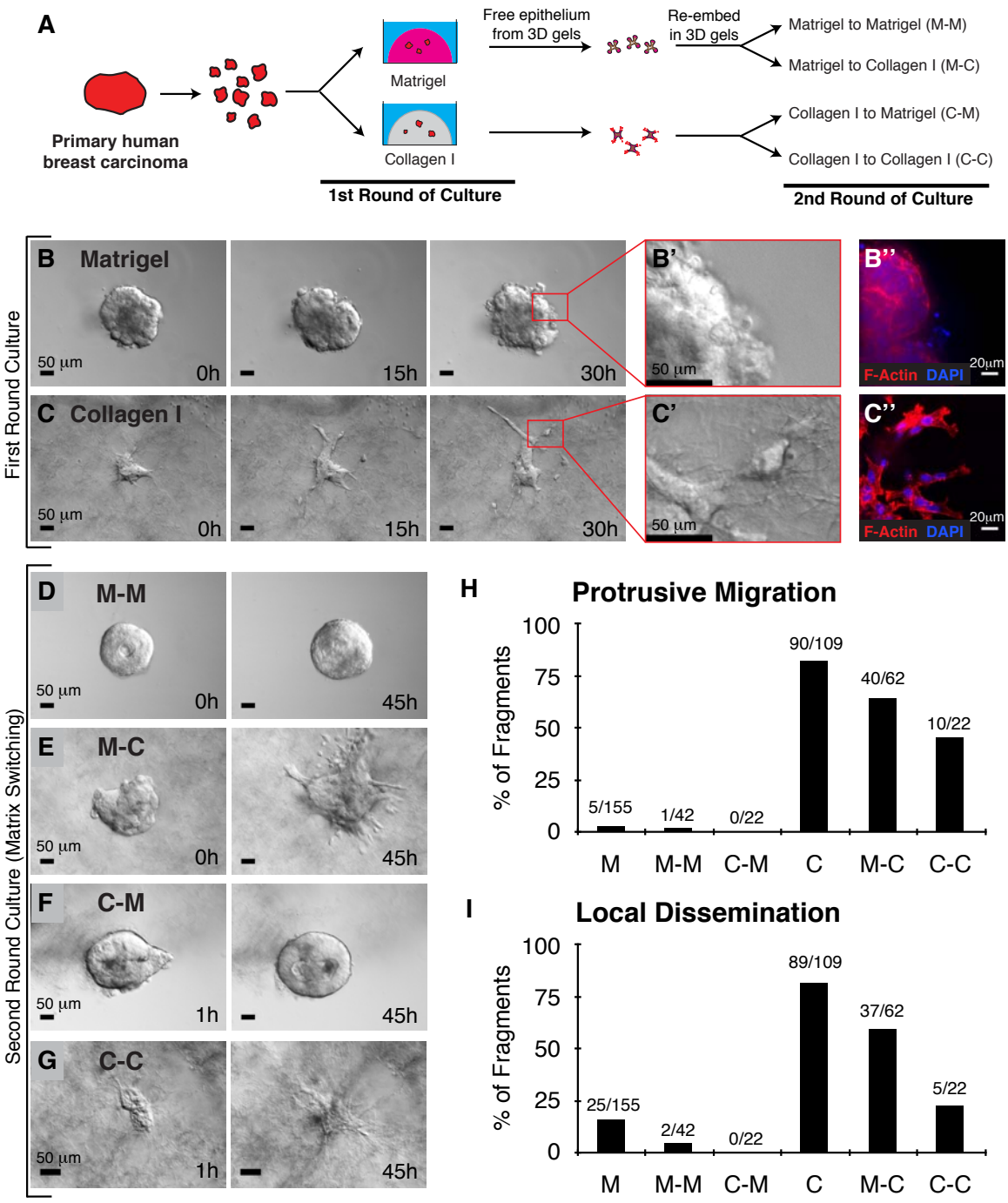
A
Primary human breast carcinoma
Matrigel
Collagen I
1st Round of Culture
Free epithelium from 3D gels
Re-embed in 3D gels
Matrigel to Matrigel (M-M)
Matrigel to Collagen I (M-C)
Collagen I to Matrigel (C-M)
Collagen I to Collagen I (C-C)
2nd Round of Culture
First Round Culture
B Matrigel
C Collagen I
B'
C'
B''
C''
50 μm
0h
15h
30h
F-Actin DAPI
20μm
Second Round Culture (Matrix Switching)
D M-M
E M-C
F C-M
G C-C
45h
1h
H
Protrusive Migration
% of Fragments
5/155
1/42
0/22
90/109
40/62
10/22
M
M-M
C-M
C
M-C
C-C
I
Local Dissemination
25/155
2/42
0/22
89/109
37/62
5/22

Figure 4-2

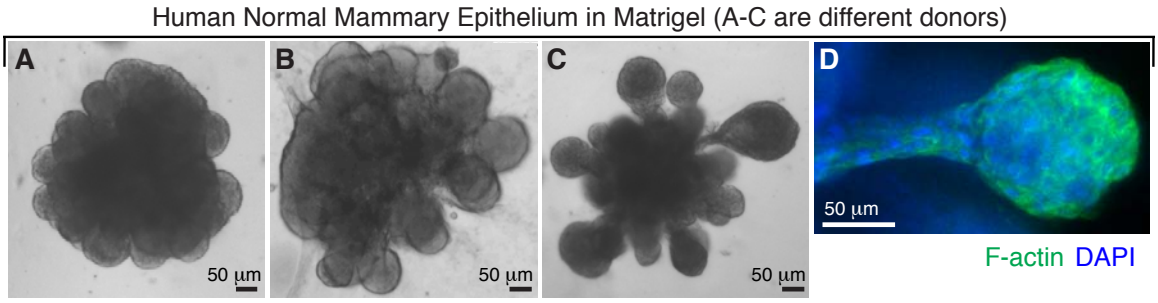

E

Sample	Age	Max Size	Pathologic Stage	# Nodes +	Mitoses	Grade	Estrogen Receptor
T01	61	0.9 cm	pT1bN0MX (Stage I)	0 of 2	5 /10 HPF	Low	90% +
T02	66	2.2 cm	pT2N1MX (Stage IIb)	1 of 2	1 / 10 HPF	Int.	60-70% +
T03	53	3.7 cm	pT2N3MX (Stage IIIc)	20 of 20	24 / 10 HPF	High	Not Reported
T04	40	Post-Chemo	ypT1micN2MX (Stage I)	2 of 10	4 / 10 HPF	Low	Not Reported
T05	30	7.5 cm	pT3N2MX (Stage IIIa)	4 of 19	17 / 10 HPF	Int.	10% +
T06	50	3.5 cm	pT2N1MX (Stage IIb)	1 of 22	Ki67: 25%	High	100%
T07	51	2.7 cm	pT2N2MX (Stage IIa)	6 of 18	KI67: 30%	High	70%

Normal human mammary epithelium undergoes branching morphogenesis in Matrigel. (A-C) Representative bright-field images of human mammary branching morphogenesis in Matrigel. (D) F-actin and DAPI staining showing the non-protrusive front of a human mammary end bud in Matrigel. (E) Pathologic stage and characteristics of human tumor samples used in this study. Six of these samples grew well in culture and exhibited strong ECM dependence in migration strategy and dissemination frequency (T01-03 and T05-T07). T04 was from a patient who had previously received chemotherapy and the residual tissue was largely intermediate ductal carcinoma in situ and fibroadenoma. T04 explants did not grow well in 3D culture. Human tissue was acquired from the Collaborative Human Tissue Network and the Johns Hopkins Hospital.

Figure 4-3

Despite intra- and inter-tumor heterogeneity, the extracellular matrix microenvironment regulates collective migration and dissemination in human breast tumors. (A-C) Representative images are presented for the range of morphologies observed in epithelial fragments from 3 human tumors when cultured in either Matrigel (top row) or collagen I (bottom row). All scale bars are 50 μm.

Figure 4-3

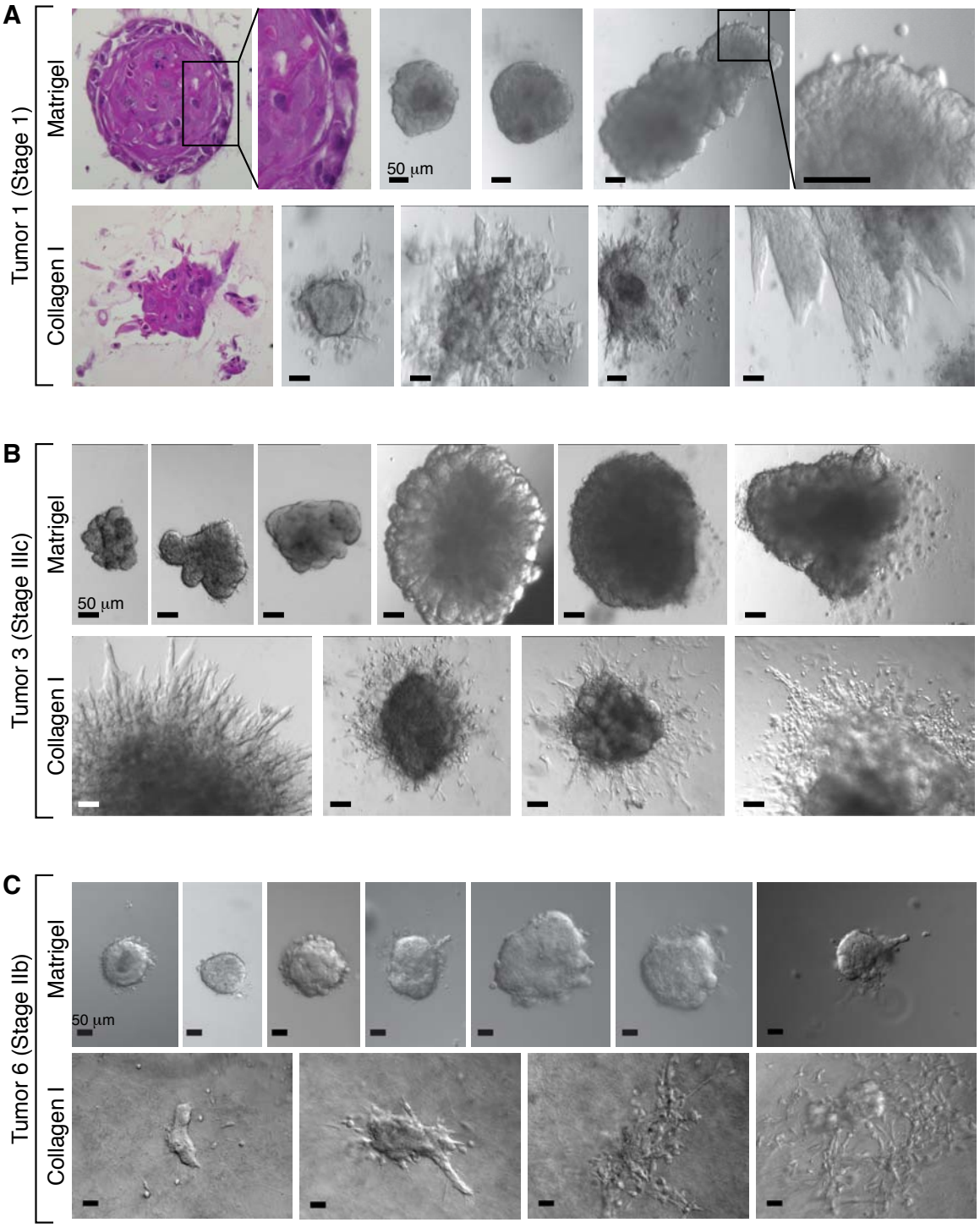
A
Tumor 1 (Stage 1)
Matrigel
Collagen I
50 μm
B
Tumor 3 (Stage IIIc)
Matrigel
Collagen I
50 μm
C
Tumor 6 (Stage IIb)
Matrigel
Collagen I
50 μm

Figure 4-4

The ECM governs the migratory pattern and disseminative behavior of both tumor and normal murine mammary epithelium. (A) Schematic description of isolation and 3D culture of murine tumor fragments. (B and C) Representative frames of DIC time-lapse movies of tumor fragments in Matrigel (B) and collagen I (C). Black arrowheads indicate disseminated cells, some of which are observed to proliferate (white arrowhead). (B' and C') Localization of actin, SMA, and DAPI in tumor fragments in Matrigel (B') and collagen I (C'). White arrowheads mark the leading fronts. (D) Percent of tumor fragments showing cell dissemination in Matrigel and collagen I. n, total number of movies (four biological replicates, Student's t test, two-tailed, unequal variance). (E) Schematic description of isolation and 3D culture of normal mammary organoids. (F and G) Representative frames from DIC time-lapse movies of normal organoids in Matrigel (F) and collagen I (G). (F' and G') Localization of actin, SMA, and DAPI in normal organoids in Matrigel (F') and collagen I (G'). White arrowheads mark the leading fronts. Yellow arrowhead indicates myoepithelial cell dissemination. (H) Percent of normal organoids showing dissemination in Matrigel and collagen I. n, total number of movies (four biological replicates, Student's t test, two-tailed, unequal variance).

Figure 4-4

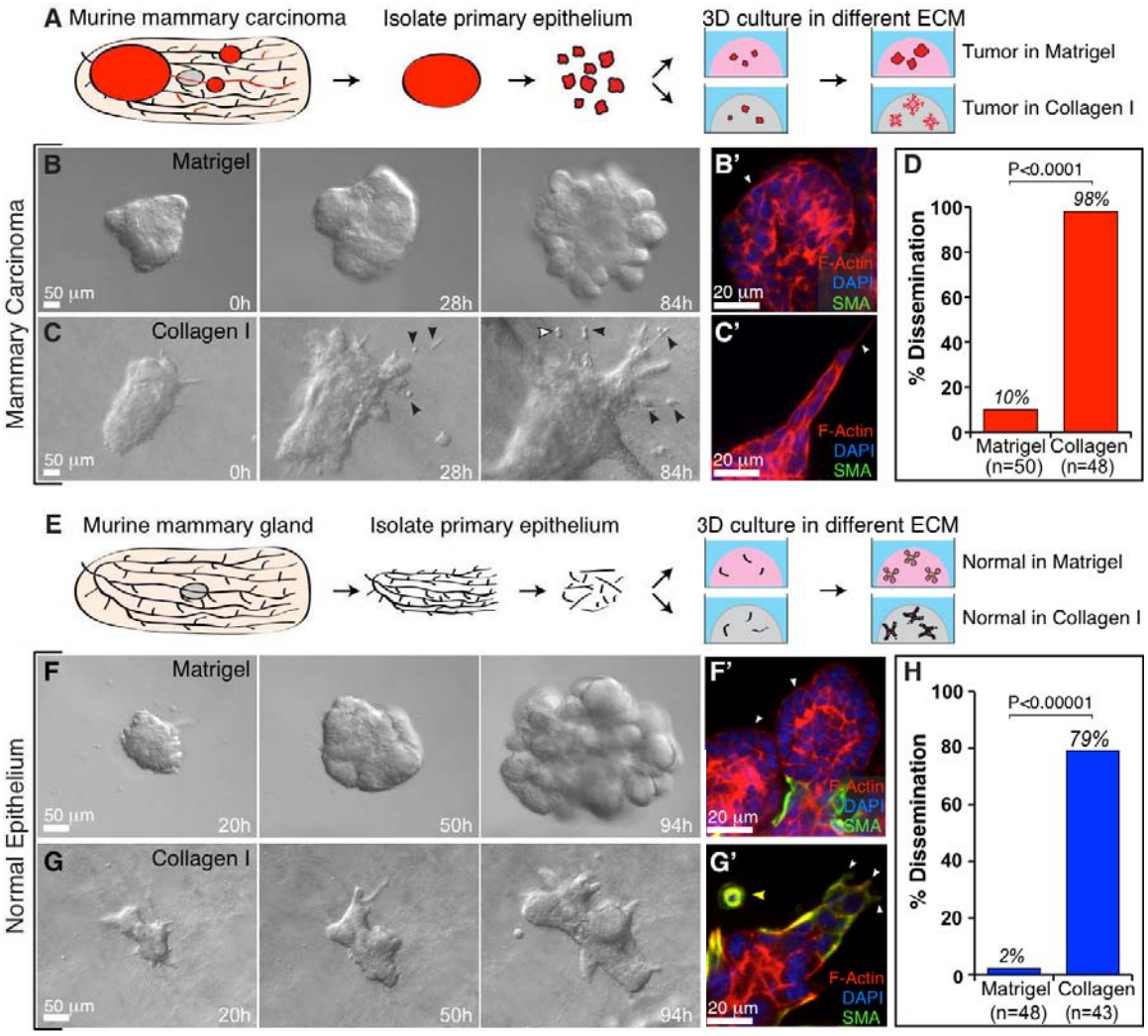
A Murine mammary carcinoma
Isolate primary epithelium
3D culture in different ECM
Tumor in Matrigel
Tumor in Collagen I
Mammary Carcinoma
B Matrigel
C Collagen I
50 μm
0h
28h
84h
B'
C'
F-Actin
DAPI
SMA
20 μm
D
P<0.0001
98%
10%
% Dissemination
Matrigel (n=50)
Collagen (n=48)
E Murine mammary gland
Isolate primary epithelium
3D culture in different ECM
Normal in Matrigel
Normal in Collagen I
Normal Epithelium
F Matrigel
G Collagen I
20h
50h
94h
F'
G'
H
P<0.00001
79%
2%
Matrigel (n=48)
Collagen (n=43)

Figure 4-5

The current, local ECM microenvironment determines the collective migration pattern of murine mammary epithelium. (A) Schematic description of isolation and 3D culture of normal mammary organoids. (B-C) Representative bright-field time-lapse movies of normal organoids in (B) Matrigel and (C) collagen I. (D) Schematic description of epithelial fragment isolation and matrix switching. (E-H) Representative bright-field time-lapse movies of normal organoids switched from (E) Matrigel to Matrigel (M-M), (F) Matrigel to collagen I (MC), (G) collagen I to Matrigel (C-M), and (H) collagen I to collagen I (C-C).

Figure 4-5

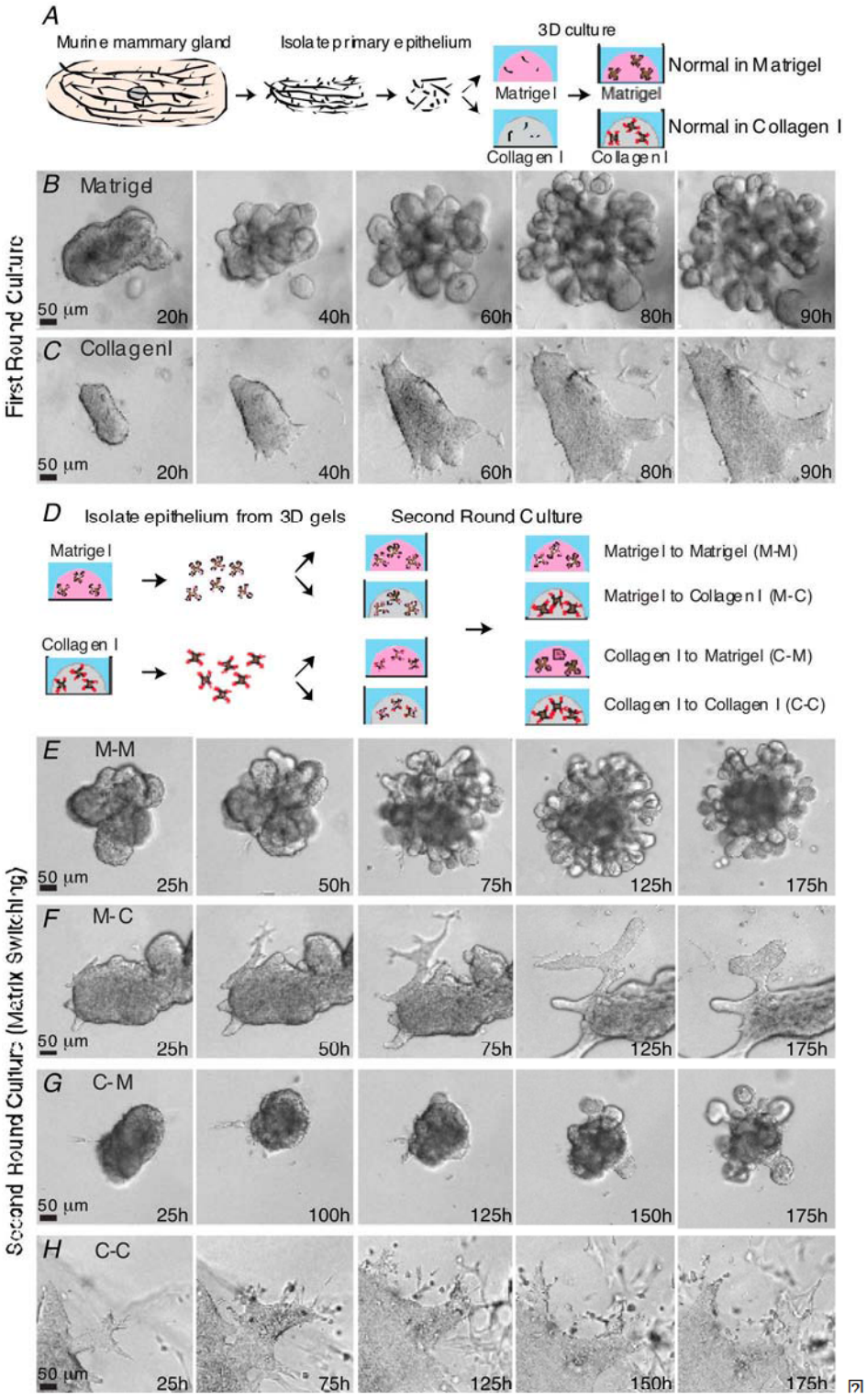
A
Murine mammary gland
Isolate primary epithelium
3D culture
Matrigel
Collagen I
Normal in Matrigel
Normal in Collagen I
First Round Culture
B Matrigel
C Collagen I
50 µm
20h
40h
60h
80h
90h
D
Isolate epithelium from 3D gels
Second Round Culture
Matrigel to Matrigel (M-M)
Matrigel to Collagen I (M-C)
Collagen I to Matrigel (C-M)
Collagen I to Collagen I (C-C)
Second Round Culture (Matrix Switching)
E M-M
F M-C
G C-M
H C-C
25h
50h
75h
100h
125h
150h
175h

Figure 4-6

Cell dissemination into collagen I is persistent in tumor and transient in normal epithelium. (A–C) Tumor cells disseminate with mesenchymal (black arrowheads) (A), amoeboid (white arrowheads) (B), and collective (black arrow) (C) morphologies. (D and E) Distribution of morphological types of dissemination (D) and fate of disseminated cells in normal and tumor organoids (E) in collagen I. n, total number of disseminated cells observed in each condition. (F and G) Representative frames from DIC time-lapse movies of tumor (F) and normal organoids (G) in collagen I. (H and I) Localization of E-cadherin and DAPI in tumor (H) and normal organoids (I) cultured in Matrigel. (J and K) Localization of E-cadherin and DAPI in tumor (J) and normal organoids (K) cultured in collagen I.

Figure 4-6

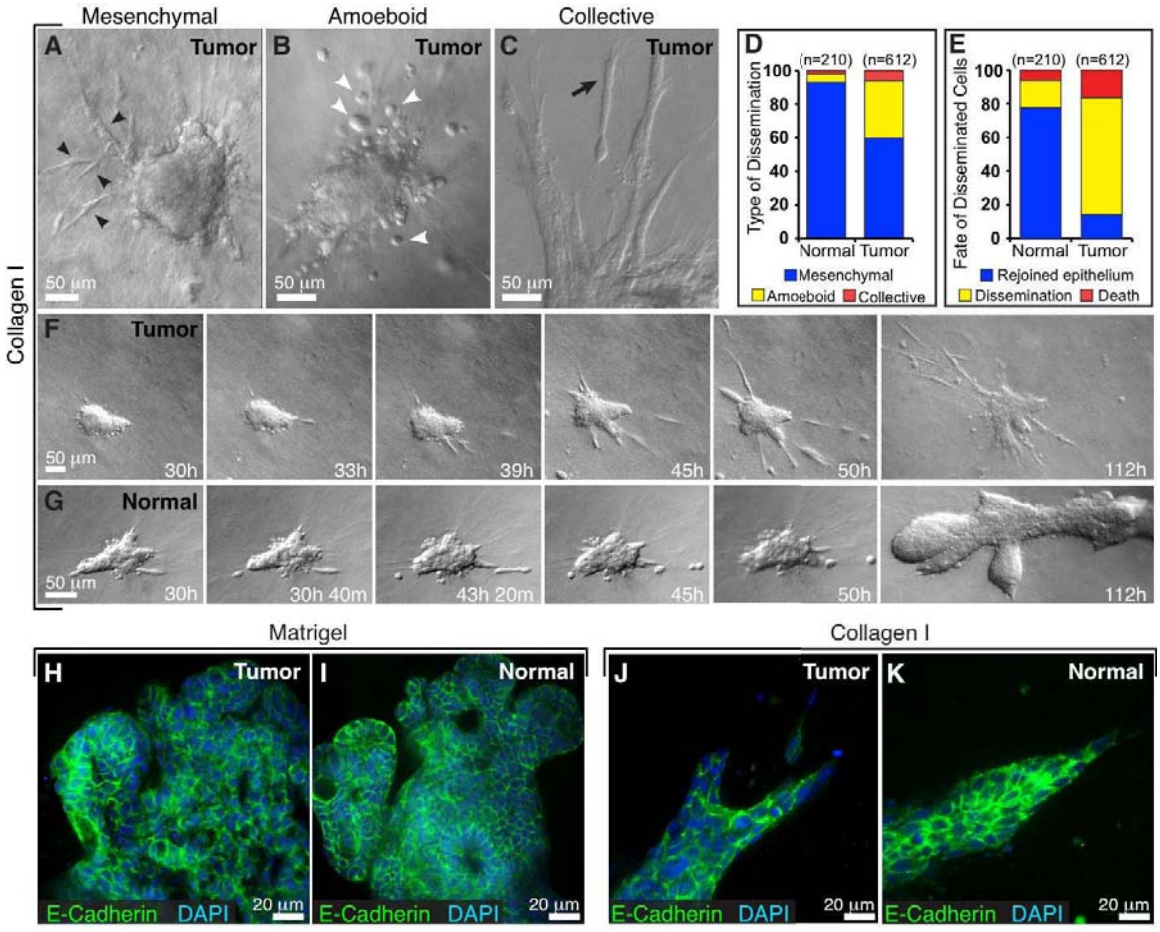
Mesenchymal
Amoeboid
Collective
A Tumor
B Tumor
C Tumor
50 µm
D
(n=210) (n=612)
Type of Dissemination
100
80
60
40
20
0
Normal Tumor
Mesenchymal
Amoeboid Collective
E
(n=210) (n=612)
Fate of Disseminated Cells
Normal Tumor
Rejoined epithelium
Dissemination Death
Collagen I
F Tumor
30h
33h
39h
45h
50h
112h
G Normal
30h
30h 40m
43h 20m
45h
50h
112h
Matrigel
Collagen I
H Tumor
I Normal
J Tumor
K Normal
E-Cadherin DAPI
20 µm

Figure 4-7

Normal epithelium transiently protrudes and disseminates into collagen I but reestablishes a complete basement membrane. (A) Representative frames of a DIC time-lapse movie of a normal organoid grown in collagen I. (A') Higher magnification of a transition from a protrusive to a smooth border with ECM. (A") Higher magnification of the reintegration of disseminated cells with the epithelial group. (B) Representative frames from a confocal time-lapse movie of a normal organoid grown in collagen I. (B') Higher magnification of transient protrusions within single myoepithelial cells. Arrows indicate individual protrusions, retractions, and epithelial reorganization. (B") Higher magnification of a multicellular extension of myoepithelial cells (blue arrows) at the leading front. (C–G) Normal epithelia in collagen reform a multicomponent basement membrane. (C–D' and F and F') Localization of actin, DAPI, and laminin 111 in a merge of all channels (C, D, and F) and in a single channel of laminin 111 (C', D', and F') in a normal organoid with a single-cell protrusion (C'), a multicellular extension (D'), and a normal organoid after reorganization (F'). All the Insets highlight negative correlation of cell protrusion (C, D, and F) and laminin 111 (C', D', and F') at the leading front. (E and E' and G and G') Localization of actin, DAPI, and collagen IV in a merge of all channels (E and G) and in a single channel of collagen IV in a normal organoid (E' and G') with multicellular extensions (E') and after reorganization (G'). (H and H') Localization of DAPI and laminin 332 in a merge of two channels (H) and a single channel of laminin 332

(H’). (I–K’) Tumor epithelia display incomplete basement membrane coverage. Single channels show the localization of actin (I, J, and K), laminin 111(I’), collagen IV (J’), and laminin 332 (K’) in tumor organoids in collagen I. Red and green arrowheads indicate actin-based protrusions and signals of basement membrane components, respectively.

Figure 4-7

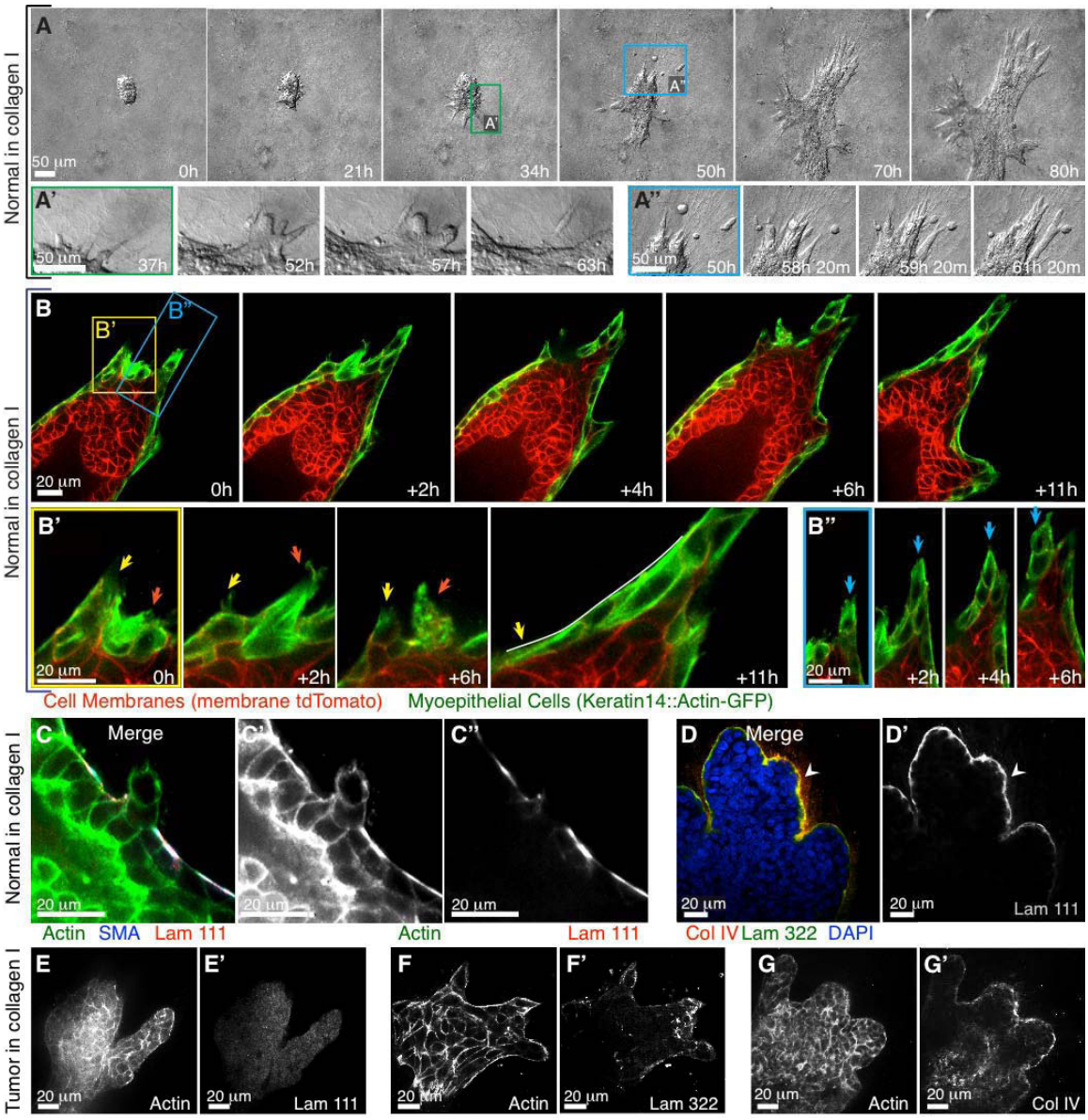
Normal in collagen I
A
A'
A''
50 μm
0h
21h
34h
50h
70h
80h
37h
52h
57h
63h
50h
58h 20m
59h 20m
61h 20m
B
B'
B''
20 μm
0h
+2h
+4h
+6h
+11h
Cell Membranes (membrane tdTomato)
Myoepithelial Cells (Keratin14::Actin-GFP)
C
Merge
C'
C''
D
Merge
D'
Actin SMA Lam 111
Actin
Lam 111
Col IV Lam 322 DAPI
Lam 111
Tumor in collagen I
E
E'
F
F'
G
G'
Actin
Lam 111
Actin
Lam 322
Actin
Col IV

Figure 4-8

Tumor and normal epithelium remain transcriptionally distinct despite morphological similarities induced by the ECM. (A) Schematic description of 3D cultures of normal and tumor murine epithelial fragments in Matrigel and collagen I for mRNA expression analyses. n = at least 3 biological replicates. (B) Complete-linkage hierarchical clustering of the experimental conditions. (C) Principal component analysis of the experimental conditions. (D) Heatmap representation of the 19,693 genes included in the microarray (blue and red indicate lower and higher expression, respectively). (E) Summary of differentially expressed genes with fold changes ≥2 and FDR ≤0.05. (F and G) Genes differentially expressed based on ECM condition in normal (F) and tumor (G). C, collagen I; M, Matrigel.

Figure 4-8

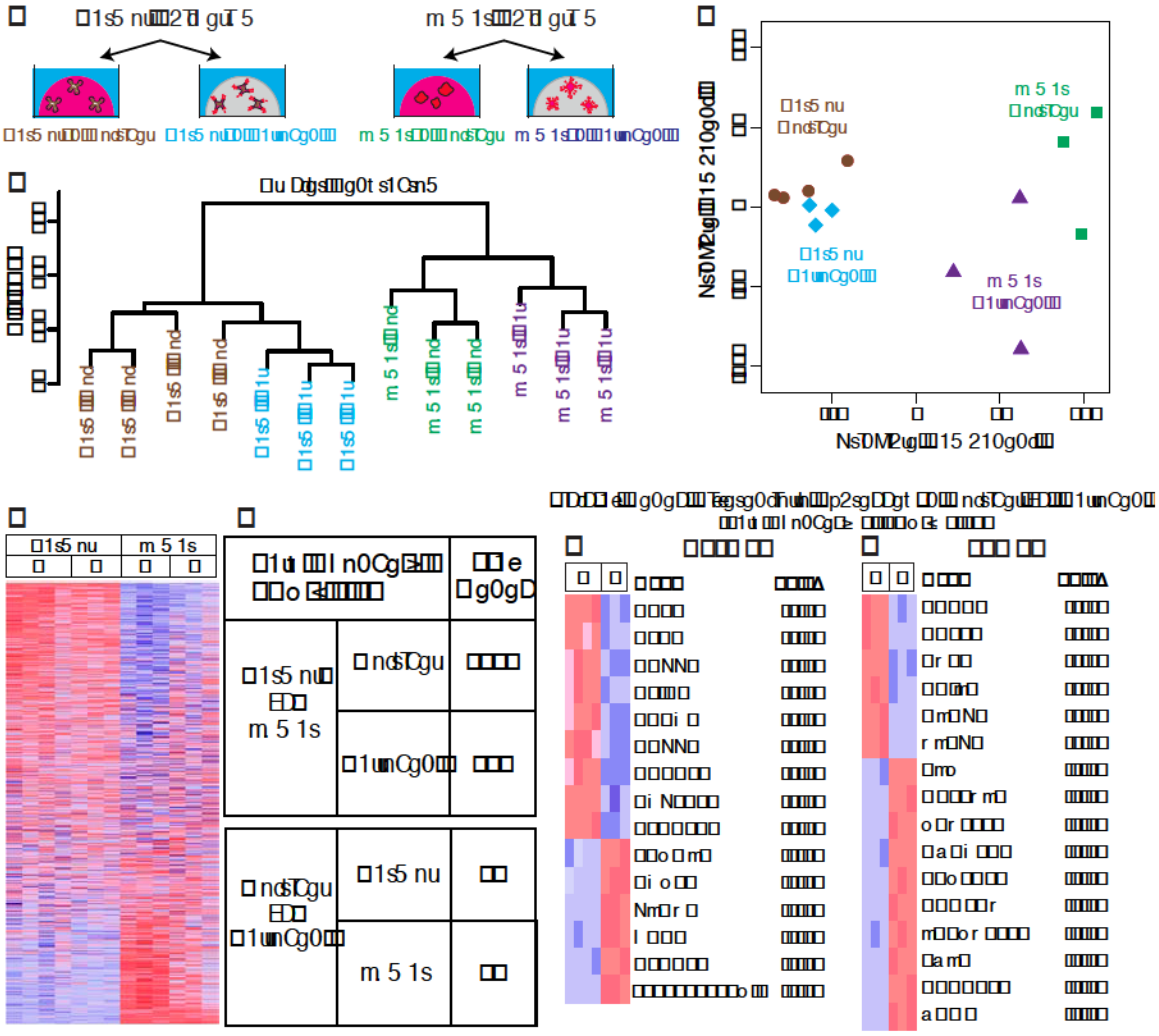

Figure 4-9

Cell-cell adhesion and extracellular genes are downregulated in tumor epithelium. (A) Analysis using DAVID functional annotation clustering. Genes with fold changes ≥ 2 and FDR ≤ 0.05 were used as input into DAVID. The top enriched categories include genes whose protein products are involved in cell adhesion, are localized to the extracellular space, or are involved in the inflammatory response. (B) Expression of structurally related genes implicated in cell-cell and cell-matrix adhesion. (C) Expression of genes associated with epithelial to mesenchymal transition (EMT). EMT genes are either upregulated in normal or are not significantly differentially expressed. For all heatmaps, *denotes p-value < 0.05; **denotes p-value < 0.001.

Figure 4-9

A

Enrichment	Cluster #	Gene Ontology (GO) Category	# of Genes	Enrichment Score	FDR
Matrigel – Higher in Normal	1	Cell Adhesion (GO:007155)	64	10.9	9.4×10^{-11}
	2	Extracellular Region (GO:0005576)	137	8.1	7.9×10^{-12}
	3	Blood Vessel Development (GO:0001568)	31	5.3	6.4×10^{-5}
	4	Heparin Binding (GO:008201)	38	4.6	6.0×10^{-3}
Matrigel – Higher in Tumor	1	Extracellular Region (GO:0005576)	138	19.3	3.3×10^{-21}
	2	Inflammatory Response (GO:0006954)	58	7.6	4.1×10^{-7}
	3	Ectoderm Development (GO:0007398)	25	3.3	7.9×10^{-3}
Collagen I – Higher in Normal	1	Extracellular Region (GO:0044421)	65	12.0	1.4×10^{-13}
	2	Cell Adhesion (GO:0007155)	44	8.7	6.9×10^{-9}
	3	Blood Vessel Development (GO:0001568)	27	8.6	1.5×10^{-7}
	4	Carbohydrate Binding (GO:0030246)	26	5.1	7.5×10^{-6}
	5	Regulation of Cell Migration (GO:0030334)	13	3.8	2.3×10^{-3}
	6	Growth Factor Binding (GO:0019838)	14	3.6	6.3×10^{-3}
Collagen I – Higher in Tumor	1	Extracellular Region (GO:0005576)	41	6.7	6.6×10^{-9}

B

Cell Adhesion Families Gene Expression

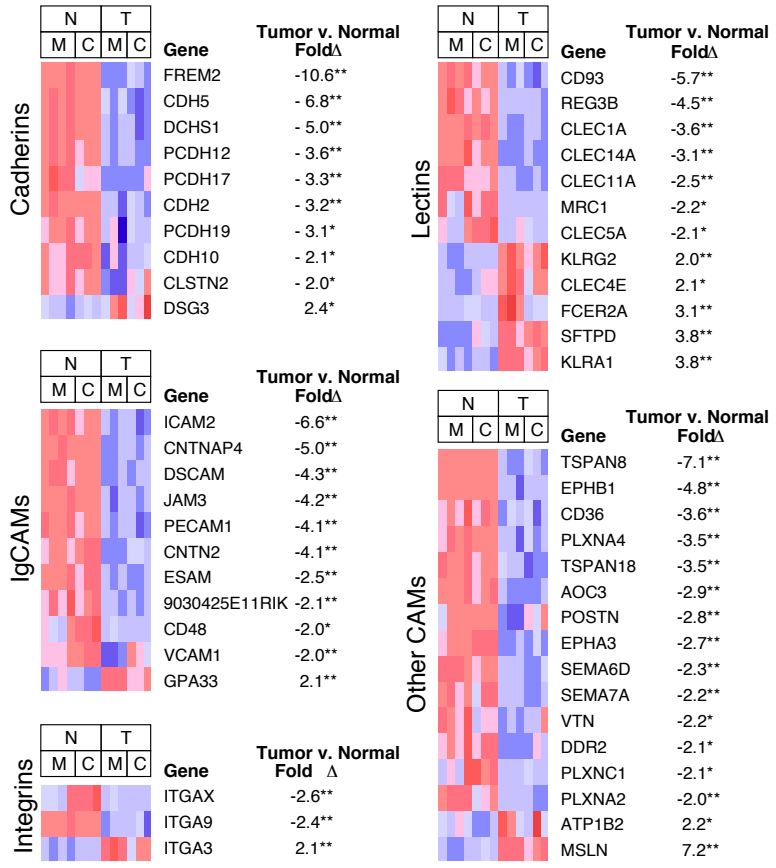

C

EMT Gene Expression

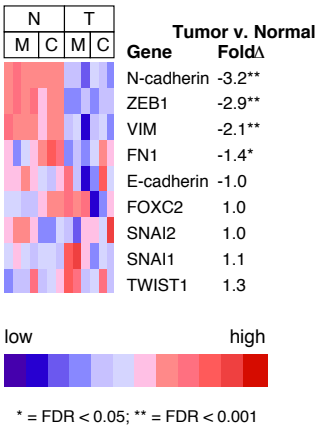

* = FDR < 0.05; ** = FDR < 0.001

Figure 4-10

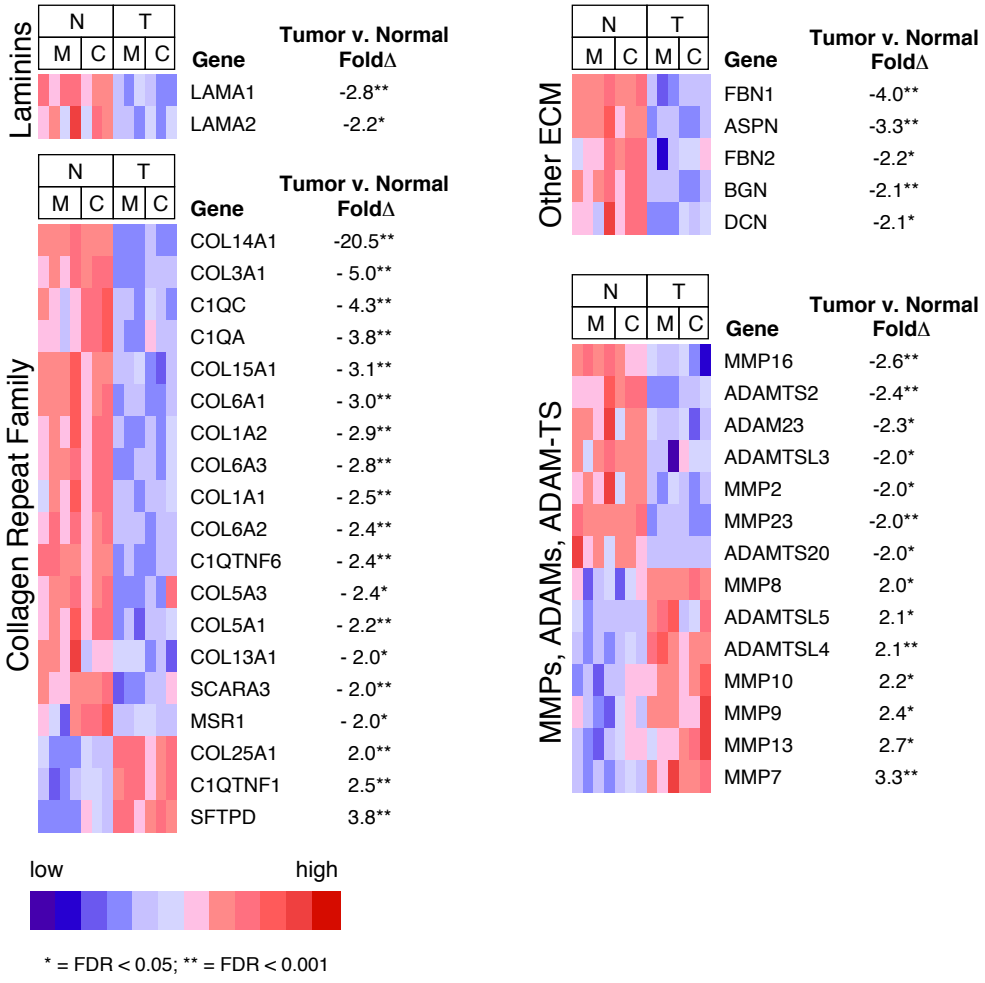

Extracellular matrix genes and metalloproteinases are differentially expressed by normal and tumor epithelium. The majority of differentially expressed genes in laminin, collagen, and other ECM gene sets were upregulated in normal epithelium. Approximately equal numbers of differentially expressed metalloproteinase genes were downregulated in normal and tumor epithelium. For all heatmaps, * denotes p-value < 0.05; **denotes p-value < 0.001.

Figure 4-11

Loss of P-cadherin causes precocious branching morphogenesis in Matrigel and enhanced, sustained dissemination into collagen I. (A and B) Representative frames from DIC time-lapse movies of (A) control [P-cadherin$^{+/+}$ (P-cad$^{+/+}$)] and (B) P-cadherin$^{-/-}$ (P-cad$^{-/-}$) epithelium grown in parallel in Matrigel. (C) Percent of P-cad$^{+/-}$ and P-cad$^{-/-}$ organoids branching in Matrigel on day 7. n, total number of organoids counted (three biological replicates; *P = 0.04; Student's t test, two-tailed, unequal variance). (D and E) Representative frames from DIC time-lapse movies of P-cad$^{+/-}$ (D) and P-cad$^{-/-}$ (E) epithelium grown in parallel in collagen I. Arrowheads indicate persistent cell dissemination. (F) Distribution of number of disseminated cells per organoid in P-cad$^{+/-}$ and P-cad$^{-/-}$ epithelia. n, total number of movies (three biological replicates; *P < 0.0001; upper one-sided $\chi 2$ test). (G) Representative frames from a confocal time-lapse movie of *P-cad$^{+/-}$, mT/mG, K14::Actin-GFP* epithelium in collagen I. Arrows indicate transient, myoepithelial-led protrusions. Arrowhead indicates a single disseminated myoepithelial cell. (H) Representative frames from a confocal time-lapse movie of enhanced myoepithelial dissemination into collagen I by *P-cad$^{-/-}$, mT/mG, K14::Actin-GFP* epithelium. (I) Proliferation of a disseminated P-cad$^{-/-}$ myoepithelial cell.

Figure 4-11

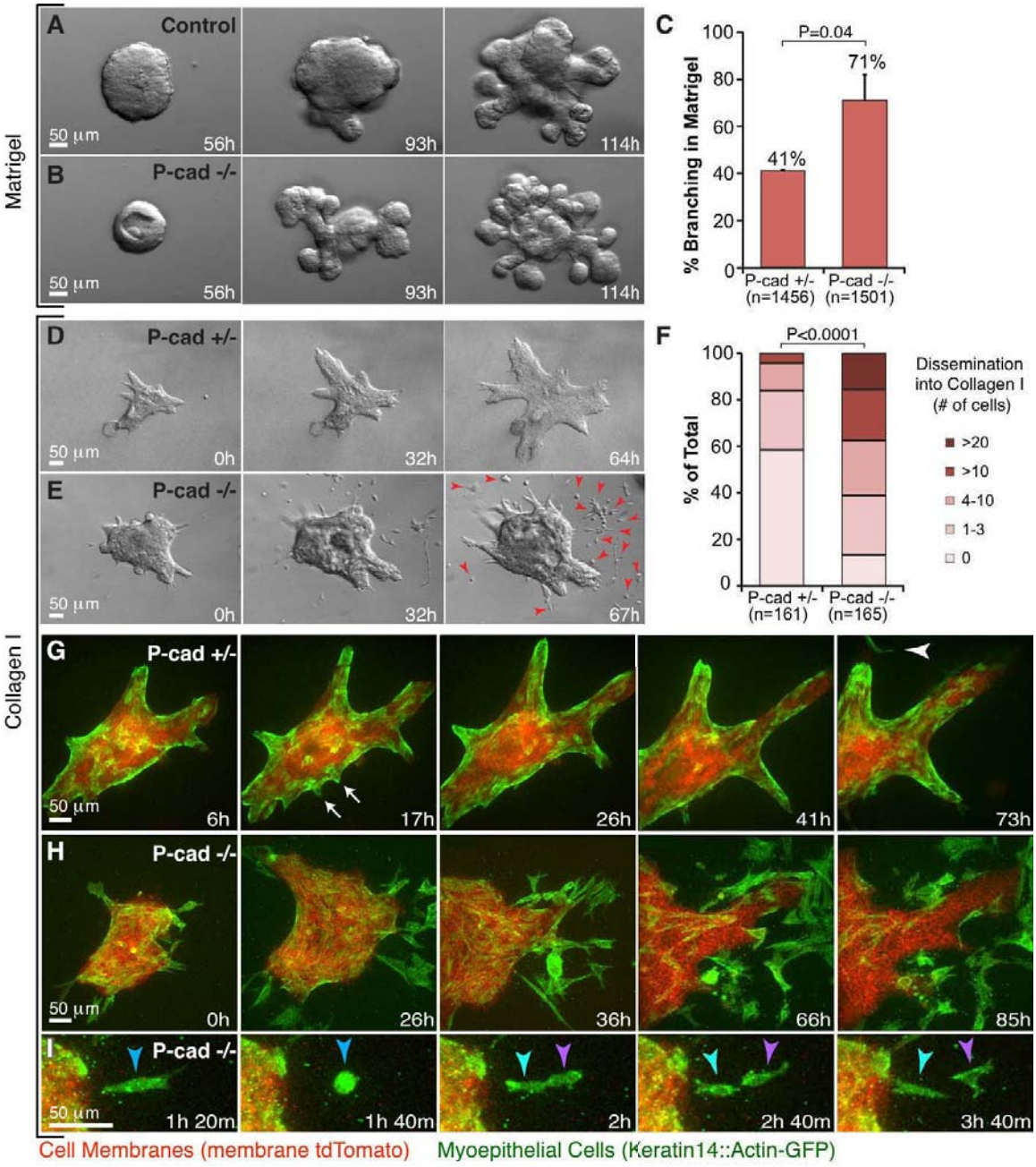
Matrigel
Collagen I
A Control
B P-cad -/-
50 µm
56h
93h
114h
C
P=0.04
71%
41%
% Branching in Matrigel
P-cad +/- (n=1456)
P-cad -/- (n=1501)
D P-cad +/-
E P-cad -/-
0h
32h
64h
67h
F
P<0.0001
% of Total
Dissemination into Collagen I (# of cells)
>20
>10
4-10
1-3
0
P-cad +/- (n=161)
P-cad -/- (n=165)
G P-cad +/-
H P-cad -/-
I P-cad -/-
6h
17h
26h
41h
73h
0h
36h
66h
85h
1h 20m
1h 40m
2h
2h 40m
3h 40m
Cell Membranes (membrane tdTomato)
Myoepithelial Cells (Keratin14::Actin-GFP)

CHAPTER 5

Epithelial cells requires actomyosin contractility to remodel collagen I fibers and maintain tissue architecture

Abstract

The fibrillar collagen type I (collagen I) is the most abundant scaffolding protein in human body. In mammary gland, localized in stroma, collagen I provide signals and scaffolds for epithelial outgrowth, the process known as branching morphogenesis. However, epithelial cells are partitioned from stromal surrounding via a basement membrane; therefore the questions of whether and how epithelial cells interact with stromal collagen I remain unclear. We recently developed collagen I-based organotypic culture assays, enabling us to study the dynamic interaction of epithelial cells and collagen I during branching morphogenesis and invasion processes. Here we show that mammary epithelial cells are capable of directly remodeling collagen I matrix. Myoepithelial cells actively align collagen I fibers through cycles of protrusion and retraction. In a pure collagen I gel, myoepithelial cells exert force on the fibers using protrusion directed to collagen I matrix, while in a mixed gel of collagen I and basement membrane proteins (Matrigel), they take advantage of protrusion internally directed to neighboring cells. Inhibition of actomyosin contractility abolishes fiber alignment, disrupts collective migration of epithelial cells, and interferes with basal epithelial organization and maintenance. These results indicate a novel function of actomyosin contractility in maintaining epithelial-stromal interface and preventing basal invasion. Our results provide the first direct evidence that epithelial cells can align with collagen I fibers without extending subcellular protrusion to the extracellular matrix.

Introduction

The mammary gland, comprised of epithelium and stroma, is a special organ in which the main developmental program occurs post-natally. Derived from ectoderm, mammary epithelium remains quiescent as a small rudiment until puberty (Hogg et al., 1983). Receiving pubertal signals, epithelial rudiments enter an active development phase, so-called branching morphogenesis, to elaborate a large ductal network throughout mammary fat pad. Derived from mesoderm, mammary stroma that includes cells and extracellular matrix (ECM) provides signals and cues for epithelial tissue to develop and function.

Mammary epithelial is built of two types of cells, including apically located luminal epithelial cells and basally located myoepithelial cells. In particular, myoepithelial cells have fusion properties of basal epithelia, and contractile muscle that is required for milk secretion. Epithelial structures are varied between developmental stages. Distinct from a simple bilayer duct with one layer of each cell type, branching epithelium acquires a stratified structure, termed as a terminal end bud (TEB), which actively drives ductal elongation and bifurcation. TEBs include multiple layers of luminal epithelial cells and a single layer of myoepithelial cells (Hinck and Silberstein, 2005).

Extracellular matrix is an important constituent of stroma and provides with scaffolding infrastructure for epithelial development and function. Basement membrane and fibrillar collagen type I (collagen I) are among the ECM microenvironments that have significant impacts on epithelial branching

morphogenesis and breast cancer. Basement membrane, or basal lamina, forms as a thin sheet, residing outside of myoepithelial cell layer and limiting epithelium within a confined compartment. Basement membrane must be a dynamic structure, whose composition and organization are constantly remodeled to accommodate different sizes of epithelial tissue during branching morphogenesis. Collagen I represents the most abundant structural protein in stroma. Produced and secreted to the extracellular space by stromal cells, collagen I proteins are assembled into fibrils, which then bundle into fibers, forming a large collagen I fiber network across mammary fat pad (Wolfe et al., 2010; Ingman et al., 2006; Brownfield et al., 2012). Although epithelial cells migrate collectively within a basement membrane, are spatially separated from stroma, and extend no epithelial protrusion directed to stromal ECMs (Ewald et al., 2008; Ewald et al., 2012), collagen I is still required for branching morphogenesis (Ingman et al., 2006; Brownfield et al., 2013). This mismatching issue raises a question about the relationship of epithelial cells that collectively migrate during ductal elongation, with stromal collagen I matrix.

Composition and organization of stromal collagen I are continuously changed throughout the entire life of mammary gland; and its abnormal alterations are associated with breast cancer progression and metastasis. In particular, the aligning feature of collagen I fibers, primarily found in breast tumor, has been used as an ECM marker for tumor invasiveness (Provenzano et al., 2006, Conklin et al., 2011; Cheung et al., 2013). In this model, in addition to

stromal cells, tumor cells that invade through basement membrane gaps are directly exposed to collagen I in stroma and able to exert force to align the fibers. Similarly, epithelial cells from normal mammary glands also invade collagen I matrix with transient cellular protrusion and dissemination (Nguyen-Ngoc et al., 2012), align or respond to collagen I fiber orientation (Guo et al., 2012; Brownfield et al., 2013). Although these evidence suggest that collagen I remodeling is a conserved program of tumor and normal epithelial cells and because the protrusive invasion does not exist during mammary branching morphogenesis, whether and how normal epithelial cells are able to remodel stromal collagen I fibers while basement membrane remains intact remain elusive.

Myosin II and its resulting contractile force play an important role in multiple cellular processes. In single cells that are highly motile and loosely adhered to one another, myosin II-generated tension orchestrates cell migration and matrix modification through several adhesion complexes. For examples, myosin II provides tension and traction for fibroblasts to align the fibers in 3D collagen matrix (Meshel et al., 2005) through integrin-based focal adhesion complex (Kubow and Horwitz, 2011). In contrast, since epithelial cells are tightly connected and their functions and development require a harmonious coordination of cells across the tissue, the contractile force is multi-directionally attributed. Actomyosin contractility is involved in forming and maintaining cell-cell junctions, cell-matrix adhesion, cell migration, and matrix modification (reviewed

by Vicente-Manzanares et al., 2009). A change in actomyosin contractility balancing influences tissue homeostasis and morphogenesis. For examples, increased contractility disrupts cell-cell adhesion collective cell migration, resulting in cell dissemination (Hidalgo-Carcedo et al., 2011); or cytoskeletal tension due to Rho/ROCK upregulation reflexes matrix stiffness, affects tissue behaviors (Paszek et al., 2005), and promotes tumorigenesis (Sanz-Moreno et al., 2011). In contrast, cellular contractility in epithelial tissue is variably required at different stages and dependent on ECM microenvironments (Ewald et al., 2012; Brownfield et al., 2013). In Matrigel, Rho/ROCK-inhibited epithelium is disorganized at adherent junction and polarity (Ewald et al., 2012), while it fails to follow fiber orientation cues in the collagen I ECM (Brownfield et al., 2013). However, in vivo epithelial tissue exists and develops in the presence of both types of ECMs; the functional contribution of cellular contractility is incompletely understood, therefore.

In this study, we used organotypic culture assays, in which parts of epithelial ducts, termed as organoids, are explanted to 3D ECM gels, to directly examine collagen I matrix remodeling and roles of actomyosin contractility in mammary branching morphogenesis.

Results

Mammary epithelial cells could align collagen I fibers

In mammary stroma, collagen type I is the most abundant protein and plays an important role in epithelial development and diseases. Structural properties of collagen I matrix is remarkably changed across developmental stages of mammary glands, which exerts a strong impact on cell fate and behavior of the epithelium. As a stromal protein, collagen I mainly localizes in the interstial space and separated from the epithelium via a basement membrane. Therefore, the majority of collagen I remodeling is carried out by stromal cells, including fibroblasts, myoblasts, macrophases. Recent studies have indicated that collagen I is involved, indirectly or directly, in regulating mammary branching morphogenesis (Ingman et al., 2006, Brownfield et al., 2013). This evidence leads to a question of whether epithelial cells could also interact and modify collagen I.

To test this question, we first examined the interaction of epithelial cells with a collagen I matrix. We used a collagen I-based invasion assay, in which epithelial organoids are explanted to 3D gels of pure collagen I. Since in vitro collagen I could be monitored to form fibrils or larger fibers, visible under differential interference contrast (DIC) microscopy. Therefore, to observe the relative interaction between epithelial cells and collagen I fibers, we used DIC time-lapse imaging to visualize the dynamic organization of the collagen I network during collective invasion (Fig. 5-1A).

We observed a striking progressive alignment of collagen fibers, correlated with epithelial elongation. Collagen fibers were displaced and progressively re-arranged from a random to an aligned array of parallel fibers, which correlated with the direction of cellular protrusion (Fig. 5-1C). To quantify the extent of fiber displacement, we utilized Deformation Quantification Analysis (DQA) software (Vanni et al., 2003) on 10 movies and observed that collagen I fibers were vectorally displaced and aligned during protrusive collective migration of epithelial cells (Fig. 5-1B).

In mammary tissue, basement membrane serves as a barrier to limit direct contact between epithelial cells and collagen I-rich stroma. Therefore, we next tested whether the presence of basement membrane proteins could interfere with collagen I fiber alignment by epithelial cells. We used a collagen I-based branching assay, in which epithelial organoids are cultured in a mixed ECM of Matrigel and collagen I and achieve a complete program of branching morphogenesis (Fig. 5-1D).

Through the similar DQA quantification, we also observed that collagen I fibers were extensively displaced mainly during bud elongation (Fig. 5-1E). Examining the local architecture of collagen I matrix, we found that 34% of epithelial buds (Fig. 5-1G) had collagen I fibers aligned and radiated either from the leading front (Fig. 5-1F') or on the sides (Fig. 5-1F"). Taken together, these data have shown that mammary epithelial cells aligned collagen I fibers in 3D gels.

Myoepithelial cells are directly involved in collagen I fiber alignment

Mammary epithelium contains two types of cells, including basal myoepithelial and apical luminal epithelial cells. We next asked which one of them could align collagen I fibers. Myoepithelial cells lead the collective invasion in the pure collagen I matrix, and from this knowledge we hypothesized that myoepithelial cells were primarily in contact with and aligned collagen I fibers. To test the hypothesis, we combined immunofluorescent staining with a myoepithelial-specific marker (smooth muscle actin (SMA)) and second-harmonic generation microscopy to observe the relative localization between myoepithelial cells and collagen I fibers.

In both pure collagen I and mixed with Matrigel, we found that collagen I fiber bundles emerged from SMA-positive cells (Fig. 5-2). In the pure collagen I gels, myoepithelial cells linked to and modified the fibers through actin-based protrusion (Fig. 5-2A, A'), which is a fibroblast-like mechanism (Wolfe et al., 2010). In the mixed ECMs, there were two scenarios of aligned collagen I fibers according to two positions of myoepithelial cells along elongating buds. First, an array of collagen I fibers aligned radically in the front of myoepithelium-covered buds. Secondly, aligned fibers formed at the position of SMA+ cells (Fig. 5-2B-B"), compared to a random meshwork (Fig. 5-2B'"). These data indicate that myoepithelial cells modulate collagen I fibers independent of basement membrane proteins.

Myoepithelial cells actively remodel collagen I fiber without ECM-directed protrusion

We next sought to understand how myoepithelial cells could remodel collagen I fibers. When growing on either 2D or 3D collagen I matrix, cells develop adhesion complexes underlying actin-based protrusion as linkages to connect the ECMs to cytoskeletal networks, so-called ECM-directed protrusion. In contrast, our in vivo and in vitro studies had revealed that mammary epithelial cells extend no subcellular protrusion to stromal ECM microenvironments during branching morphogenesis. Instead, live imaging and super-resolution microscopy exhibited that epithelial cells residing within the tissue have interdigitating membrane protrusion, which we term it as cell-directed protrusion (Ewald et al., 2012). To test whether myoepithelial cells could use cell-directed protrusions to remodel collagen I matrix, we combined confocal imaging to visualize epithelial cell morphology by fluorescent labeling with DIC imaging to visualize collagen I fiber structure (Fig. 5-3).

We found that myoepithelial cells located near the front of the bud were in line and actively pulling collagen I fibers (Fig. 5-3A, A') and acquired a protrusive morphology (Fig. 5-3B', arrowheads). However, 3D reconstruction with luminal epithelial cells revealed that myoepithelial cell protrusions were limited within the tissue and the basal surface were smooth and non-protrusive (Fig. 5-3C, C'). Throughout eight time-lapse movies with 10 minute intervals, we never observed any epithelial cells extending protrusion toward collagen I fibers. These data

suggest that myoepithelial cells use internal cell-directed protrusion to remodel collagen I matrix.

Myoepithelial cells were highly contractile

To examine the dynamics of myoepithelial cell protrusion in aligning collagen I fibers, we used the transgenic myoepithelial reporter mouse line (keratin 14::actin-GFP; mT/mG). Tracking protrusive activities of GFP+ cells over time in the pure collagen I, we observe that collective invasion of myoepithelial cells were highly dynamic and contractile. They undergo cycles of protrusion/extension and retraction (Fig. 5-4A), resulting in elongation and recruitment of luminal epithelial cells into the elongating group (Fig. 5-4A'). In addition, analysis from our DIC imaging also exhibited that the cyclic process of epithelial protrusion was correlated with collagen I fiber remodeling (Supplemental data). Taken together, these data suggest that contractility of myoepithelial cells was required for fiber alignment.

Actomyosin contractility is required for matrix displacement and fiber alignment

We next tested whether fiber remodeling depended on actomyosin contractility using inhibitors for Rho kinase (Y27632) and myosin II (Blebbistatin) before protrusion was initiated. We found that after drug addition, the collagen matrix was released from the tension, and collagen fibers stayed unchanged.

The long invasion of thin cell protrusions did not interfere the organization of collagen fibers (Fig. 5-4B', C'). DQA quantification revealed a loss in vectorial displacement and a reduction in the extent of displacement (Fig. 5-4B", C").

Actomyosin contractility is required for collective migration

Since multicellular extension is correlated with collagen I fiber remodeling, we asked whether loss of actomyosin contractility influenced collective invasion. Although inhibition of both Rho kinase and myosin II did not affect single cell protrusion, they intefered the retraction following protrusion (Fig. 5-4B"' and 4C"'). Inhibition of Rho kinase reduced the retraction (Fig. 5-4B'") while inhibition of myosin II completely blocked it (Fig. 5-4C"'). Due to the loss of retraction, almost all of initial protrusions were retained throughout culture and cells invaded the matrix with long and spiky protrusions.

Since myoepithelial cells were contractile and leading in both single and multicellular extension, we hypothesized that loss of actomyosin contractility mainly influenced their cellular behaviors. Upon Rho kinase inhibition, myoepithelial cells quickly extended multiple spiky protrusions (Fig. 5-4D, D'). In a few cases, the myoepithelial cells formed multicellular extensions including either only small groups of only myoepithelial cells (Fig. 5-4D') or with the association of luminal epithelial cells (Fig. 5-4D"). However, neither single protruding cells nor multicellular groups were able to expand and develop into broad elongating branches. These data suggest that actomyosin activity plays an important role in the retraction, coordination and migration of epithelial cells.

Actomyosin contractility is required for epithelial re-establishment

As we previously showed, at the late stage of invading to collagen I matrix, epithelial cells transition from protrusive to non-protrusive migration to reorganize the epithelial tissue (Fig. 5-5A, ref). Since the retraction following protrusion was blocked by the inhibition of Rho kinase or myosin II, we hypothesized that treated organoids were unable to re-establish their epithelial organization.

Staining for F-actin and SMA, we found distinct effects of Rho kinase and myosin II inhibition on incomplete re-establishment of epithelium. When myosin II was inhibited, there were many protrusions remained at the leading front as well as at the side of the branch (Fig. 5-5B-B”). Most of the basal protrusions were SMA+ (Fig. 5-5B”). However, myoepithelial cell coverage remained almost intact. Likewise, in the organoids that Rho kinase is inhibited, thin and spiky protrusions of myoepithelial cells were all over the ECM interface (Fig. 5-5C). Different from myosin II inhibition, Rho kinase inhibition resulted in disruption in myoepithelial cell layer (Fig. 5-5C”). Confocal time-lapse imaging also revealed that protrusive myoepithelial cells gradually lost their cell-cell contact, resulting in large breaks in myoepithelial cell coverage (Fig. 5-5C”, D-D’) and allowing a direct access and invasion of luminal cells into ECM (Fig. 5-5C’, D”). We conclude that contractility is required for the reorganization of myoepithelium, preventing epithelial cells from invasion to ECM.

Actomyosin contractility is involved in epithelial tissue integrity and branching morphogenesis

We next asked whether actomyosin contractility is required for maintenance of tissue integrity. To test this, we applied Blebbistatin treatments in two conditions of when epithelium was fully restored in a pure collagen I ECM and when it underwent branching morphogenesis in mixed ECMs. Upon drug treatments, the tissue interface with ECMs lost the smooth morphology (Fig. 5-6A-B). First, in a pure collagen I ECM, single to strands of cells re-invaded collagen I with extensive protrusion. Invasion occurred at the front end and at the side of the bud as well (Fig. 5-6A' and A") The invasion began with single spiky protrusions and quickly transitioned to broader strands or cell dissemination (Fig. 5-6A' and A"). Time-lapse imaging also revealed that organoids were spreading out and partially lost their three-dimension architecture (Fig. 5-6A, first panel vs last panel). Secondly, in a mix of collagen I and Matrigel, inhibition of myosin II activity induced local invasion and interfered with the branching morphogenesis program (Fig. 5-6B-C). Epithelial cells failed to migrate collectively into ECM microenvironments for new bud initiation and elongation (Fig. 5-6C, C'). In addition, loss of actomyosin contractility resulted in an incomplete coverage of myoepithelial cell layer and basement membrane, allowing luminal epithelial cell invasion (Fig. 5-6D-E). These data indicate that actomyosin contractility is indispensable for preservation of non-protrusive epithelium-ECM interface during quiescent and developing stages.

Discussion

In this study, we used 3D organotypic culture based on collagen I-rich ECMs to directly examine the dynamic interaction between mammary epithelial cells and collagen I matrix. We showed that myoepithelial cells can directly align the fibers either during protrusive invasion in pure collagen I or during branching morphogenesis in mix of collagen I and Matrigel. When invading collagen I gel, myoepithelial cells were highly contractile, going through cycles of protrusion followed by retraction. In addition to diminishing collagen I fiber alignment, we found that inhibition of actomyosin contractility caused other cellular consequences. First, loss of actomyosin contractility reduced cell retraction, resulting in sustained invasion to the matrix. Second, it disrupted the coordination among epithelial cells required for onward collective migration, leading to a failure of branching morphogenesis. Lastly, it induced local basal invasion of epithelial tissue. Taken together, these data revealed multiple cellular functions of actomyosin contractility in epithelial tissue homeostasis and branching morphogenesis.

Cell migration within 3D collagen I matrix is preceded by actin-based protrusion, under which cells form integrin-mediated adhesions and exert pulling force on collagen I fibers, resulting in local fiber alignment or global matrix remodeling (Kubow and Horwitz, 2011; Kubow et al., 2013). Myoepithelial cells acquire a protrusive morphology when exposed to collagen I matrix (Nguyen-Ngoc et al., 2012). The protrusion was directed to the ECM and highly

contractile. The cycles of extension and retraction might be correlated with those of pulling on and releasing to eventually align collagen I fibers. Although in vivo myoepithelial cells are confined within basement membrane and are not invading to stromal ECM, these data indicate an intrinsic ability of epithelial cells to remodel collagen I fibers in stroma.

Mammary epithelial cells develop and exist in a collagen I-rich stroma. Despite spacial separation from the epithelium due to basement membrane, collagen I plays an important role in orienting epithelial branching (Brownfield et al., 2013), in ductal elongation and myoepithelial cell coverage (Nguyen-Ngoc and Ewald., 2013), in terminal end bud structure and elongation (Ingman et al., 2006). Therefore, the long-standing question is whether and how epithelial cells are able to interact with collagen I in stroma during branching morphogenesis. Using the 3D mixed gels containing both collagen I and Matrigel, in which organoids collectively migrate without ECM-directed protrusion, we demonstrate that myoepithelial cells were capable of grasping, pulling and then aligning collagen I fibers. This result indicates that basement membrane proteins did not interfere myoepithelial cells from interacting with the fibers. Surprisingly, to interact with collagen I fibers myoepithelial cells utilized internal protrusions extending on their neighboring cells and toward elongation direction. We speculate two possibilities for this interaction. First, basement membrane proteins, such as laminins, collagen IV, or entactin, may serve as linkers to relay the contractile force from myoepithelial cells to collagen I fibers. Second, as an

epithelial duct elongates, basement membrane must be constantly remodeled (Hanuraga et al., 2014), involving both phases of assembly and disassembly of protein meshwork. The remodeling process may result in a transient gap of basement membrane, allowing myoepithelial cells directly interact with collagen I fibers in stroma.

Mammary epithelium forms a well-defined interface to surrounding stroma via a basement membrane, whose components are mainly contributed by myoepithelial cells (Gudjonsson et al., 2002). Therefore, the existence of the myoepithelial layer and basement membrane is mutually dependent on one another; a disruption of either of them can increase tumor invasion in breast cancer (Polyak, 2010). In this study, we described a novel function of actomyosin contractility in establishing and maintaining myoepithelial layer and basement membrane continuity. In the pure collagen I ECM, which contained no basement membrane proteins, and with loss of cellular contractility before protrusion cessation, the epithelial tissue failed to restore and retained a protrusive basal surface. In the ECM conditions that basement membrane proteins were secreted by myoepithelial cells or supplemented in 3D gels, once actomyosin contractility was inhibited, protrusion was relapsed. In particular, Rho kinase inhibition resulted in large gaps in myoepithelial cell layers and basement membrane organization. We conclude that the contractile force generated by actomyosin networks is required for myoepithelial layer integrity and basement membrane continuity to maintain epithelial tissue homeostasis and prevent tumor invasion.

Materials and methods

Mouse lines and breeding. All experiments were done in accordance with an approved protocol from the Johns Hopkins University Animal Care and Use Committee. Most experiments were done with Charles River FVB/N mice. For confocal time-lapse imaging, myoepithelial cells were visualized using keratin-14::actin-GFP transgenic mice (Vaezi et al., 2002), in which the keratin-14 promoter drives cell-type specific expression of an actin-GFP fusion protein. Cell membranes were visualized using the membrane TdTomato signal in the mT/mG transgenic line (Muzumdar et al., 2007). Keratin-14::actin-GFP were generously provided by Elaine Fuchs (Rockefeller University, NY, NY, USA), and mT/mG mice were obtained from Jackson Laboratory and back-crossed to FVB/N.

Isolation of primary mouse mammary organoids. We isolated organoids following previously described protocols (Ewald et al., 2008; Nguyen-Ngoc et al., 2012). In short, we collected mammary glands, minced the tissue with a sterile scalpel, and isolated the epithelial fraction following collagenase and trypsin treatment. Epithelial organoids were separated from single cells by differential centrifugation.

Collagen gel preparation. We used acid-solubilised rat tail collagen I (BD Bioscience #354326) as starting material. We combined 8 µL NaOH 1N, 25 µL 10X DMEM and 217 µL collagen I into 250 µL of solution. The volume was scaled up as necessary. Collagen solution was mixed until it had a stable, uniform color. The pH was adjusted to 7.0–7.5. The concentration of collagen I

varies between commercial lots and was always adjusted to 3 mg mL−1 by 1x DMEM. 10–20 µL of the collagen I solution was used to make a thin underlay for each well. The rest of the collagen I solution was pre-incubated at 4°C, on wet ice, from 5 min to 2 h (Fig. 2-1A). At the end of the specified pre-incubation interval, the collagen I solution was mixed with epithelial organoids, and the mixture was plated on top of the underlay and incubated at 37°C for 1 h to allow gelation before addition of culture medium. To generate the mixed gels, preassembled collagen I solutions (3 mg mL−1, pre-incubated for 1 h at 4°C) were mixed with Matrigel (BD Biosciences #354230, Growth Factor Reduced) in 3:7, 5:5, and 7:3 (v/v) ratios. The mixtures were then combined with epithelial organoids plated, and incubated at 37°C for 1 h for gelation. Organoids were combined at an approximate ratio of two organoids per microliter of ECM solution.

Drug treatment. Blebbistatin (25 μM) (Sigma, B0560-5MG) and ROCK inhibitor Y-27632 (50 μM) (Sigma, Y0503-5MG) were added to the culture at specific time.

Antibody staining. Organoids cultured in all matrix conditions were fixed with 4% (v/v) paraformaldehyde in PBS for 20 min, washed twice with PBS for 10 min, permeabilised with 0.5% (v/v) Triton X-100 in PBS for 20 min, and washed twice for 10 min. Samples were then blocked with 10% FBS (v/v) in PBS for 2 h, incubated with primary antibody in 10% FBS for 2 h at RT, washed twice, and blocked another 1 h in 10% FBS in PBS. They were next stained with secondary antibody for 1h and washed twice with 10% FBS in PBS before imaging. F-actin

was stained with Alexa 647 Phallodin (1:100) (Invitrogen A22287), and nuclei were stained with DAPI (1:1000) (Invitrogen D3571). Primary antibodies were mouse anti-laminin 1α (1:100) (R&D System MAB2549) and anti smooth muscle actin-FITC conjugate (1:250) (F3777, Sigma).

Time-lapse imaging. Live DIC imaging was conducted using a Zeiss Cell Observer system with a Zeiss AxioObserver Z1 and an AxioCam MRM camera. Images were collected at 20 min intervals with exposure time of approximately 250 ms and analysed by Axiovision software. Live confocal imaging was performed using a custom spinning disc microscope (Ewald et al., 2008; Ewald, 2010) and Zeiss 780. Temperature was maintained at 37°C and CO2 at 5%.

Image acquisition. Confocal images were acquired using a custom spinning disc microscope with 40× c-APO oil and 20× air objectives. Second harmonic generation (SHG) was conducted using a Zeiss LSM 710 laser-scanning microscope with a 25× water objective. SHG excitation was via a Coherent Inc. Chameleon laser tuned to 880 nm. For SHG imaging, laser power was set to 35, gain was in the range of 800–1000 depending on sample intensity, the digital offset was 1200, and the digital gain was 1.0. SHG images in the figures were collected with equivalent gain settings and are presented with equivalent digital contrast, brightness, and levels. DIC-confocal time-lapse imaging was conducted using a Zeiss 780 confocal microscope. Images were assembled using Imaris software.

References

1. Brownfield DG, Venugopalan G, Lo A, Mori H, Tanner K, Fletcher DA, Bissell MJ. (2014) Patterned collagen fibers orient branching mammary epithelium through distinct signaling modules. Curr Biol. 23(8):703-9.
2. Cheung KJ, Gabrielson E, Werb Z, Ewald AJ. (2013) Collective invasion in breast cancer requires a conserved basal epithelial program. Cell. 155(7):1639-51.
3. Conklin MW, Eickhoff JC, Riching KM, Pehlke CA, Eliceiri KW, Provenzano PP, Friedl A, Keely PJ. (2011) Aligned collagen is a prognostic signature for survival in human breast carcinoma. Am J Pathol. 178(3):1221-32.
4. Ewald AJ, Brenot A, Duong M, Chan BS, Werb Z (2008) Collective epithelial migration and cell rearrangements drive mammary branching morphogenesis. Dev Cell. 14(4):570-81.
5. Ewald AJ, Huebner RJ, Palsdottir H, Lee JK, Perez MJ, Jorgens DM, Tauscher AN, Cheung KJ, Werb Z, Auer M (2012) Mammary collective cell migration involves transient loss of epithelial features and individual cell migration within the epithelium. J Cell Sci. 125(Pt 11):2638-54.
6. Gudjonsson T1, Rønnov-Jessen L, Villadsen R, Rank F, Bissell MJ, Petersen OW. (2002) Normal and tumor-derived myoepithelial cells differ in their ability to interact with luminal breast epithelial cells for polarity and basement membrane deposition. J Cell Sci. 115(Pt 1):39-50.
7. Harunaga JS, Doyle AD, Yamada KM. (2014) Local and global dynamics of the basement membrane during branching morphogenesis require protease activity and actomyosin contractility. Dev Biol. 394(2):197-205.
8. Hidalgo-Carcedo C, Hooper S, Chaudhry SI, Williamson P, Harrington K, Leitinger B, Sahai E. (2011) Collective cell migration requires suppression of actomyosin at cell-cell contacts mediated by DDR1 and the cell polarity regulators Par3 and Par6. Nat Cell Biol. 13(1):49-58.
9. Hinck L, Silberstein GB. (2005) Key stages in mammary gland development: the mammary end bud as a motile organ. Breast Cancer Res. 7(6):245-51.
10. Hogg NA, Harrison CJ, Tickle C. (1983) Lumen formation in the developing mouse mammary gland. J Embryol Exp Morphol. 73:39-57.
11. Ingman WV, Wyckoff J, Gouon-Evans V, Condeelis J, Pollard JW. (2006) Macrophages promote collagen fibrillogenesis around terminal end buds of the developing mammary gland. Dev Dyn. 235(12):3222-9.
12. Kubow KE, Conrad SK, Horwitz AR. (2013) Matrix microarchitecture and myosin II determine adhesion in 3D matrices. Curr Biol. 23(17):1607-19.
13. Kubow KE, Horwitz AR. (2011) Reducing background fluorescence reveals adhesions in 3D matrices. Nat Cell Biol. 13(1):3-5.
14. Meshel AS, Wei Q, Adelstein RS, Sheetz MP. (2005) Basic mechanism of three-dimensional collagen fibre transport by fibroblasts. Nat Cell Biol. 7(2):157-64.

15. Muzumdar MD, Tasic B, Miyamichi K, Li L, Luo L. (2007). A global double-fluorescent Cre reporter mouse. Genesis. 45:593-605.
16. Nguyen-Ngoc KV, Cheung KJ, Brenot A, Shamir ER, Gray RS, Hines WC, Yaswen P, Werb Z, Ewald AJ. (2012). The ECM microenvironment regulates collective migration and local dissemination in normal and malignant mammary epithelium. Proc Natl Acad Sci U S A. 109(39):E2595-604.
17. Nguyen-Ngoc KV, AJ Ewald. (2013). Mammary ductal elongation and myoepithelial migration are regulated by the composition of the extracellular matrix. J Microsc. 251(3):212-23.
18. Paszek MJ, Zahir N, Johnson KR, Lakins JN, Rozenberg GI, Gefen A, Reinhart-King CA, Margulies SS, Dembo M, Boettiger D, Hammer DA, Weaver VM (2005) Tensional homeostasis and the malignant phenotype. Cancer Cell. 8(3):241-54.
19. Polyak K. (2010) Molecular markers for the diagnosis and management of ductal carcinoma in situ. J Natl Cancer Inst Monogr. 2010;2010(41):210-3.
20. Provenzano PP, Eliceiri KW, Campbell JM, Inman DR, White JG, Keely PJ. (2006) Collagen reorganization at the tumor-stromal interface facilitates local invasion. BMC Med.4(1):38.
21. Sanz-Moreno V, Gaggioli C, Yeo M, Albrengues J, Wallberg F, Viros A, Hooper S, Mitter R, Féral CC, Cook M, Larkin J, Marais R, Meneguzzi G, Sahai E, Marshall CJ. (2011) ROCK and JAK1 signaling cooperate to control actomyosin contractility in tumor cells and stroma. Cancer Cell. 20(2):229-45.
22. Vaezi A, Bauer C, Vasioukhin V, Fuchs E (2002) Actin cable dynamics and Rho/Rock orchestrate a polarized cytoskeletal architecture in the early steps of assembling a stratified epithelium. Dev Cell 3(3):367-381.
23. Vanni S, Lagerholm BC, Otey C, Taylor DL, Lanni F. (2003) Internet-based image analysis quantifies contractile behavior of individual fibroblasts inside model tissue. Biophys J. 84(4):2715-27.
24. Vicente-Manzanares M, Ma X, Adelstein RS, Horwitz AR (2009) Non-muscle myosin II takes centre stage in cell adhesion and migration. Nat Rev Mol Cell Biol. 10(11):778-90.
25. Wolf K, Alexander S, Schacht V, Coussens LM, von Andrian UH, van Rheenen J, Deryugina E, Friedl P. (2009) Collagen-based cell migration models in vitro and in vivo. Semin Cell Dev Biol. 20(8):931-41.

Figure 5-1

Mammary epithelial cells could remodel collagen I matrix. (A) Representative DIC time-lapse movies of epithelial organoid grown in pure collagen I. (B) Matrix displacement quantification performed within certain periods of time. (C) Higher magnification of collagen I fiber alignment. (D) Representative DIC image of epithelial organoids that aligned collagen I fiber in the mixed ECMs. (D'-D") Higher magnification of collagen I fiber alignment.

Figure 5-1

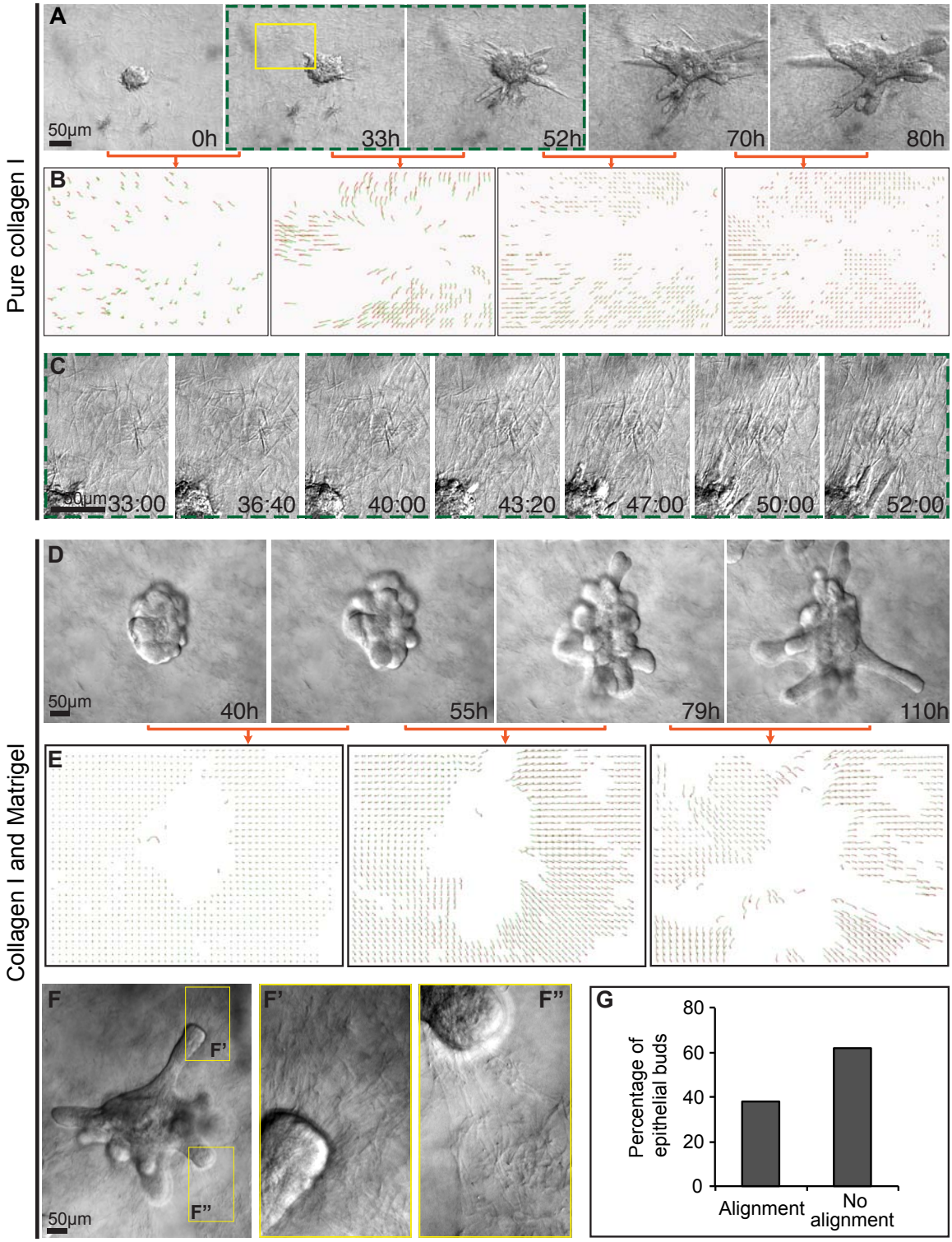
Pure collagen I
A
50μm
0h
33h
52h
70h
80h
B
C
50μm
33:00
36:40
40:00
43:20
47:00
50:00
52:00
Collagen I and Matrigel
D
50μm
40h
55h
79h
110h
E
F
F'
F''
50μm
F'
F''
G
Percentage of epithelial buds
80
60
40
20
0
Alignment
No alignment

Figure 5-2

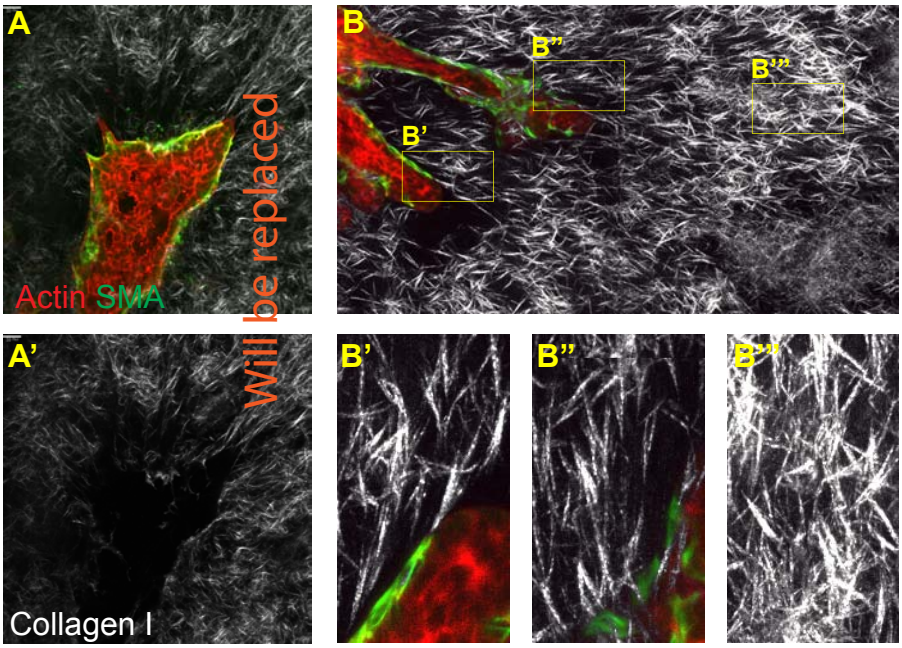

Myoepithelial cells are involved in collagen I fiber alignment. (A) Representative multiphoton micrograph of epithelial organoids aligning the fibers in collagen I matrix. (A') Higher magnification of myoepithelial cells and fiber alignments. (B) Representative multiphoton micrograph of epithelial organoids aligning the fibers in the mixed ECMs. (B'-B") Higher magnifications of myoepithelial cells and collagen I fiber interaction. (B"') Higher magnifications of collagen I meshwork.

Figure 5-3

Myoepithelial cells are pulling collagen I fibers without ECM-directed protrusion. (A, B, C) Representative time-lapse movie presented in (A) DIC and green channel, (B) only green channel, and (C) green and red channels of epithelial organoid grown in a mix of collagen I and Matrigel. (A') Higher magnification of myoepithelial cells actively pulling collagen I fibers. (B') Higher magnification of morphology of single myoepithelial cells. (C') Higher magnification of cell-directed protrusion of myoepithelial cells within a growing bud.

Figure 5-3

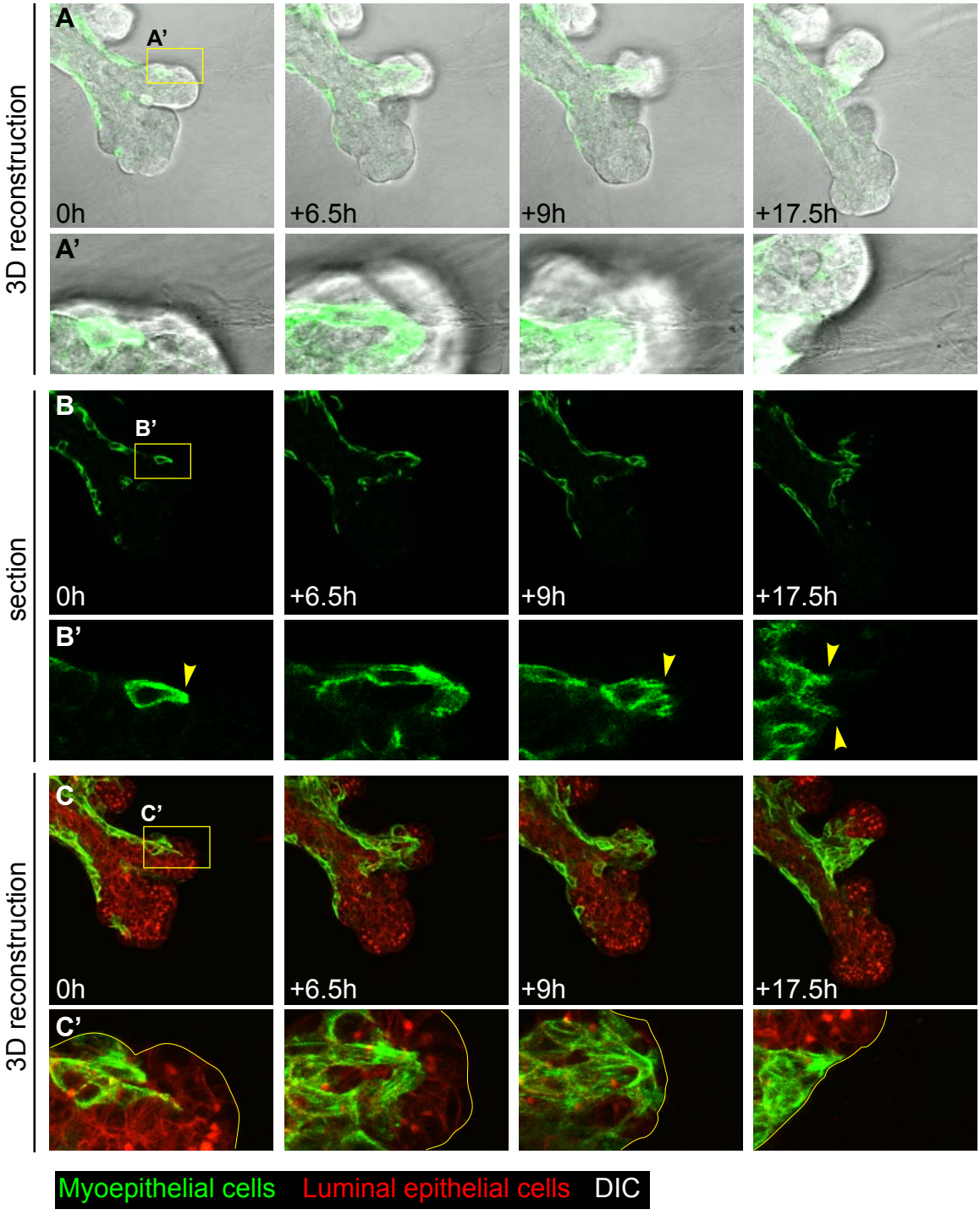
3D reconstruction
section
3D reconstruction
A
A'
B
B'
C
C'
0h
+6.5h
+9h
+17.5h
Myoepithelial cells
Luminal epithelial cells
DIC

Figure 5-4

Actomyosin contractility is required for collagen I alignment and cell retraction. (A) Representative confocal time-lapse image of invasive epithelium grown in a pure collagen I ECM. (A') Schematic description of contractile invasion of epithelium in a pure collagen I ECM. (B-C) Representative DIC time-lapse movie of epithelial organoids treated with (B) Rho kinase inhibitor and (C) Blebbistatin. (B'-C') Higer magnification of unchanged collagen I matrix under (B') Rho kinase inhibitor and (C') Blebbistatin treatments. (B"-C") Displacement quantification of collagen I matrix under (B") Rho kinase inhibitor and (C") Blebbistatin treatments. (B"'- C"') Higher magnification of cell invasion dynamics under (B"') Rho kinase inhibitor and (C"') Blebbistatin treatments. (D) Representative confocal time-lapse movie of epithelial organoids treated with Rho kinase inhibitor. (D'-D") Higher magnification of (D') groups of myoepithelial cells and (D") collection of myoepithelial and luminal epithelial cells.

Figure 5-4

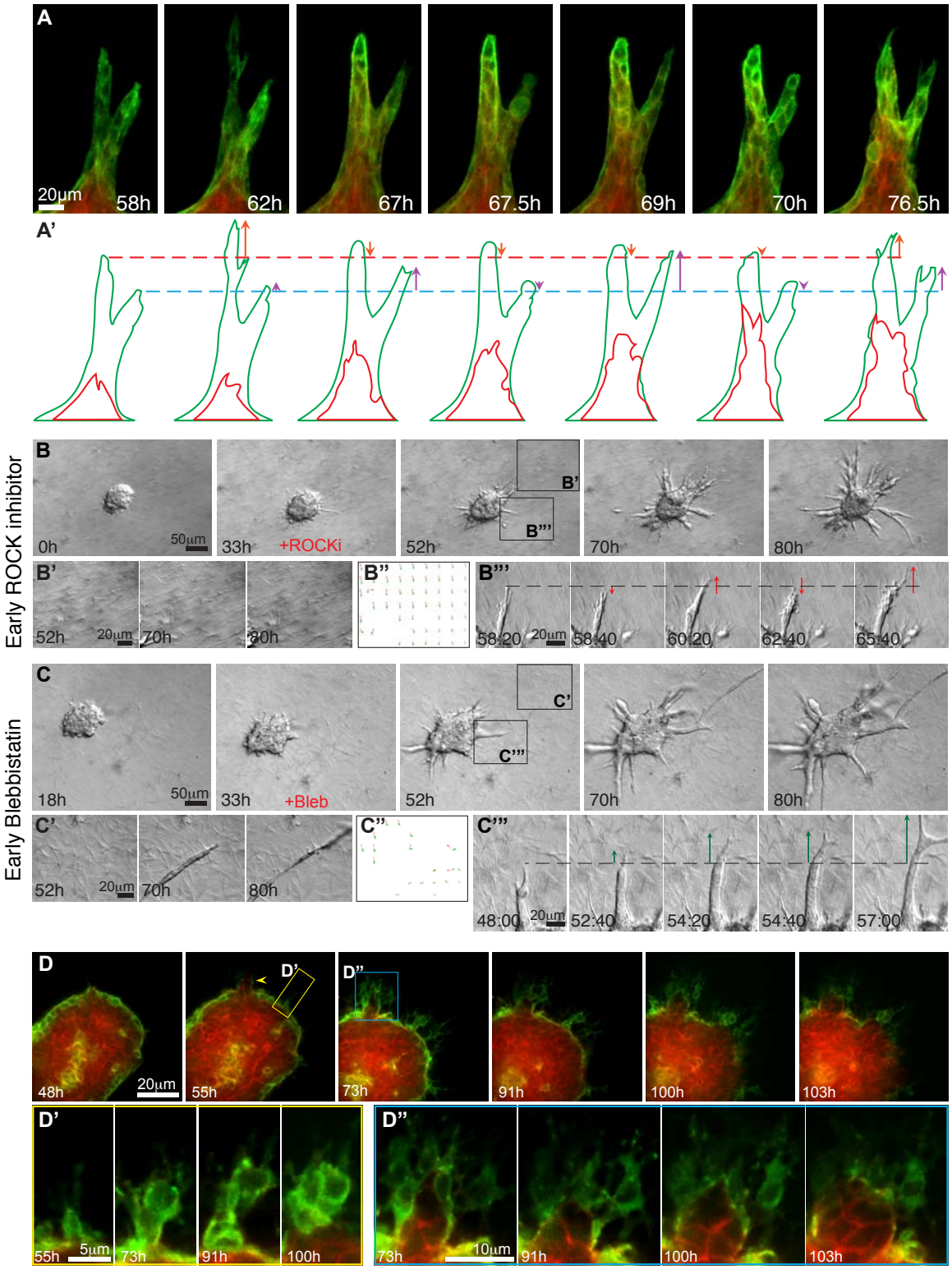
A
20μm
58h
62h
67h
67.5h
69h
70h
76.5h
A'
Early ROCK inhibitor
B
0h
50μm
33h
+ROCKi
52h
B'
B'''
70h
80h
B'
52h
20μm
70h
80h
B''
B'''
58:20
20μm
58:40
60:20
62:40
65:40
Early Blebbistatin
C
18h
50μm
33h
+Bleb
52h
C'
C'''
70h
80h
C'
52h
20μm
70h
80h
C''
C'''
48:00
20μm
52:40
54:20
54:40
57:00
D
48h
20μm
55h
D'
D''
73h
91h
100h
103h
D'
55h
5μm
73h
91h
100h
D''
73h
10μm
91h
100h
103h

Figure 5-5

Actomyosin contractility is required for establishing tissue-ECM interface. (A-C) Epithelial organoids grown in a pure collagen I ECM under (A) Control, (B) Blebbistatin, and (C) Rho kinase inhibitor conditions. (A'-C') Higher magnification of epithelial branches in (A-C), respectively. (A"-C") Localization of SMA of epithelial branches in (A-C), repectively. (A'"-C'") Localization of actin of epithelial branches in (A-C), repectively. (D) Representative confocal time-lapse movies of epithelial organoids treated with Rho kinase inhibitor. (D') Higher magnification of myoepithelial cell layer break. (D") Higher magnification of luminal epithelial invasion.

Figure 5-5

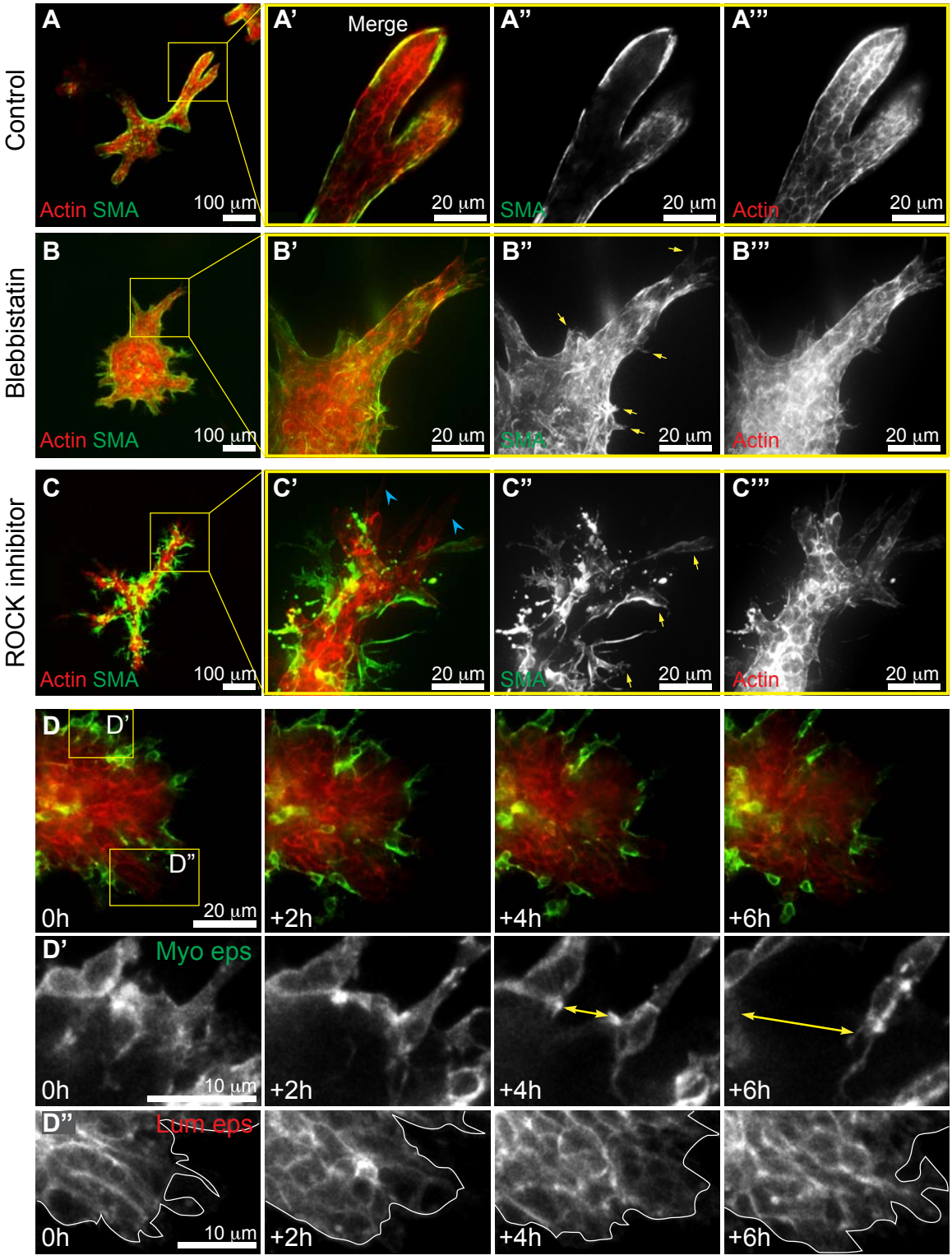
Control
Blebbistatin
ROCK inhibitor
A
A'
Merge
A''
A'''
B
B'
B''
B'''
C
C'
C''
C'''
Actin SMA
SMA
Actin
100 μm
20 μm
D
D'
D''
0h
+2h
+4h
+6h
Myo eps
Lum eps
10 μm

Figure 5-6

Actomyosin contractility is required for maintenance of epithelial integrity. (A) Representaive DIC time-lapse movies of epithelial organoids grown in a pure collagen I ECM and treated with Blebbistatin at later time points. (B'-B") Higher magnification of basal invasion induced by drug treatment (B') on the side and (B") in the leading front. (B-C) Representaive DIC time-lapse movies of epithelial organoids grown in a mix of collagen I and Matrigel (B) as a control and (C) treated with Blebbistatin. (C') Higher magnification of invasion process in (C). (D-E) Localization of Actin, SMA and Laminin 332 in (D) control epithelial tissue, and (E) Blebbistatin-treated tissue.

Figure 5-6

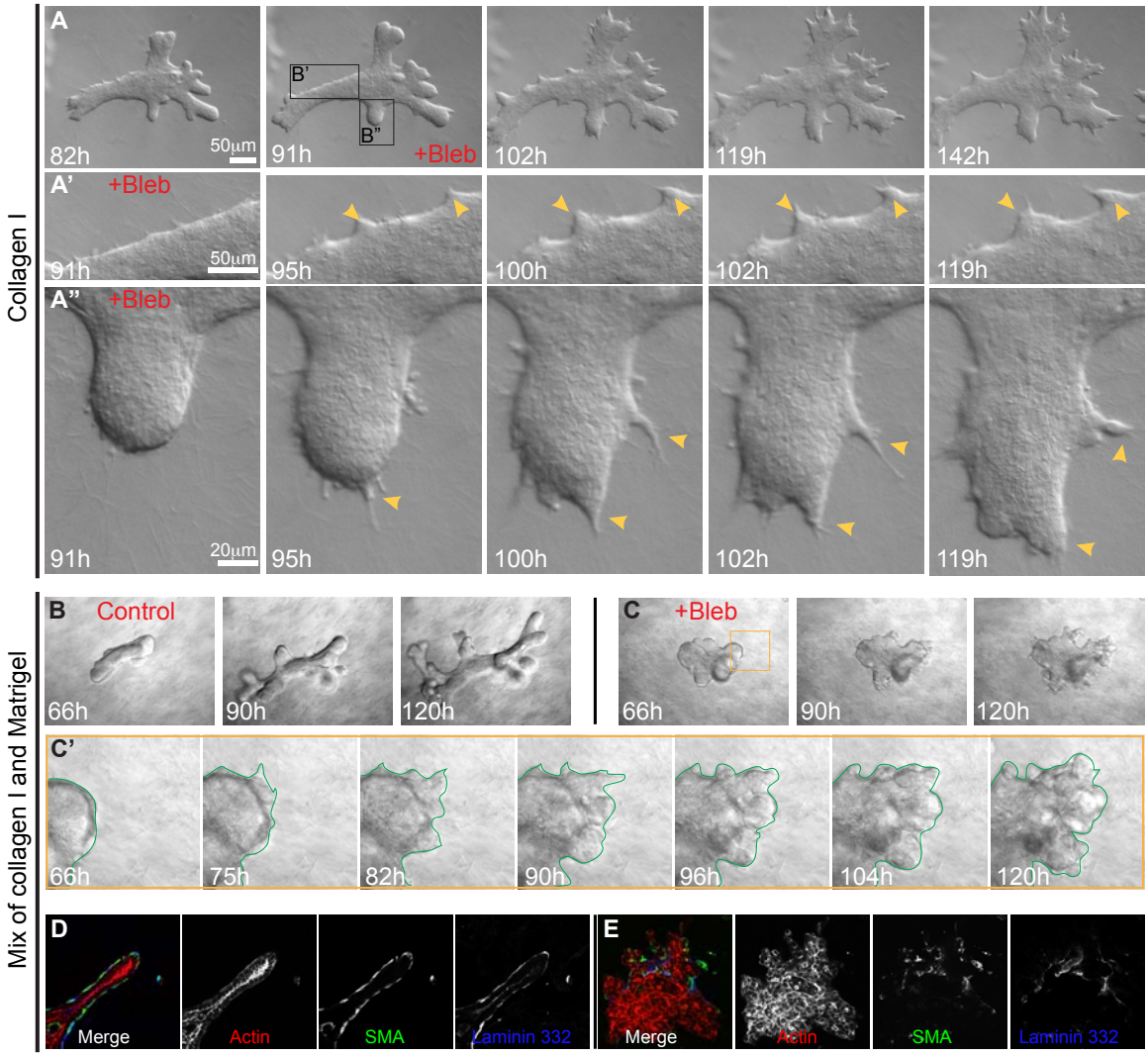
Collagen I
A
82h
50μm
B'
B"
91h
+Bleb
102h
119h
142h
A'
+Bleb
91h
50μm
95h
100h
102h
119h
A"
+Bleb
91h
20μm
95h
100h
102h
119h
Mix of collagen I and Matrigel
B
Control
66h
90h
120h
C
+Bleb
66h
90h
120h
C'
66h
75h
82h
90h
96h
104h
120h
D
Merge
Actin
SMA
Laminin 332
E
Merge
Actin
SMA
Laminin 332

CHAPTER 6

Concurrent deletion of non-muscle myosin IIA and IIB is sufficient to induce proliferation in the mammary epithelium

Abstract

Non-muscle myosin II (NMII) plays an essential role in diverse cellular processes. In epithelial tissues, NMII is required for the formation and maintenance of cell-cell and cell-matrix adhesions. Recent studies have shown that increased NMII signaling can lead to increases in the stiffness of the extracellular matrix and increased cortical tension within the cell, each of which can promote mammary tumor progression. In contrast, the impact of reduced NMII signaling on cell proliferation and tissue growth in the mammary gland is less well understood. To answer this question, we assayed the consequences of conditional deletion of NMIIA and/or NMIIB in primary mammary epithelial tissues. Surprisingly, deletion of both NMIIA and NMIIB (NMIIA,B) induces excessive proliferation in 3D culture models of quiescent ducts and during growth factor-induced branching morphogenesis. Genetic mosaic analysis revealed that the NMIIA,B hyper-proliferation phenotype is cell non-autonomous, as both NMIIA,B-null and neighboring wild-type cells proliferated. Consistent with our 3D culture experiments, loss of both NMIIA,B also induces spontaneous proliferation in mature epithelial ducts *in vivo*. Taken together, our data suggest a novel, cooperative role of NMIIA and NMIIB as negative regulators of proliferation in mammary epithelial tissue.

Introduction

Cell proliferation and tissue growth need to be tightly regulated to ensure normal development and homeostasis. Excessive proliferation is a hallmark of cancer and can be induced by constitutive activation of mitogenic signals, inactivation of growth suppressors, or escape from contact inhibition of proliferation (Weinberg and Hanahan, 2011). For example, loss of the cadherin/catenin complex can induce uncontrolled proliferation and tumor growth (Jeanes et al., 2008). However, most studies of the genetic regulation of proliferation have been conducted in conventional 2D cell culture, which only partially recapitulate the structure and dynamics of epithelial tissues, and the molecular mechanism by which cells sense and regulate proliferation in three-dimensional contexts remains incompletely understood.

Non-muscle myosin II (NMII) is expressed in most cell types and it plays a central part in various cellular processes including cell adhesion, cell migration, and cell division (Vicente-Manzanares et al., 2009). NMII is exists in three isoforms: NMIIA, NMIIB, and NMIIC. Each NMII is composed of three pairs of proteins: two regulatory light chains, two essential light chains, and two heavy chains (Vicente-Manzanares et al., 2009). The specificity of the NMII complex is determined by the identity of the heavy chain, which in mammals can be encoded by three genes NMII heavy chains A, B, and C (NMHC IIA, IIB, IIC) (Vicente-Manzanares et al., 2009). NMII molecules bind to and crosslink the actin cytoskeleton to form networks of actomyosin filaments, which support cell

architecture and function (Vicente-Manzanares et al., 2009). In single cell migration, NMII molecules orchestrate integrin-mediated adhesion to extracellular matrix (ECM) substrates (Choi et al., 2008) and cell polarity to ensure directional movement (Yam et al., 2007). In multicellular systems such as epithelia, NMIIs are required for the establishment and maintenance of apical junctions in early developing tissues, such as the visceral endoderm (Conti et al., 2004) and the spinal neuroepithelium (Ma et al., 2007), and in mature organs such as the intestinal epithelium (Naydenov et al., 2014) and the epidermis (Sumigray et al., 2012). Using a variety of genetic tools including isoform specific ablation and replacement, Adelstein and colleagues have discovered both specific and redundant functions of NMII isoforms (Ma and Adelstein, 2014). NMIIA and NMIIB can be exchangeable in regulating spinal neuroepithelial intercellular junction 5 whereas NMIIA is uniquely required for mouse placental blood vessel formation, and NMIIB is uniquely required for neuronal cell migration (Ma et al., 2004). Exchanging the two isoforms only partially rescues organ defects in the non-redundant cases. Distinct molecular functions of NMIIA and NMIIB have also been found during the spatio-temporal regulation of E-cadherin-based junction in epithelial cell sheet (Smutny et al., 2010). These findings demonstrate the importance of NMII molecules in epithelial tissue architecture and function, and also stimulate questions about how loss of NMII could disrupt tissue homeostasis and promote pathogenesis.

Disruption of NMII-mediated cellular contractility is associated with many

types of diseases, in particular cancer. Cell binding to surrounding ECM activates NMII molecules and the Rho/ROCK pathway, enforcing cell-matrix adhesion affinity 3. However, a sustained elevation of NMII-mediated cellular tension in response to increasing matrix stiffness and rigidity can promote cell proliferation and tumorigenesis (DuFort et al., 2011). Similarly, inducible expression of p190-B Rho GTPase disrupted mammary tissue architecture and resulted in increased cell proliferation (Chakravarty et al., 2000). In contrast, reduced contractility due to loss of NMIIA in a tumor susceptible background promotes cell proliferation and metastasis in squamous cell carcinoma (Schramek et al., 2014). This emerging evidence indicates that NMIIA is a tumor suppressor (Schramek et al., 2014); however, the molecular mechanisms by which loss of NMII proteins regulate cell proliferation remain elusive.

Here we sought to understand the role of NMII in epithelial organization and development, using the mammary epithelium as a model system. We combined 3D culture of primary epithelial organoids with adenoviral delivery of Cre-recombinase and timelapse imaging to reveal the cellular consequence of deletion of NMII in mammary epithelium. Surprisingly, we found that combined deletion of NMIIA and NMIIB is sufficient to induce epithelial tissue growth and cell proliferation in a cell non-autonomous fashion, even in the absence of exogenous growth factors signals.

Results

Isoform specific deletion of NMII in mammary organoids

We first examined the expression and localization of myosin II isoforms A, B, and C in the mammary epithelium using both *NMIIA-GFP* and *NMIIB-GFP* knock-in mice and immunofluorescent staining to detect endogenous proteins. The mammary epithelium consists of two major cell types: an inner luminal epithelial cell layer, surrounded by a basally-positioned myoepithelial cell layer. Consistent with previous reports (Beach et al., 2011), NMIIA was expressed equally in both luminal and myoepithelial cells, NMIIB was predominantly observed in myoepithelial cells, and NMIIC was restricted in the luminal epithelial cell layer (Fig. 6-1A-C). In luminal epithelial cells, we additionally detected low levels of NMIIB protein localized near the apical limit of the cell membranes (Fig. 6-1B).

To study the consequences of loss of NMII in the mammary epithelium, we used Cre recombinase to delete the NMHCIIA and NMHCIIB genes in primary mammary epithelial organoids embedded within 3D extracellular matrix (ECM) gels (Matrigel) (Fig. 6-1A). In these assays, wild-type organoids will arrest as polarized cysts in basal medium and will undergo branching morphogenesis when additionally supplemented with FGF2 (Ewald et al., 2008; Nguyen-Ngoc et al., 2015). In subsequent paragraphs, since the heavy chain confers the specificity of the NMII complex, we refer to the deletion of NMHCIIA and NMHCIIB and loss of NMIIA and NMIIB interchangeably. We first tested the

efficiency of Cre-lox-based gene deletion using a tamoxifen inducible Cre-ER. Treatment of the organoids with tamoxifen was sufficient to deplete NMHCIIA and NMHCIIB proteins from mammary organoids (Fig. 6-2A-B). As a control for any effects of tamoxifen and as a strategy for generation of genetic mosaics, we alternately utilized adenovirally delivered Cre recombinase (Ad-Cre) to delete NMHCIIA or NMHCIIB, typically in the range of 50-75% of cells (Shamir et al., 2014). Ad-Cre was also effective in depleting NMIIA and NMIIB.

Deletion of both NMIIA and NMIIB is sufficient to induce proliferation in quiescent mammary epithelium

We first investigated the consequences of loss of NMIIA and/or NMIIB in basal medium without exogenous growth factor, our cyst forming assay (Nguyen-Ngoc et al., 2014; Fig. 6-3A-B). Control epithelial organoids typically maintained their size or compacted slightly (Fig. 6-3C). Deletion of two or three alleles of the NMHCIIA and NMHCIIB genes did not grossly affect epithelial tissue growth (Fig. 6-3D-H). Surprisingly, homozygous deletion of all four alleles of NMHCIIA and NMHCIIB resulted in a striking increase in epithelial growth, inferred from the change in projected area of organoids in timelapse movies (Fig. 6-3I-J). This apparent increase in tissue growth in NMIIA,B-deleted organoids was substantiated by a higher mitotic index (Fig. 6-3K), calculated from the fraction of total cells that stained positive for phospho-Histone H3 (pH-H3). Representative images from this analysis reveal the large increase in mitotic cells in organoids

lacking NMIIA and NMIIB (green), compared to control organoids or organoids lacking either NMIIA or NMIIB singly (Fig. 6-3L-O). Taken together, these data indicate that concurrent loss of both NMIIA and NMIIB is sufficient to induce extensive mitosis in the mammary epithelium under normally quiescent conditions.

Loss of NMIIA and NMIIB synergizes with exogenous FGF2 to promote proliferation

During puberty, mammary epithelial cells undergo branching morphogenesis in response to proliferative signals mediated through both steroid hormones and growth factors 15. We have previously shown that this process can be modeled through addition of nanomolar concentrations of FGF2, in our "branching assay" 11,12 (Fig. 6-4A). FGF2 addition induced cell division and resulted in the formation of branched epithelial structures (Fig. 6-4B), with a corresponding increase in size (~4 fold, Fig. 6-4I). Deletion of 1-3 alleles of NMHCIIA and NMHCIIB correlated with a non-significant reduction in tissue growth and was compatible with relatively normal branching (Fig. 6-4C-G, I). However, deletion of all four alleles led to a striking and significant increase in tissue growth (~9 fold), inferred from the change in projected area of organoids in time-lapse movies (Fig. 6-4H). Consistent with their apparent growth in time-lapse movies, NMIIA,B double null organoids were more proliferative than those in control organoids, as assayed by pH-H3 staining (Fig. 6-3J-M). These data

demonstrate that loss of both NMIIA and NMIIB can also synergize with growth factor signaling to further promote excess proliferation. Taken together, we conclude that NMIIA and NMIIB cooperatively serve as negative regulators of mammary epithelial proliferation.

The hyperproliferation caused by loss of NMIIA,B is cell non-autonomous

We next asked whether the excess proliferation we observed was limited to NMHCIIA$^{-/-}$;NHMCIIB$^{-/-}$ cells. To address this question, we crossed a bifluorescent Cre reporter into the floxed myosin II line (*NMIIA$^{fl/fl}$;NMIIB$^{fl/fl}$;mTmG*). With the mTmG reporter, there is a membrane-localized Tomato (mT; red fluorescence) that is expressed constitutively in all cells 16. Cre activity excises the mT allele and brings a membrane-localized GFP (mG) into proximity of the promoter 16 (Fig. 6-5A). Green fluorescence therefore serves as a direct reporter for Cre activity and an indirect reporter for NMHCIIA and NMHCIIB deletion. In our cyst formation assay, control organoids rarely contain mitotic cells. We inferred the genotype of dividing cells by collecting timelapse movies of Ad-Cre infected *NMIIA$^{fl/fl}$;NMIIB$^{fl/fl}$;mTmG* and determining the fluorescent protein expression of the dividing cells. Red cells were Cre negative and inferred to be wildtype, while green cells had active Cre and were inferred to have lost both NMIIA and NMIIB. Surprisingly, we found that organoids with mosaic loss of NMIIA and NMIIB exhibited extensive division of both double null cells (Fig. 6-5C) and wildtype cells (Fig. 6-5C-D). Our tracking

and quantification (5 movies, each 30 hours long; 10 minutes time-lapse interval) revealed that 75% of dividing cells were wild-type and 25% were double null cells (Fig. 6-4E). We concluded that loss of NMIIA and NMIIB can induce cell non-autonomous proliferation.

NMIIA,B deletion increases sporadic cell proliferation in epithelial ducts *in vivo*

Our genetic mosaic analysis in 3D culture revealed that loss of NMIIA,B resulted in excess growth of mammary epithelium and triggered cell proliferation in both subsets of wild-type and NMIIA,B-null cells. We next tested the *in vivo* consequences of NMIIA,B deletion specifically in polarized mammary epithelial ducts. We isolated and orthotropically transplanted organoids from *ER-Cre; NMIIA$^{fl/fl}$;NMIIB$^{fl/fl}$;mTmG* and *CreER; NMIIA$^{fl/+}$; mTmG* mice, waited 6 weeks for ductal network formation, then induced NMIIA,B deletion by tamoxifen injection, then waited for 6 weeks before mammary glands were collected and analyzed for mitotic cells (Fig. 6-6A). Similar to organoids in our cyst forming assay (Fig. 6-6B), control epithelial ducts contained very few pH-H3+ mitotic cells (Fig. 6-6C-E). In contrast, both organoids (Fig. 6-6B') and epithelial ducts in which both NMIIA and NMIIB were deleted displayed excess mitotic cells (Fig. 6-C'-E'). We calculated the number of proliferative cells per 40x field of view and observed a statistically significant increase following loss of NMIIA and NMIIB (Fig. 6-6F). Finally, proliferation was observed in both red (Cre-) and green (Cre+) cells, thus

demonstrating that the effect of NMIIA,B deletion on proliferation was also cell non-autonomous *in vivo* (Fig. 6-6G-H').

The MMTV-Cre transgene was able to accomplish deletion of NMHCIIA and NMHCIIB in culture but not *in vivo*

We next sought to determine the consequences of loss of NMIIA and NMIIB during pubertal branching morphogenesis, through mammary epithelial-specific expression of Cre under control the MMTV long terminal repeat 17 (*MMTV-Cre; NMIIA$^{fl/fl}$;NMIIB$^{fl/fl}$;mTmG*). Using the mTmG Cre reporter, we confirmed that Cre was specifically expressed and active in luminal epithelial cells (Fig. 6-7A-D). Although we observed a range of epithelial architectures, we observed essentially no proliferating cells in these samples (Fig. 6-7A-D). This negative outcome could result from two possibilities. First, it was possible that NMIIA and NMIIB proteins were not depleted in the mammary epithelial tissue. Second, MMTV-Cre-driven loss of NMIIA and NMIIB might not be sufficient to induce proliferation *in vivo*. To distinguish these possibilities, we isolated organoids from *MMTV-Cre; NMIIA$^{fl/fl}$;NMIIB$^{fl/fl}$;mTmG* mice into two groups, one for immediate analysis of NMIIA and NMIIB protein levels by Western blot (*in vivo* samples) and one for growth in organotypic culture. After 5 days, we analyzed NMIIA and NMIIB protein levels and proliferation index in the cultured organoids (Fig. 6-7E-L).

As a positive control, both tamoxifen-induced Cre-ER and Ad-Cre infection

were able to efficiently deplete the protein levels of NMHCIIA and NMHCIIB (Fig. 6-7F, lanes 1, 2). However, we found that NMIIA and NMIIB protein levels in the *in vivo* MMTV-Cre samples were indistinguishable from wildtype (Fig. 6-7F, lanes 4, 5). Surprisingly, protein levels of NMIIA and NMIIB in organoids from *MMTV-Cre; NMIIA$^{fl/fl}$;NMIIB$^{fl/fl}$;mTmG* mice were significantly reduced in the *in vitro* cultured samples (Fig. 6-7F, lanes 3). Consistent with the loss of protein, the cultured organoids from *MMTV-Cre; NMIIA$^{fl/fl}$;NMIIB$^{fl/fl}$;mTmG* mice displayed significantly elevated levels of proliferation (Fig. 6-7G-L). These data indicate that the MMTV-Cre driver was not able to deplete NMIIA and NMIIB proteins in mammary epithelium *in vivo* and that switching to *in vitro* culture enabled the protein reduction, resulting in hyper-proliferation. Taken together, our data reveal across three Cre delivery approaches (Er-Cre, Ad-Cre, MMTV-Cre) that combined loss of NMIIA and NMIIB is sufficient to induce epithelial hyperproliferation.

Discussion

The study of NMII was motivated by our previous results which demonstrate the requirement of actomyosin contractility in epithelial organization and ductal elongation during branching morphogenesis (Ewald et al., 2008). We initially aimed to understand the role of individual NMII isoforms in the mammary epithelium using 3D organotypic culture technique. We surprisingly found that concurrent loss of NMIIA and NMIIB isoforms not only triggers cell proliferation in the quiescent epithelial tissue, but also significantly increases proliferation in actively growing epithelium. The hyper-proliferation effect only occurs when all four alleles of the two isoforms are deleted simultaneously. The deletion of NMIIA and NMIIB in a subset of cells can induce neighboring wild-type cells to proliferate. Collectively, our data reveal a novel, cooperative role of NMIIA and NMIIB in controlling cell proliferation at different developmental stages of mammary epithelium.

How epithelial tissues control their size and how epithelial cells communicate and regulate one another have been long-standing questions. Architecture of epithelial tissues is based on multiple types of adhesions, which help epithelial cells adhere to one another and attach to surrounding ECMs. Cell tension derived from NMII-based contractility is not only required to support these adhesion complexes, but also responds to the resistance from adjacent cells or ECM microenvironment. Therefore, either an elevation or reduction of cell tension would change cell behavior, tissue organization, and other consequences

like tumor formation and invasion. Growing evidence indicates that activation of Rho/ROCK and increasing actomyosin contractility in response to or in combination with matrix stiffness can enhance proliferation and tumor growth (Paszek et al., 2005; Butcher et al., 2009; Samuel et al., 2011). Stiff matrix and cellular tension feedback loops promote cell proliferation either through the Ras/MAPK pathway, a downstream of FAK/Src kinase activated by integrin clustering (Schlaepfer et al., 1994), or through a downstream transcription factor of Hippo pathway, YAP, linking mechano-transduction to gene expression and proliferation (Dupont et al., 2011; Schlegelmilch et al., 2011). In contrast, our data reveal the opposite effect and support the notion that NMII molecules can function as negative regulators of cell growth. Since NMIIA and NMIIB provide mechanical tension for the establishment and dynamics of junction complexes (Smutny et al., 2010) and loss of junctional components such as E-Cadherin (Derksen et al., 2006), and Par3 (McCaffrey et al., 2012) accelerates mammary tumor progression, it is likely that loss of NMII isoforms trigger cell proliferation by destabilizing these junctions or disrupting mechano-sensation and transduction within epithelial tissue.

NMIIA and NMIIB are of the most essential structural proteins and required for multiple functions at the cell and tissue levels. Therefore, it may not be favorable for tumor growth and invasiveness both isoforms are completely depleted from the tissue. Instead, through a non-cell autonomous machinery, the effect of NMIIA,B deletion in a subset of cells could benefit the growth of adjacent

cells and tissues. This suggests that concurrent loss of NMIIA and NMIIB could occur in a certain population of tumor cells.

Cell proliferation is tightly controlled by multiple redundant signaling pathways. Tumor formation requires multiple genetic alterations. Although mosaic deletion of NMIIA,B strikingly induces cell proliferation in our 3D culture assays, we observe a modest increase in proliferation with relatively normal epithelial structure using orthotropic transplantation. This data suggests that loss of NMIIA,B may not be sufficient and requires additional genetic perturbations to trigger tumor formation. In line with this concept, knock-down of NMIIA accelerates tumor growth on a TβRII-null background (Schramek et al., 2014). Future work should focus on studying the deletion of NMIIA and NMIIB in the context of tumor formation with long latency.

Evolved from one gene of NMII in metazoans, mammalian cells own three distinct NMII isoforms, whose specific and cooperative roles in many organs remain obscure. NMIIA and NMIIB are indispensable genes for embryogenesis because their knock-out pups are not viable (Conti et al., 2004; Tullio et al., 2001). The expression and localization of NMII isoforms become distinguishable and tissue-specific at the early embryo (Ma and Adelstein, 2014). The fact that there are more than one NMII isoforms expressed in either luminal or myoepithelial cells indicates that their functions may be substituted. Defects in tight junction leading to loss of epidermal homeostasis are observed only when both NMIIA and NMIIB are concurrently deleted (Sumigray et al., 2012). Our

genetic variance analyses reveal that at least one allele of either NMIIA or NMIIB is sufficient in controlling epithelial cell proliferation; the hyper-proliferative effect is achieved only with a complete deletion of all four alleles. Moreover, using the MMTV-Cre driver with the *in vitro* assay, which NMIIA,B gene deletion is limited in luminal epithelial cells, we still observe increased proliferation. This result indicates that the phenotype does not require both types of mammary epithelial cells and raises a question about the involvement of NMIIC in regulating luminal epithelial cell proliferation.

The MMTV-Cre transgene has been commonly used for specific conditional gene deletion in mammary epithelial tissue (Robinson and Hennighausen, 2011). Previous studies have observed incomplete MMTV-Cre-mediated gene deletion and a complete gene deletion could be achieved after multiple rounds of estrus cycles (Lu et al., 2008). However, in this study using MMTV-Cre transgene line D, we are unable to deplete NMII proteins in mammary epithelium. Although we observe an extensive expression of Cre enzyme in luminal epithelial cells via the mTmG biosensor, NMIIA and NMIIB proteins of epithelial tissue carrying NMIIAfl/fl; NMIIBfl/fl remain unchanged. This result reveals another caveat of the MMTV-Cre driver, which might be caused by several reasons. First, genomic loci are variably accessible for Cre-mediated recombination. Targeting mTmG in the ROSA26 locus will be likely more accessible than to the loci of NMHCIIA and NMHCIIB genes, probably leading to low levels of recombination. Second, Cre activity and efficiency are context-

dependent. Our experiment setting reveals that NMIIA and NMIIB proteins from the same source of tissue are depleted *in vitro*, but not *in vivo*. It is possible that microenvironmental changes and stress during experimental procedure and *in vitro* culture might enable Cre to access and perform genomic excision. Third, as the important structural proteins, NMIIA and NMIIB might be more resistant to degradation, resulting in longer turnover and retention.

Materials and methods

Mouse strains. The *NMIIA*$^{fl/fl}$ *and NMIIB*$^{fl/fl}$ mouse lines (Jacobelli et al., 2010; Ma et al., 2009) were a gift from R. Adelstein (National Heart, Lung, and Blood Institute, NIH, Bethesda, MD). The *R26::Cre-ER* mouse line was a gift of J. Nathans (Johns Hopkins University – Baltimore, MD). The *MMTV-Cre* line D (Wagner et al., 1997) and *mT/mG* (Muzumdar et al., 2007) mouse lines were acquired from the Jackson Laboratory. Mouse husbandry and procedures were all conducted under an Institutional Animal Care and Use Committee–approved animal protocol.

3D culture assays of primary mammary epithelial organoids. We used a combined mechanical and collagenase/trypsin digestion, followed by differential centrifugation to isolate groups of mammary epithelial ducts, termed as organoids, as previously described (Ewald et al., 2008, 2012; Nguyen-Ngoc et al., 2014). Organoids were then embedded in 3D Matrigel TM (Corning) at 2-3 organoids/μl as 150-μl suspensions in a 24-well multiwell glass bottom plate or 2-well chamber coverglass (Thermo). Gels were allowed to polymerized for 40 min at 37°C and then cultured with organoid medium including DMEM (Life Technology) with 1% insulin-transferrin-selenium (Gibco) and 1% penicillin-streptomycin (Sigma-Aldrich). Basal organoid media was used in the cyst forming and co-culture assays while supplementation with 2.5 nM FGF2 (Sigma) was used to initiate branching morphogenesis.

Adenoviral delivery of Cre recombinase. As previously described (Shamir et al., 2014), prior to embedding in 3D Matrigel, organoids were infected with Adeno-CMV-Cre (Vector BioLabs) at the ratio of ~10^7 PFU per 1000 organoids. Infections were conducted in a 50 μl DMEM for 1.5 – 2h at 37°C.

Orthotropic transplantation to mammary fat pad. For transplantation of mammary organoids followed by gene deletion induction, we isolated and incubated organoids overnight at 37°C in organoid medium with 2.5 nM FGF2 in HydroCell 96-well microplates (174907, Thermo Fisher Scientific). The next day, organoids were suspended in a DMEM:Matrigel (1:1) solution at a density of 20 – 30 organoids/μl and kept on ice throughout the transplantation procedure. We used 3-wk-old NOD/SCID mice to perform orthotropic transplantation in a sterile hood. In brief, mice were anesthetized and immobilized. A mid-sagittal cut followed by an oblique cut from the initial incision to one hip. Skin was retracted to expose the no. 4 mammary gland. The no. 5 gland and the region surrounding the lymph node in the no. 4 gland were removed. The organoid suspension was injected into the cleared no. 4 gland using a 1-in needle syringe. The same procedure was repeated in the contralateral mammary gland. We transplanted control organoids (*Cre-ER; mTmG; NMIIA*$^{fl/+}$) in one gland and experimental organoids (*Cre-ER; mTmG; NMIIA*$^{fl/fl}$*; NMIIB*$^{fl/fl}$) in the other. The wounds were closed with 9-mm autoclips. Triple antibiotic ointment was applied to wounding sites. For deletion of NMIIA and NMIIB in mature ductal networks, after transplantation we allowed NOD/SCID mice to grow for 6 weeks, and then

injected three doses of 100 μl of 10mg/ml tamoxifen i.p every other day. Glands were collected 6 weeks after injection.

Differential interference contrast (DIC) microscopy. DIC time-lapse imaging was performed with an LD Plan-Neofluar 20×/0.4 Korr Ph2 objective lens and a Cell Observer system with an AxioObserver Z1 and an AxioCam MRM camera (Carl Zeiss). 100 – 200 positions were captured in paralleled for 5 days with 20-min intervals. Temperature was set at 37°C and CO_2 at 5%. AxioVision (Carl Zeiss) was used to acquire and analyze the movies, place scale bars, and export time frames in TIFFs. Photoshop CS5 was used to adjust levels and brightness on entire images.

Confocal microscopy. Confocal imaging was conducted on on a spinning-disk confocal microscope (Solamere Technology Group Inc.) with an XR/MEGA-10 S30 camera (Stanford Photonics, Inc.), as previously described (Ewald et al., 2011). A Fluar 20×/0.75 objective lens (Carl Zeiss) was used for intermediate magnification images, an LD C-Apochromat 40×/1.1 W Korr objective lens (Carl Zeiss) for high magnification single and time-lapse image acquisition, with water and oil used as the imaging mediums, respectively. Acquisition was done with a combination of μManager (Edelstein et al., 2010) and Piper (Stanford Photonics, Inc.). For time-lapse imaging to observe cell division, images were captured with 20-min intervals for 16 – 18h, and temperature was set at 37°C and CO_2 at 5%. Imaris (Bitplane) was used to analyze images, add scale bars, and export individual TIFFs. Photoshop CS5 was used to adjust levels and gamma for each

channel.

Immunofluorescent staining. Organoids and mammary gland tissues were collected, fixed, and stained as previously described (Nguyen-Ngoc et al., 2014). Briefly, organoids embedded in 3D Matrigel were fixed in 2% paraformaldehyde (PFA) for 25 min and mammary gland tissues in 4% PFA for 3h. The samples were then rinses three time with PBS for 10 min, embedded in Optimal Cutting Temperature compound (OCT), frozen at -80°C. OCT blocks were sectioned at 100-μm thickness for cultured organoid samples and 50-μm thickness for gland tissue. Sections were placed on Superfrost Plus Gold microscope slides (15-188-48; Fisherbrand) and stored at -80°C. For antibody staining, slides were thawed at room temperature, rinsed twice with PBS to wash off OCT, permeabilized with 0.5% Triton X-100 for 1h. Samples were then blocked with 10% FBS 1% BSA in PBS solution for 2 – 3h, incubated with primary antibody solution overnight at 4°C. Slides were then rinsed twice with 10% FBS 1% BSA in PBS solution, then incubated with secondary antibody diluted in 1% FBS 1% BSA in PBS solution overnight at 4°C. Slides was rinsed twice with 1% FBS 1% BSA in PBS for 10 min, and once with PBS for 10 min before mounted with Fluoromount (F4680; Sigma-Aldrich), and sealed with coverslips. Nuclei were stained with DAPI (1:1000, D3571, Invitrogen). Immunofluorescent staining for each antibody was done at least three independent biological replicates. Mouse anti-Phospho-Histone H3 (1:300, 9706L, Cell Signaling Technology) was used as primary antibody and Alexa Fluor-647 goat anti-mouse (1:200, Invitrogen) as secondary

antibody.

Protein extraction. Organoids that were freshly isolated from mammary gland tissue were directly suspended in RIPA buffer to obtain cell lysate. For organoids grown in 3D Matrigel, medium was aspirated, the gels were rinsed once with 1 ml cold PBS, and then dissolved in 1 ml cold PBS/EDTA buffer. The suspension was transferred to centrifuge tubes, mixed by pipetting, incubated on shaker for 15 min at 4°C, and then centrifuged at 1500 rpm for 5 min at 4°C. Supernatants were removed and pellets were suspended with 50 – 100 μl of RIPA lysis buffer. Lysis buffer was prepared by diluting 10x RIPA buffer with ultrapure water. Immediately before added to cell pellets, lysis buffer was supplemented with 0.1% SDS, 5% glycerol, 3 mM EDTA, 1 mM NaF, 1 mM PMSF, 1.5 mM $NaVO_4$, Aprotinin (A6279; Sigma-Aldrich), and a mini protease inhibitor tablet (11836153001; Roche). The suspension in RIPA buffer was left on ice for 40 – 60 min and vortexed every 10 min. Tubes were centrifuged for 10 min at 13 000 rpm at 4°C. Supernatants were transferred to another tubes and stored at -80°C.

Western blotting. Cell lysates were thawed or directly used after preparation. Samples were mixed with Laemmli sample buffer (161–0747; Bio-Rad Laboratories) and β-mercaptoethanol, heated at 70°C for 10 min. Samples were loaded for equal amount of protein based on bicinchoninic acid (BCA) analysis (Thermo Fisher Scientific) in in 4–15% Mini-PROTEAN TGX precast gels (456–1084; Bio-Rad Laboratories). SDS-PAGE was run at 115V for 1h until the dye came off the gels. Gels were transferred onto nitrocellulose membranes (45-000-

948; GE Healthcare) at 100 V for 1 h at 4°C. Membranes were blocked in 10 ml 10mL Odyssey Blocking Buffer for 1h at room temperature on shaker before incubated with primary antibody in 50:50 Odyssey Blocking Buffer/TBST at 4°C overnight. Primary antibodies used were rabbit anti-NMIIA (1:1000; 3403; Cell Signaling Technologies), rabbit anti-NMIIB (1:1000; PRB-445P; Covance), Mouse anti-Beta Tubulin (1:1000; T5201; Sigma). Membranes were washed three times with TBST for 5 min, before incubated with secondary antibody (IR-conjugated Licor) in 50:50 Odyssey blocking buffer/TBST for 1 h at room temperature on shaker. Secondary antibodies used were Goat anti-Rabbit 800CW (1:10,000, 827-08365; Licor) and Goat anti-Mouse 680RD (1:10,000; 926-68170; Licor). Membranes were then washed twice with TBST for 5 min, once with TBS for 5 min, before imaged wet on the Licor Odyssey CLx. Bands were quantified using Image Studio 4.0 software.

Author contribution

K-V. N-N principally designed, performed the experiments and analyzed the data. K-V. N-N also wrote the manuscript.

References

1. Beach JR, Hussey GS, Miller TE, Chaudhury A, Patel P, Monslow J, Zheng Q, Keri RA, Reizes O, Bresnick AR, Howe PH, Egelhoff TT (2011) Myosin II isoform switching mediates invasiveness after TGF-β-induced epithelial-mesenchymal transition. Proc Natl Acad Sci. 108(44):17991-6.
2. Chakravarty G, Roy D, Gonzales M, Gay J, Contreras A, Rosen JM (2000) P190-B, a Rho-GTPase-activating protein, is differentially expressed in terminal end buds and breast cancer. Cell Growth Differ. 11(7):343-54.
3. Choi CK, Vicente-Manzanares M, Zareno J, Whitmore LA, Mogilner A, Horwitz AR (2008) Actin and alpha-actinin orchestrate the assembly and maturation of nascent adhesions in a myosin II motor-independent manner. Nat Cell Biol. 10(9):1039-50.
4. Conti MA, Even-Ram S, Liu C, Yamada KM, Adelstein RS (2004) Defects in cell adhesion and the visceral endoderm following ablation of nonmuscle myosin heavy chain II-A in mice. J Biol Chem. 279(40):41263-6.
5. Derksen PW, Liu X, Saridin F, van der Gulden H, Zevenhoven J, Evers B, van Beijnum JR, Griffioen AW, Vink J, Krimpenfort P, Peterse JL, Cardiff RD, Berns A, Jonkers J (2006) Somatic inactivation of E-cadherin and p53 in mice leads to metastatic lobular mammary carcinoma through induction of anoikis resistance and angiogenesis. Cancer Cell. 10(5):437-49.
6. DuFort CC, Paszek MJ, Weaver VM (2011) Balancing forces: architectural control of mechanotransduction. Nat Rev Mol Cell Biol. 12(5):308-19.
7. Dupont S, Morsut L, Aragona M, Enzo E, Giulitti S, Cordenonsi M, Zanconato F, Le Digabel J, Forcato M, Bicciato S, Elvassore N, Piccolo S (2011) Role of YAP/TAZ in mechanotransduction. Nature.474(7350):179-83.
8. Edelstein A, Amodaj N, Hoover K, Vale R, Stuurman N (2010) Computer control of microscopes using μManager. Curr Protoc Mol Biol. Chapter 14:Unit14.20.
9. Ewald AJ, Brenot A, Duong M, Chan BS, Werb Z (2008) Collective epithelial migration and cell rearrangements drive mammary branching morphogenesis. Dev Cell. 14(4):570-81.
10. Ewald AJ, Huebner RJ, Palsdottir H, Lee JK, Perez MJ, Jorgens DM, Tauscher AN, Cheung KJ, Werb Z, Auer M (2012) Mammary collective cell migration involves transient loss of epithelial features and individual cell migration within the epithelium. J Cell Sci. 125(Pt 11):2638-54.
11. Hanahan D, Weinberg RA (2011) Hallmarks of cancer: the next generation. Cell. 144: 646–674.
12. Jacobelli J, Friedman RS, Conti MA, Lennon-Dumenil AM, Piel M, Sorensen CM, Adelstein RS, Krummel MF (2010) Confinement-optimized three-dimensional T cell amoeboid motility is modulated via myosin IIA-regulated adhesions. Nat Immunol. 11(10):953-61.
13. Jeanes A, Gottardi CJ, Yap AS (2008) Cadherins and cancer: how does

cadherin dysfunction promote tumor progression? Oncogene 27: 6920–6929.
14. Lu P, Ewald AJ, Martin GR, Werb Z (2008) Genetic mosaic analysis reveals FGF receptor 2 function in terminal end buds during mammary gland branching morphogenesis. Dev Biol. 321(1):77-87.
15. Ma X, Adelstein RS (2014) The role of vertebrate nonmuscle Myosin II in development and human disease. Bioarchitecture. 4(3):88-102.
16. Ma X, Bao J, Adelstein RS (2007) Loss of cell adhesion causes hydrocephalus in nonmuscle myosin II-B-ablated and mutated mice. Mol Biol Cell. 18(6):2305-12.
17. Ma X, Takeda K, Singh A, Yu ZX, Zerfas P, Blount A, Liu C, Towbin JA, Schneider MD, Adelstein RS, Wei Q (2009) Conditional ablation of nonmuscle myosin II-B delineates heart defects in adult mice. Circ Res. 105(11):1102-9.
18. McCaffrey LM, Montalbano J, Mihai C, Macara IG (2012) Loss of the Par3 polarity protein promotes breast tumorigenesis and metastasis. Cancer Cell. 22(5):601-14.
19. Muzumdar MD, Tasic B, Miyamichi K, Li L, Luo L (2007) A global double-fluorescent Cre reporter mouse. Genesis. 45(9):593-605.
20. Naydenov N, Feygin A, Conti MA, Adelstein RS, Ivanov A (2014) Intestinal epithelium specific knockout of nonmuscle myosin II A disrupts epithelial barrier and exaggerates experimental colitis (60.5) FASEB, 28(1).
21. Nguyen-Ngoc KV, Shamir ER, Huebner RJ, Beck JN, Cheung KJ, Ewald AJ (2015) 3D culture assays of murine mammary branching morphogenesis and epithelial invasion. Methods Mol Biol. 1189:135-62.
22. Paszek MJ, Zahir N, Johnson KR, Lakins JN, Rozenberg GI, Gefen A, Reinhart-King CA, Margulies SS, Dembo M, Boettiger D, Hammer DA, Weaver VM (2005) Tensional homeostasis and the malignant phenotype. Cancer Cell. 8(3):241-54. Butcher DT, Alliston T, Weaver VM (2009) A tense situation: forcing tumour progression. Nat Rev Cancer. 9(2):108-22.
23. Robinson GW, Hennighausen L (2011) MMTV-Cre transgenes can adversely affect lactation: considerations for conditional gene deletion in mammary tissue. Anal Biochem. 412(1):92-5.
24. Samuel MS, Lopez JI, McGhee EJ, Croft DR, Strachan D, Timpson P, Munro J, Schröder E, Zhou J, Brunton VG, Barker N, Clevers H, Sansom OJ, Anderson KI, Weaver VM, Olson MF (2011) Actomyosin-mediated cellular tension drives increased tissue stiffness and β-catenin activation to induce epidermal hyperplasia and tumor growth. Cancer Cell. 19(6):776-91.
25. Schlaepfer DD, Hanks SK, Hunter T, van der Geer P (1994) Integrin-mediated signal transduction linked to Ras pathway by GRB2 binding to focal adhesion kinase. Nature. 372(6508):786-91.
26. Schlegelmilch K1, Mohseni M, Kirak O, Pruszak J, Rodriguez JR, Zhou D, Kreger BT, Vasioukhin V, Avruch J, Brummelkamp TR, Camargo FD (2011) Yap1 acts downstream of α-catenin to control epidermal

proliferation. Cell. 144(5):782-95.
27. Schramek D, Sendoel A, Segal JP, Beronja S, Heller E, Oristian D, Reva B, Fuchs E (2014) Direct *in vivo* RNAi screen unveils myosin IIa as a tumor suppressor of squamous cell carcinomas. Science. 343(6168):309-13.
28. Shamir ER, Pappalardo E, Jorgens DM, Coutinho K, Tsai WT, Aziz K, Auer M, Tran PT, Bader JS, Ewald AJ (2014) Twist1-induced dissemination preserves epithelial identity and requires E-cadherin. J Cell Biol. 204(5):839-56.
29. Smutny M, Cox HL, Leerberg JM, Kovacs EM, Conti MA, Ferguson C, Hamilton NA, Parton RG, Adelstein RS, Yap AS (2010) Myosin II isoforms identify distinct functional modules that support integrity of the epithelial zonula adherens. Nat Cell Biol. 12(7):696-702.
30. Sumigray KD, Foote HP, Lechler T (2012) Noncentrosomal microtubules and type II myosins potentiate epidermal cell adhesion and barrier formation. J Cell Biol. 199(3):513-25.
31. Tullio AN, Bridgman PC, Tresser NJ, Chan CC, Conti MA, Adelstein RS, Hara Y. (2001) Structural abnormalities develop in the brain after ablation of the gene encoding nonmuscle myosin II-B heavy chain. J Comp Neurol. 433(1):62-74.
32. Vicente-Manzanares M1, Ma X, Adelstein RS, Horwitz AR (2009) Non-muscle myosin II takes centre stage in cell adhesion and migration. Nat Rev Mol Cell Biol. 10(11):778-90.
33. Wagner KU, McAllister K, Ward T, Davis B, Wiseman R, Hennighausen L (2001) Spatial and temporal expression of the Cre gene under the control of the MMTV-LTR in different lines of transgenic mice. Transgenic Res. 10(6):545-53.
34. Wagner KU, Wall RJ, St-Onge L, Gruss P, Wynshaw-Boris A, Garrett L, Li M, Furth PA, Hennighausen L (1997) Cre-mediated gene deletion in the mammary gland. Nucleic Acids Res. 25(21):4323-30.
35. Yam PT, Wilson CA, Ji L, Hebert B, Barnhart EL, Dye NA, Wiseman PW, Danuser G, Theriot JA (2007) Actin-myosin network reorganization breaks symmetry at the cell rear to spontaneously initiate polarized cell motility. J Cell Biol. 178(7):1207-21.

Figure 6-1

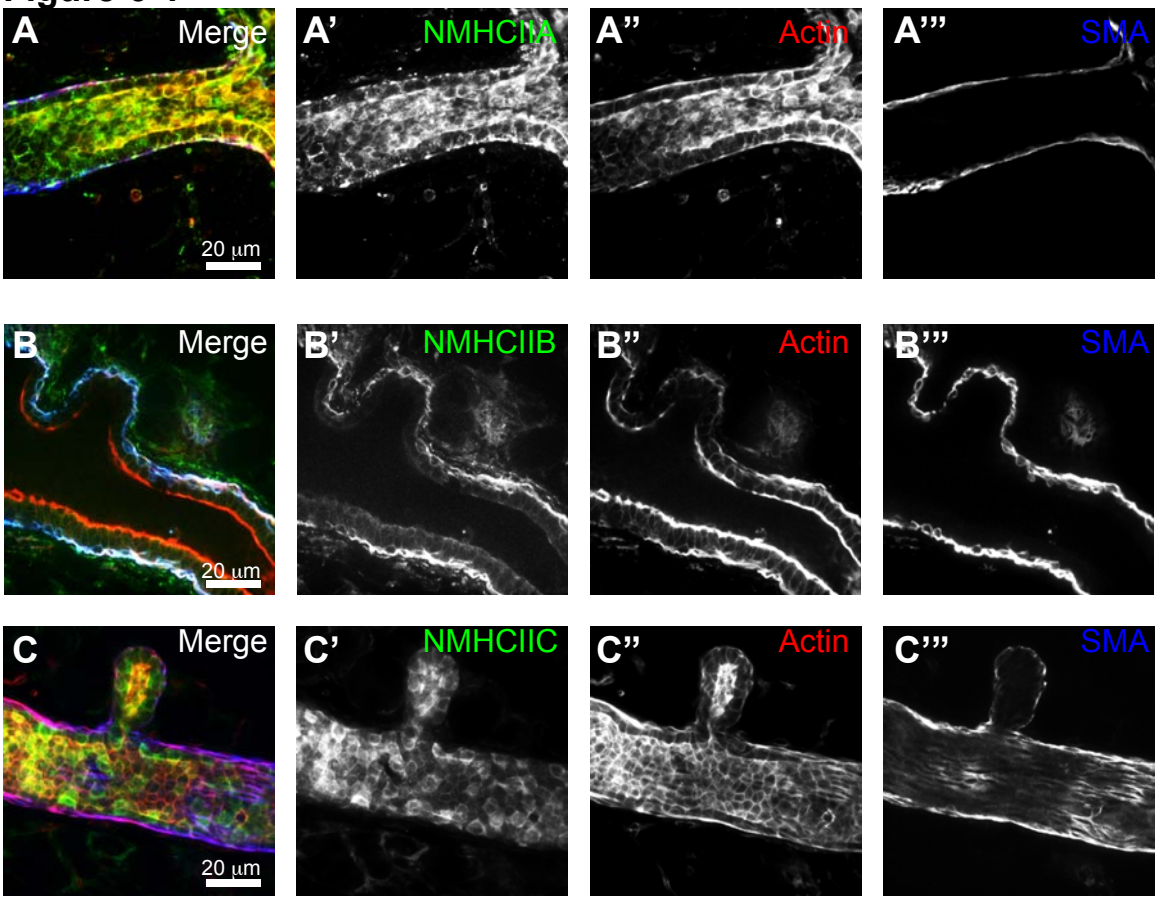

Expression and localization of NMII isoforms in mammary epithelium. (A-C) Mammary epithelial ducts were stained with (A) NMIIA, (B) NMIIB, (C) NMIIC together with F-actin and SMA (smooth muscle actin). (A') NMIIA, (B') NMIIB, C' (NMIIC). (A"-C") F-actin. (A'"-C'") SMA. (D) Western blot, NMIIA and NMIIB proteins were reduced in organoid samples after 4-5 days in culture.

Figure 6-2

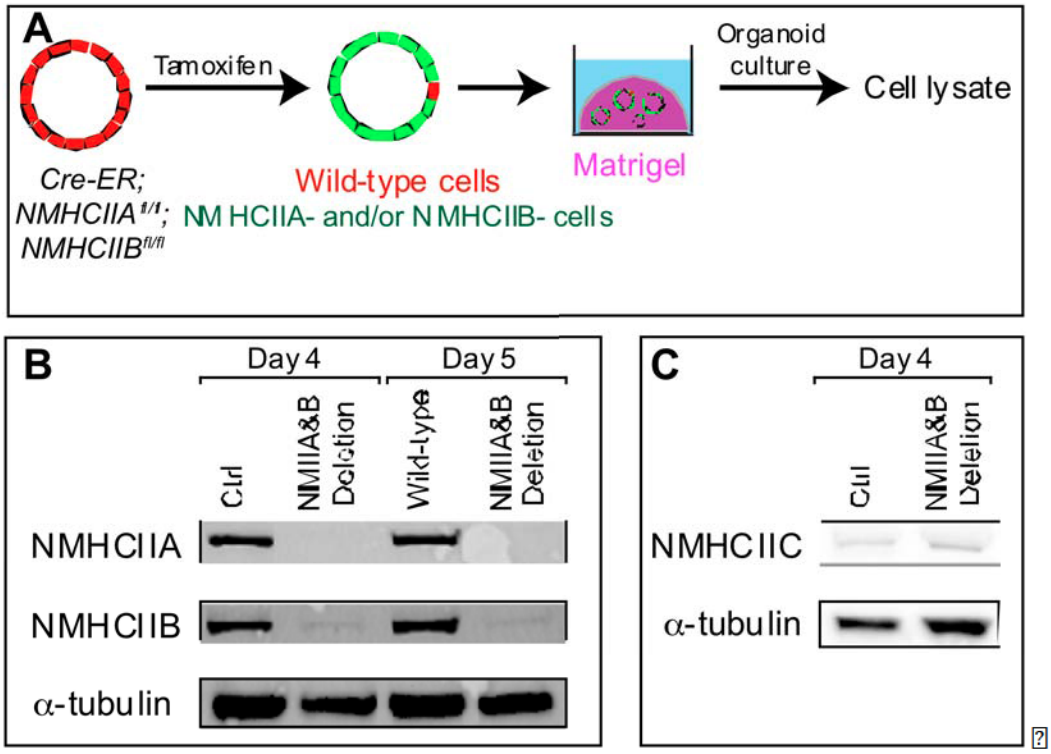

Deletion of NMIIA and NMIIB using the Cre-ER inducible system. (A) NMIIA and NMIIB were completely deleted in *NMIIA*$^{fl/fl}$; *NMIIB*$^{fl/fl}$ organoids with tamoxifen treatment, cultured in Matrigel, and collected for protein lysate. (B) Western blot, NMIIA and NMIIB expression levels from control and experimental samples after 4-5 days in culture. (C) Western blot, NMIIC expression levels from control and experimental samples after 4 days in culture.

Figure 6-3

Deletion of NMIIA,B induced excessive growth in quiescent mammary epithelium. (A) Control and genetic mosaic NMIIA and/or NMIIB deleted organoids was cultured in basal media. (B-H) Still images from time-lapse movies of organoids carrying different genetic variants of *NMIIA*$^{fl/fl}$*; NMIIB*$^{fl/fl}$ alleles. (I) Tissue growth rates were quantified by measuring organoids area normalized to the initial size. n: the number of time-lapse movies. Stars highlighted the significant difference across samples at the same time point by one-way ANOVA ($P<0.0001$). (J) Proliferation rates were quantified as the number of P-H3-positive cells was divided by the number of cells per organoid. $P<0.0001$ two-tailed unpaired t test. (K-N) Organoids were stained for P-H3 (green) and nuclei (blue). White dash lines marked the shape of organoids.

Figure 6-3

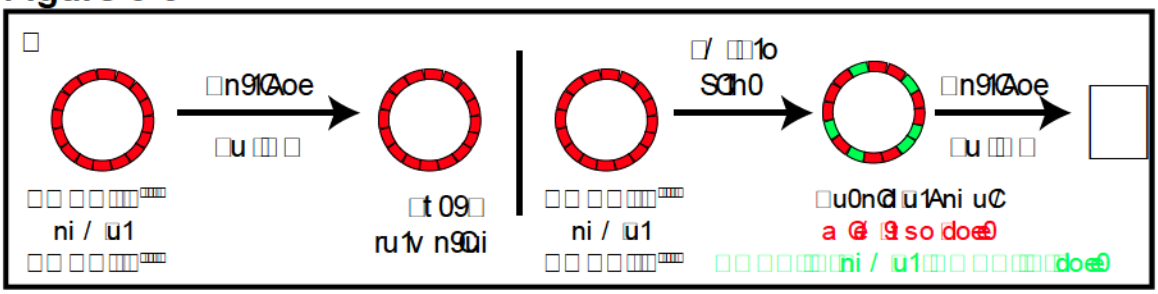

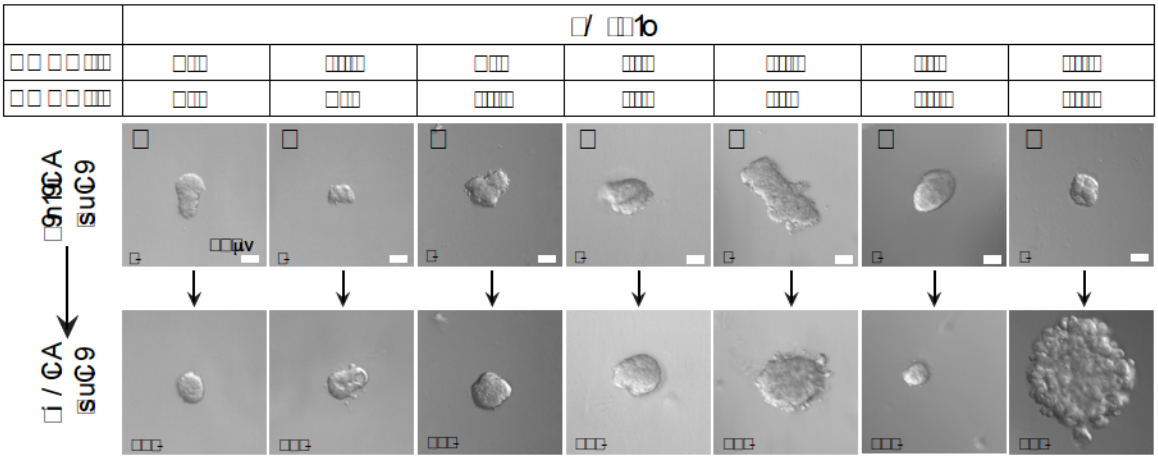

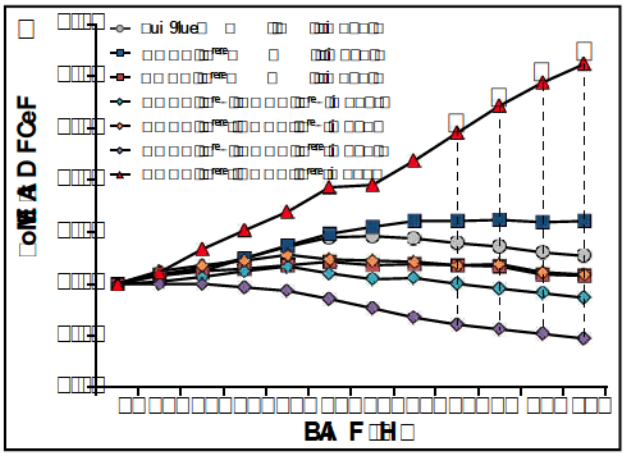

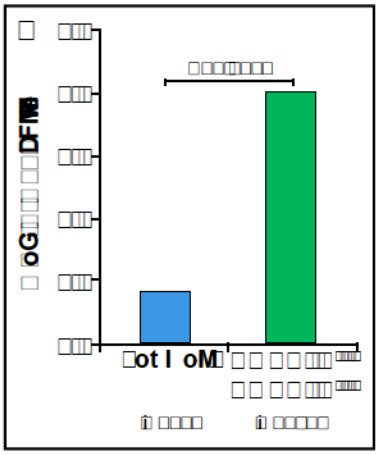

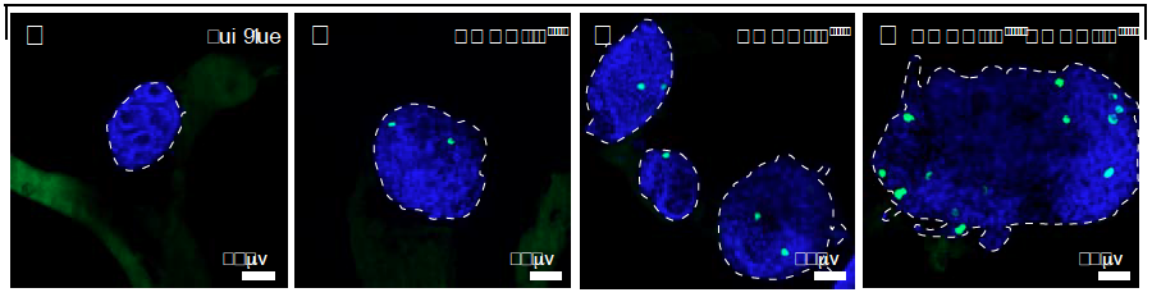

Figure 6-4

Loss of NMIIA,B enhanced epithelial growth beyond growth factor. (A) Control and genetic mosaic tissues were tested for tissue growth in the branching assay. (B-H) Still images from time-lapse movies of organoids carrying different genetic variants of *NMIIA*$^{fl/fl}$*; NMIIB*$^{fl/fl}$ alleles. (I) Tissue growth rates were quantified by measuring organoids area normalized to the initial size. n: the number of time-lapse movies. Stars highlighted the significant difference across samples at the same time point by one-way by ANOVA ($P<0.0001$). (J-M) Organoids were stained for P-H3 (green) and nuclei (blue). White dash lines marked the shape of organoids.

Figure 6-4

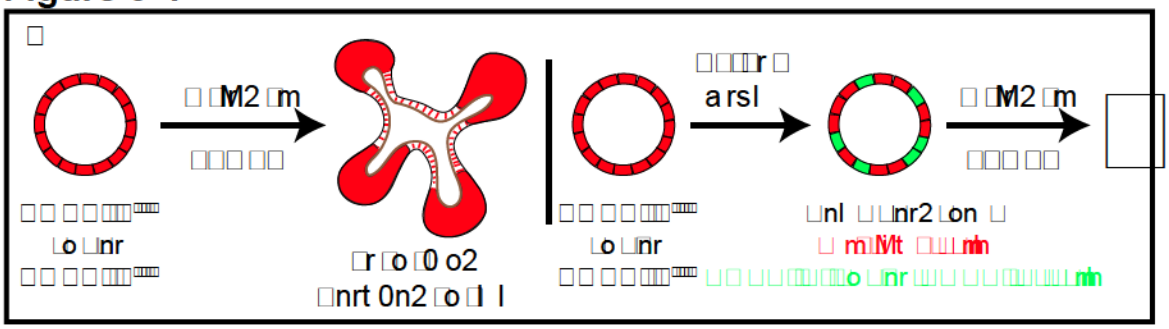

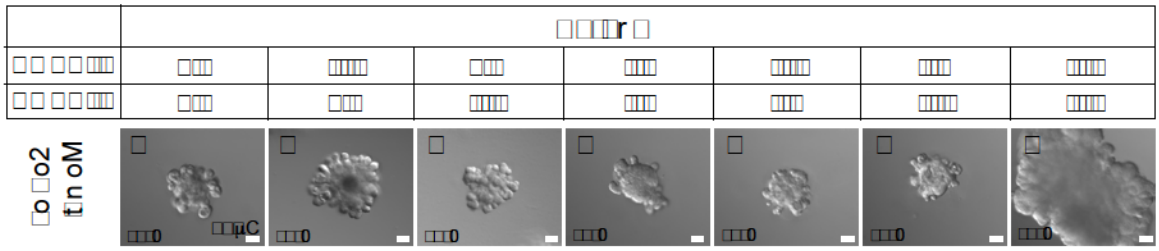

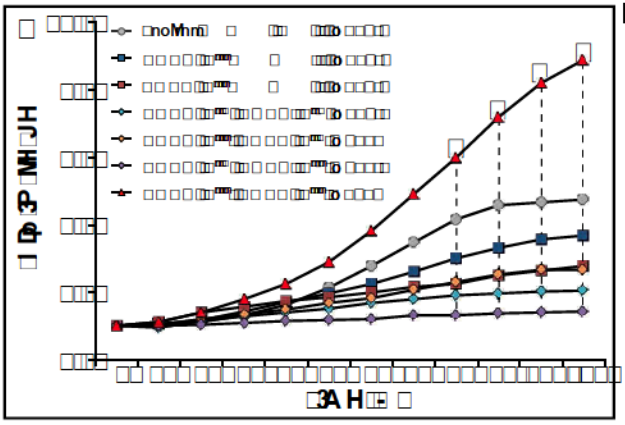

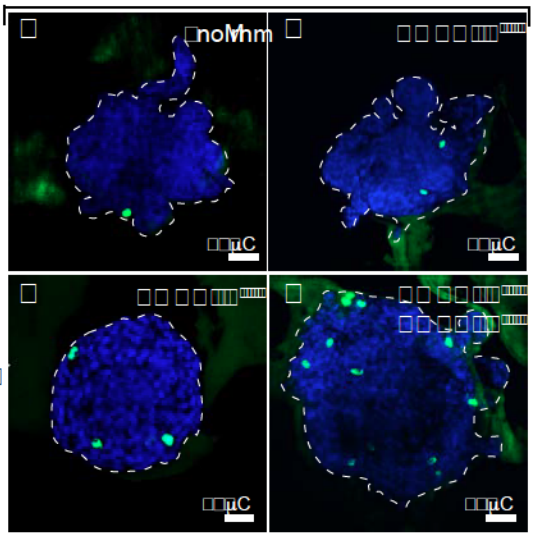

Figure 6-5

The hyper-proliferation is a non-cell autonomous effect. (A) Control and genetic mosaic tissues were individually cultured or co-cultured in basal media to test for cell autonomy. (B) Frames from a confocal time-lapse movie of a genetic mosaic NMIIA,B-deleted organoid. (C) Insets of the green channel to depict cell division in NMIIA,B-null cells. (D) Insets of the red channel to depict cell division in wild-type cells. White dash lines marked changes in cell shape throughout the division. (E) Percentage of dividing cells that were tracked from 5 confocal time-lapse movies. (F-H) Co-cultured organoids were stained with P-H3 (pink) and nuclei (blue). (I) Distribution of the number of P-H3+ cells in co-cultured organoids. Both $P<0.002$, $P<0.07$ values were calculated by two-tailed unpaired t tests.

Figure 6-5

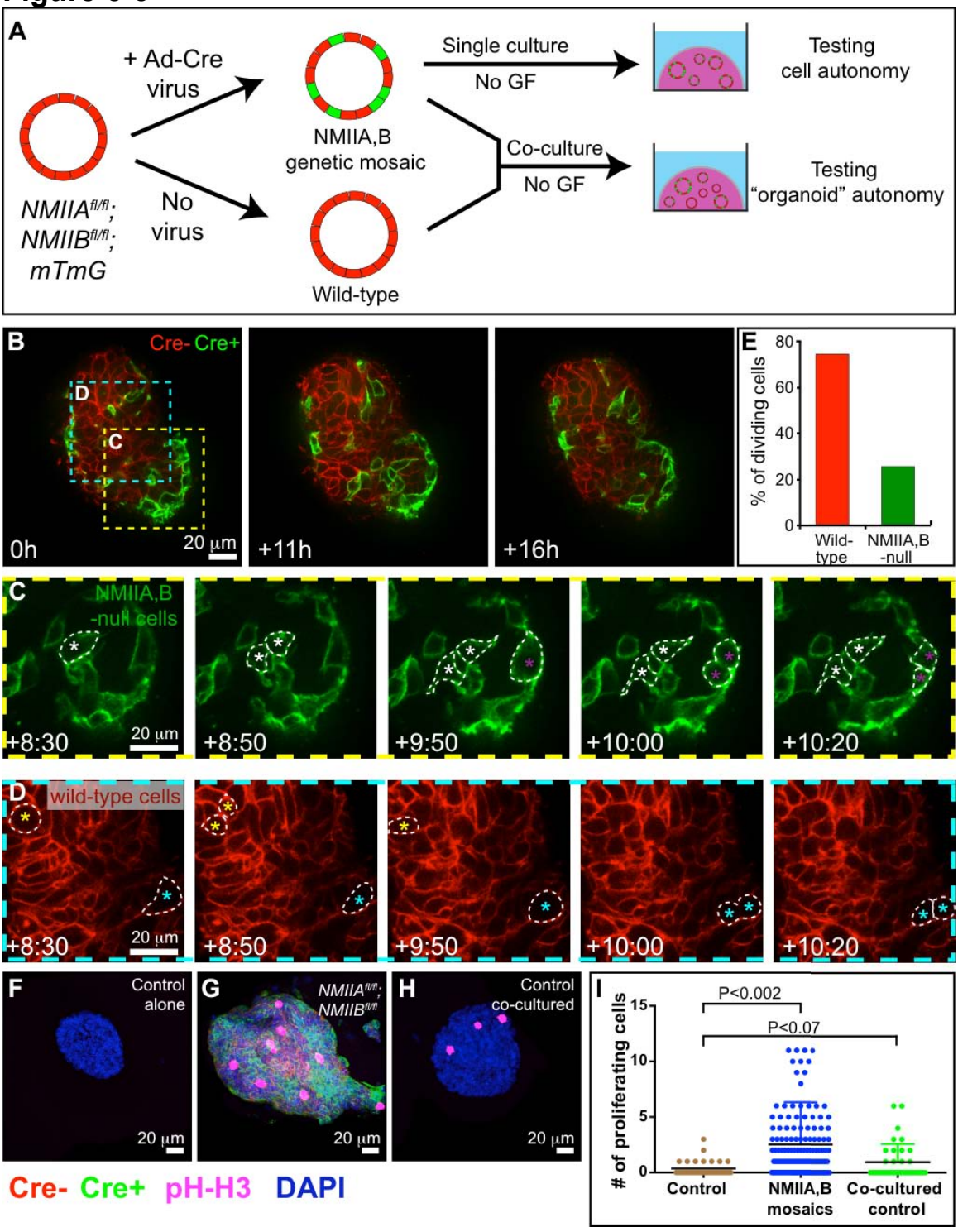
A
+ Ad-Cre virus
No virus
NMIIA^fl/fl; NMIIB^fl/fl; mTmG
NMIIA,B genetic mosaic
Wild-type
Single culture
No GF
Co-culture
No GF
Testing cell autonomy
Testing "organoid" autonomy
B
Cre- Cre+
D
C
0h
20 μm
+11h
+16h
E
% of dividing cells
80
60
40
20
0
Wild-type
NMIIA,B -null
C
NMIIA,B -null cells
+8:30
20 μm
+8:50
+9:50
+10:00
+10:20
D
wild-type cells
+8:30
20 μm
+8:50
+9:50
+10:00
+10:20
F
Control alone
20 μm
G
NMIIA^fl/fl; NMIIB^fl/fl
20 μm
H
Control co-cultured
20 μm
Cre- Cre+ pH-H3 DAPI
I
# of proliferating cells
P<0.002
P<0.07
15
10
5
0
Control
NMIIA,B mosaics
Co-cultured control

Figure 6-6

NMIIA,B deletion increased spontaneous proliferation in mammary epithelium. (A) Schematic description of orthotropic transplantation and inducible gene deletion. (B-D) Different epithelial structures found in the control glands. (B'-D') Different epithelial structures with random P-H3+ cells found in NMIIA,B-deleted glands. (E) The average number of P-H3+ cells per epithelial duct imaged at 40x magnification. (F-G) Different section views of the same epithelial duct. (F'-G') Insets of proliferating NMIIA,B-null and wild-type cells.

Figure 6-6

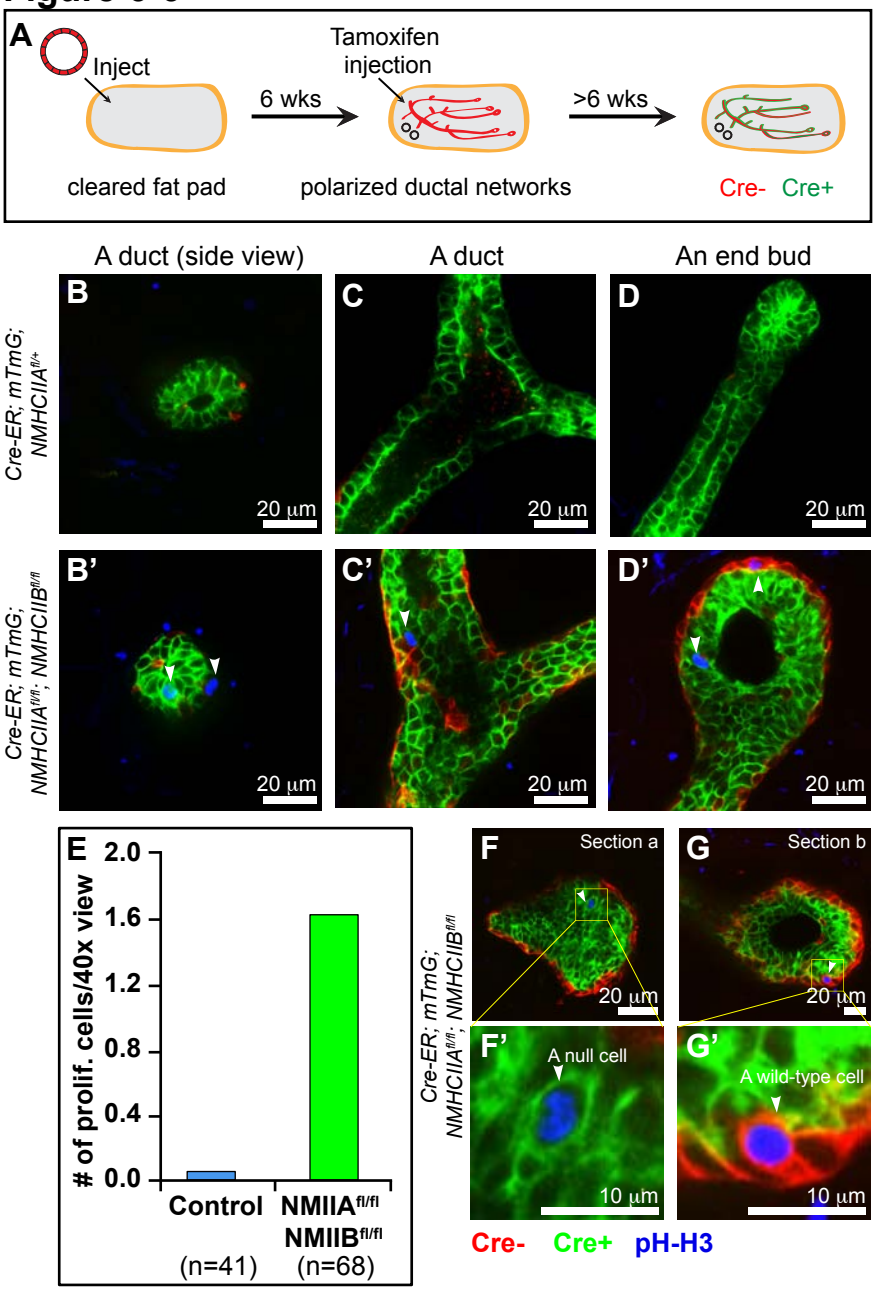
A
Inject
Tamoxifen injection
6 wks
>6 wks
cleared fat pad
polarized ductal networks
Cre- Cre+
A duct (side view)
A duct
An end bud
Cre-ER; mTmG; NMHCIIA fl/+
Cre-ER; mTmG; NMHCIIA fl/fl; NMHCIIB fl/fl
B
C
D
B'
C'
D'
20 μm
E
# of prolif. cells/40x view
2.0
1.6
1.2
0.8
0.4
0.0
Control
NMIIA fl/fl NMIIB fl/fl
(n=41)
(n=68)
F
Section a
G
Section b
F'
A null cell
G'
A wild-type cell
10 μm
Cre-ER; mTmG; NMHCIIA fl/fl; NMHCIIB fl/fl
Cre- Cre+ pH-H3

Figure 6-7

MMTV-Cre failed to deplete NMIIA and NMIIB proteins *in vivo*, but succeeded *in vitro*. (A-D) Mammary epithelial ducts from mice carrying *MMTV-Cre; mTmG* with different combinations of $NMIIA^{fl/fl}$; $NMIIB^{fl/fl}$ alleles. (E) Schematic description to examine NMIIA and NMIIB protein levels from *in vivo* and *in vitro* samples that were isolated from *MMTV-Cre* mice. Parts of cultured organoids were fixed and stained with P-H3 to test for proliferation. (F) Western blot, NMIIA and NMIIB expression levels from *in vivo* and *in vitro* samples. (G) Distribution of the numbers of P-H3+ cells of organoids carrying different combinations of $NMIIA^{fl/fl}$; $NMIIB^{fl/fl}$ alleles. $P<0.0001$ values were calculated by two-tailed unpaired t tests. (I-L) Cultured organoids carrying *MMTV-Cre; mTmG* $NMIIA^{fl/fl}$; $NMIIB^{fl/fl}$ alleles were fixed and stained with P-H3 (pink).

Figure 6-6

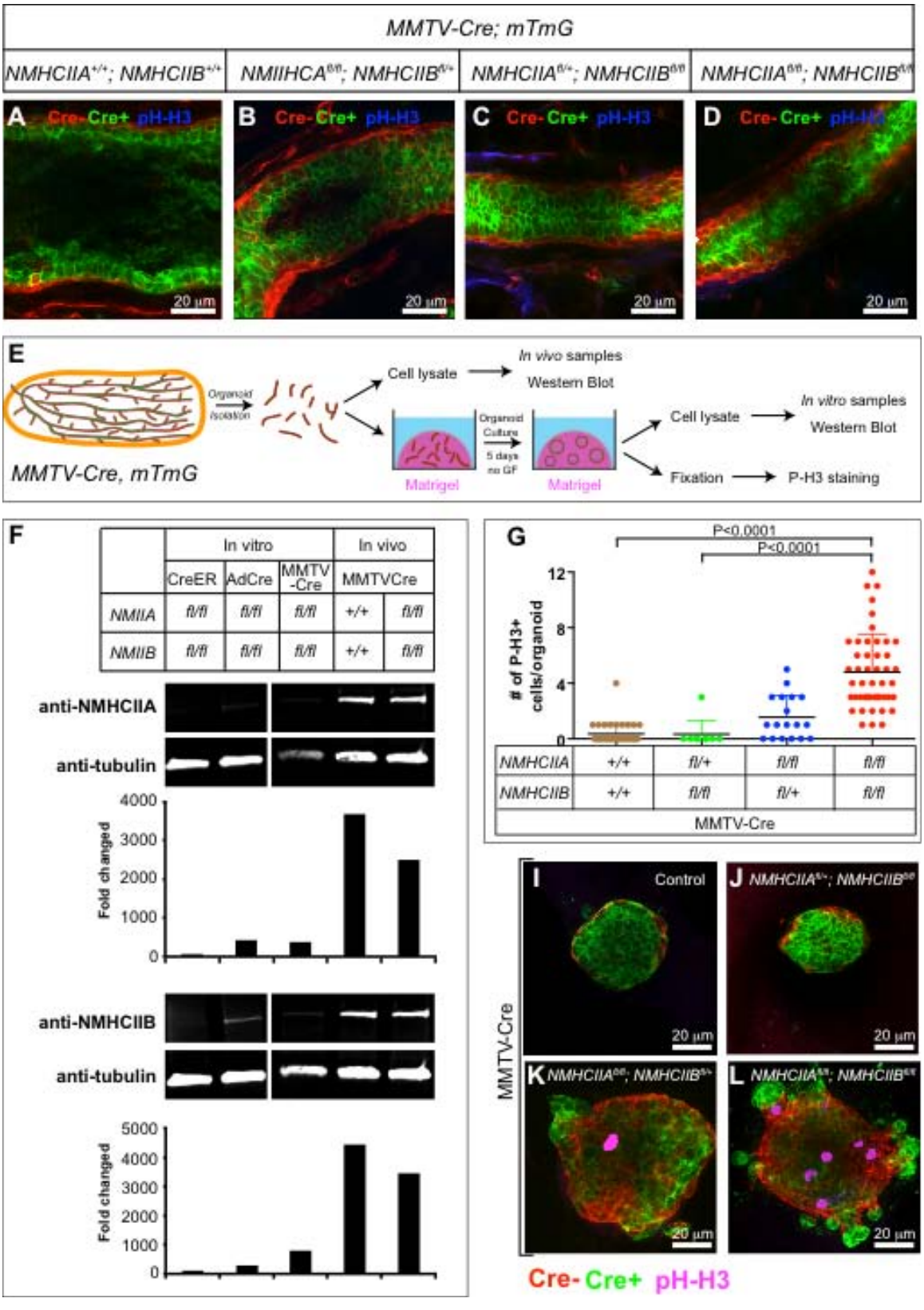
MMTV-Cre; mTmG
NMHCIIA+/+; NMHCIIB+/+
NMIIHCA fl/fl; NMHCIIB fl/+
NMHCIIA fl/+; NMHCIIB fl/fl
NMHCIIA fl/fl; NMHCIIB fl/fl
A Cre- Cre+ pH-H3
B Cre- Cre+ pH-H3
C Cre- Cre+ pH-H3
D Cre- Cre+ pH-H3
20 μm
E
Organoid Isolation
MMTV-Cre, mTmG
Cell lysate
In vivo samples
Western Blot
Organoid Culture
5 days no GF
Matrigel
Matrigel
Cell lysate
In vitro samples
Western Blot
Fixation
P-H3 staining
F
In vitro
In vivo
CreER
AdCre
MMTV -Cre
MMTVCre
NMIIA
NMIIB
fl/fl
+/+
anti-NMHCIIA
anti-tubulin
Fold changed
anti-NMHCIIB
anti-tubulin
Fold changed
G
P<0.0001
P<0.0001
# of P-H3+ cells/organoid
NMHCIIA
NMHCIIB
MMTV-Cre
I Control
J NMHCIIA fl/+; NMHCIIB fl/fl
K NMHCIIA fl/fl; NMHCIIB fl/+
L NMHCIIA fl/fl; NMHCIIB fl/fl
MMTV-Cre
Cre- Cre+ pH-H3

CHAPTER 7

Conclusion: Novel functions of the extracellular matrix and non-muscle myosin II in regulating mammary epithelium

Mammary epithelium develops and functions within a stromal microenvironment that is rich in ECMs. Directly surrounding the epithelium is a basement membrane which functions as a physical boundary to stroma, and provides molecular signals for establishing the epithelial architecture and maintaining homeostasis (Muschler and Streuli, 2010). In quiescent epithelium, the basement membrane controls, and limits, the penetration of stromal cells into epithelial space and vice versa, preventing epithelial cells from invading into stromal ECMs (Liotta et al., 1980). Pioneering work from Bissell and colleagues established the importance of basement membrane proteins (Matrigel) and collagen I for milk production of *in vitro* cultured mammary epithelial cells (Lee et al., 1984; Li et al., 1987). The impact of fibrillar collagen I has recently been the major focus of tumor microenvironment because abnormal alterations in collagen concentration and structure were correlated with breast cancer progression and metastasis (Egeblad et al., 2010). Although invasion through the basement membrane is a hallmark of invasive breast cancer, it remains unclear how and why a change from basement membrane to collagen I-rich ECM can trigger the invasive phenotype. This observation also led to an implication that exposure to, and remodeling of stromal collagen I ECM, are specific characteristics of stromal and tumor cells. In addition, tumors, themselves, contain thousands of genetic mutations (Stephens et al., 2009), which allow them to acquire cell plasticity during migration. Underlying actin-based protrusion are multiple adhesion complexes that permit stromal cells to adhere to, and migrate on, the fibrillar

collagen I substrate (Kubow and Horwitz, 2011).

The mammary epithelium has several distinct stages of development, in which it acquires different epithelial architectures (Hinck and Silberstein, 2005). After puberty epithelial ducts comprise a bilayer of quiescent, polarized and tightly connected cells. In contrast, the terminal end buds (TEBs) are a stratified structure of proliferative and motile epithelial cells during branching morphogenesis. The elongation of TEBs involves collective cell migration (Ewald et al., 2008), and follows both molecular and scaffolding cues in the fat pad (Nelson and Bissell, 2006; Brownfield et al., 2014). In contrast to the smooth basal surface, the internal epithelial cells that are not in contact with basement membrane ECMs retain their protrusive morphology (Ewald et al., 2012). Therefore, it is possible that normal epithelial cells possess an intrinsic ability to: 1) re-activate their motile and invasive properties, which are dormant in the homeostatic state, and 2) interact with stromal collagen I matrix, to sense and follow scaffolding cues, and to remodel collagen fibers.

Three dimensional (3D) culture models with various ECM substrates have been widely used to recapitulate tissue developments and cancer biology (Shamir and Ewald, 2014). Due to the abundance and importance of ECMs in many cellular processes, Matrigel and collagen I matrix are among the most common experimental substrates for modelling the basement membrane and stromal ECMs, respectively. The *in vitro* sources of these ECMs provide researchers with a great flexibility to manipulate the physical and supramolecular

characteristics of ECM microenvironment. However, there is an important limitation in such an approach: the *in vitro* fibrillogenesis and assembly of collagen I fibers are very variable and dependent on experimental conditions, which leads to a large variation in experimental results (Wolf et al., 2009). Thus, there is a need to establish a consistent collagen I-based assay in which the physical and supramolecular properties are controllable.

These questions converge into a general one: how do ECM composition and structure influence the behavior of mammary epithelial cells? I first established a collagen I-based assay with consistent supramolecular structure, to control epithelial growth (Nguyen-Ngoc and Ewald, 2013). I tested the acute response of varying ECM conditions using the organotypic culture technique, in which epithelial ductal groups, termed “organoids”, were explanted into 3D ECM gels (Nguyen-Ngoc et al., 2012; Nguyen-Ngoc et al., 2015). Using both pharmacological perturbation and Cre-lox based gene deletion of actomyosin contractility, I aimed to unravel the underlying mechanism by which ECMs regulate epithelial cell behavior and tissue organization.

The ECM microenvironment regulates epithelial migration during branching morphogenesis and tumor invasion

I first monitored the experimental conditions that allow *in vitro* solubilized collagen I to form 3D gels, and tested the effects of collagen matrix on epithelial growth. *In vitro* collagen fibrillogenesis is highly dependent on a pre-incubation

time prior to gelation. Epithelial organoids grew extensively in fiber-rich collagen ECMs while remaining unchanged in the non-fiber counterpart. This result suggested that *the presence of fibers in collagen I gel is essential for epithelial growth and migration*. Thus, the fiber-rich collagen I matrix was used for further investigation.

We next sought to distinguish the relative contribution of the alternations in the genetic and ECM microenvironment on tumor invasion. We explanted organoids from tumor and normal mammary epithelium to 3D gels of Matrigel and fiber-rich collagen I matrix. In Matrigel, normal and tumor organoids always maintained a non-protrusive interface. In contrast, both types of organoids invaded the collagen I ECM with extensive protrusion and dissemination. This unexpected result indicates that *cellular responses to the ECM microenvironment are conserved during tumor progression*. Moreover, the tumor cells invaded persistently with single or collective cell dissemination into the collagen I matrix. Despite initiating similar protrusions, myoepithelial cells in normal epithelium ceased to protrude by re-establishing basement membrane. Taken together, these data demonstrate that ECM microenvironment and genetic mutations are co-opted to promote tumor invasion, and myoepithelial cells and their secreted basement membrane proteins are crucial for suppressing tumor invasion.

I next tested whether the presence of Matrigel suppressed invasive behavior in mixed gels that contained collagen I. The organoids underwent branching morphogenesis, while retaining a non-protrusive interface with

Matrigel-containing ECMs. In addition, *the density of collagen I was correlated with the extent of ductal elongation and myoepithelial cell coverage*, (features of epithelial branching morphogenesis that were absent in pure Matrigel). In particular, I identified that *the 3:7 ratio of Matrigel and collagen I in the mixed gel was the most physiologically suitable microenvironment for branching morphogenesis*, with elongated ducts and full coverage of myoepithelial cells. Our data have highlighted the importance of both basement membrane and collagen I ECM to mammary branching morphogenesis. We speculate that collagen I fibers are involved in regulating myoepithelial cell proliferation and migration, to maintain the coverage and provide guiding signals and cues for ductal elongation.

I then used the collagen I-based assay to understand how epithelial cells interact with collagen I fibers. I used imaging analyses and cell marker staining to describe the cellular events involved in modifying surrounding collagen I fibers during branching morphogenesis. I observed that *collagen I fibers were progressively aligned during, and at the conclusion of, ductal elongation*. The fiber linearization was correlated with the localization and cellular contractility of myoepithelial cells. Importantly, I observed that myoepithelial cells used protrusions, which were not directed to the ECM, to bind and exert pulling force on collagen I fibers. We conclude that mammary epithelial cells can remodel the collagen I matrix, which in turn orients the ductal elongation. We further speculate that the dynamic remodeling of basement membrane creates transient

gaps, and allows epithelial cells to interact with collagen I.

My work provided new insights into the mechanisms by which the ECM microenvironment regulates epithelial cell migration. The ECM microenvironment plays a pivotal role in dictating the migratory behaviors of normal and malignant cells. Both normal and tumor cells own an intrinsic ability to invade, and to remodel, collagen I matrix. Either pre-existence or *de novo* formation of basement membrane can inhibit cell invasion. In normal tissue, the harmonious coordination of basement membrane and stromal collagen I is required to achieve a complete program of epithelial branching morphogenesis, and maintain tissue homeostasis. In tumor tissue, the breaching basement membrane allows tumor cells to directly expose to collagen I rich stroma and acquire the trait of persistent invasion. My work also established *ex vivo* assays for in depth study of the cellular and molecular basis of epithelial branching morphogenesis and tumor invasion in our laboratory.

Concurrent loss of non-muscle myosin IIA and IIB induces proliferation in mammary epithelium

Non-muscle myosin II (NMII) is central to the interplay of cellular response to ECM microenvironments (Vicente-Manzanares et al., 2009). Our analysis of time-lapse imaging of normal organoids grown in collagen I ECM revealed that the invasion and epithelial reorganization were correlated with cycles of extension and retraction, indicating an involvement of cellular contractility.

Indeed, *pharmacological inhibition of actomyosin contractility abolished tissue reorganization and basement membrane re-establishment, which enabled persistent invasion*. This result indicates that NMII-mediated contractility contributes to preventing invasion.

Myosin II also mediates several important cellular processes in epithelial tissue; and its deregulation leads to multiple embryogenesis defects and diseases (Ma and Adelstein, 2014). To further elucidate the functional contribution of NMII isoforms to epithelial organization, we used Cre-lox based deletion to genetically perturb NMII isoforms A and/or B, which are indispensable for embryogenesis and crucial for epithelial cell adhesions. Surprisingly, *concurrent deletion of NMIIA and NMIIB (NMIIA,B) simultaneously induced epithelial growth in both quiescent and actively growing tissues,* which were correlated with mitotic index and proliferation rate. Interestingly, analysis in genetic mosaic NMIIA,B deletion revealed that *both NMIIA,B-null and wild-type cells were dividing extensively*. Collectively, our data demonstrate the novel, cooperative function of NMIIA and NMIIB as a negative regulator of epithelial tissue growth. Through the non-cell autonomous machinery, the effect of NMIIA,B deletion could be beneficial to the growth of neighboring cells.

Our data led us to rethink how epithelial tissue controls its shape and size. We speculate that epithelial cells can use the network of myosin II-generated contractile force to relay molecular signals, and/or mechanical cues, between cells within the tissue. Myosin II may be a regulator underlying the contact

inhibition of proliferation. Therefore it is plausible that concurrent loss of NMIIA and NMIIB may break the contractile integrity within epithelial tissue, resulting in loss of growth control, and fostering sustained proliferation during tumor progression. Future work may focus on analysis of the expression profile of NMIIA,B-deleted tissue to understand how cell proliferation is induced by loss of NMIIA,B at the molecular level. In addition, *in vivo* deletion of NMIIA,B in a tumor susceptible background may further reveal the functional contribution of myosin II to tumorigenesis.

References

1. Brownfield DG, Venugopalan G, Lo A, Mori H, Tanner K, Fletcher DA, Bissell MJ. (2014) Patterned collagen fibers orient branching mammary epithelium through distinct signaling modules. Curr Biol. 23(8):703-9.
2. Egeblad M, Rasch MG, Weaver VM. (2010) Dynamic interplay between the collagen scaffold and tumor evolution. Curr Opin Cell Biol. 22(5):697-706.
3. Ewald AJ, Brenot A, Duong M, Chan BS, Werb Z (2008) Collective epithelial migration and cell rearrangements drive mammary branching morphogenesis. Dev Cell. 14(4):570-81.
4. Ewald AJ, Huebner RJ, Palsdottir H, Lee JK, Perez MJ, Jorgens DM, Tauscher AN, Cheung KJ, Werb Z, Auer M (2012) Mammary collective cell migration involves transient loss of epithelial features and individual cell migration within the epithelium. J Cell Sci. 125(Pt 11):2638-54.
5. Hinck L, Silberstein GB. (2005) Key stages in mammary gland development: the mammary end bud as a motile organ. Breast Cancer Res. 7(6):245-51.
6. Kubow KE, Horwitz AR. (2011) Reducing background fluorescence reveals adhesions in 3D matrices. Nat Cell Biol. 13(1):3-5.
7. Lee EY, Parry G, Bissell MJ. (1984) Modulation of secreted proteins of mouse mammary epithelial cells by the collagenous substrata. J Cell Biol. 98(1):146-55.
8. Li ML, Aggeler J, Farson DA, Hatier C, Hassell J, Bissell MJ. (1987) Influence of a reconstituted basement membrane and its components on casein gene expression and secretion in mouse mammary epithelial cells. Proc Natl Acad Sci U S A. 84(1):136-40.
9. Liotta LA, Tryggvason K, Garbisa S, Hart I, Foltz CM, Shafie S. (1980) Metastatic potential correlates with enzymatic degradation of basement membrane collagen. Nature. 284(5751):67-8.
10. Ma X, Adelstein RS (2014) The role of vertebrate nonmuscle Myosin II in development and human disease. Bioarchitecture. 4(3):88-102.
11. Muschler J, Streuli CH. (2010) Cell-matrix interactions in mammary gland development and breast cancer. Cold Spring Harb Perspect Biol. 2(10).
12. Nelson CM, Bissell MJ. (2006) Of extracellular matrix, scaffolds, and signaling: tissue architecture regulates development, homeostasis, and cancer. Annu Rev Cell Dev Biol. 22:287-309.
13. Nguyen-Ngoc KV and AJ Ewald. (2013). Mammary ductal elongation and myoepithelial migration are regulated by the composition of the extracellular matrix. J Microsc. 251(3):212-23.
14. Nguyen-Ngoc KV, KJ Cheung, A Brenot, ER Shamir, RS Gray, WC Hines, P Yaswen, Z Werb and AJ Ewald. (2012). The ECM microenvironment regulates collective migration and local dissemination in normal and malignant mammary epithelium. Proc Natl Acad Sci U S A. 109(39):E2595-604.

15. Shamir ER, Ewald AJ. (2014) Three-dimensional organotypic culture: experimental models of mammalian biology and disease. Nat Rev Mol Cell Biol. 15(10):647-64.
16. Stephens PJ, McBride DJ, Lin ML, Varela I, Pleasance ED, Simpson JT, Stebbings LA, Leroy C, Edkins S, Mudie LJ, Greenman CD, Jia M, Latimer C, Teague JW, Lau KW, Burton J, Quail MA, Swerdlow H, Churcher C, Natrajan R, Sieuwerts AM, Martens JW, Silver DP, Langerød A, Russnes HE, Foekens JA, Reis-Filho JS, van 't Veer L, Richardson AL, Børresen-Dale AL, Campbell PJ, Futreal PA, Stratton MR. (2009) Complex landscapes of somatic rearrangement in human breast cancer genomes. Nature. 462(7276):1005-10.
17. Vicente-Manzanares M1, Ma X, Adelstein RS, Horwitz AR (2009) Non-muscle myosin II takes centre stage in cell adhesion and migration. Nat Rev Mol Cell Biol. 10(11):778-90.
18. Wolf K, Alexander S, Schacht V, Coussens LM, von Andrian UH, van Rheenen J, Deryugina E, Friedl P. (2009) Collagen-based cell migration models in vitro and in vivo. Semin Cell Dev Biol. 20(8):931-41.

CURRICULUM VITAE FOR Ph.D. CANDIDATE
The Johns Hopkins University School of Medicine

KIM-VY NGUYEN-NGOC 02.15.2015

Educational History:

Ph.D.	2015	BCMB Program	Johns Hopkins School of Medicine
(expected)		Mentor: Andrew Ewald Ph.D.	
M.Sc	2008	MMD Program	Radboud University Nijmegen
B.S.	2005	Biotechnology	University of Sciences

Professional Experiences

05/2010 – present: Ewald Lab (PhD thesis lab). Departments of Cell Biology & Oncology, Johns Hopkins School of Medicine.

04/2009 – 08/2009**:** Brugge Lab. Department of Cell Biology, Harvard University School of Medicine.

01/2008 – 03/2009: Sterneck Lab (Master thesis lab). Laboratory of Cell and Developmental Signaling, National Cancer Institute at Frederick, National Institute of Health.

02/2007 – 12/2007: Lohrum Lab (Internship). Department of Molecular Biology, Nijmegen Center for Molecular Life Sciences, Radboud University Nijmegen. The Netherlands.

Scholarships, fellowships

2013 ASCB Graduate Student Travel Award. Annual Meeting in New Orleans, LA.

2013 Lewis Travel Award. Department of Cell Biology. Johns Hopkins School of Medicine.

2013 – 2014 Isaac Morris Hay and Lucille Elizabeth Hay Graduate Fellowship. Department of Cell Biology. Johns Hopkins School of Medicine.

2008 KWF Internship Grant for Pre-doctoral Students for an abroad internship in cancer research. *KWF: Dutch Cancer Society*.

2006 – 2008 DELTA Scholarship for international students. *DELTA: Dutch Education: Learning at Top Level Abroad.*

2006 – 2008 Fellowship of Dutch Blind Foundation.

2004 AMCHAM Scholarship – awarded to 20 outstanding students of Vietnam National University in Ho Chi Minh City. *AMCHAM: the American Chamber of Commerce in Vietnam.*

2004 The encouraging prize – a contest for "Students in science research", University of Sciences, Ho Chi Minh City.

Publications

Research papers:

Nguyen-Ngoc, K.-V., and Ewald, A.J. 2013. Mammary ductal elongation and

myoepithelial migration are regulated by the composition of the extracellular matrix. J Microsc. 251(3):212-23.

Nguyen-Ngoc, K.-V., Cheung, K.J., Brenot, A., Shamir, E.R., Gray, R.S., Hines, W.C., Yaswen, P., Werb, Z., and Ewald, A.J. 2012. The ECM microenvironment regulates collective migration and local dissemination in normal and malignant mammary epithelium. PNAS. 109, E2595-2604.

Kim, J.H., Cho, A., Yin H., Schafer, D.A., Mouneimne, G., Simpson, K.J., **Nguyen, K.-V.,** Brugge, J.S., and Montell, D.J. 2011. Psidin, a conserved protein that regulates protrusion dynamics and cell migration. Genes Dev. 25(7):730-41.

Book chapters:

Nguyen-Ngoc, K.-V., Shamir, E.R., Huebner, R.J., Beck, J.N., Cheung, K.J., and Ewald, A.J. 2015. 3D culture assays of murine mammary branching morphogenesis and epithelial invasion. Methods Mol Biol. 1189:135-62

Presentations

Talks:

American Society of Cell Biology Annual Meeting, *Minisymposium 20 – Cancer Cell Biology*: "Downregulation of Non-muscle Myosin II Induces Cell Proliferation in Mammary Epithelium". New Orleans, LA. December 2013.

Biochemistry, Cellular & Molecular Biology (BCMB) Annual Program Retreat: Student Research Talk, "Coordinated Regulation of Epithelial Migration by ECM and Actomyosin Contractility". Baltimore, MD. October 2012.

Posters:

American Society of Cell Biology Annual Meeting: "Coordinated Regulation of Epithelial ECM and Actomyosin Contractility." San Francisco, CA. December 2012.

Annual Safeway Breast Cancer Research Retreat: "Effects of collagen type I on mammary branching morphogenesis and breast cancer metastasis." Baltimore, MD. May 2011.

American Society of Cell Biology Annual Meeting: "Coordinated Regulation of Epithelial Migration by ECM and Actomyosin Contractility." Philadelphia, PA. December 2010.

NCI-CCR NIAID Symposium: "The C/EBPδ-regulated interleukin 1 member 9 (IL-1F9, IL-1H1) is a potential survival factor for mammary epithelial and breast tumor cells." Bethesda, MD. June 2008.

Spring Research Festival at NCI-Frederick: "Verification and characterization of apoptosis-related target genes of CCAAT/enhancer binding protein delta (C/EBPδ)." NCI-Frederick campus. Frederick, MD. June 2008.